EFFECT OF PARTIAL DEBONDING OF PRESTRESSING STRANDS ON BEAM END CRACKING

By

Melissa Donoso Vidales

A THESIS

Submitted to
Michigan State University
in partial fulfillment of the requirements
for the degree of

MASTER OF SCIENCE

Civil and Environmental Engineering

2011

ABSTRACT

EFFECT OF PARTIAL DEBONDING OF PRESTRESSING STRANDS ON BEAM END CRACKING

By

Melissa Donoso Vidales

The use of shielded strands is an effective technique to reduce high tensile stresses in the end region of prestressed concrete members. However, damage in the ends of prestressed beams with shielded strands has been increasingly experienced during production. Guidelines on the use of debonded strands, such as the AASHTO Bridge Design Specifications are mainly to address concerns regarding the shear strength of pre-tensioned concrete elements. The bond behavior of shielded 0.6 in. (15.2 mm) diameter strand was experimentally evaluated by conducting studies on unstressed (pull-out tests) and stressed (pretensioned beams) concrete elements. The strands were debonded using flexible sheathing. Experimentally calibrated finite element (FE) models were developed to simulate bond behavior of shielded strand and assessed the induced stress state in the elements. The effect of partial strand debonding on the anchorage zone of bridge girders was studied through FE simulations within the context of a skew U-beam case study for which evidence of damage exists. Pull-out test results showed no evidence of residual bond on singular or doubly sheathed strand. However, experimentally calibrated numerical simulations showed that strand debonded with flexible-slit sheathing leads to high radial stresses along the debonded length in the concrete due to strand dilation from Poisson’s effect. The use of rigid oversized sheathing was shown to decrease stresses in the transfer region and along the unbonded length. A staggered distribution of the debonded strands can reduce the longitudinal shear stresses created by the uneven distribution of prestress forces in the beam-cross section.

DEDICATION

To God, my parents, and my husband

ACKNOWLEDGEMENT

I give special thanks to my advisor, Dr. Rigoberto Burgueño, for giving me the opportunity of working with him, all the advice and encouragement, to keep doing my very best even when I felt that things were not going the way that I wanted. I never imagined being a research assistant and it was a great experience that I will not ever forget; thank you Dr. Burgueño.

I thank Yi Sun and Mr. Sia Ravanbaskh for all the technical support. Yi, I will never forget the countless hours of fun work at the CIL. That was an extraordinary experience. I also thank all of the students and staff at the Department of Civil and Environmental Engineering at Michigan State University for all their support. I thank Dr. Robert J. Frosch (Purdue University) for sharing valuable information with us, which was of great contribution to the work presented herein.

I want to deeply thank my great-uncle Guillermo Murillo for his support during my studies in the U.S. Without his helped this would have not been possible. I am grateful for the support that my parents have given me, all the moments that I thought this was tough, they always will be there for me. I am grateful to my husband Darren for his moral support and understanding, for being there for me in good and not so good times. And the most important thank you, to God, who keeps me alive; helping me to do my very best every day of my life. Never give up your dreams; there are the motor of our lives.

Table of Contents

LIST OF TABLES

LIST OF FIGURES

CHAPTER 1 INTRODUCTION: MOTIVATION AND DESCRIPTION OF THE PROBLEM

1.1 Introduction

This chapter presents the motivation of this research and preliminary background information. In addition, this chapter presents the description of the problem for which this research was undertaken and examples that provide a better description of the issue. Moreover, the research hypotheses, research objectives, the project phases, and the organization of the report are also presented.

1.2 Background

Prestressed concrete members are extensively used as bridge girders. The concrete is precompressed when the tensile force in steel strands is released into the concrete member. Prestressed concrete members are made of high strength materials. However, when the prestressing force is released into the concrete member the anchorage zone is highly stressed, which can result in beam-end cracking.

The use of debonded strands in the precast/prestressed industry, especially for bridge girders, has been beneficial as it permits the reduction of the high tensile stresses close to the free end of the members. In addition, by debonding some strands the free length of the strand is increased by reducing the restraining effect at the beam ends [19].

Partially debonded strands are considered a better solution than the use of draped strands because of its easier implementation. Debonding is achieved by placing plastic tubing around the strand along the desired length in order to prevent bonding between the steel and the surrounding concrete [27], as shown in Figure 1-1 and Figure 1-2. However, cracking in the anchorage zones of prestressed concrete beams containing unbonded strands have been observed during the production process, as shown in Figure 1-3 and Figure 1-4. There are many factors that can contribute to beam-end-cracking in prestressed concrete beams with blanketed strands, such as the strand diameter, the compressive strength, the strand release rate and sequence, the restraint effect due to free lengths strand, etc. Thus, detailed evaluation of this complex problem has been elusive.

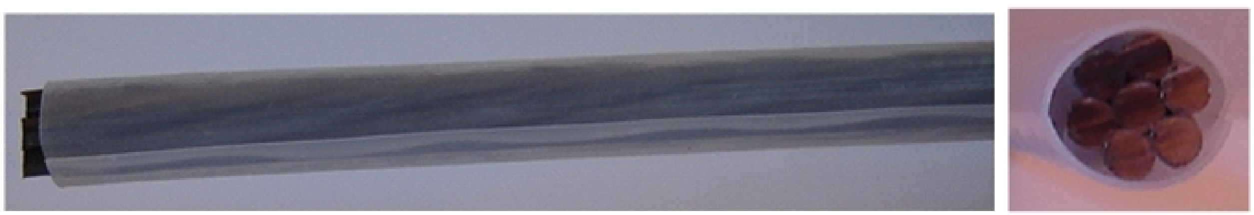

Figure 1-1 Debonded Strand using Flexible Sheathing

(For interpretation of the references to color in this and all other figures, the reader is referred to the electronic version of this thesis)

Figure 1-2 Photograph of a Shielded Strand using Rigid Debonding Material

There have not been many studies conducted regarding the causes for end cracking in prestressed beams. One of the most recognized works is the one conducted by Mirza and Tawfik [19]. They conducted experimental studies and developed a one-dimensional numerical model to sutdy the restraint effect in beam cracking. Mirza and Tawfik found that the short free strand length can cause beam-end cracking and recommended the free strand length to be 5 percent of the casting bed. Another representative study is that of Kannel et al. [13] who conducted research to study the effects of strand release sequence on beam-end cracking. Kannel et al. [13] used experimentally validated three-dimensional continuum-type finite element models with the purpose of simulating the end region of a prestressed concrete beam. This study also verified that unbonded strands can minimize stress levels in beam-end regions by increasing the free strand length and thus minimizing the axial restraint effect.

Since the problem of beam-end cracking is concentrated in the anchorage zone and the involved parameters are many, a full experimental assessment is cost-prohibitive. Numerical simulations are thus more feasible; but they need to be realistic enough to represent geometry, component interaction, and nonlinear material response.

Even though precast concrete fabricators follow the lastest design guidelines when dealing with debonded strands, end-cracking is still being observed during the production of some units. This is an important aspect that needs to be resolved in order to obtain high quality products and maximize potential serviceability or durability performance. It shall be recognized that the guidelines for the use of debonded strands provided by codes such as the AASHTO Bridge Design Specifications [2] and the AASHTO Bridge Design Construction Specifications [2] are mainly related to the shear performance of girders under service loads. Thus, these recommendations are not aimed at avoiding possible end-cracking in girders with blanketed strands during production.

While strand debonding has been in use with relative success for some time, the cracking of beam-ends continues to be a problem. Furthermore, the idealized assumption that an “unbonded” strand does not transfer any forces to the concrete beam has been proven wrong through ad-hoc tests [6]. Thus, a detailed evaluation on the bond behavior of debonded strand, and its effect on the transfer of prestressing forces at the ends of beams including cracking potential is needed.

1.3 Problem Description

Blanketing of prestressing strands has become an effective technique to alleviate the high tensile stresses in the anchorage region of pre-tensioned concrete beams during the strand release procedure. However, end-cracking has been observed in some prestressed concrete beams containing debonded strands. Two examples made accessible for this study are the damage in the end region of skew bridge beams with U- and Box-type cross section [8][23][31] as shown in Figure 1-3 and Figure 1-4. Figure 1-3 shows the end-cracking on the bottom of a skew-box girder that occurred upon release of the prestressing strands. The skew angle of the box girder was 40 degrees. Debonding of the strands was accomplished with double slit flexible sheathing around the strand. In this study, the slit flexible sheathing will be also referred as soft debonding material. The cross section of the box-girder is shown in Figure 1-5. The reinforcing details and location of debonded and fully bonded strands are also shown in this figure.

The damage to a skewed U-beam containing partially debonded strand is shown in Figure 1-4. The skew angle was 18 degrees. The strands were also debonded using a soft sheathing material. The cross section of the U-beam, the location of the fully bonded strands, and the strand debonding pattern are shown in Figure 1-6. The U-girder was taken as case study for the numerical simulations presented in Chapter 5 to investigate the effect of debonded strands on end-cracking in full-size beams.

Figure 1-3 Skew Box-beam damage observed during production [31]

Figure 1-4 End-cracking seen on U-beam during production [23]

The box beam had an overall debonding percentage of 37 percent. The bottom row of strands (Figure 1-5), 24 percent were debonded, and row 5 had 67 percent of its strands debonded. The AASHTO Bridge Design Specifications [2] limit the number of debonded strands to 25 percent in total and to no more than 40 percent in a given single row.

Soft (slit) sheathing material offers a tight fit against between the strand and the surrounding concrete, which could lead to high radial pressure at the interface of the two materials as the strand tries to recover its original diameter upon release of the pre-tensioning force. In some cases, it may be advisable to use a rigid (un-split) and oversized debonding material to eliminate any degree of prestressing force that could be transferred along the debonded zone and to ensure that radial stresses would not develop as the strand dilates. Pavelchak [23] and Sun [31] have recommended the use of un-split (rigid) debonding material when effectiveness of debonding becomes essential.

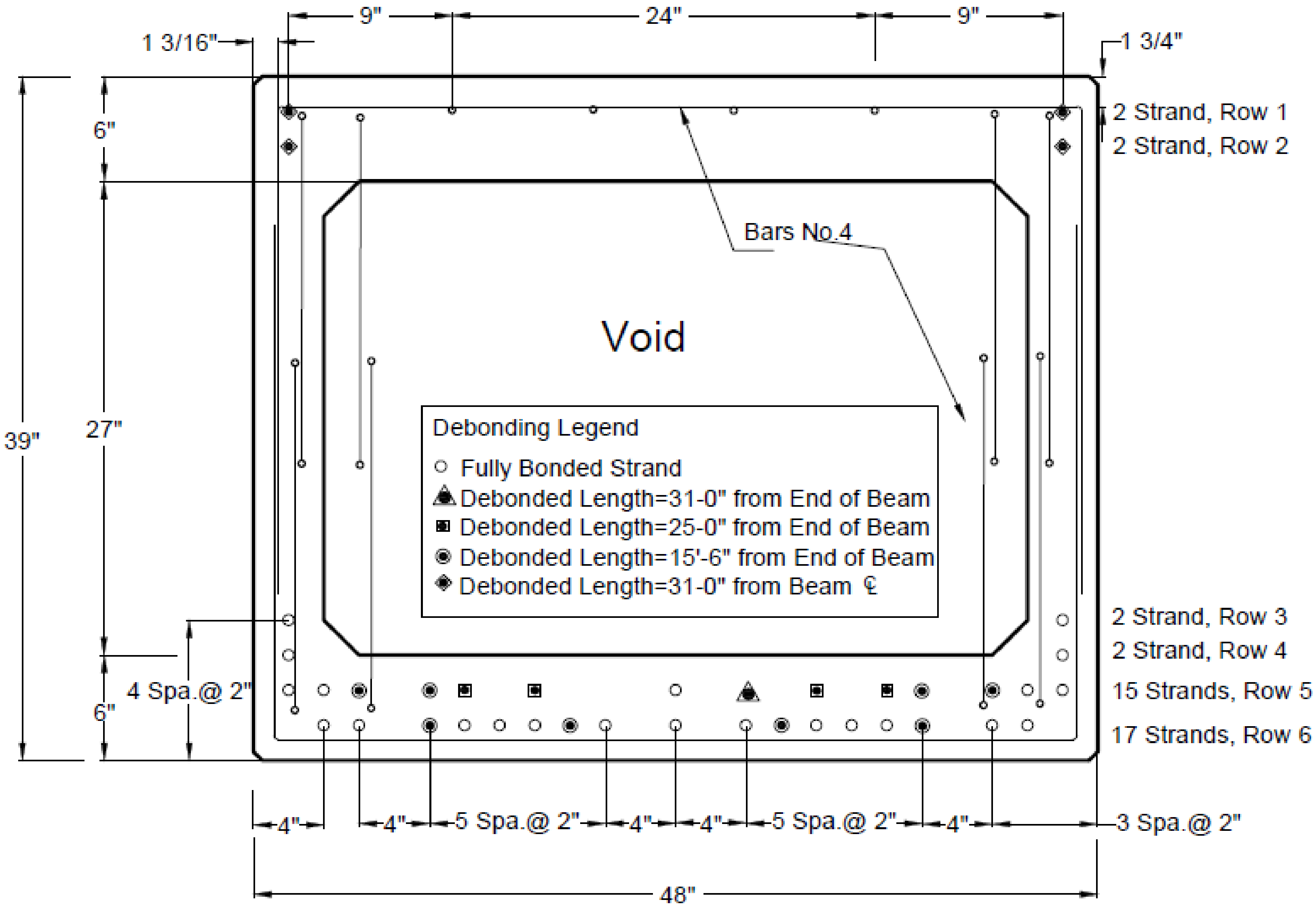

Figure 1-5 Box-girder - cross section details. Adapted from [31]

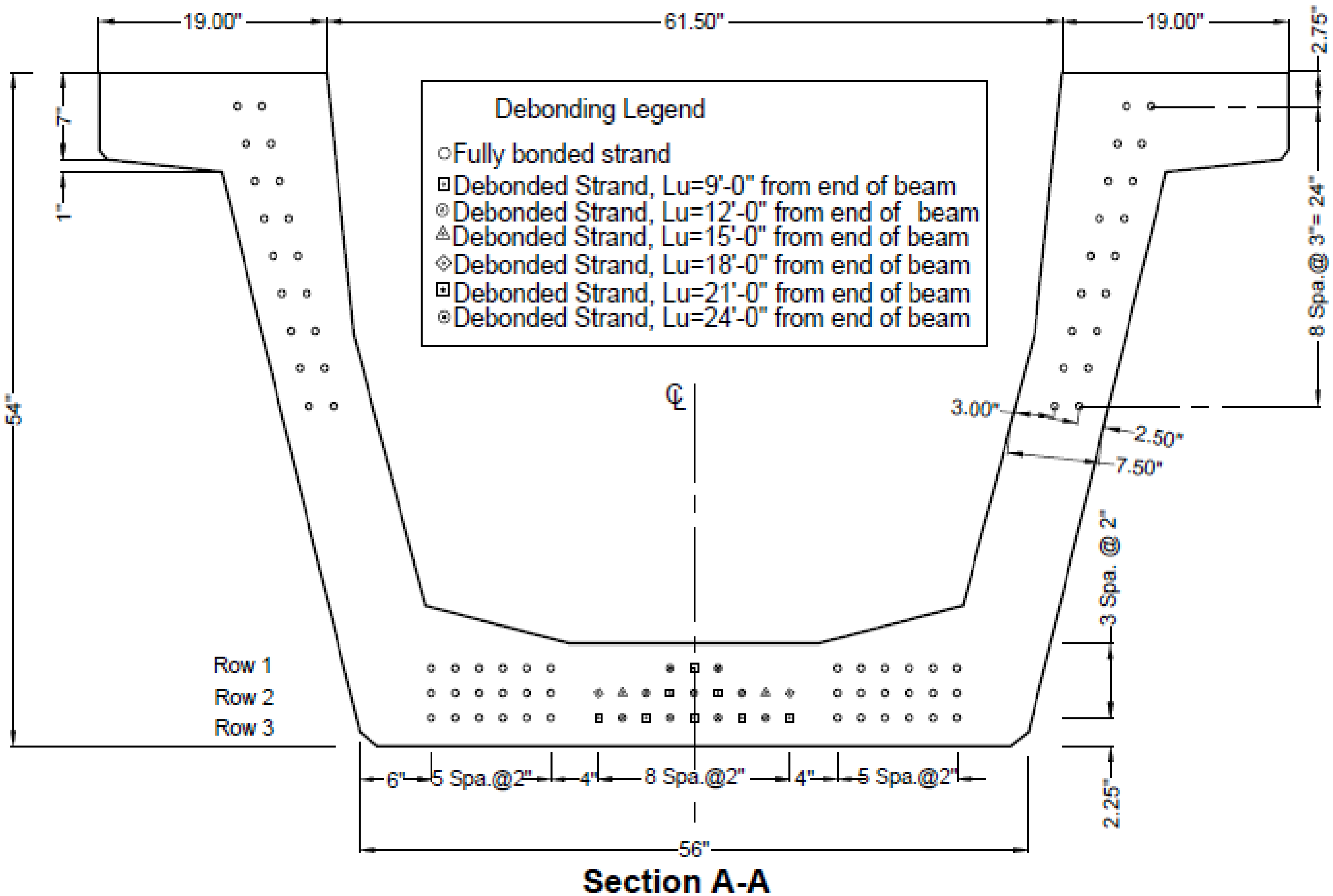

Figure 1-6 U-beam cross section details. Adapted from [8][23]

1.4 Hypotheses and Objective

Even though the use of debonded strands decreases the high tensile stresses in the end-region of prestressed concrete members, cracking in this zone has been observed during production. The research hypotheses behind this damage are:

1) Beam-end cracking could occur because the debonding mechanism used does not effectively break the bond between the strand and the surrounding concrete, thus allowing some transfer of the prestressing force where it was not accounted for.
2) The radial stresses caused by the increased dilation of the partially debonded strands can be quite significant in the end region and the cause for cracking at the beam end.
3) The strand debonding pattern could lead to unbalanced forces resulting in high longitudinal shear stresses if all the blanketed strands are grouped together, which can induce shear cracking at the beam end or a high-stress region in the anchorage zone that can compromise the shear strength.

The research objective of this study was to obtain a better understanding on the bond behavior of partially debonded strands and its effect on beam-end cracking upon release of the prestressing force into the concrete member. Moreover, it was of importance to investigate the influence of concrete, concrete fluidity and confinement reinforcement. Thus, the specific research aims were:

- To characterize the basic bond behavior of bonded and debonded 0.6-in.-diameter (15.2 mm) Grade 270 (1860 MPa) low relaxation prestressing strand.
- To study the effect of concrete fluidity using normal consolidated concrete and self-consolidating concrete with bonded and debonded 0.6-in.-diameter (15.2 mm) strand.

- To study the effect of confinement from steel reinforcement on the bond behavior of bonded and debonded 0.6-in.-diameter (15.2 mm) strand.
- To develop high-fidelity finite element models that can emulate strand bond behavior to further investigate the mechanisms of bond stress transfer and potential sources of damage.
- To study the effects of strand debonding on beam end cracking in the anchorage zones of small and full size beams through numerical simulations.

The research hypotheses were evaluated after analyzing the experimental and numerical simulation results as presented in Chapters 3, 4, and 5. The objectives were achieved by separating the study into three tasks as presented next.

1.5 Project Research Tasks

The research project was subdivided into the following three tasks: (1) strand bond behavior assessment, (2) strand bond behavior simulation, and (3) simulation studies on anchorage zones.

Task 1 focused on determining the fundamental bond behavior of 0.6-in.-diameter (15.2 mm) Grade 270 (1860 MPa) low relaxation prestressing strand under fully bonded and partially unbonded conditions. The objective of this first task was to generate data to calibrate three-dimensional finite element models for strand bond behavior simulation in Task 2. The parameters considered for the experimental phase (Task 1) were: (1) concrete hydraulic head, (2) concrete fluidity (SCC), (3) confining reinforcement, and (4) single vs. double layered slit sheathing for debonding of the strand. Basic bond behavior was assessed through pull-out tests on 6” (150 mm) diameter, 24” (610 mm) long cylinders with concentric 0.6-in.-diameter (15.2

mm) strand. The effects of concrete fluidity were studied conducting pull-out tests on wall-type blocks containing 0.6-in.-diameter (15.2 mm) unstressed strand and built with normally consolidated (NCC) and self-consolidating concrete (SCC) Finally, the stress transfer behavior of fully bonded and debonded 0.6-in.-diameter (15.2 mm) strand was evaluated through laboratory-scale pre-tensioned concrete beams.

In Task 2, 3-D nonlinear FE beam models were developed for the laboratory-scale beams of Task 1 using the commercial finite element program ABAQUS [1] and calibrated with experimental data. The models used a concentric fully bonded or partially debonded strand with tight fit. The strand was simulated as a cylindrical rod and bond was simulated by the definition of normal and tangential surface interaction properties between the steel and concrete parts of the model. The coefficient of friction used in the tangential surface contact interaction definitions was calibrated with experimental data. The calibrated models were used to study the effect of confining reinforcement along the transfer zone and debonded length.

Task 3 focused on the stress analysis of the anchorage region of a large-scale beam models. A U-type cross section beam (seen Figure 1-6) was selected as case study based on evidence of damage during production (Figure 1-4). Three-dimensional nonlinear numerical models were developed using ABAQUS [1]. Four U-beam FE models were created and analyzed to study the effect of sheathing material and the arrangement of debonded strands.

1.6 Scope

The effectiveness of debonding using a single layer or double layer of flexible-slit sheathing was evaluated by conducting experimental studies on unstressed 0.6-in. (15.2 mm) diameter fully bonded and debonded strand. Pull-out tests on unstressed strands were conducted to evaluate basic bond behavior associated with chemical adhesion and mechanical interlock. The effects of concrete fluidity and hydraulic head on the possible paste infiltration of slit sheathed strand were evaluated through pull-out tests on wall-like blocks. Finally, stress-transfer behavior of fully-bonded and debonded strands was studied with laboratory-scale pretensioned concrete beams.

Additional investigations were carried out through high-fidelity numerical simulations. Models of the laboratory-scale beam units were established and calibrated with the experimental data to determine effective parameters for the simulation of bond-slip response between strand and concrete. Stress analyses on the anchorage zone of U-beam were then used to evaluate the effect of flexible tight fitting debonding vs. rigid debonding material as well as the influence of strand debonding pattern on beam-end damage.

It was the goal of this study to provide recommendations to the precast/prestressed industry on the effects of the type of sheathing material, slit-flexible or rigid (oversized), arrangement of strand debonding distribution, and reinforcing confinement in the end zone of pre-tensioned concrete members during production.

1.7 Organization of the Report

The present report has been organized into six chapters. Chapter 2 provides a literature review on the fundamental concepts of bond phenomena, end-cracking on prestressed concrete beams, top-strand effect, bond behavior on units cast with self-consolidating concrete, and a summary of the most relevant studies related to the above mentioned topics. Chapter 3 reports on the experimental program: tests units details, procedures, results, findings, and discussion of the results. Chapter 4 presents the numerical simulation of strand bond behavior on small-scale beam models calibrated using experimental data. Results from the finite element models, relevant findings, and a discussion of the results are provided. This chapter also presents theoretical concepts behind the numerical models, such as the modeling of inelastic concrete behavior and the modeling of friction contact interaction to simulate bond. Chapter 5 provides numerical studies on anchorage zones of skew U-girders, including the evaluation of “the as-built” condition, parametric studies, and discussion of relevant findings. The conclusions and recommendations of this study are presented in Chapter 6. The Appendix section provides supplementary documentation of the results obtained in the experimental and numerical tasks.

CHAPTER 2 BACKGROUND

2.1 Introduction

One of the goal of this investigation was to study the bond behavior of "unbonded" strands since it may be possible that the use of flexible tight fitting sheathing could lead to high radial stresses in the anchorage region can cause end-cracking. First, it is needed to study bond behavior in fully bonded strand to assess the different bond mechanisms. Thus, a literature review on this topic and how this has been studied in the past is presented in this chapter. In addition, a literature review on beam-end cracking in prestressed concrete beams upon release with and without debonded strands is also presented here. Moreover, code recommendations on the use of unbonded strands in pretensioned concrete members are also summarized. Finally, an overview of some of the possible causes behind the end-cracking in beams with debonded strands is presented. The chapter is organized as follows:

- Bond behavior in pretensioned concrete member including bond mechanisms,
- Transmission of prestresing force,
- End-cracking in pretensioned concrete beams, and
- Use of shielded strands in prestressed concrete girders.

2.2 Bond Phenomena in Pretensioned Concrete Members

When the steel is prestressed, bond is needed to hold the steel under tension and consequently precompress the concrete [27]. In prestressed concrete applications, the tensile stresses of the pretensioned strand are fully transmitted into the concrete member by bond. The bond transfer varies from zero at the beam end and increases until the tensile force in the strand is constant, reaching the effective prestressing force f_{se}. The region along which the prestressing force is transferred to the concrete is often called the transmission or transfer zone. If cracking takes place in the concrete member, the bond between the strand and the surrounding concrete plays a significant role in governing flexural response and shear [12]. Thus, it is important to ensure a satisfactory bond quality to prevent bond-slip and thus undesired failure mode in a member. The bond mechanisms in pretensioned concrete members are presented in the following to better understand the components of bond between strand and the surrounding concrete.

2.2.1 Bond Mechanisms

The main factors that contribute to the bond between strand and the surrounding concrete are [12] adhesion, friction, and mechanical interlock. The bond between strand and concrete is created by the chemical adhesion of the cement paste to the strand. Mechanical interlock resistance follows from the geometry of the helical strand, which provides shear resistance against the surrounding concrete. When the steel is prestressed, the diameter is reduced, and as the prestressing force is released into the concrete member the strand expands due to its Poisson's ratio and creates a wedging effect in the anchorage region [12]. In addition, the increase in the strand diameter causes a radial pressure at the interface with the surrounding concrete. As result, the longitudinal frictional forces preventing strand slip are increased. The frictional forces depend on the radial pressure exerted on the surrounding concrete due to the dilation of the strand and on the coefficient of friction between the two surfaces in contact. The value of the coefficient of friction depends on the surface conditions of the strand and it also depends on the character of the cement paste [12].

However, adhesion plays a minimal role because once there is some relative slip of the strand the chemical adhesion mechanism is broken. On the other hand, friction has a significant contribution in the development of transmission of shear or bond stresses because it prevents strand-slip along the transfer zone. The strand upon release from its pretensioned state at the abutments locally recovers its original diameter causing a wedging effect in the end-region (see Figure 2-1) known as Hoyer’s effect. To develop frictional bond stresses, radial compressive stresses are needed. These radial compressive stresses have been attributed to the Hoyer effect because the reduced diameter of the steel causes radial stresses as the strand tries to recover its original diameter upon release. The Poisson’s expansion causes compression perpendicular to the steel-concrete interface as shown in Figure 2-1. As a result, the concrete is precompressed. Moreover, shrinkage of the concrete can also contribute to the radial compressive stresses that cause frictional resistance [4]. Figure 2-1 shows an schematic of the Hoyer effect upon detensioning and the radial stresses at the interface of the strand and the surrounding concrete. Figure 2-2 shows a schematic of the transverse tension from the pretensioned strand to the wire and transverse compression toward the strand. High bond stresses thus develop in the zone of the radial compressive forces due to the Hoyer effect, which is the main contributor to bond between the strand and the surrounding concrete.

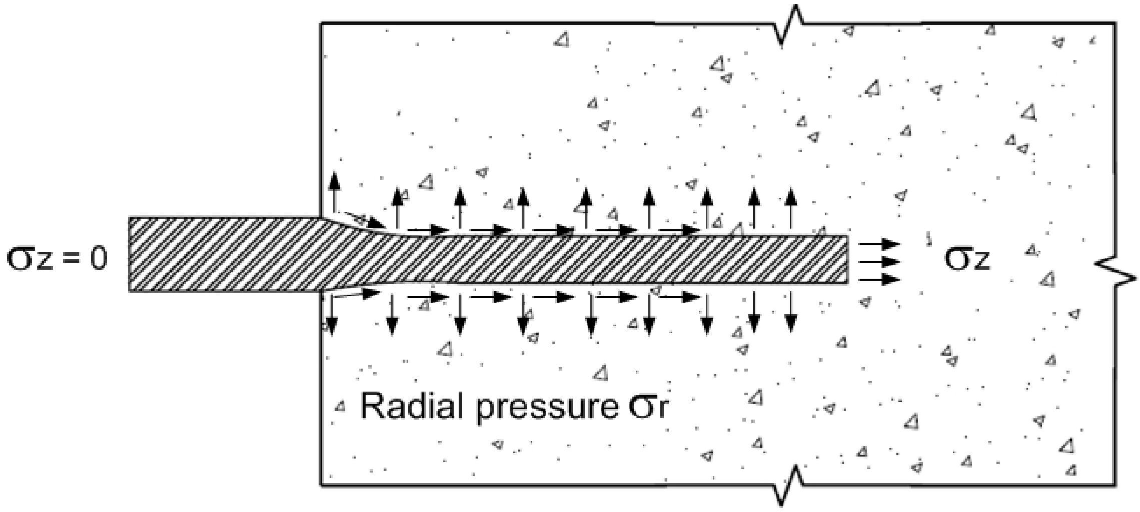

Figure 2-1 Schematic of bond stresses and wedging effect. Adapted from [16]

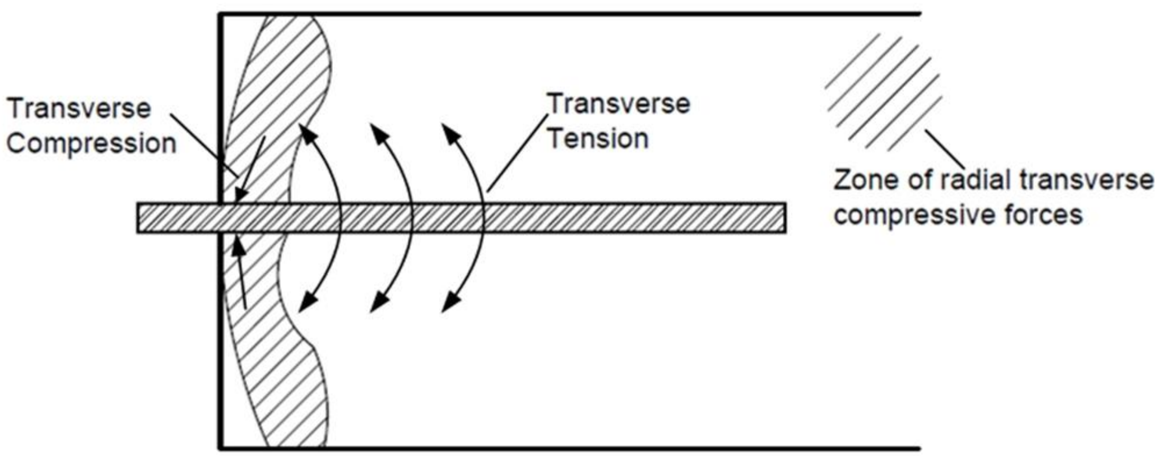

Figure 2-2 Bond stresses distribution at the anchorage-zone. Adapted from [16]

2.2.3 Bond Strength Determination

The bond between steel and the surrounding concrete can be determined by means of analytical, experimental or numerical approaches. A summary of some of the most relevant studies on bond strength determination are presented next.

Several researchers have developed expressions to estimate bond stresses. The equations have been based on different assumptions according the type of units built and tested for the purpose of determination of bond. In this section, some of the theoretical expressions most commonly cited in the literature are presented.

Janney, 1954

Janney [12] conducted one of the earliest studies on bond behavior. In addition to conducting experimental tests on bond transfer and flexural bond, he also presented theoretical considerations to determine bond stresses. If the strand is free to expand, a decrease in the pretensioning force from its initial value will result in an increase of the strand diameter. If the concrete section is large compared to the radius of the prestressed steel the elastic theory of thick walled cylinders gives a relation to find the increment of the steel using Equation 2-1.

$$\Delta r = r\sigma_r \frac{1+\upsilon_c}{E_c} \qquad \textbf{Equation 2-1}$$

In Equation 2-1, σ_r is the radial stress in the steel (see Figure 2-3); υ_c is the Poisson's ratio of the concrete; E_c is the elastic modulus of the concrete; and, r represents the strand effective radius. The radial stress is equal to the contact pressure between the steel and the surrounding concrete. Figure 2-4 shows the change in diameter of the strand at each stage: unstressed, prestressed, and after detensioning. As the prestressing force is released, the strand expands creating radial pressure at the interface between the strand and concrete as shown in Figure 2-3.

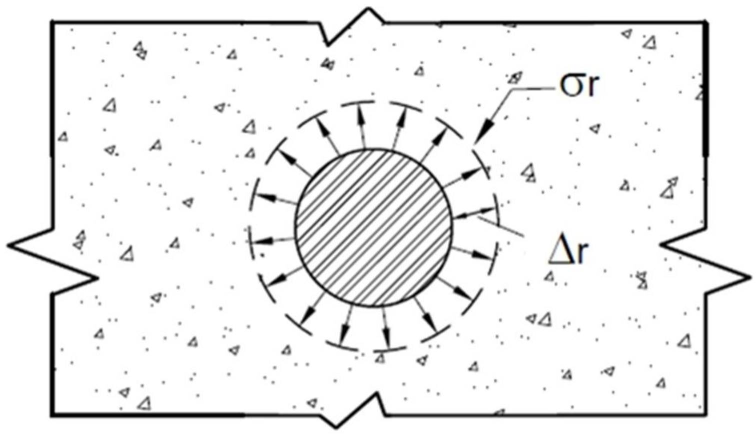

Figure 2-3 Radial Stresses at the interface of concrete and strand upon releasing the prestressing force

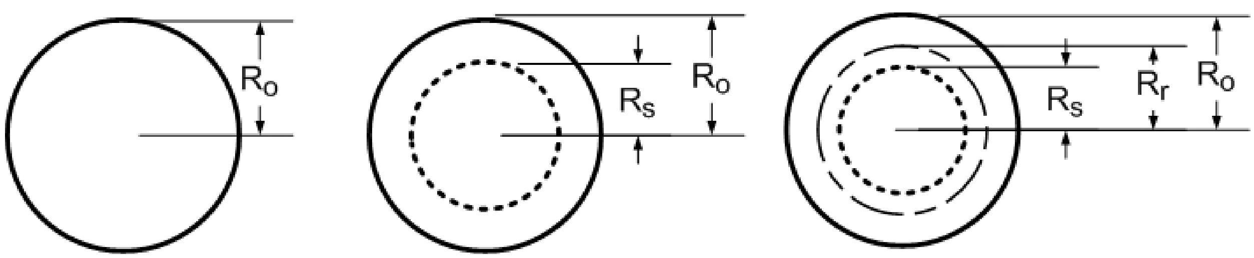

Figure 2-4 Dilation of the prestressing strand

$$\sigma_r = \frac{(f_{se} - f_s)\upsilon_s}{1 + (1 + \upsilon_c)\dfrac{E_s}{E_c}} \qquad \textbf{Equation 2-2}$$

Thus, the magnitude of the radial stress can be found using Equation 2-2, where 2-2, f_{se} represents the prestressing force in the steel; f_s is the tensile stress in the steel at any point; υ_s is the Poisson's ratio of the steel; and E_s is the Young's modulus of the steel. Prestress bond stresses at any location along the transmission zone are equal to the slope of the stress transfer curve multiplied by r/2 [12] as represented in Eq.2-3.

$$u = \frac{dfs}{dl}\frac{r}{2}$$ **Equation 2-3**

If the bond between strand and the surrounding concrete is entirely due to the friction (ϕ) between the strand and the surrounding concrete, bond stresses can be related to radial stresses (σ_r) using Equation 2-4 as proposed by Janney [12]. However, it is well known that while friction is one of the main bond mechanisms, there are other mechanisms involved in prestress bond transfer.

$$u = \phi\sigma_r$$ **Equation 2-4**

Bond can be experimentally measured by conducting different types of bond assessment. One of the simplest ways to measure bond strength is by conducting pull-out tests on unstressed strand. A schematic of a simple pull-out test is shown in Figure 2-5. Most pull-out tests are conducted on unstressed strands; thus, the bond contribution from Hoyer and Poisson's effects cannot be accounted for in this type of test. The bond strength by means of this test is determined using Equation 2-5. Where, F_{max} is the peak pull-out force (lbs. [N]), d_b is the nominal diameter of the strand (in. [mm]), and L_e is the embedment length (in. [mm]).

$$u = \frac{\mathrm{F_{max}}}{(4/3)\pi \mathrm{d_b L_e}}$$ **Equation 2-5**

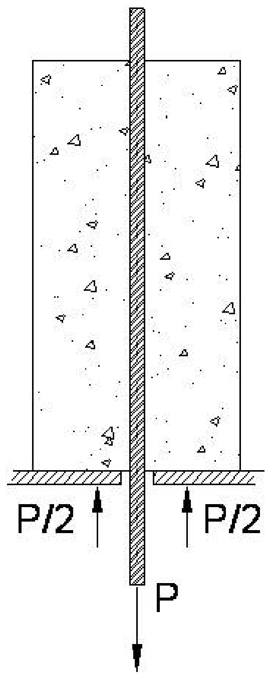

Figure 2-5 Schematic of Simple Pull-out Test. Adapted from [16]

2.3 Transmission of Prestresing Force

The pre-tension force in the stressed strand is released when the concrete has attained enough compressive strength. Once the strand is released, it tends to shorten and it dilates. The pretensioning force in the strands is purely transmitted into the concrete member by bond, and as a result the concrete is precompressed. According to Moon et al. [20], both sudden (flame-cuting) and gradual (hydraulic jacking) cause a very rapid strain change of the stress state at the end of the concrete beam. Some of the primary factors affecting the structural integrity of a prestressed concrete member are the prestress release method and the bond integrity between the strand and concrete. Cracks may thus develop in the end zone of a pretensioned concrete member due to an undesirable tensile strain change during the detensioning procedure [20].

Prestress bond transfer takes place from the end of the concrete member, release end, to a point in which the stress in the strand remains constant. This constant level of stresses in the strand is termed the effective prestress, f_{se}. The length over which the entire prestressing level is transmitted into the concrete members is known as transfer length. The transfer length mainly depends on the degree of prestressing force, surface condition of the prestressing strand, concrete compressive strength at release, release method [9], quality of the bond, radial pressure, and transverse reinforcement [16]. Beyond the transfer length, the stress in the steel remains constant as shown in Figure 2-7. The determination of transfer lengths has been extensively studied since it is an important design parameter in pretensioned concrete structures [4][5][12][20][22][23][25][26][30]. Numerous experimental studies on the evaluation of transfer length have been conducted since this is a parameter that can be easily measured and used for calibration of numerical models (as was case of this investigation). Results have then been commonly used for the development of empirical expressions to determine transmission length. However, this is not the scope of this investigation.

If the transmission length is short, it may lead to high compressive stresses that can cause spalling or bursting cracks in the end region of the concrete member (see Figure 2-6). On the other hand, long transfer lengths could reduce the shear capacity of the beam and longer development lengths will be required, which may affect flexural behavior [5]. Previous studies [4][22][27][31] have shown that sudden release of the prestressing force results in larger transfer lengths. This phenomenon is mainly related to the dynamic effects associated with the transfer energy from the strand to the concrete member [4].

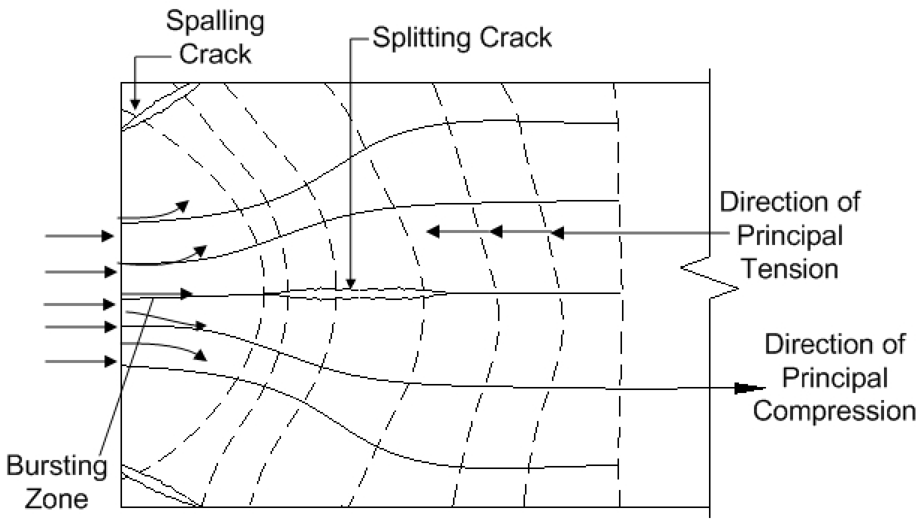

Figure 2-6 Bursting zone and appearance of spalling and splitting cracks upon detensioning. Adapted from [21]

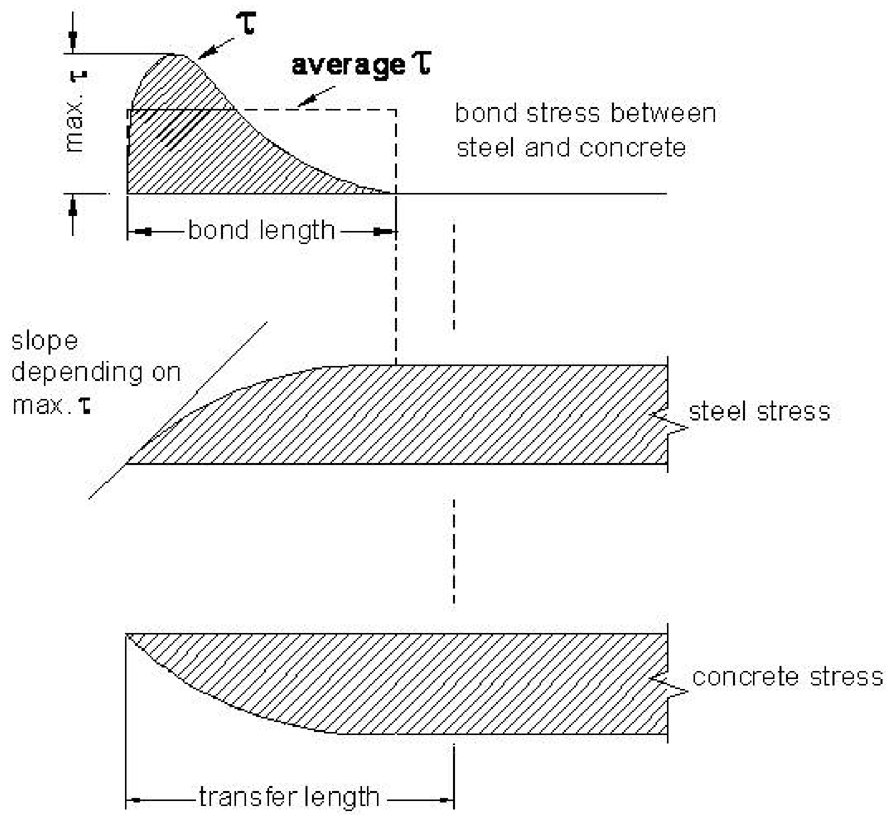

Figure 2-7 Bond stresses distribution in the end-region. Adapted from [16]

Transfer lengths can be experimentally measured using different approaches. The most common is to measure the development of compressive strains in the concrete along the transfer region. This can be done by taking measurements on the surface of the concrete element or by using strain gages on the prestressing strand or an instrumented rod embedded in the concrete. Other simple methods, such as the measurement of the strand end-slip, or "suck-in," into the beam have also been used. Only the first method, that of using surface strain measurements is reviewed here since it is the approach used in this study.

Concrete surface strains can be measured using mechanical gages metal disks that are installed along a surface path of interest. The distance between target points is measured before and after release of the pretensioning force. The difference between the final and initial reading upon the initial reading gives the strain over certain gage length. Strain values are plotted along the beam length in the form of a profile. A common method to obtain the transfer length from the compressive strain profile is the 95 percent average maximum strain (AMS) method [26]. The AMS is obtained from the strain values near the plateau of the trend once the prestressing force has become uniform. The 95% AMS value is plotted on the strain profile and the point at which the 95% AMS line intersects the curve defines the transfer length. The 95% AMS method was proposed by Russell et al. [26] and it has been well accepted by other researchers. This method was used for the experimental program of this investigation (see Section 3.6.1)

2.4 End Cracking in Pretensioned Concrete Members

Prestressed concrete I-girders often experience cracking at their ends upon strand detensioning. Such initial cracking accelerates the deterioration of the anchorage region of the girder with the presence of moisture principally by accelerating chloride ingres and corrosion initiation of shear reinforcement and prestressing steel [14]. The probability of end-cracking in a prestressed member upon release can increase when the free strand length is short since the restraining force increases [19]. Moreover, the restraint force will be larger when the strand is not simultaneously released at the two free ends [19].

The formation of cracks in the end-zone of prestensioned concrete girders is primarily caused by the high concentration of stresses in the end-zone upon release of the prestressing strands. In the case of Type-I girders, cracks are usually horizontal and take place near the joint of the bottom flange and the web [33] as shown in Figure 2-8. According to Tuan et al. [33] the distribution of high stresses in the anchorage zone of prestressed concrete members is dependent of the location of strands, the degree of the prestressing force in the strands, the amount of concrete surrounding the strands, the amount of draped strands in the beam-end zone, the geometry of the girder, and the concrete characteristics.

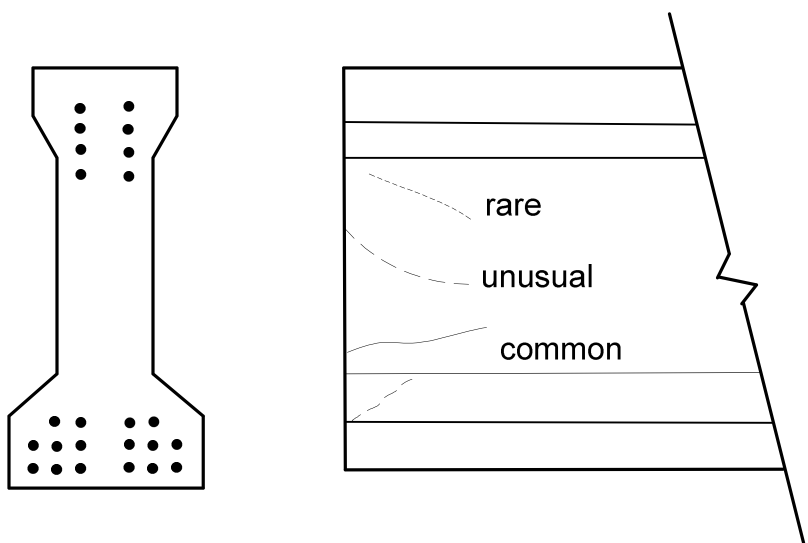

Figure 2-8 Cross section of a Type-I girder and typical cracks observed in the anchorage region. Adapted from [9].

In accordance with preliminary studies, Zia [19] concluded that one possible reason for the end-cracking problem was the restraining effect caused by unreleased strands. If the distance between abutments and casting bed is relatively small, this restraining effect can be significant. The debonding of strands increases the strand free length, which could reduce the high stresses induced in the concrete element due to the releasing of the prestressing force.

2.4.1 Studies on Beam-end Cracking upon Detensioning

The amount of studies conducted regarding beam-end cracking upon release is few. The most recognized studies in this topic are those by Mirza and Tawfik [19] and Kannel et al. [13]. A recent study by Sun [31] has also addressed the problem and it is a companion to this study. However, the research by Sun included the use of debonded strands and a summary of Sun's investigation and main findings are presented in Section 2.5.2 and Section 2.5.3. An overview of the first two works is presented next.

Mirza and Tawfik, 1978

Mirza and Tawfik [19] conducted a detailed investigation to understand the causes behind the appearance of vertical cracks at the ends of prestressed concrete beams. Their study included experimental and analytical components on the development of a model to estimate tensile stresses from the restraint effect from free strand lengths. The experimental phase of their research was conducted on Type- III AASHTO girders of approximately 73 ft. (22.3 m) in length to study beam-end cracking during production. The main goal of the experimental investigation was to study the restraining effect from the short length of unreleased strands in beam-end cracking upon strand detensioning. The experimental study was performed on small-scale beams with 3/8-in. (9.5 mm) diameter strands. The study's principal criterion was to cause enough cracking in the concrete due to the strand restraining effect. Prestressing force was transferred into the concrete by simultaneous release at the beam ends at three intermediate points (two beams in a line). Mirza and Tawfik found that the release restraint effect can be significant if the strand free length is short.

The analytical model resulting from this work was a one-dimensional representation of the casting bed, concrete beams and prestressing strands. Beam members and each length of free strand were represented using individual springs. The mathematical model was based on the following assumptions: a) the materials were modeled using linear-elastic properties, b) no friction was provided between beams and casting bed, c) dynamic effects were neglected, and d) the stress calculation was based on beam theory. The model provided useful information in respect to the effect of the free strand length in the casting bed and its distribution when casting multiple beams in a single line. The numerical model did not attempt to replicate the three-dimensional stress distribution in the end the regions of the prestressed concrete member, and thus the regions subjected to high stress were not identified and bond behavior was not replicated in the model. Satisfactory agreement between the model and the experimental results was observed after half of the strands were released. The effects of un-released strand and free strand length were successfully investigated with the model. Mirza and Tawfik recommended that the free strand length shall be equal or greater to 5% of the length of the casting bed.

Kannel, French, and Stolarski (1997)

Kannel, French, and Stolarski [13] studied the cracking at beam ends within the context of the sequence of strand release during detensioning, the debonding of strands to increase free length, and the pre-cutting of some strands. They conducted experimental and numerical studies and their approach was to utilize experimentally calibrated finite element models to account for the stress components that take place in the transfer of prestress forces into the concrete member. Their finite element model was developed using the program ABAQUS [1] and calibrated with experimental data. The strands were modeled using discrete truss elements, thus, the Poisson's and Hoyer effects due to the dilation of the strand upon detensioning was not replicated. The concrete was modeled using 3-D continuum elements (along the region of interest) and linear-elastic material properties. The experimental studies were conducted on 54 in. (1370 mm) deep prestressed concrete beams. The main objective was to study release patterns that could prevent cracking, thus the researchers did not consider important to model the inelastic behavior of the concrete and the model was considered to be truthful until the first crack developed. They observed that the faster the stress concentration at the base of the web increased in proportion to the rate upon which the compression is transmitted into the concrete member. Thus, they recommended combining pre-releasing of the strands with debonding of some strands to prevent shifting the vertical cracking further into the concrete member when using debonded strands. They also found that altering the release sequence and using debonded strands could help to reduce the negative restraint effect that can cause end cracking. The model was judged satisfactory, showing general trends, such as the ones related to altering the strand release order.

2.5 Use of Debonded/Shielded Strands in Prestressed Concrete Girders

Strand debonding consists in the elimination of the strand-concrete bond over a portion of the strand in a prestressed concrete element, and it is an option to regulate the high compressive and tensile stresses in the prestressed concrete members [27]. Debonding practice has been established based on constrained empirical data and engineering judgment. Strand debonding is an option to the more traditional method to reduce high stresses in the end zone of prestressed concrete members by draping the strands upward, which modifies the center of gravity of the strands and thus efficiently decreases concrete stresses in the anchorage region [27].

Strand debonding, or sheathing, is done by placing plastic tubing around the strand to separate it from the concrete and thus eliminate bond resistance. The sheathing material is of two general types: soft polyethylene slit tubing used in either a single or double layer with opposing locations for the slit opening (see Figure 1-1), or a more rigid oversized plastic tubing (see Figure 1-2). In this study, two types of debonding material were considered: soft (tight fitting) and rigid (loose fitting) as shown in Figure 1-1 and Figure 1-2, respectively. Soft slit sheathing fits closely to the strand and it is easily “squeezed” for a tight fit by the fresh concrete; thus creating geometric contact between the strand and the concrete, albeit separated by the polymer. By contrast, the oversized polymer tube is stiff enough that it does not collapse with the fresh concrete and thus leaves a gap between the strand and concrete.

The use of partially debonded strands reduces the axial tension because the effective free length of the strand is increased. This effect can be debated. Yet, with the use of debonded strands, the axial restraint effect decreases, shear stress distribution is improved, and the shear stresses are reduced. Moreover, the stress concentration at the base of the web, as in the case of girders, is also decreased after full release of the strands due to the decrease in compressive force transferred at the end of the concrete member [13]. Hence, the use of debonded strands has been beneficial in reducing the occurrence of cracking in the beam-end regions.

As introduced before, strand debonding has been generally successful in minimizing beam-end cracking. However, concerns have recently emerged on the effect that partially debonded strand may have on the damage in beam ends (see Figure 1-3 and Figure 1-4) [8][23][31]. Unfortunately, only limited research has been done to evaluate the unstressed and stressed response of shielded, or debonded, strands, and code guidelines do not address fundamental parameters of influence in beam-end cracking and they focus mainly on the possible reduced shear strength rather than on the potential damaging effects from production. The next sections provide an overview of current code provisions and research related to debonded strand in prestressed concrete.

2.5.1 Code Guidelines: Provisions and Limitations

The AASHTO LRFD Bridge Design Specifications [2] on the use of debonded are mainly based on concerns related to shear performance. ACI-318 [3] does not present any type of limitations or recommendations related to the use of debonded strands in pretensioned girders except for the expression to calculate development length. The recommendations provided in both codes are summarized next.

a) AASHTO LRFD Bridge Design Specifications 2010

The AASHTO LRFD Bridge Design Specifications [2] address debonded strands mainly by placing limits on the number of partially debonded strands that can be used, which shall not exceed 25% of the total number of strands. In addition, the number of unbonded strands in any horizontal row shall not exceed 40% of the number of strands in that row. Moreover, the debonded length of any strand shall satisfy all limit states considering the total development of the member's resistance at any section under consideration. In addition, unbonded strands shall be in a symmetrical pattern with respect to the beam-center line. The debonded length of strand pairs with respect to the center line shall be the same. Not more than four strands or 40 percent of the unbonded strands, whichever is greater, shall have the same unbonded length. The AASHTO Specifications also establish that were bonding does not extend to the end of the concrete member, the development length of partially debonded strands shall be twice the calculated one for fully bonded strands. Finally, debonding of strands is limited to interior strands.

According to Shahawy and Hassan [28] if debonded effects are not accounted for in the design of girders containing shielded strands, cracking in the member and bond failure could occur during the service life of the girder. This finding has been taken into account in the AASHTO Specifications [2] by limiting the number of debonded strands to 25% of the total number in a girder. Thus, the limitations on the percentage on the use of debonded strands in the AAHSTO Specifications are related to concerns regarding shear performance.

a) ACI-318

The ACI-318 2008 recommendations [3] note that the contribution of debonded strands to the overall behavior of the prestressed concrete member begins at the point where the fully effective stress starts, at the end of the transmission zone, and beyond that point. The development length of debonded strands is to be twice the calculated for fully bonded strands using Equation 2-6. However, the guidelines also states that at sections where the pretensioned strands are not fully developed, it is common to assume that both transmission and development lengths are doubled.

$$Ld \geq \left(\frac{fse}{3}\right)db + \left(fps - fpe\right)db \text{ [ksi, in.]} \quad \textbf{Equation 2-6}$$

c) Florida DOT Structures Guidelines

The Florida Department of Transportation Structures Guidelines [7] establishes that for the design of prestressed concrete girders containing debonded strands, the distribution of the shielded strands needs to be even throughout the strand pattern. Whenever possible, debonded strands should be separated in all directions by at least one fully bonded strand. This recommendation on the use of staggered debonding pattern has not been adopted by the AASHTO Bridge Design Specifications or the ACI-318 Recommendations.

2.5.2 Literature Review on Experimental and Numerical Studies on the use of Shielded Strands in Pretensioned Concrete Beams

Experimental studies on debonded strand behavior and its effect on prestressed concrete beams are limited. This may follow from the fact that the strand is assumed to be perfectly debonded from the concrete. Mirza and Tawfik [19] (see Section 2.4.1) included the use of debonded strands in their experimental studies after end-cracking was experimentally observed. The use of shielded strand seemed to be beneficial in reducing the restraint effect since the strand free length increases with the use of unbonded strands. Kannel et al. [13] (see Section 2.4.1) conducted experimental and numerical studies that included the use of debonded strands. They found that the greatest benefit of using debonded strands is when the shielded stands are cut last and some of the fully bonded strands are pre-cut first, such that the high tensile stresses are not simply shifted to the onset of the fully bonded zone of the blanketed strands. While the studies of Mirza and Tawfik and Kannel et al. addressed debonded strands, this was not a main objective in their study. The following summarizes the research studies known to have specifically focused on issues related to debonded strand.

a) Experimental studies

Russell, Burns, and ZumBrunnen, 1994

Russell et al. [27] conducted experiments on AASHTO Type-I beams to evaluate their flexural resistance. Each beam contained eight 0.5-in. (12.7 mm) diameter strands and four of those strands were either concurrently debonded or staggered debonded. Concurrent debonded strands were shielded strands having the same debonded lengths and staggered debonded strands had different debonding lengths. The variables in the study were embedment length and the debonded strand lengths, either staggered or concurrent. Debonding was achieved using plastic tubing made from a semi-rigid plastic with a satisfactory tight fit.

Based on their experimental work, Russell et al. recommended the use of staggered debonded strands as they found that the use of staggered shielded strands is likely to increase the resistance of the prestressed concrete member to cracking and that staggered debonding pattern required shorter embedment length than concurrent debonding pattern. They also concluded that the appearance of flexural cracking along the transmission region of partially debonded strands causes the strand to slip, affecting strand anchorage and leading to bond failure. Moreover, they recommended that for simply supported beams the debonded strand length shall not be greater than 15 percent of the total span length measured from the ends.

Moon, Kim, Lee, and Kim, 2010

Moon et al. [20] studied the effects of the use of confinement reinforcing, debonded of some strands using PVC, and detensioning method in the strain history change in the end region by conducting experimental studies on small-scale pretensioned concrete beams. The units had a cross section of 6 in. x 6 in. (150 mm x 150 mm) and 13 ft. (4 m) long. Two of the beams had a concentric 0.5-in. (12.7-mm) diameter strand and the rest contained a concentric 0.6-in. (15.2 mm) diameter strand. One of the beams was partially debonded, and the others were fully bonded. The debonded length was 8 in. (200 mm) from each end, and the confinement was placed after the debonded region. The detensioning process was flame-cutting and gradual release with a hydraulic jack. Moon et al. found that the use of debonded strand efficiently diminished harmful effects at the cut-end from the flame-cutting procedure. When the strand was gradually released, the effect on the debonded region was negligible.

Pavelchak, 2009

Pavelchak [23] studied the effectiveness of different debonding materials such as flexible-slit (tight fit) sheathing, un-slit (rigid [oversized]) debonding, and PVC tubing. The flexible sheathing material was obtained from three different manufacturers. The study was conducted after damaged was observed on the U-beam girder shown in Figure 1-4 upon strand detensioning. To assess the efficacy of several debonding materials, small-scale prismatic prestressed concrete beams were built using different sheathing products to study the effectiveness of debonded strands. The specimens had a cross section of 4”x4” (100 mm x 100 mm). The length of the beams was 10 ft. (3050 m) and 14 ft. (4270 m). Five of the 10 ft-long (3050 m) beams contained a concentric partially debonded strand and the blanketed length was 2 ft (600 mm) from each end. The debonded length for the concentric partially debonded strands in the 14 ft (4270 mm) long beams was 4 ft (1220 mm) from each end and six beams were built with these characteristics. The strand was 0.5- in. (12.7 mm) diameter and the initial prestressing force was 0.75 f_{pu}. The test consisted on the gradual release of the prestressing force.

Pavelchak noted that the 2-ft (610 mm) debonded length was not sufficient to develop adequate friction to transfer the prestressing force. He also noted that as the debonded length was increased, the effectiveness of the debonding appears to decrease. Pavelchak concluded that un-split (rigid) sheathing shall be used when the efficacy of the debonding is essential since this type of debonding provides excellent blanketing performance.

Yi Sun, 2010

Sun [31] evaluated basic bond behavior on small-scale beams containing fully bonded and partially debonded strands. The strand release rate, type of sheathing material (flexible or rigid), strand debonded length, and strand adjacent effects were the variables incorporated for the experimental phase of the study. The goal of the study was to understand how these parameters affect the bond behavior along the unbonded zone and to produce data to calibrate finite element. In the experimental program four different cross sections with three different strand configurations were considered: monostrand, twin-strand, and four strand. The strand used for the experimental phase was 0.6 in. (15.2 mm) diameter and prestressed to 0.75 fpu. The test consisted of the sudden or gradual release of the prestressing force into the concrete members. Concrete surface strain profiles were obtained along the neutral axis of the beam units and internal measurements were taken using an embedded instrument (strain gages) rod at the centroid of the beams.

Sun observed different strain values between the readings taken from the surface of the beam and from internal measurements. The reason was determined to be creep and shrinkage effects, which has also been observed by other researchers [22]; and which was also seen in the results obtained in the experimental program of this study (see Section 3.6.2). Sun found that sudden release led to longer transfer lengths, ~ 58% compared to values obtained from a gradual release process. Strand debonding with rigid material exhibited larger transfer lengths compared to beams with fully bonded strands and about 49% larger than values obtained from beam units with debonded strand using flexible sheathing. Thus, Sun found that when flexible sheathing is used the transfer length is not only affected by stored energy along the unbonded zone, but also by the residual bond stresses along the debonded zone.

b) Numerical Studies

Sun, 2010

Sun [31] developed numerical models based on the laboratory-scale beam models built and tested for the experimental program (see Section 2.5.2-a) to evaluate basic bond behavior. The numerical models were developed using the finite element program ABAQUS [1]. The aim of the simulation of the small-scale beam models was to assess basic bond behavior to investigate the causes of end cracking in pre-tensioned concrete beams. Flexible sheathing was simulated providing a tight fit around the strand along the unbonded zone, which continued throughout the fully bonded zone, and rigid sheathing was simulated by providing oversize hole around the strand along the blanketed length. Surface contact interaction models (see Section 4.3) were used to simulate strand-concrete bond behavior. The calibrated parameter was the coefficient of friction and the values were obtained by matching the experimental concrete internal strain profile with the numerical results. The coefficient of friction along the unbonded zone was zero for the debonded strands with tight-fitting sheathing and no interaction was defined for the debonded strands using rigid (oversized) debonding. Results from the study showed that the tight-fitting debonding caused high stresses along the unbonded zone and that the high stresses extended further into the fully bonded zone. The high stresses along unbonded zone when using flexible (tight fit) sheathing were attributed to Poisson's and Hoyer effects because the strand upon detensioning tries to dilate and the debonding mechanism does not provide the strand with space to expand.

2.5.3 Literature Review on Numerical Models on Beam-end Cracking on Full-size Beams with Shielded Strands

Simulations on end cracking in full-size pre-tensioned girders containing shielded strands are not many. Kannel et al. (see Section 2.4.1) [13] incorporated the use of debonded strands in their numerical models to study their effect in the stress state in the anchorage region. The model was validated with experimental data. However, Kannel et al. simulated the strand using truss elements and along the unbonded zone truss elements were not provided in order to emulate the debonding mechanism. With this modeling approach, the effect of the use of debonded strands on release sequence can be accounted for, yet the dilation of the unbonded strand upon release using a tight fit (flexible sheathing) along the debonded length cannot be taken into account. Kannel et al. found that the use of debonded strands is beneficial as this increase the strand free length and reduces the probability of end cracking.

Sun, 2010

Sun [31] investigated beam-end cracking in a skew box-girder containing unbonded strands for which evidence of damage existed (see Figure 1-3). The box-type cross section beam is shown in Figure 1-5. Sun created and analyzed large-scale beam models using the finite element program (ABAQUS) [1] to study the stress state in the anchorage region upon release.

The variables considered for the study were: (a) type of debonding material, flexible (tight fit) and rigid (oversized) sheathing; and, (b) the skew angle of the beam since the beam had a skew angle of 40°. Linear-elastic material properties were used for the entire model and cracking damaged was assessed by using an elastic limit of $7.5\sqrt{f'_{ci}}$ (psi).

Sun found good agreement between the damage predicted in the simulation and the actual damage observed during production. However, he observed that a tight fit (flexible sheathing) seems to significantly contribute to beam-end cracking since the stresses observed from the model with oversized hole (rigid sheathing) around the strands were lower than those observed from the model with a tight fit (flexible sheathing). In addition, it seems that the large skew angle of 40° had a strong influence in the resulting beam-end cracking. Nonetheless, the type of debonding material was noted to have the greatest effect on end cracking upon strand detensioning.

CHAPTER 3 EXPERIMENTAL ASSESSMENT ON BOND BEHAVIOR OF BONDED AND SHIELDED STRAND

3.1 Introduction

This chapter presents the experimental assessment of bond behavior of bonded and shielded 0.6-in.-diameter (15.2 mm) prestressing strand. The unbonded strands were blanketed using single and double layers of slit-flexible sheathing. Bond behavior was evaluated for the stressed and unstressed conditions for normal consolidated concrete (NCC) and self-consolidating concrete (SCC). Bond strength on unstressed strands was evaluated through pull-out tests on simple cylinders and wall-like blocks using fully bonded and debonded strands. Pull-out tests on cylinders evaluated simple bond strength while the pull-out tests on wall blocks were used to study the effects of concrete hydraulic head and concrete fluidity. Bond stress transfer behavior of stressed strands was studied on laboratory-scale prestressed concrete beams containing a concentric 0.6-in.-diameter (15.2 mm) strand for fully bonded and debonded (shielded) strand. Results and main findings of the experimental program are presented in this chapter.

3.2 Description of the Experimental Program

In order to evaluate basic bond behavior, two types of pull-out tests were carried out containing unstressed 0.6-in.-diameter (15.2 mm-diameter) Grade 270 (1860 MPa) low relaxation fully bonded and shielded strands. Sixteen 6”x24” (150 mm x 610 mm) cylinders containing concentric debonded strands were built for conducting simple pull-out tests on the unstressed strands. In addition, two 72” (1830 mm) high wall like blocks with 24”x24” (610 mm x 610 mm) in cross section were also built for conducting pull-out tests on 18 strands located at different heights in the block. To assess the transfer of prestressing forces into the concrete members, twelve 20 ft-long (6.1 m) beams with a 6”x6” (150 mm x 150 mm) cross section were built and tested by gradually releasing the prestressed strands. The parameters taken into account for the experimental phase were:

1) bonded and debonded (shielded) strand condition,

2) single vs. double layered slit sheathing for debonding of the strands,

3) concrete fluidity,

4) reinforcing confinement, and

5) hydraulic head effect (top-strand effect).

3.3 Assessment of Strand Quality

The bond quality of the 0.6 in.-diameter (15.2 mm-diameter) strand was verified by conducting a large block pull-out test (LBPT). The LBPT proposed by Logan [17] containing six 0.5-in.-diameter (12.7 mm-diameter) Grade 270 (1860 MPa) strands, with an embedment length of 18” (455 mm), was slightly modified for the 0.6-in. (15.2 mm) diameter strand. The difference was the strand embedment (bonded) length, which was changed from 18” (455 mm) to 20” (510 mm). The mix design was kept similar to the one recommended by Logan. The mix design used for the LBPT in this study is given in Appendix A.

According to Logan, the LBPT first slip force benchmark for 0.5-in.-diameter (12.7 mm-diameter) strands is 16 kip (71.2 kN). Logan also recommended the benchmark for the average peak load to be 36 kip (160.1 kN). The bond stress values for the recommended average first slip force and peak were calculated to obtain the benchmark values for 0.6-in.-diameter (15.2 mm-diameter) strand and an embedment length of 20” (510 mm). The corresponding average first slip force and the average maximum pull-out force benchmark values were thus found to be 21 kip (93.4 kN) and 48 kip (213.5 kN), respectively. The geometry and reinforcement details for the 24”x24” (610 mm x 610 mm) large block pull-out are shown in Figure 3-2 and Figure 3-2. Specifications for the strand are provided in Appendix A.

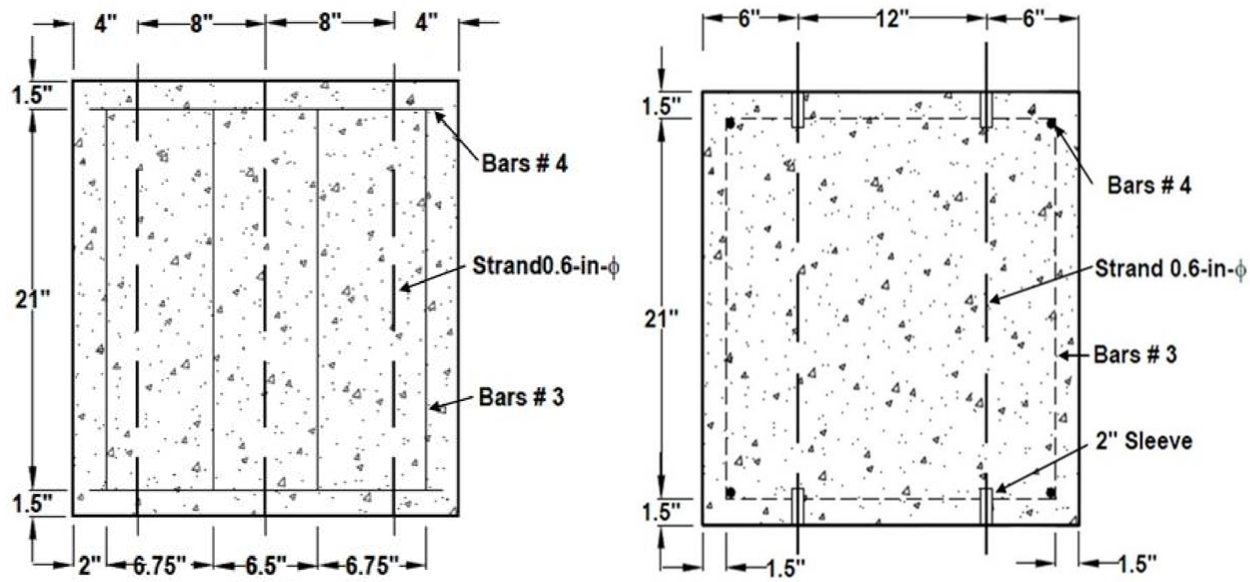

a) Front Elevation **b) Side Elevation**

1 inch = 25.4 mm

Figure 3-1 Reinforcing details of large block: Front and side elevation

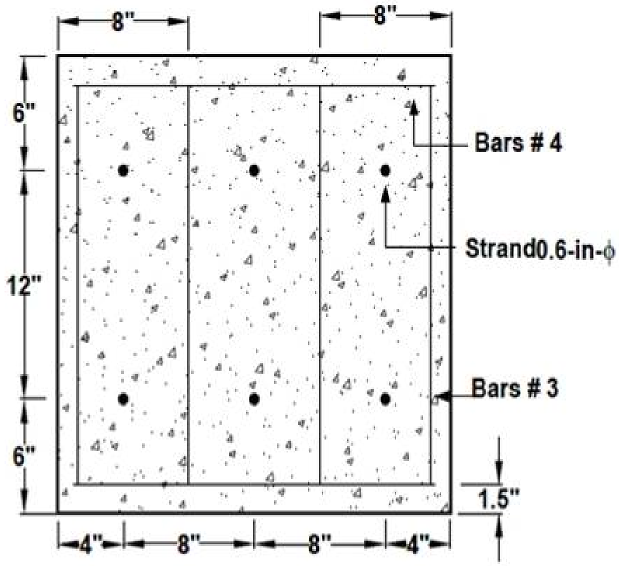

a) Top Elevation **b) Photograph of the Top View**

Figure 3-2 Reinforcing details of the pull-out block

The block was cast with the strands in the vertical position as shown in Figure 3-2-b. The average compressive strength obtained for the block at day of the test (~2 days after casting) was 6,400 psi (44.1 MPa). The pull-out test was done with a hollow hydraulic jack (6" [150 mm] stroke and 200 kip [890 kN] capacity). Load was measured with a 100 kip (445 kN) load cell and strand movement was measured on the loading (live) and back (dead) ends of the strand with displacement potentiometers. A schematic and a picture of the test setup are shown in Figure 3-3 and Figure 3-4, respectively.

To conduct the test, the block was rotated to lay on its side so that the strands were in the horizontal position (Figure 3-4). The loading rate recommended by Logan was about 20 kip/minute (89 kN/minute). However, the loading rate in this case varied between 9 kip (40 kN) and 13 kip (57.8 kN) per minute. The test was stopped when the maximum pull-out force dropped significantly or the strand was pulled out about 6 in. (150 mm), whichever occurred first. In average, this procedure took about 5 to 6 minutes per strand.

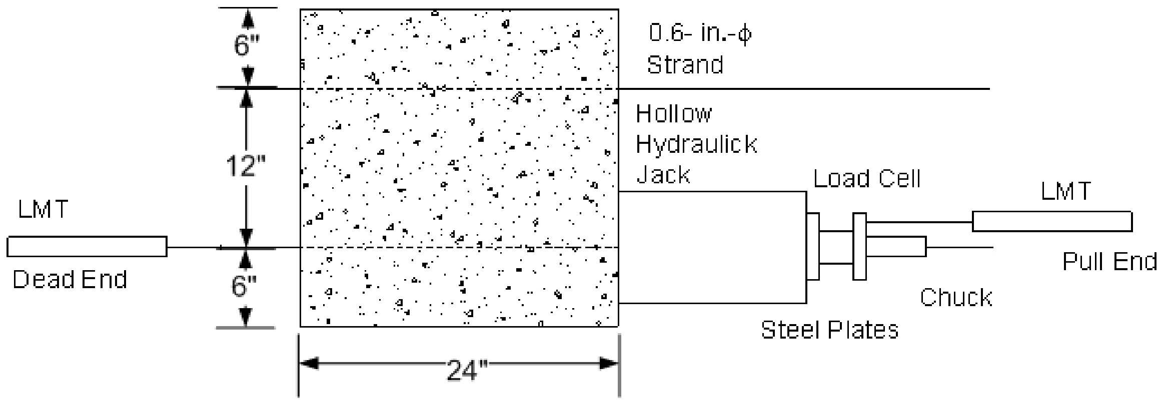

Figure 3-3 Large-block pull-out test set up

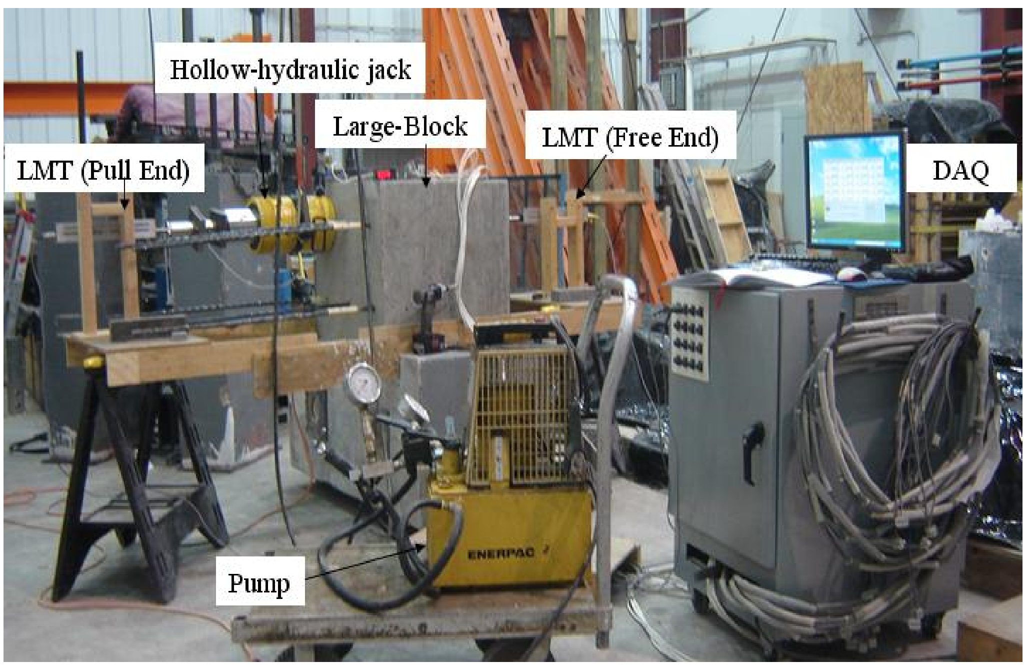

Figure 3-4 Overview of the large block pull-out test set up

Results from the large-block pullout test are shown in Figure 3-5. The average maximum pull-out force was 55 kip (244.6 kN) and the average first slip pull-out force was 35 kip (155.7 kN). Recalling, the compressive strength at the day of the test was 6,400 psi (44.1 MPa). It shall be noted that one of the strands performed poorly based on the found benchmark values.

Therefore, one of the six values was discarded and the noted average results were obtained from five (5) strands. The results thus met the pre-qualification benchmark.

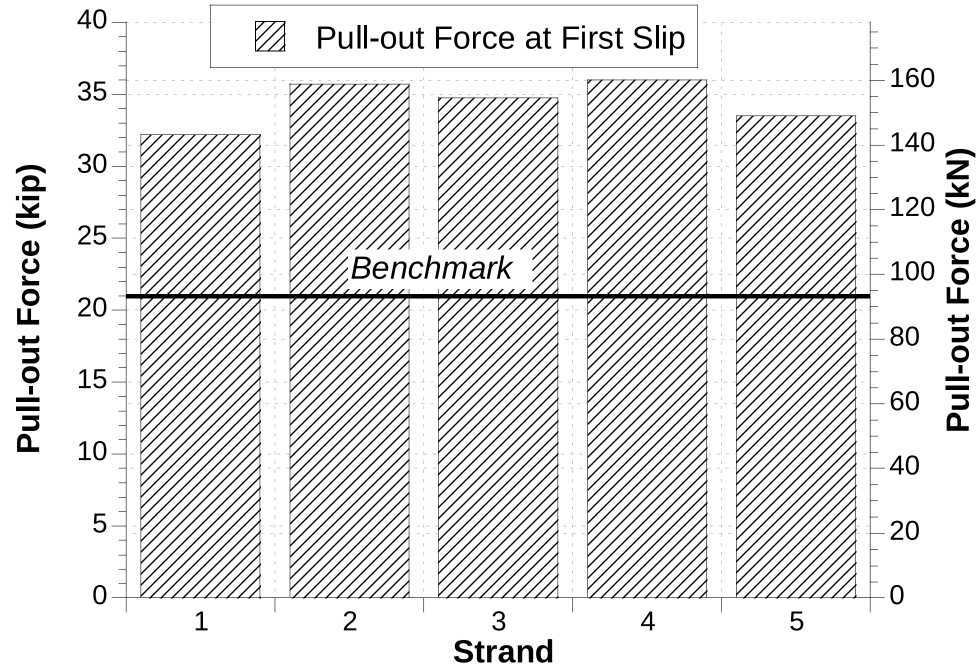

a) First slip pull-out force

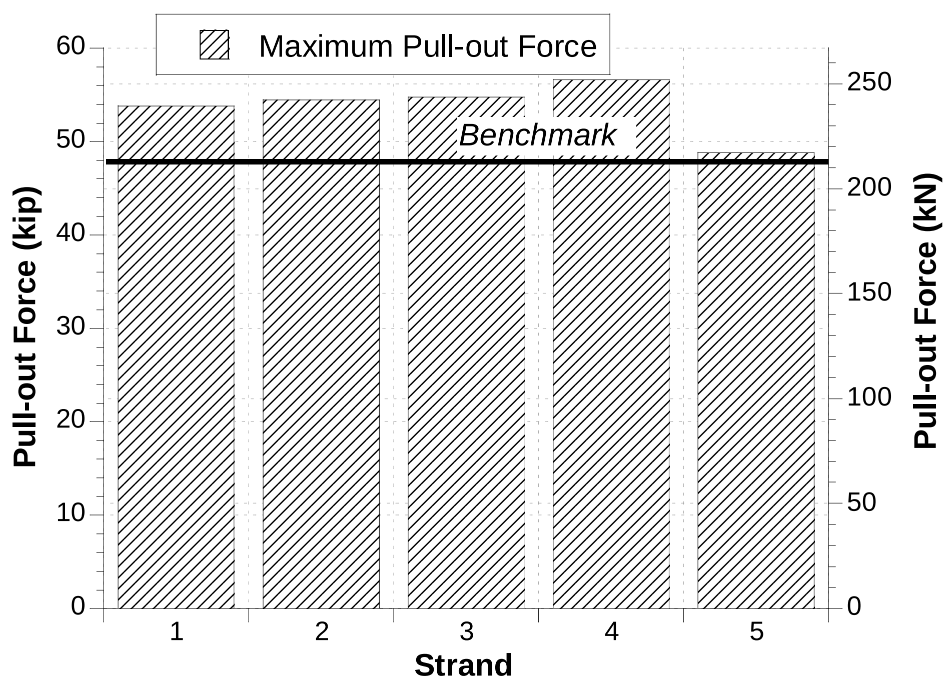

b) Maximum pull-out force

Figure 3-5 Large block pull-out test results

3.4 Bond Evaluation of Unstressed Strand through Cylinder Pullout Tests

In order to assess the bond behavior between the strand and the surrounding concrete and assess the effect of concrete fluidity, simple pull-out tests on concrete cylinders containing concentric non-stressed strand were built and tested using normal consolidated concrete (NCC) and self-consolidating concrete (SCC). The built and tested cylinders were 6-in.-diameter (15.2 mm) and 24 in.- (610 mm) long, with an embedment length of 20” (510 mm). Some of the cylinders contained debonded strand using double layer slit sheathing, others were fully bonded, and the rest were fully bonded with confinement reinforcement.

3.4.1 Test plan, description, and construction

Confinement reinforcement was provided for three cylinders in each batch, NCC and SCC, using Grade 60 (414 MPa) #3 bars as shown in Figure 3-6. The pitch of the spiral confinement was 2” (51 mm) and the outside diameter of the spiral was 3” (75 mm). PVC pipes, 0.75-in.- diameter (20 mm) and 2 in.-long (50 mm) were placed from each end, thus leaving an embedment length of 20 in. (510 mm). The strands were cleaned with a dry towel prior to placement in the forms. The cylinders were cast in a group with the strand in the vertical direction (see Figure 3-6). The naming convention given to the pull-out cylinders is given in Figure 3-7. The amount of pull-out cylinders cast and tested is given in Table 3-1.

The soft “slit” sheathing tubing was placed along the embedment length in the case of the debonded strands using two layers. The NCC samples were cast in two layers with vibration after each layer. No vibration was provided to the SCC cylinders and the concrete was poured in a single step.

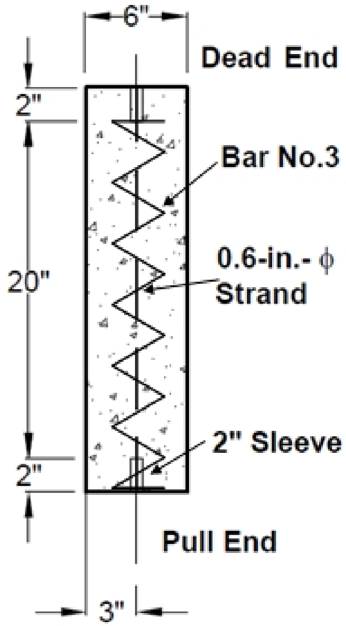

a) Reinforcing details **b) Formwork and strand set up**

Figure 3-6 Reinforcement and geometry details of pull-out tests on cylinders

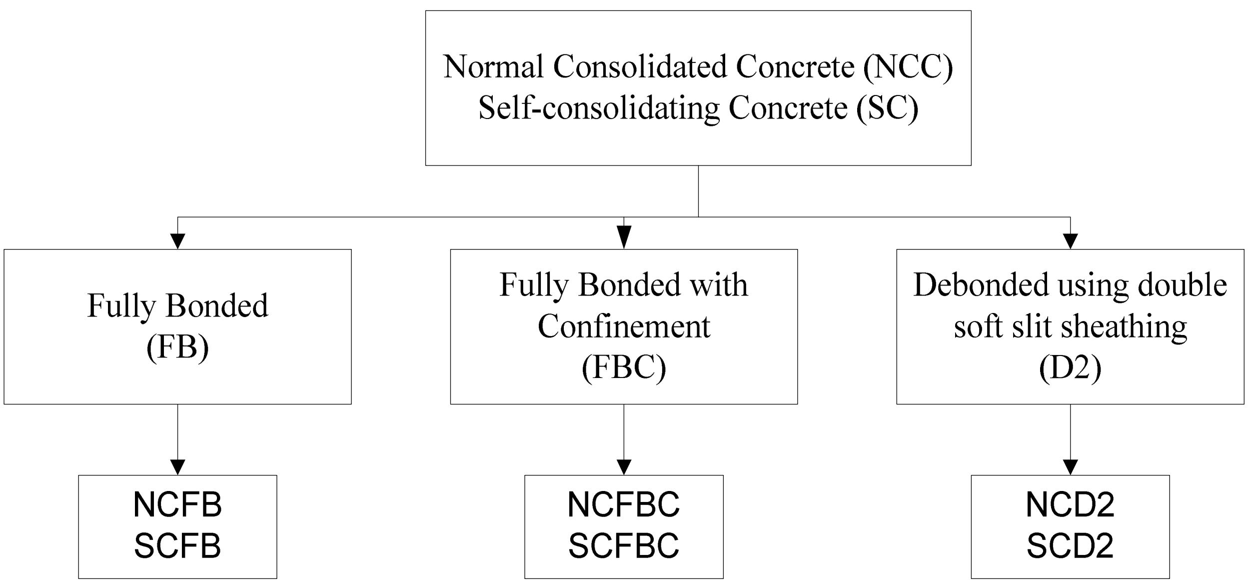

Figure 3-7 Test matrix and naming and matrix convention for cylinder pull-out tests

Table 3-1 Amount of pull-out cylinders cast per batch

Condition of Strand	Type of Concrete	
	NCC	SCC
FB	3	3
FBC	2	3
D2	2	3
Total	7	9

3.4.2 Test Procedure

The concrete compressive strength for concrete used in the pull-out cylinder tests was determined according to ASTM-C873 using 4”x8” (100 mm x 200 mm) cylinders. Three cylinders were kept in a curing room and the rest were left next to the test units in the laboratory test bay. The average compressive strength at the day of test (~6 days after casting) was 7,300 psi (50.3 MPa) for the normal consolidated concrete (NCC), and 9,400 psi (64.8 MPa) for the self-consolidating concrete (SCC). The NCC and SCC mix designs are given in Appendix A.

The set up for the pull-out test on cylinders was similar to the one shown for the large-block in Figure 3-3. The equipment used for the pull-out test on cylinders was the same as the one used for the large block pull-out test (see Section 3.4.2). Figure 3-8 shows an overview picture of the test set-up. Strand-slip was monitored at both ends, pull and dead (see Figure 3-8), and readings were recorded using a data acquisition system (DAQ). The pull-out test was stopped when the strand was pulled out about 6 in. (150 mm) or when the peak load suddenly dropped, whichever happened first.

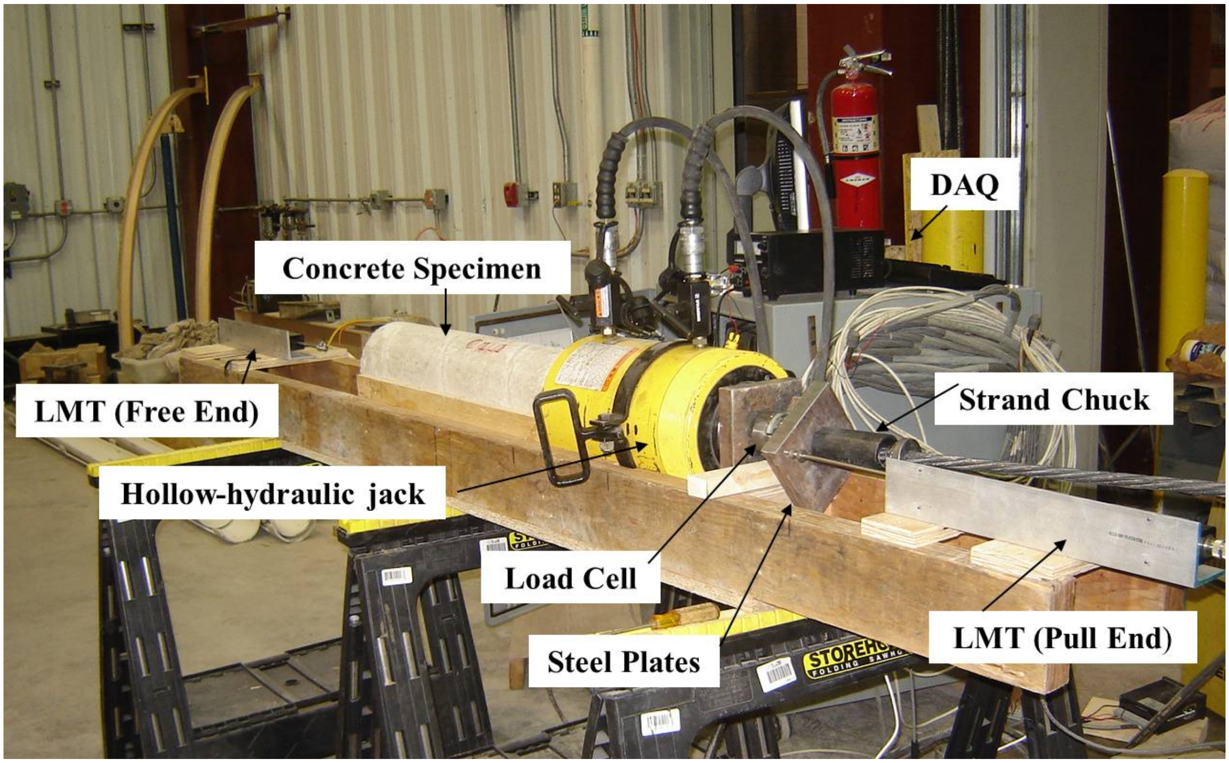

Figure 3-8 Photograph of the cylinder pull-out test setup

3.4.3 Cylinder Pull-out Test Results

Longitudinal cracks along the concrete cylinder (see Figure 3-9) were observed after hearing a strong noise and observing on the DAQ-computer that the pull-out force had dropped considerably. The cracks started at the pull-end close to the strand and extended to the surface of the cylinder. The crack then propagated along the cylinders towards the dead end. In no case did the crack reach the dead end. Cracking did not occur in the cylinders containing a single concentric debonded strand.

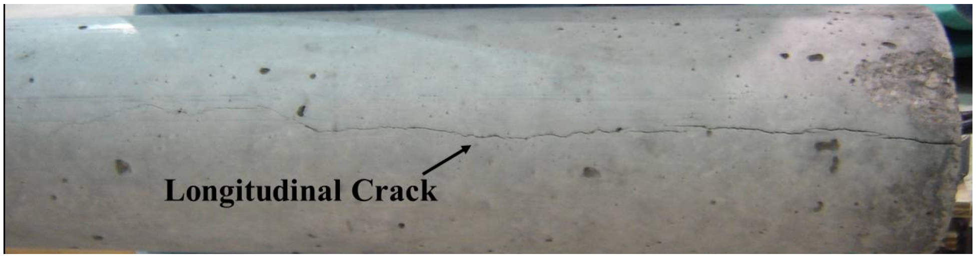

Figure 3-9 Pull-out cylinder with longitudinal cracking

A typical pull-out curve response from the pull-out tests is shown in Figure 3-10. Three main points are highlighted: a) the first slip force, b) the strand-slip at first slip force, and c) the peak pull-out load; as described below:

a) First slip force: is the force that causes the initial movement of the strand. The first slip force coincides with the end of the elastic region along the pull-end curve.

b) Strand slip at first slip force: is the distance that the strand moves at the pull end that coincides with the initiation of movement at the dead end.

c) Peak Load: is the maximum load reached when pulling the strand and it remains approximately constant exhibiting a plateau.

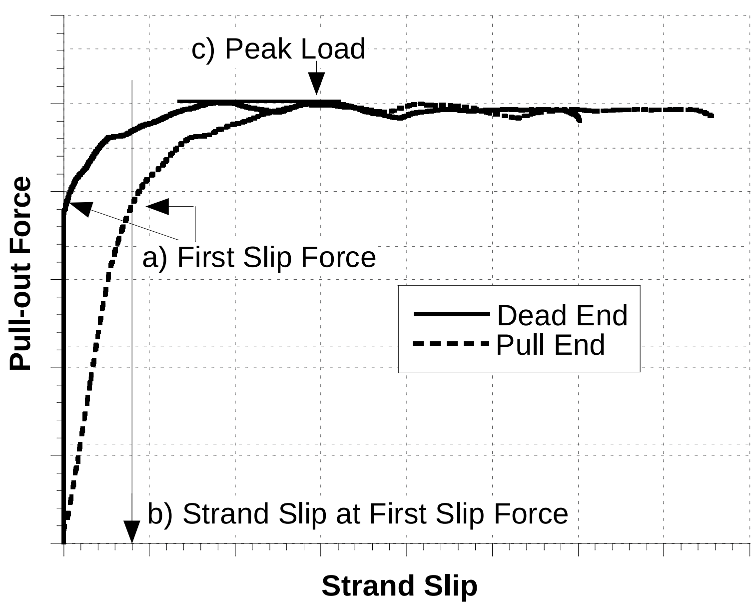

Figure 3-10 Typical force-slip response from pull-out test

The obtained average maximum pull-out forces are presented in Table 3-2. It can be seen that the fully bonded strand with confinement (FBC) exhibited the maximum pull-out force for each set, NCC and SCC. Figure 3-11 and Figure 3-12 show the pull-out response curve for the three different strand conditions: fully bonded (FB), fully bonded confined (FBC), and debonded with two layers (D2) (see Figure 3-7) for both sets. Supplementary pull-out curves are given in Appendix B.

Table 3-2 Summary of maximum pull-out force on cylinders

Strand Denomination	NCC (f'_{ci}= 7330 psi) (50.3 MPa) Maximum Pull-out force -kip (kN)		SCC (f'_{ci}= 9450 psi) (64.8 MPa) Maximum Pull-out force -kip (kN)	
	Mean	**St.dev**	**Mean**	**St.dev**
FBC	51.1 (227.3)	8.16 (36.3)	49.4 (319.73)	2.02 (8.98)
FBU	46.59 (207.2)	7.53 (33.5)	44.73 (199)	1.4 (6.23)
D2	0.26 (1.16)	0.07 (0.31)	0.18 (0.80)	0.12 (0.53)

1 kip= 4.448 kN

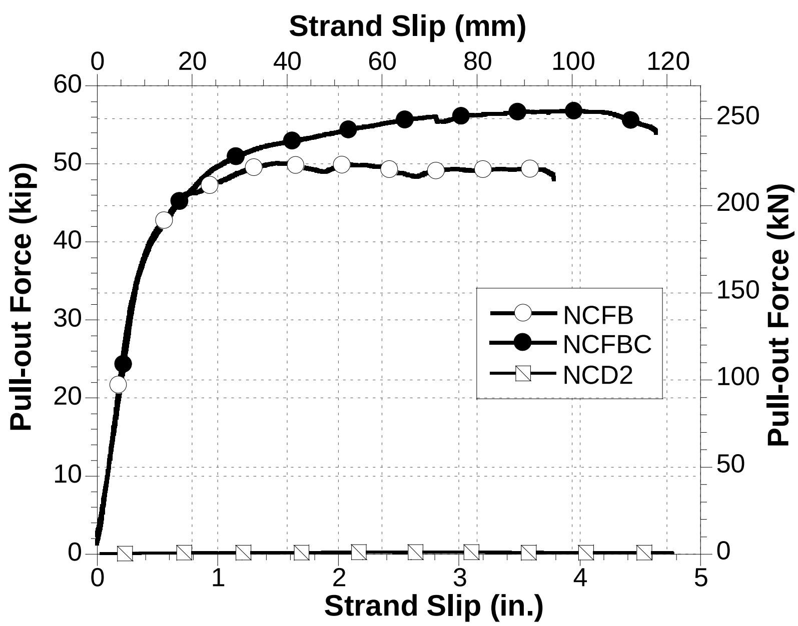

Figure 3-11 Pull-out response for strand in NCC cylinders

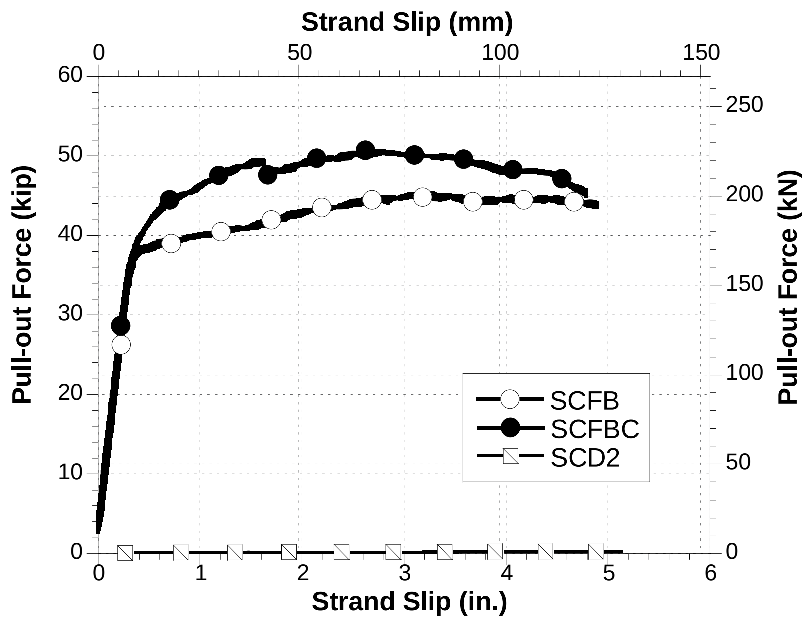

Figure 3-12 Pull-out response for strand in SCC cylinders

The average maximum bond strength, *u*, was calculated from the average maximum pull-out forces for the corresponding embedment length of 20" (510 mm), and the surface area of the 0.6-in.-diameter (15.2 mm) strand. Equation 2-5 was used to obtain the average bond strength values. Since the simple pull-out tests on cylinders were conducted using two different types of concrete, NCC and SCC, the bond stress values were normalized in respect to $\sqrt{f'_{ci}}$ for each set. The normalized bond strength values, *u'*, were obtained using Equation 3-1. The maximum pull-out force, the calculated bond strength values, and the normalized bond strength are shown in Table 3-3. Figure 3-13 shows a graph with the normalized bond strength values with respect to $\sqrt{f'_{ci}}$.

$$u' = \frac{u}{\sqrt{f'_{ci}}} \qquad \textbf{Equation 3-1}$$

Table 3-3 Maximum pull-out forces and bond strength values obtained from pull-out tests on cylinders

Strand Denomination	Maximum Pull-out Force - kip (kN)	Bond Strength (*u*)-psi (MPa)	$u' = \frac{u}{\sqrt{f'_{ci}}}$	$\frac{u'}{u'\,NCFB}$
NCFBC	51.1 (227.3)	1017 (7.0)	11.9	1.1
NCFB	46.6 (207.3)	927 (6.4)	10.9	1.0
SCFBC	49.4 (219.7)	983 (6.8)	10.1	0.9
SCFB	44.7 (198.8)	890 (6.1)	9.2	0.9

1 kip= 4.448 kN
1 MPa= 145 psi

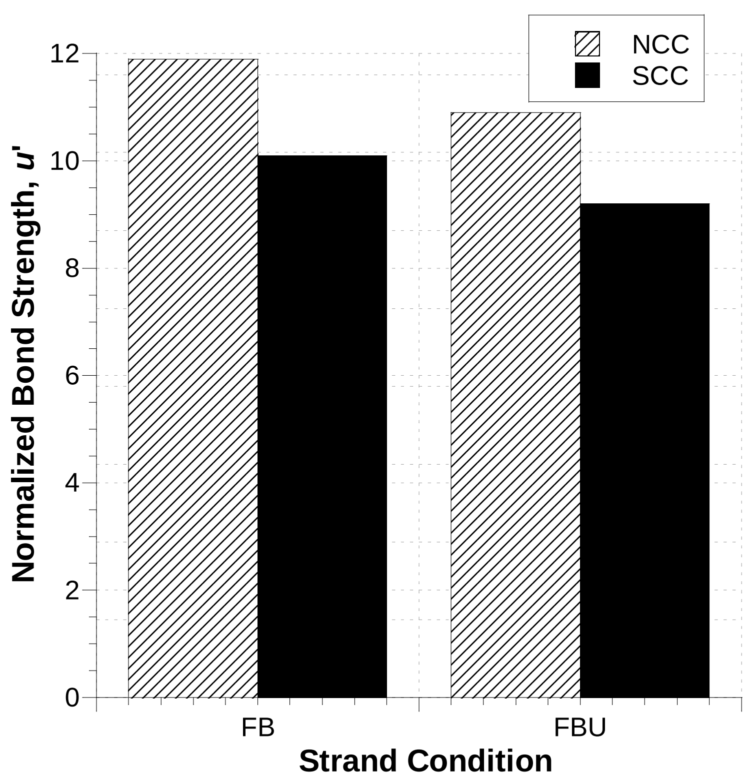

Figure 3-13 Normalized peak bond strength values with respect to $\sqrt{f'_{ci}}$

3.4.4 Bond Evaluation of Unstressed Strand through Cylinder Pullout Tests

From the pull-out test results on simple cylinders it was observed that the strand provided with spiral confinement reached a greater average pull-out peak load than those without spiral (Table 3-2). From the NCC tests set, the NCFBC group attained greater pull-out force than the NCFBU group by 8.8%. For SCC set of cylinders, the SCFBC pull-out tests reached an average maximum pull-out greater than the SCFBU tests by about 9.5%. In addition, it can be seen in Table 3-2 that the pull-out tests on SCC had more uniform results as the standard deviation values were lower compared to the NCC tests. Even though the compressive strength for the SCC tests was about 2000 psi (13.8 MPa) greater than the NCC set, the average maximum pull-out force reached from every subgroup of SCC cylinders (FBC, FBU, and D2) was lower than for the NCC units.

As shown in Figure 3-11 and Figure 3-12, the fully bonded cylinders with confinement and fully bonded pull-out cylinders without confinement curves response were quite similar along the elastic region, indicating similar level of stiffness. From Table 3-2 it can be seen that the debonding mechanism, double layer flexible slit sheathing, effectively broke the bond between the unstressed strand and the surrounding concrete, thus paste infiltration did not occur even when using high fluidity concrete (SCC).

3.5 Evaluation of Hydraulic Head Effect on Bond through Wall-like Blocks Pull-out Tests

The effect of concrete hydraulic head was evaluated on debonded strands to investigate if high concrete fluidity can cause bonding of the unbonded strands due to paste infiltration and if deformations on the sheathing material can take place due to concrete pressure, thus preventing full debonding of the strand and the surrounding concrete when using flexible slit sheathing. These possible effects were evaluated with pull-out tests on wall-like blocks containing unstressed debonded strands, where debonding was accomplished using single and double layer flexible slit sheathing.

Recent studies to evaluate the top-strand effects in prestressed concrete members and its effect on bond behavior have been conducted by Peterman [24]. It was observed that the main factor causing the top-strand effect is the amount of fresh concrete cast above the strands. In addition, Peterman observed that an increase in concrete fluidity will cause a decreased in bond capacity. This effect was more evident for those strands closer to the top surface of the prestresed concrete member.

3.5.1 Test plan description and construction

In order to study the hydraulic head effect and its influence on bond behavior for shielded strand, pull-out tests on unstressed strand were done on two 72” (1830 mm) high wall-like blocks with a cross section of 24”x 24” (610 mm x 610 mm) using normal consolidated concrete (NCC) and self-consolidating concrete (SCC). Each block had eighteen (18) strands as shown in Figure 3-15. The strands designated as NCFB and SCFB were fully bonded. Six strands were debonded using single flexible slit sheathing (NCD1 and SCD1), and the others were debonded by means of double soft slit sheathing (NCD2 and SCD2).

The naming convention for the wall-like blocks is shown in Figure 3-14. NC and SC refer to the type of concrete used. NC refers to normal consolidated concrete (NCC) and SC refers to self-consolidating concrete (SCC). The other two letters correspond to the type of strand, either bonded or debonded. For instance, for NCD2 the NC stands for NCC and D2 for debonded strand using double soft slit sheathing.

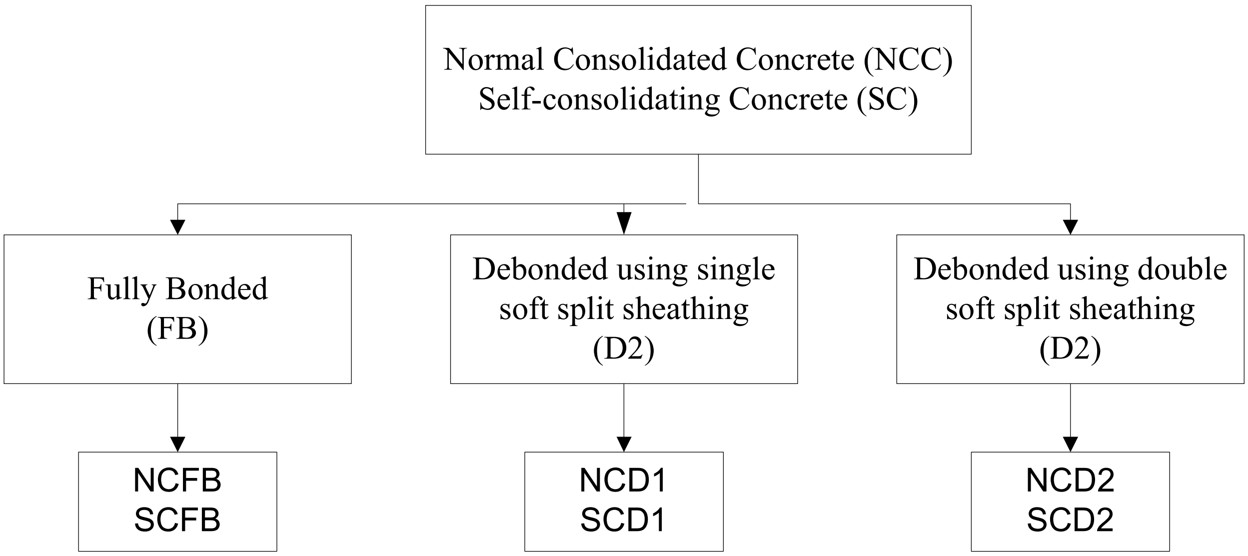

Figure 3-14 Test matrix and naming convention for wall-like block tests

The wall-like blocks were reinforced using bars #4 at each corner as shown in Figure 3-15a. Ties (#3 bar sizes) were placed every 12" (305 mm) center-to-center (see Figure 3-15). In total, four #4 bars and five #3 ties were used as reinforcement for each wall-like block. The 0.6-in.-diameter (15.2 mm) strands were spaced at every 12" (305 mm). The upper strands were located at 6" (150 mm) from the top of the block, and the lower strands were placed at 6" (150 mm) from the bottom of the block as shown in Figure 3-15. The blocks were filled with concrete from the top, with the strands in a horizontal position as shown in Figure 3-16.

The wall-like blocks were demolded about 2 days after the concrete was poured. The compressive strength of the concrete was verified by testing three 4"x8" (100 mm x 200 mm) concrete cylinders the day of demolding the wall-block formwork. The wall block cast with NCC was filled out in three layers with vibration. No vibration was done for the wall block cast with SCC.

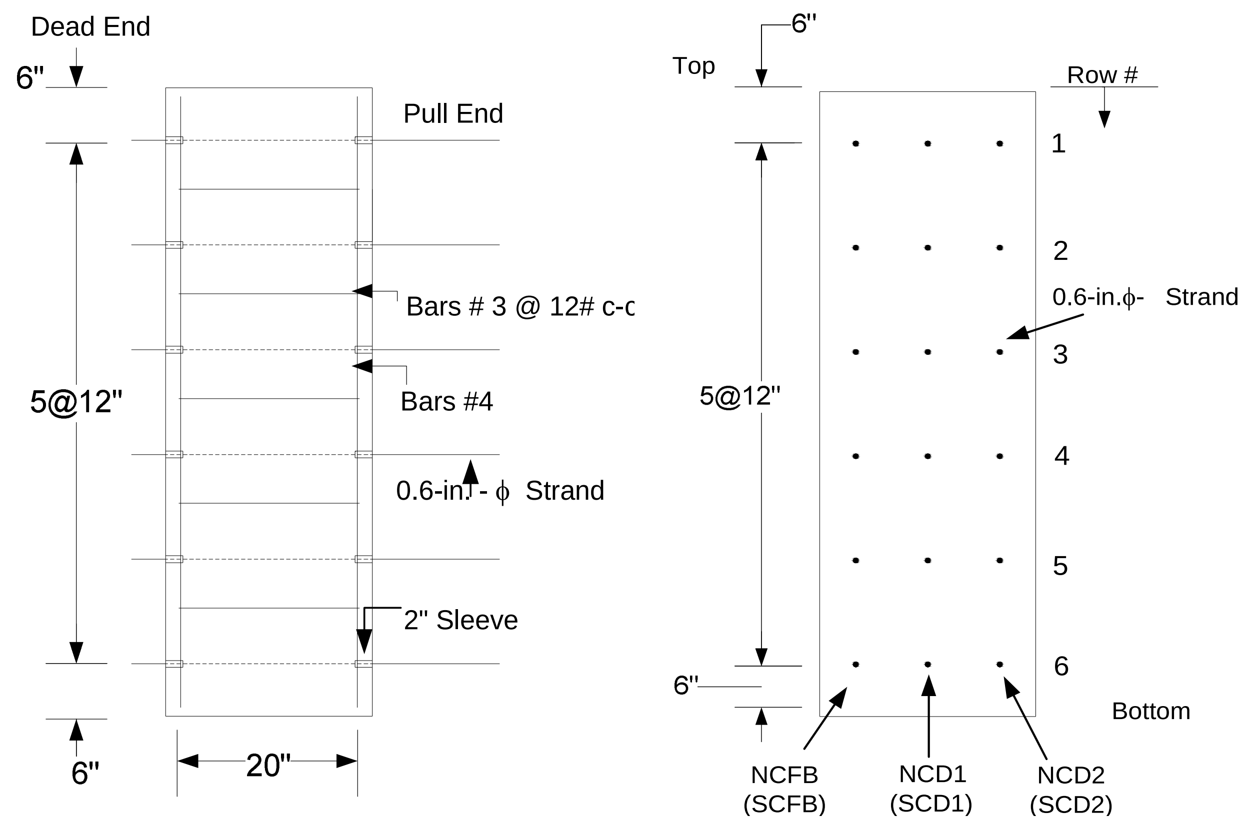

a) Side view **b) Front view**

Figure 3-15 Wall-like block geometry details: side and front view

3.5.2 Wall-like Block Test Procedure

The concrete compressive strength for the concrete in the wall-like blocks was assessed with 4”x8” (100 mm x 200 mm) cylinders according to ASTM-C873. Three cylinders were kept in a curing room and the rest were kept in the laboratory floor next to the wall-blocks. The average compressive strength at the day of testing (~6 days after casting) was 7,300 psi (50.3 MPa) and 9,400 psi (64.8 MPa) for the NCC and SCC blocks, respectively.

The pull-out test set-up on the wall-like blocks was similar to the ones used for the large block pull-out test and the simple pull-out test on cylinders. Figure 3-17 shows an overview of the wall-like block pull-out test set up. Readings from the load cell and linear potentiometers were recorded with a data acquisition system (DAQ).

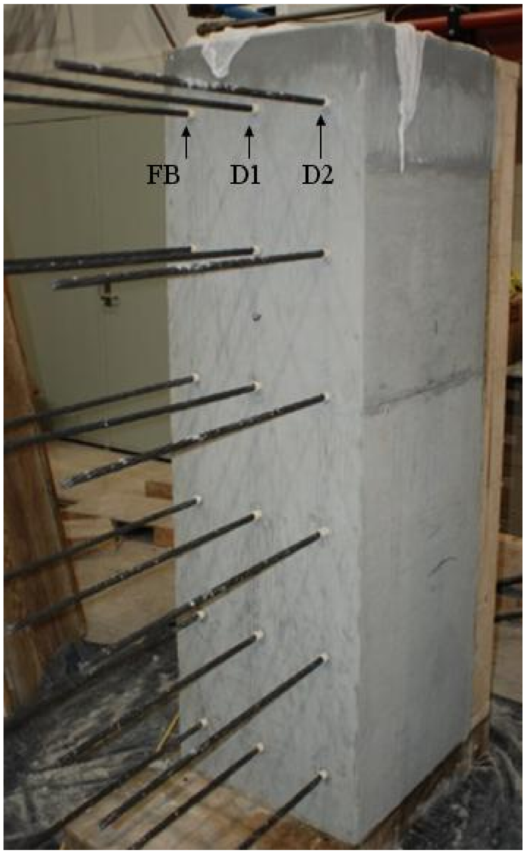

a) Photograph of construction details   b) Photograph

Figure 3-16 Wall-like block reinforcing details

Figure 3-17 Overview of the wall-like block pull-out test

3.5.3 Wall-like Blocks Pull-out Test Results

Typical pull-out force vs. strand slip curves obtained from the NCC wall-like block at a height of 18 in. (455 mm) (see Figure 3-16) are shown in Figure 3-18. Supplementary results obtained for each strand are given in Appendix B. Results for the debonded strands, using single and double slit sheathing layer, in the NCC wall-like block at 18 inches (455 mm) from the block bottom are seen in Figure 3-18. The observed top-strand effect on both wall-like blocks is clearly shown in Figure 3-19 for the three different strand conditions, i.e., fully bonded and fully debonded. It is seen in Figure 3-19 that the fully bonded strands located toward the bottom of the block exhibited larger peak pull-out forces compared to the strands located toward the top of the block (first three upper strands). On the other hand, the maximum pull-out force obtained from the debonded strands was considerably small compared to the fully bonded strand group. Thus, hydraulic head effect had little or no effect on the behavior of the blanketed strands. The data indicates that the top strand effect was higher for the NCC block than for the SCC block, which can be seen in Figure 3-19. The compressive strength at the day of testing and the average peak pull-out forces for each strand condition are shown in Table 3-4. The bond strength values for each case were calculated using Equation 2-5 and Figure 3-20a shows the peak bond stresses from both wall blocks normalized with respect to $\sqrt{f'_{ci}}$.

Table 3-4 Summary of average maximum pull-out forces: wall-like blocks

Strand Denomination	NCC (f'_{ci}= 7200 psi) (49.6 MPa) Maximum Pull-out Force – kip (kN)		SCC (f'_{ci}= 9600 psi) (66.2 MPa) Maximum Pull-out Force – kip (kN)	
	Average	**Standard Deviation**	**Average**	**Standard Deviation**
FB	46.3 (206.0)	7.3 (32.4)	52.5 (233.4)	4.3 (19.3)
D1	3.4 (15.3)	2.2 (9.8)	1.3 (5.7)	0.5 (2.1)
D2	0.5 (2.2)	0.2 (1.0)	0.15 (0.4)	0.2 (0.7)

1 kip= 4.448 kN

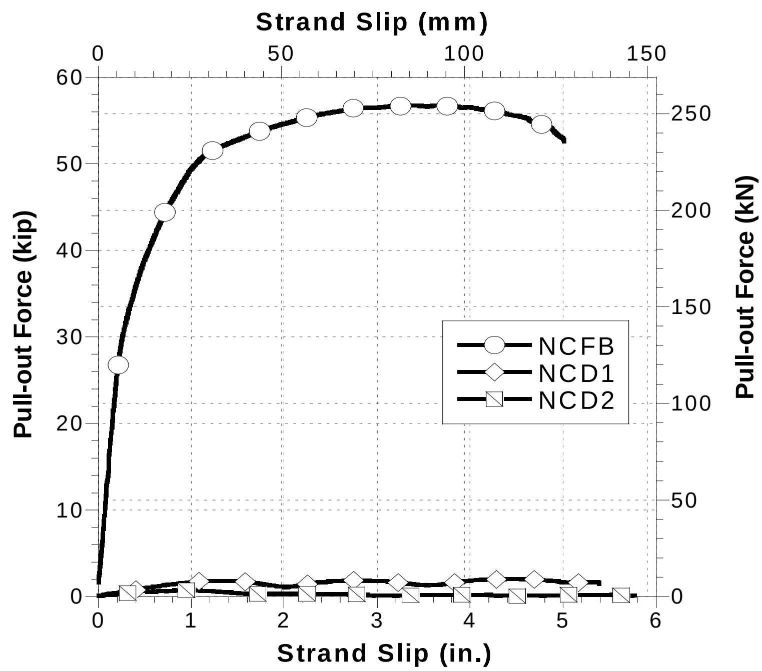

a) Wall-like block cast with NCC

Figure 3-18 Pull-out curve response of the 5th row strand on wall-like blocks

Figure 3-18 cont'd

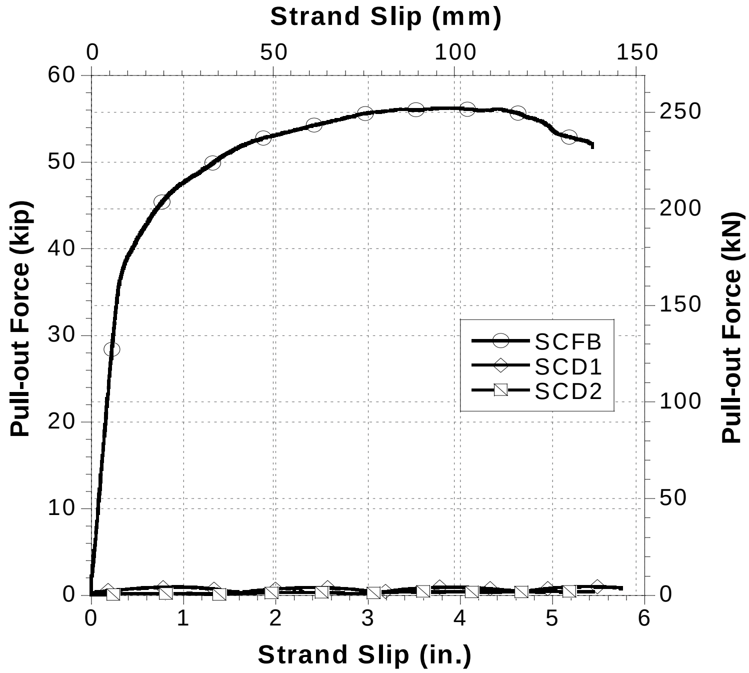

b) Wall-like block cast with SCC

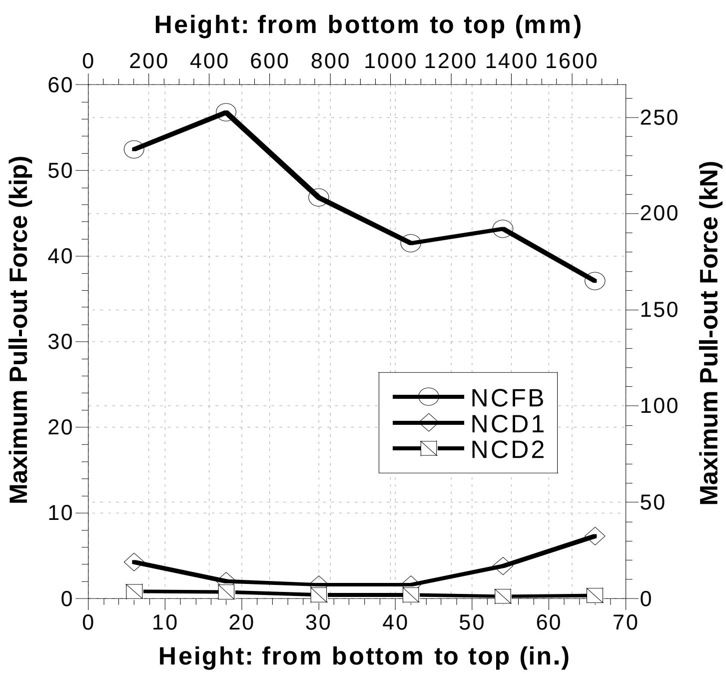

a) Wall-like block cast with NCC

Figure 3-19 Top-strand effect on wall-like blocks

Figure 3-19 cont'd.

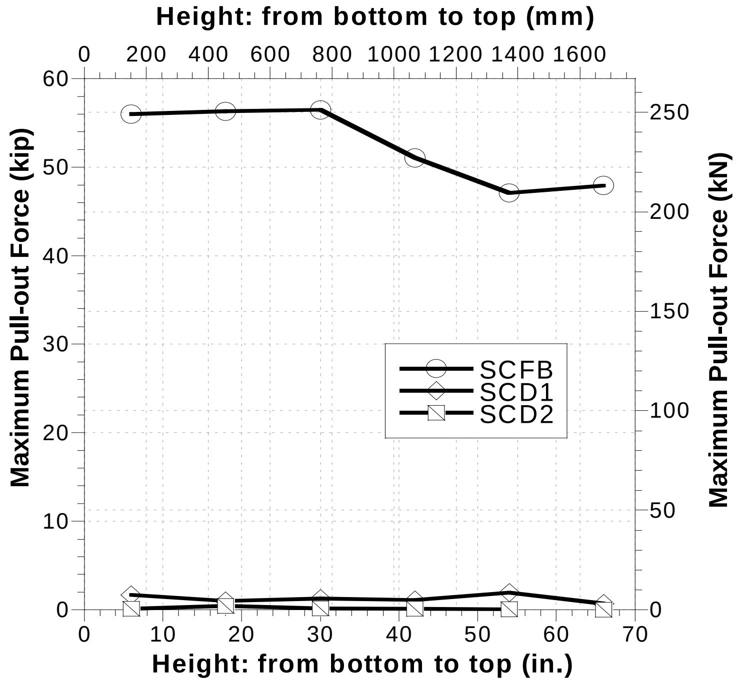

b) Wall-like block cast with SCC

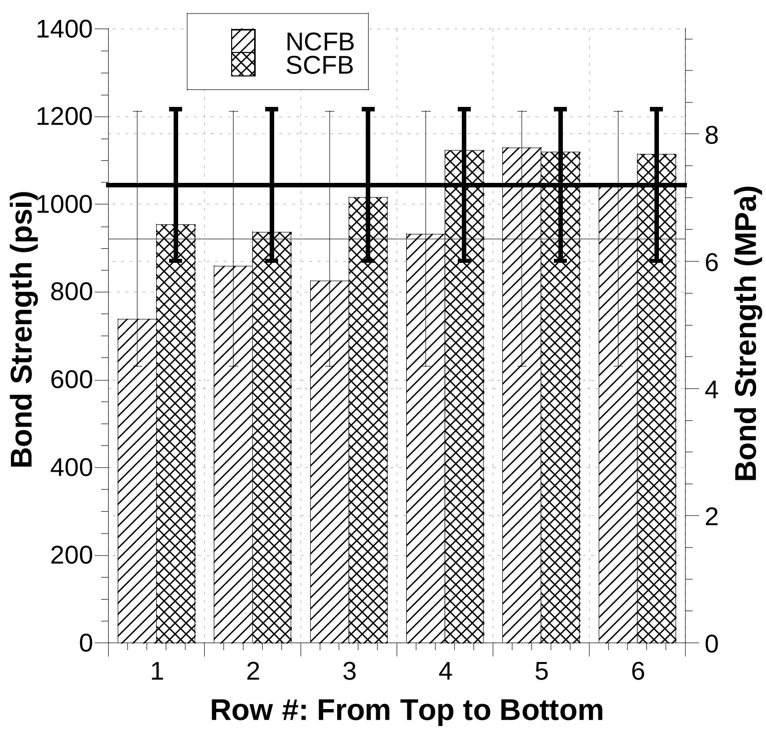

a) Peak bond stress

Figure 3-20 Bond stresses: Fully bonded strands in wall-like blocks

Figure 3-20 cont'd.

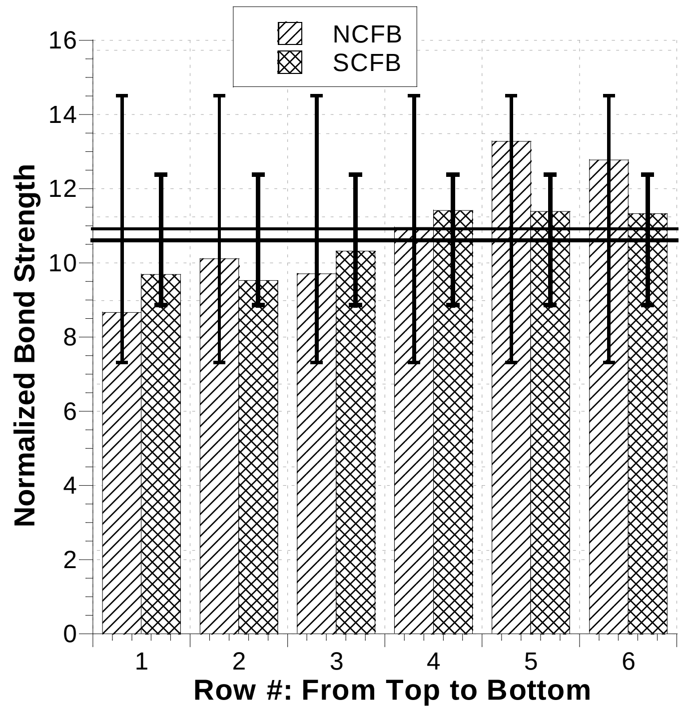

b) Normalized peak bond strength

3.5.3 Hydraulic Head Effect: Wall-like Blocks

The maximum pull-out force reached for the group of debonded strands was very small compared to the fully bonded strands, which indicates that in this type of setting (unstressed strand) the debonding mechanism was effective. The top-strand effect was clearly observed as seen in Figure 3-19, where the upper strands reached lower peak pull-out load values compared to the strands located toward the bottom of the blocks. In Figure 3-19a, the NCD1 upper strand exhibited the maximum peak load in that group and this could be attributed to the fast hardening of the concrete when pouring the last layer of concrete when casting the NCC block. As shown in Figure 3-19b, the SCFB group of strand performed more uniformly than the NCFB strands. The three lower SCFBC strands reached about the same maximum pull-out force. This was not observed in the NCC wall-like block since the strand located at 18” (455 mm) from the bottom had the largest pull-out force among the NCFBC strands. However, in both NCC and SCC wall blocks, the upper fully bonded strand exhibited a lower maximum pull-out force compared to the other five fully bonded strands in the blocks. The peak load for the SCFB group of strands increased gradually from top to bottom, and the three lower strands had a similar maximum pull-out load.

The peak pull-out force from the SCFB strands was, on average, about 65% less than the NCFB strand group as shown in Table 3-4. In Figure 3-20a the peak bond stress values for the SCFB strands are shown to be higher in most cases since greater peak pull-out loads were obtained from the SCC wall block for fully bonded strands. However, it is shown in Figure 3-20b that if the peak bond stresses are normalized respect to $\sqrt{f'_{ci}}$ the bond strength values for NCFB strands were higher in most cases.

3.6 Prestress Bond Transfer in Beams

The bond stress transfer behavior of fully bonded and shielded (debonded) 0.6-in.-diameter (15.2 mm) prestressing strand on normally consolidated and self-consolidating concrete (NCC and SCC) was studied by conducting tests on laboratory scale beams. Six beams with a single concentric strand were tested for each type of concrete. Stress transfer behavior was assessed by measuring the strains transmitted to the concrete upon gradual release of the pretensioned strand. The strand was debonded using flexible slit (tight fit) sheathing in either a single or double layer.

3.6.1 Geometry, Reinforcing, and Prestressing Details

The beams units were 6”x6” (150 mm x 150 mm) in cross section and 20 ft long (6.1 m), with a single concentric 0.6-in.-diameter (15.2 mm) strand (see Figure 3-21). Twelve beams were tested; cast in two groups of six, one group with NCC and the other with SCC. From the six beams in a given batch two had fully bonded strands, two had partially debonded strands with single slit sheathing, and the rest had partially debonded strands with double slit sheathing. When applicable, the debonded strand length was 24” (610 mm) from each end of the beam. Three of the six beams had confinement (see Figure 3-21), i.e., one of the beams containing a single fully bonded strand, one of the beams containing a single debonded strand using one slit sheathing layer, and one of the beams containing a single debonded strand using double slit flexible sheathing. The provided confinement reinforcement was the same one as the one used in the pull-out on cylinders (see Section 3.5.1), and it was placed in the anchorage region as shown in Figure 3-21. For beams with partially debonded strands, the confinement was placed at the end of the debonded length, starting at 24” (610 mm) from the end of the beam. For the beam with fully bonded strand the confinement was placed as close as possible to the releasing end. Figure 3-22 shows a photograph of one of the fully bonded beams containing spiral confinement in the anchorage region. This picture corresponds to the stage prior to casting the beams.

The test matrix and naming convention for the beams is shown in Figure 3-23. The naming convention was based on the type of concrete, condition of the strand (bonded or partially debonded), and the provision or not of confinement. The first two letters, NC or SC, correspond to the type of concrete. The following two letters refer to the condition of the strand, i.e., partially debonded using single or double slit sheathing or fully bonded. The last letter, C or U, refers to the addition of confinement in the beam, where C stands for a beam with confinement and a U refers to a beam without confinement. For instance, NCFBU beam refers to a beam cast with normally consolidated concrete (NCC), the strand was fully bonded, and no spiral confinement was provided.

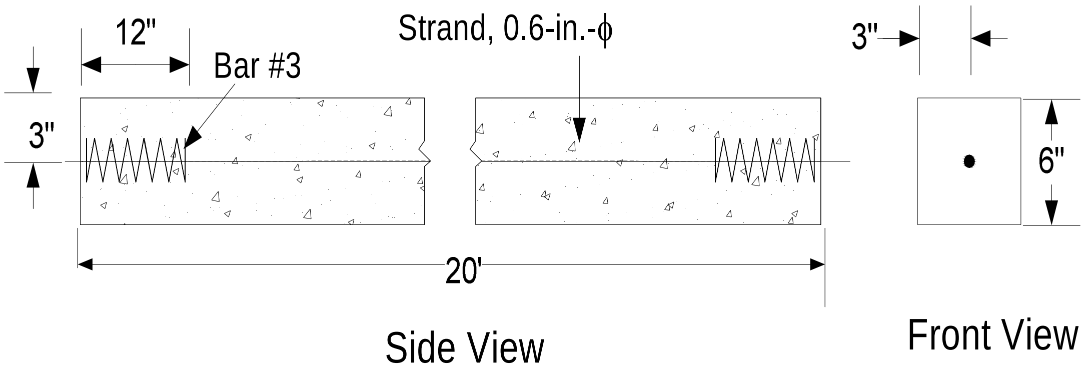

Figure 3-21 Geometry of beam with fully-bond strand and with confinement

The test setup for this study was essentially the casting bed for the beams, as shown in the plan view drawing in Figure 3-24 and the photograph in Figure 3-25. As seen in these Figures, two beams were placed for each line of strand. This was done for both sets, NCC and SCC.

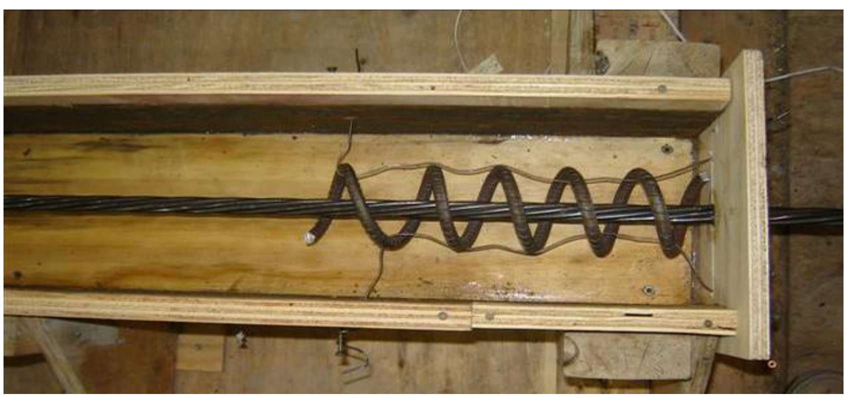

Figure 3-22 Photograph of end of fully bonded beam with confinement

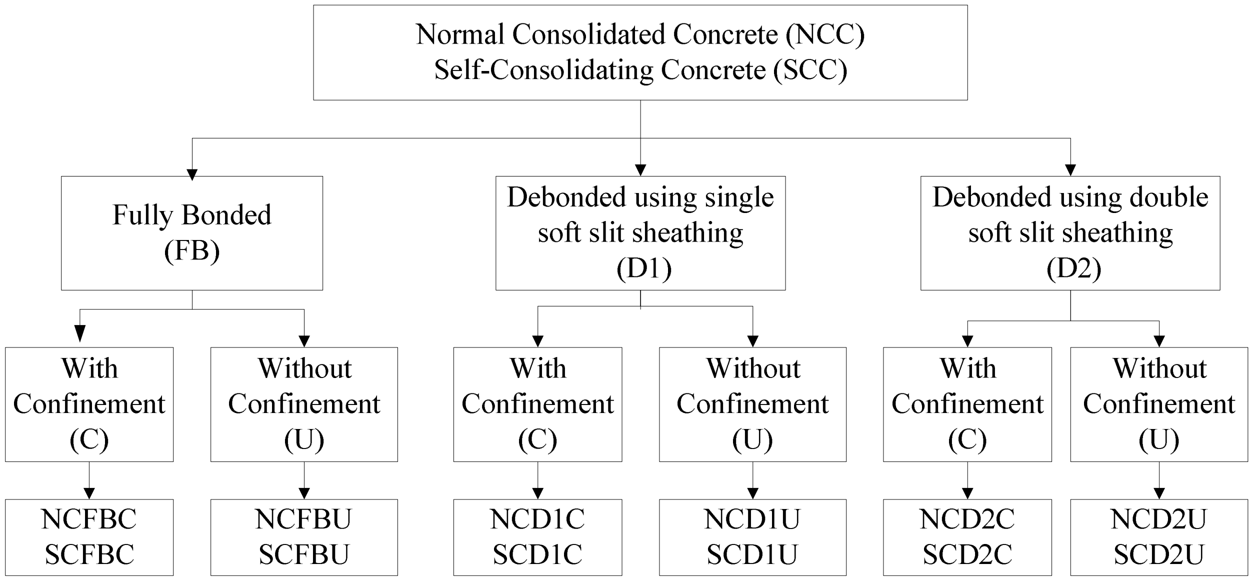

Figure 3-23 Test matrix and naming convention for beam tests

The prestressing action took place approximately two days before casting. The strands were pretensioned so as to reach a stress level of $0.7f_{pu}$ after all significant losses. During the strand tensioning operation the strain in each stand was monitored with a strain gauge and the pulling load was measured with a load cell. In addition, the stretching of each strand was monitored by manually measuring the strand elongation and its relaxation after release of the jacking force. Strain gages were also placed on the strands at dead end, east to the anchor block (see Figure 3-24) to monitor losses due to relaxation prior to casting, which was typically done 2 days after strand detensioning. The maximum strain due to relaxation prior to release into the hardened concrete beam was about 80 με. Casting took place two days after strand tensioning for the NCC beams and fourteen days after tensioning for the SCC beams.

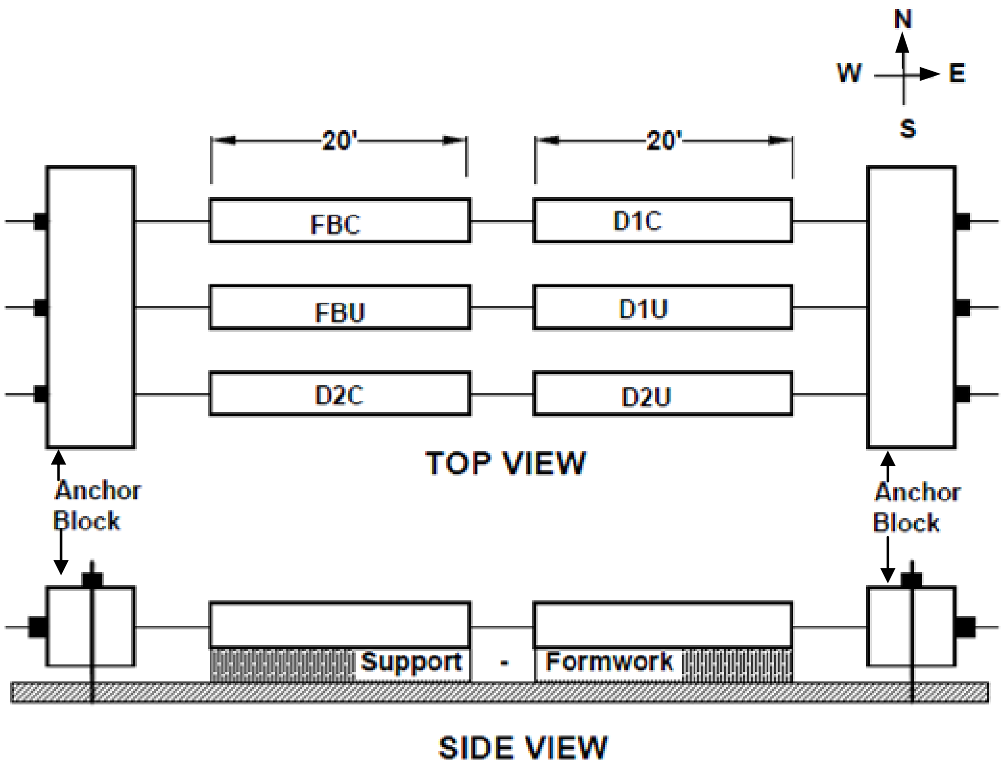

Figure 3-24 Schematic beams layout

Figure 3-25 Overview photograph of the beams layout

3.7.2.1 Concrete Surface Strain Profiles

Concrete surface strain profiles (CSSP) were obtained using a detachable mechanical (DEMEC) strain measuring system with target disks pre-installed at 2 in. (50 mm) on the beam side along the section centroid. Only one side in one end of each beam was instrumented. The first metal disk was placed at 1” (25.4 mm) from the end of the beam (see Figure 3-24 and Figure 3-26). The measurement length for beams with fully-bonded strands was about 115” (2920 mm), and for beams with debonded strands was approximately 150” (3810 mm). An overview of the test setup showing the prepared/instrumented ends of the beams is shown in Figure 3-27.

Strains were determined from measurements over a gage length of 8 in. (200 mm). Three readings were taken before and after release of the strand, respectively. The three readings were averaged (respectively) for post-processing and calculation of strains. Once the strain profile curves were obtained the curves were smoothed using the procedure depicted in Figure 3-28 as proposed by Russell et al. [26]. This technique is used to determine the so-called “transfer length” and it is well known as the 100% average maximum strain (AMS) method [26]. The procedure is well accepted and has been commonly used by other researchers.

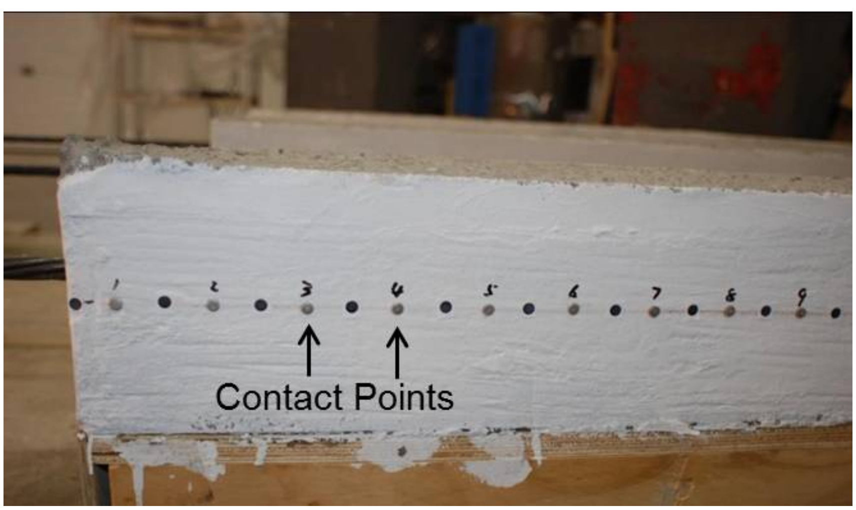

Figure 3-26 Beam side prepared for strain measurement with DEMEC system

Figure 3-27 Overview of beam test setup and instrumentation at beam ends

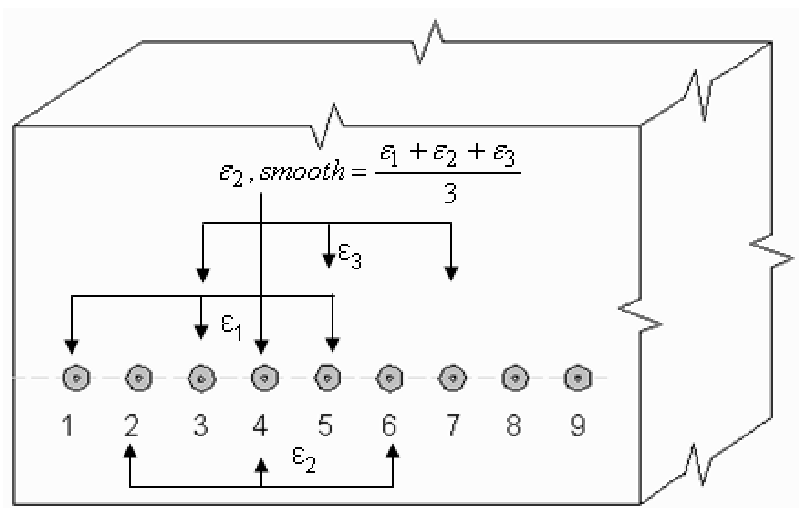

Figure 3-28 Smoothing method for concrete surface strain profiles. Adapted from [32]

3.6.1 Test Procedure: Transfer of Prestressing Force into the Concrete Member

At the day of testing, i.e., gradual release of the prestressed strands, six 4" x 8" (100 mm x 200 mm) cylinders were tested according to ASTM-C873. Three of the cylinders were kept in a curing room and the rest of the cylinders were kept in the laboratory floor next to the beams.

The strands for all pretensioned beams were gradually released by means of annealing. The strand release was typically done six days after casting. The delay was due to the time needed for demolding the specimens and instrumentation setup. The gradual prestress release into the concrete member was achieved by heat annealing of the strand along the three free strand regions in a given beam line (see Figure 3-24). The reduction of strand pretension due to the heat-induced relaxation of the steel was monitored with strain gages connected near one of the releasing ends. The annealing process took between 12 to 15 minutes. The release sequence for the NCC set was NCD2C, NCFBU, and NCFBC. Since two beams were placed per strand line, the prestressing force was transmitted into two beams at the same time. The releasing sequence for the self-consolidating concrete (SCC) batch was the same as the one described for the NCC set of beams.

Figure 3-29 Photograph of the three points where the strand was released

The time at which the DEMEC strain measurements were taken differed from beam to beam. Table 3-5 shows a summary of the time at which readings from each beam were taken after releasing the prestressing strands. The times at which measurements were taken are given because it is well-documented that transfer length increases with time, particularly during early age of the concrete beam.

Table 3-5 Times at which final DEMEC were taken after strand release

Beam ID	Time hours (min)
NCFBC	3.00 (180)
NCFBU	5.00 (300)
NCD1C	6.30 (380)
NCD1U	6.00 (360)
NCD2C	0.50 (30)
NCD2U	7.25 (435)
SCFBC	3.50 (210)
SCFBU	5.00 (300)
SCD1C	4.60 (280)
SCD1U	6.30 (378)
SCD2C	0.50 (30)
SCD2U	9.00 (540)

3.6.2 Results of Bond Transfer in Beams

The results obtained from the prestress bond transfer tests are presented next. The compressive strength at the day of test (release) for the NCC beams was 7,300 psi (50.3 MPa) and for the SCC beams it was 9,400 psi (64.8 MPa).

3.6.4.1 Concrete Surface Strain Profiles

The set of three DEMEC readings before and after strand release were averaged and then used to calculate the raw strain profile. A smoothed strain profile was determined by using a running average of 3 points as defined by Equation 3-2 below.

$$\varepsilon_{i,smooth} = \frac{\varepsilon_{i-1} + \varepsilon_i + \varepsilon_{i+1}}{3}$$ **Equation 3-2**

The 100% average measurement strain (AMS) method was used [32] to obtain the transfer length using the concrete surface strain profiles. This is a subjective technique and the average strain is calculated from those points near to the plateau of the strain profile. The onset of the plateau is the transfer length strain point. Figure 3-30 shows unsmoothed vs. smoothed concrete surface strain profile curves. It can be observed that the smoothed curve is more uniform and it takes care of peak values that may affect the average strain level. In some cases, some outlier peak levels were observed and they were eliminated because those points were far away from the trend.

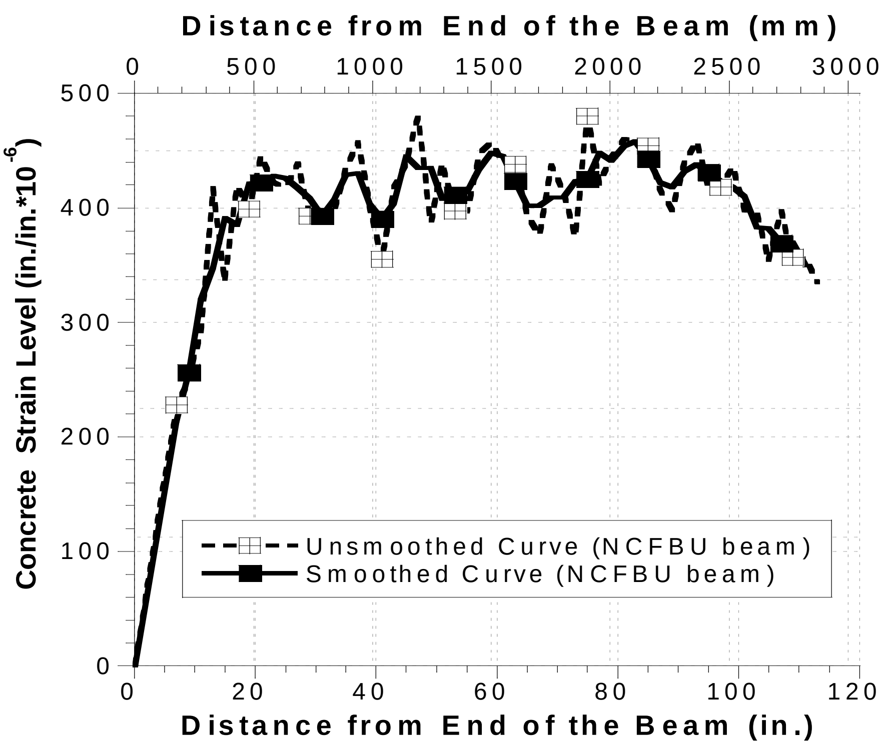

Figure 3-30 Concrete surface strain profile: smoothed vs. unsmoothed curves

Concrete strain profile curves obtained for the NCC beams are shown in Figure 3-31 and Figure 3-32. Representative results obtained for the SCC beams are shown in Figure 3-33 and Figure 3-34. In all these figures f_{pj} is the initial prestressing force after sitting losses. It can be observed from Figure 3-31, Figure 3-32, and Figure 3-34 that some level of prestressing force was transferred along the debonded length. For the beams containing partially debonded strands, the transfer length was defined as that from the end of the debonded length until the strain level became uniform, i.e., a plateau level was reached. The 100% AMS procedure [32] was also applied.

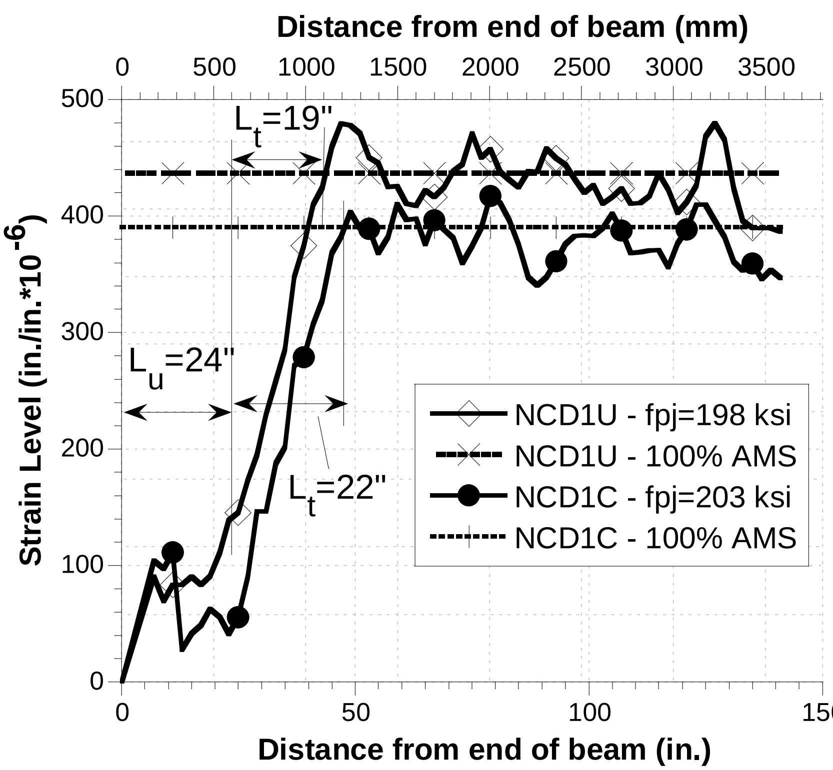

Figure 3-31 Concrete surface strains profiles for NCD1C and NCD1U beams

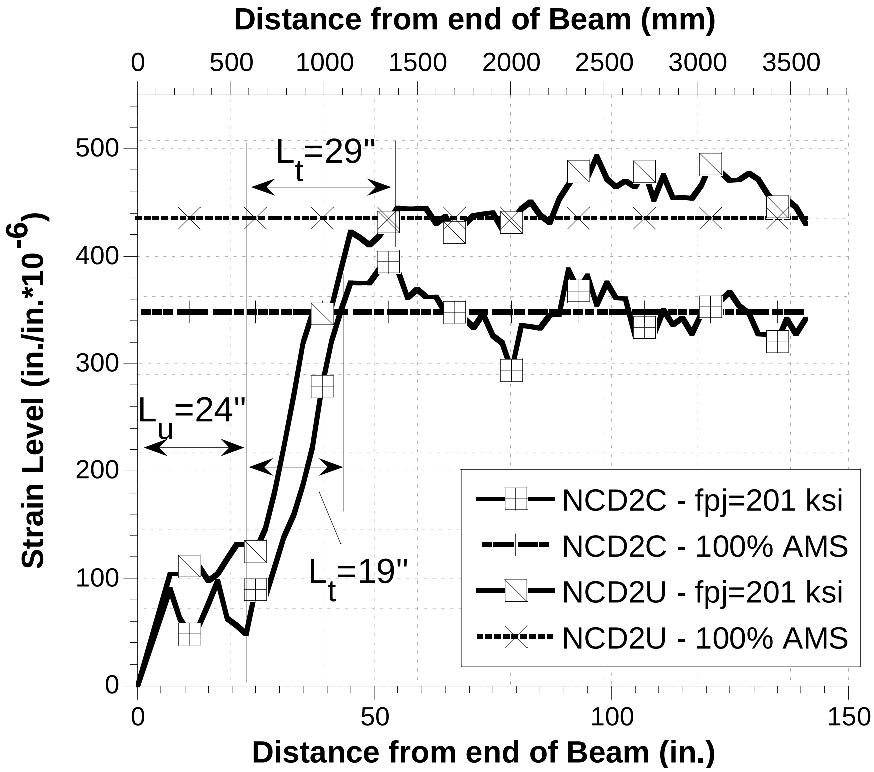

Figure 3-32 Concrete surface strain profiles for NCD2C and NCD2U beams

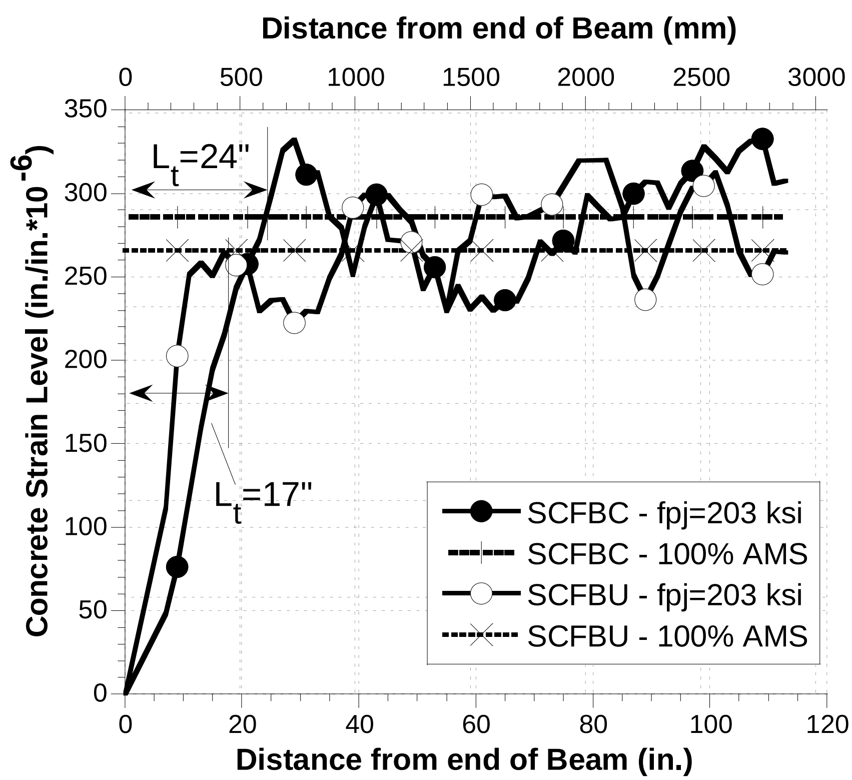

Figure 3-33 Concrete surface strain profiles for SCFBC and SCFBU beams

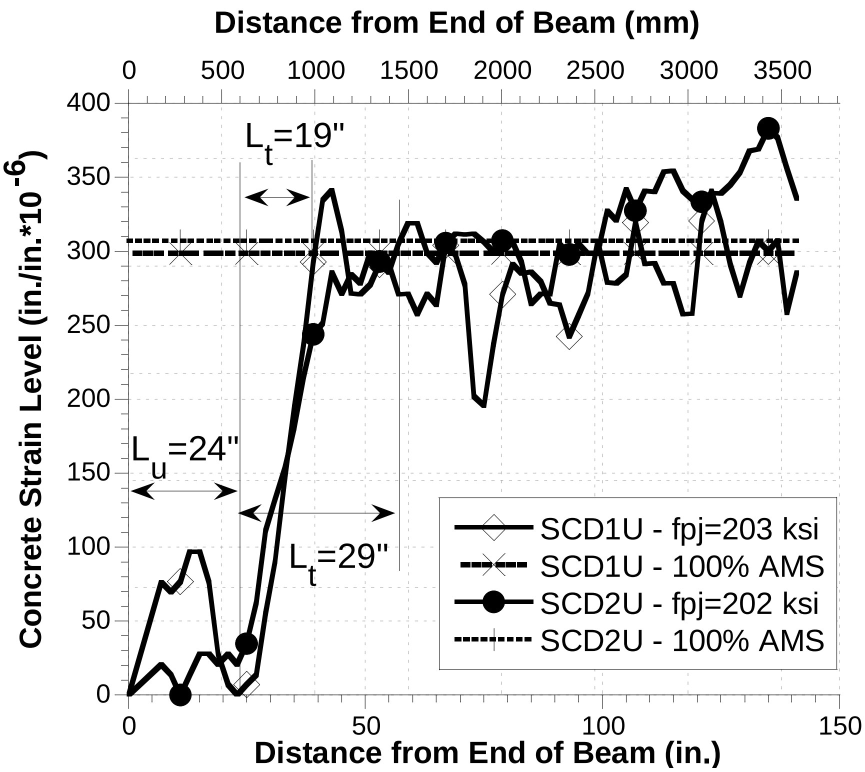

Figure 3-34 Concrete surface strain profiles: SCC beams containing partially debonded strand without confinement reinforcement

It can be seen in Figure 3-32 and Figure 3-34 that even though the beams shared the same strand line the average concrete surface strain level was different, which indicates that creep and shrinkage effects affected the final strain measurements. Table 3-6 and Table 3-7 summarize the determined transfer lengths for all beams. The force designated as f_{pj} in Table 3-6 and Table 3-7 is the applied jacking force minus the sitting losses during the pre-tensioning procedure.

Table 3-6 Transfer lengths for NCC beams

	NCFBC	NCFBU	NCD1C	NCD1U	NCD2C	NCD2U
Transfer Length (in)	19	23	22	19	19	29
f_{pj} (ksi)	203	198	203	198	201	201

1 inch = 25.4 mm, 1 ksi = 6.89 MPa

Table 3-7 Transfer lengths for SCC beams

	SCFBC	**SCFBU**	**SCD1C**	**SCD1U**	**SCD2C**	**SCD2U**
Transfer Length (in)	24	17	16	15	N/A	27
f_{pj} (ksi)	203	203	203	203	202	202

1 inch = 25.4 mm, 1 ksi = 6.89 MPa

The average transfer length for the NCC beams was found to be 22 in. (560 mm) and 20 in. (510 mm) for the SCC beams. These average values fall within two standard deviations for both sets. The transfer length values were normalized with respect to time since it is well documented that the transfer length increases with time. Transfer lengths were normalized with respect to a chosen time of six (6) hours by calculating the creep strains at this time using Equation 3-3.

$$Lt_{norm} = Lt_{measured} \frac{CreepStrain_{6hours}}{CreepStrain_{beam}} \qquad \textbf{Equation 3-3}$$

In Equation 3-3, creep strain at 6 hours is the calculated strain value due to creep effects for each batch, and creep strain in beam is the creep value calculated for each beam according to the time at which the DEMEC measurements were taken. The measured and normalized transfer length values for each beam in each set are given in Table 3-8. The normalized transfer length for beam NCD2C is not provided since the obtained value was far from the normalized average transfer length.

The initial stress values, losses due to shortening, and the calculated theoretical transfer strain values for each beam are shown in Table 3-9. In addition, the theoretical values of transferred strains obtained after taking into account creep and shrinkage, and the measured strains at 100% average strain level are also shown in this table. Creep and shrinkage effects were taken into account since they were found to be significant when comparing the experimental results to code estimates and numerical results. It was found that creep strains were particularly high. Therefore, creep strain values were added to the calculated strain values caused by the release of the prestressing force. The experimental strain level for the SCD2C beam is not shown in Table 3-9 since the results obtained from that beam were not satisfactory. Therefore, the results were discarded.

Table 3-8 Time normalized transfer lengths

Beam ID	Measured Transfer Length (in.)	Normalized Transfer Length (in.)
NCFBC	19	23
NCFBU	23	25
NCD1C	22	22
NCD1U	19	19
NCD2C	19	-
NCD2U	29	28
SCFBC	24	28
SCFBU	17	18
SCD1C	16	17
SCD1U	15	15
SCD2U	27	24

1 inch = 25.4 mm

As shown in Table 3-8, the determined and normalized transfer length values were below the 60 times nominal diameter value recommended by the AASHTO LRFD Bridge Design Specifications [2] for 0.6-in.-diameter (15.2 mm) strands, which is 36 in. (915 mm). In addition, Table 3-8 shows that the normalized transfer length values for the beams containing fully bonded strand were slightly larger than the ones obtained for debonded strand. This is attributed to the partial bond resistance along the sheathed strand length due to strand dilation, as supported by the numerical simulations presented in Chapter 4. The force transferred along the unbonded length as a percentage of the effective prestressing force was 15% and 17% for the NCC and SCC beams, respectively.

Table 3-9 Theoretical and experimental transferred strains

Beam ID	f_{pj} (ksi)	Losses due to shortening (ksi)	Theoretical strain level w/o including creep strain (μs)	Theoretical strain level including creep strain (μs)	Experimental strain level using 100% AMS method (μs)
NCD2C	201	7.0	241	292	357
NCD2U	201	7.0	241	391	435
NCFBU	198	6.9	238	370	432
NCD1U	198	6.9	238	377	436
NCFBC	203	7.1	244	360	535
NCD1C	203	7.1	244	387	368
SCD2C	202	6.2	215	270	N/A*
SCD2U	202	6.2	215	335	300
SCFBU	203	6.3	216	317	266
SCD1U	203	6.3	216	324	289
SCFBC	203	6.3	216	307	286
SCD1C	203	6.3	216	322	291

1 ksi = 6.89 MPa

As shown in Table 3-9, the calculated theoretical precompression strain level before taking into account creep and shrinkage effects did not match the experimental concrete surface strain levels. Nonetheless, once creep and shrinkage effects were taken into consideration the theoretical and experimental strain values were much closer (see Table 3-9). Figure 3-35 and Figure 3-36 show a comparison between the theoretical and experimental concrete prestress levels for both sets of beams. It is seen from these figures that the experimental results obtained from the NCC set of beams was quite higher than the theoretical calculations even though creep and shrinkage effects were included for the calculated values. However, the average difference between the experimental and calculated concrete strain values is about 13% excluding the results obtained from the NCFBC beam. On the other hand, the experimental concrete strain values measured from the SCC beam units were lower than the calculated ones about 12%.

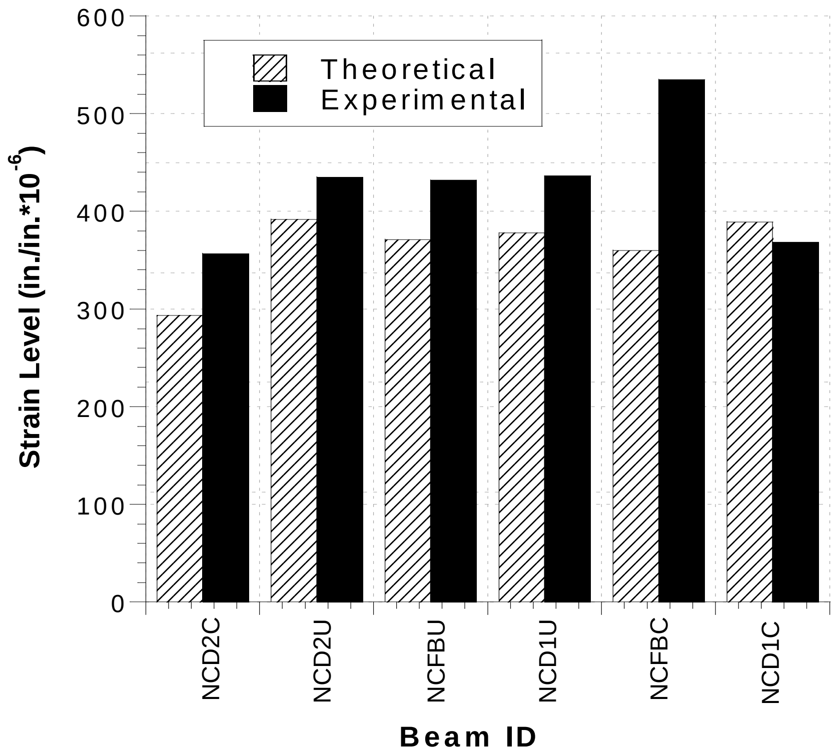

Figure 3-35 Theoretical and experimental strain level comparison – NCC beams

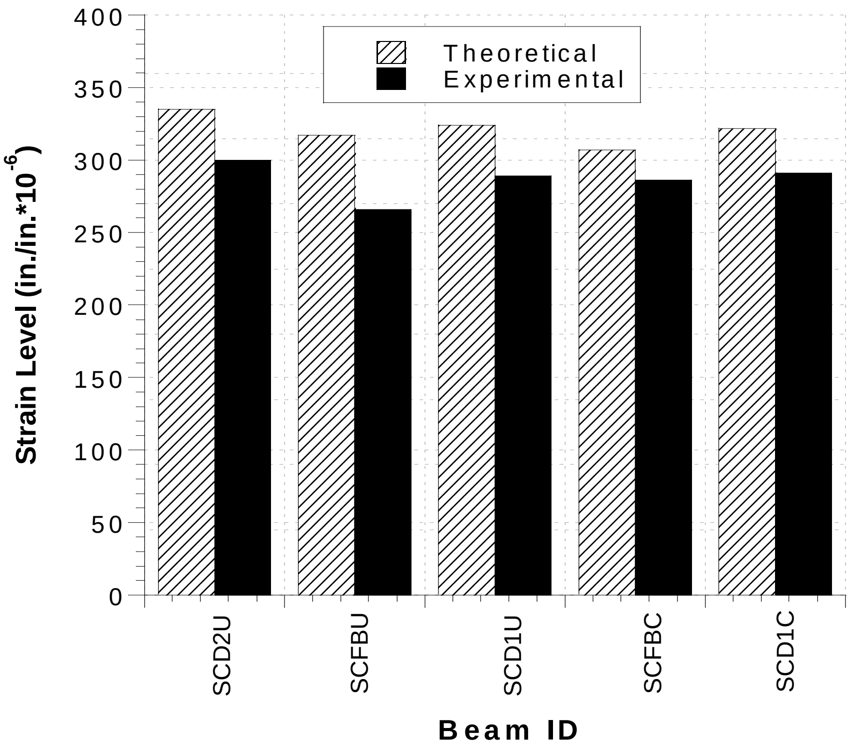

Figure 3-36 Theoretical and experimental strain level comparison – SCC beams

3.7 Findings and Discussion

The most relevant findings in the experimental program using normally-consolidated (NC) and self-consolidating (SC) concrete were:

- From pull-out tests on cylinders it was observed that the use of confinement reinforcement improved the bond strength on unstressed strands by about 11%. This was the average obtained from pull-out tests on cylinders cast with NCC and SCC.
- The maximum peak pull-out loads on simple cylinders and wall-like blocks obtained from debonded strands, whether debonding by using single or double layer flexible slit sheathing, was significantly small compared to the average peak-pull out load obtained for fully bonded strands.

- The effect of concrete hydraulic head and concrete fluidity was investigated on unbonded strands through pull-out tests on wall-like blocks. The average peak pull-out load obtained from the debonded strands was close to zero for wall blocks cast with NCC and SCC. Thus, flexible slit (tight fit) sheathing effectively eliminates the bond between the unstressed debonded strand and the surrounding concrete in a unstressed condition.
- The bond behavior of debonded strands studied using laboratory-scale beams showed that with the use of flexible slit (tight fit) sheathing, single or double layer, about 17% of the prestressing force was transferred along the debonded zone based for both, NCC and SCC beams.
- The use of confinement reinforcement along the transfer zone of two fully bonded beams did not show any improvement in bond stress transfer behavior, as judged from the concrete surface strain profiles obtained along the beam.
- Measured concrete surface strains showed that creep and shrinkage effects at an early age greatly influenced the determined transfer lengths (larger values).

CHAPTER 4 COMPUTATIONAL ASSESSMENT

4.1 Introduction

Three-dimensional nonlinear finite element models were created to study prestress bond transfer in small-scale beams containing concentric fully bonded or partially debonded strand using soft sheathing (tight fit). The models were developed using the finite element program ABAQUS [1]. The effect of additional stresses caused by the dilation of the partially debonded strands due to Poisson's effect was investigated and the influence of confinement reinforcement was incorporated. The models were calibrated with experimental data obtained from small-scale beams results (see Section 3.7). The calibrated parameter was the coefficient of friction, which was used for a nonlinear-friction model that controlled the contact interaction between the simulated strand and concrete parts in the finite element models. In addition, inelastic-material behavior of concrete was considered.

4.2 Concrete Damaged Plasticity Model

Concrete behaves as a brittle material under low confining pressure, and when the concrete is subjected to high confining pressures crack propagation in the brittle material is not observed [1]. The concrete damaged plasticity (CDP) model, option available on ABAQUS [1], gives a general capability for modeling concrete and other quasi-brittle materials such as rocks and ceramics. The model accounts for concepts of isotropic damaged elasticity combining isotropic tensile and compressive plasticity to represent the inelastic behavior of concrete. The main formulation aspects behind for the concrete damaged plasticity model are:

- Strain rate decomposition,

- Stress-strain relations,
- Hardening parameters,
- Yield function, and
- A flow rule.

The rate strain decomposition for the rate independent model is shown in Equation 4-1 [1].

$$\dot{\varepsilon} = \dot{\varepsilon}^{el} + \dot{\varepsilon}^{pl} \qquad \textbf{Equation 4-1}$$

where, the rate strain $\dot{\varepsilon}$ is decomposed into an elastic strain rate, $\dot{\varepsilon}^{el}$, and a plastic strain rate, $\dot{\varepsilon}^{pl}$. The concrete damaged plasticity model is one of the possible constitutive models that can be used to simulate failure and the recognition of crack patterns in concrete [11]. The fundamentals of any model based on the classical theory of plasticity are the yield criterion, the flow rule, and the hardening rule. The CDP model is based on the principles of the Mohr Coulomb and Drucker-Prager, which in their general formulation follow Equation 4-2.

$$F(\sigma) = c \qquad \textbf{Equation 4-2}$$

In Equation 4-2, $F(\sigma)$ is a function of the stress components and σ may be identified with the cohesion or some constant multiplier [18]. The initial part of the yield surface can be described with $c = f_{c0}$, and failure is reached when c attains its maximum along a given loading path [18]. The formation of microcracks in the concrete is represented macroscopically as softening behavior of the material, which results in localization and redistribution of strain in a structure [15].

The response from tensile and compressive damage on quasi-brittle materials are different; thus, it is not realistic to represent all damage states by a single parameter. If two state variables (f_t and f_c) representing uniaxial tensile strength and compressive strength of the material, respectively, describe the yield function, the admissible stress states are constrained by the condition shown in Equation 4-3.

$$\tilde{F}(\sigma, f_t, f_c) \leq 0 \qquad \textbf{Equation 4-3}$$

According to experimental observations, in most quasi-brittle materials, including concrete, the tendency is that the compressive stiffness is recovered upon crack closure as the load changes from tension to compression. In contrast, as the load changes from compression to tension, the tensile stiffness is not recovered once micro-cracks have developed.

The concrete damaged plasticity model [1] uses a yield condition based on the yield function proposed by Lubliner et al. [18] and incorporates the modification proposed by Lee and Fenves [15] to account for different evolutions of strength under tension and compression. The evolution of the yield surface is controlled by the hardening parameters. The yield function can be expressed in terms of effective stress, $\bar{\sigma}$, as shown in Equation 4-4 [1].

$$F\left(\bar{\sigma}, \tilde{\varepsilon}^{pl}\right) = \frac{1}{1-\alpha}\left(\bar{q} - 3\alpha\bar{p} + \beta\left(\tilde{\varepsilon}^{pl}\right)\left\langle\hat{\bar{\sigma}}_{\max}\right\rangle - \gamma\left\langle-\hat{\bar{\sigma}}_{\max}\right\rangle\right) - \bar{\sigma}_c\left(\tilde{\varepsilon}_c^{pl}\right) \leq 0 \qquad \textbf{Equation4-4}$$

where,

α and γ = dimensionless material constants,

$\bar{p} = -\frac{1}{3}\bar{\sigma} : I$ = hydrostatic pressure,

$\bar{q} = \sqrt{\frac{3}{2}\bar{S} : \bar{S}}$ = equivalent effective stress,

$\bar{S} : \bar{p}I + \bar{\sigma}$ = deviatoric part of the effective stress tensor $\bar{\sigma}$,

$\hat{\bar{\sigma}}_{\max}$ = algebraically maximum eigenvalue of effective stress tensor, and

$$\beta\left(\bar{\varepsilon}^{pl}\right) = \frac{\bar{\sigma}_c\left(\tilde{\varepsilon}_c^{\,pl}\right)}{\bar{\sigma}_t\left(\tilde{\varepsilon}_t^{\,pl}\right)}(1-\alpha)-(1+\alpha).$$

From the last expression, $\bar{\sigma}_t(\tilde{\varepsilon}_t^{\,pl})$ and $\bar{\sigma}_c(\tilde{\varepsilon}_c^{\,pl})$ are the effective tensile and compressive cohesion stresses, respectively. The variable α is determined using Equation 4-5 [1].

$$\alpha = \frac{(\sigma_{b0}/\sigma_{c0})-1}{2(\sigma_{b0}/\sigma_{c0})-1};0 \le \alpha \le 0.5 \qquad \textbf{Equation 4-5}$$

From Equation 4-5, σ_{c0} is the uniaxial compressive yield stress and σ_{b0} is the equibiaxial compressive yield stress. Another parameter that needs to be defined is the ratio of the second stress invariant on the tensile meridian, $q(TM)$, to that on the compressive meridian, $q(CM)$, K_c, at initial yield for any given value of the pressure invariant p such that the maximum principal stress is negative, $\hat{\bar{\sigma}}_{\max} < 0$ (see Figure 4-1**)** [1].

The plastic flow is governed by a flow potential function $G(\bar{\sigma})$ according to a nonassociative flow rule as shown in Equation 4-4.

$$\dot{\varepsilon}^{pl} = \dot{\lambda}\frac{\partial G(\bar{\sigma})}{\partial \bar{\sigma}} \qquad \textbf{Equation 4-6}$$

From Equation 4-4, $\dot{\lambda}$ is a nonnegative plastic multiplier [1]**.** The plastic potential is defined in the effective stress space as shown in Figure 4-2.

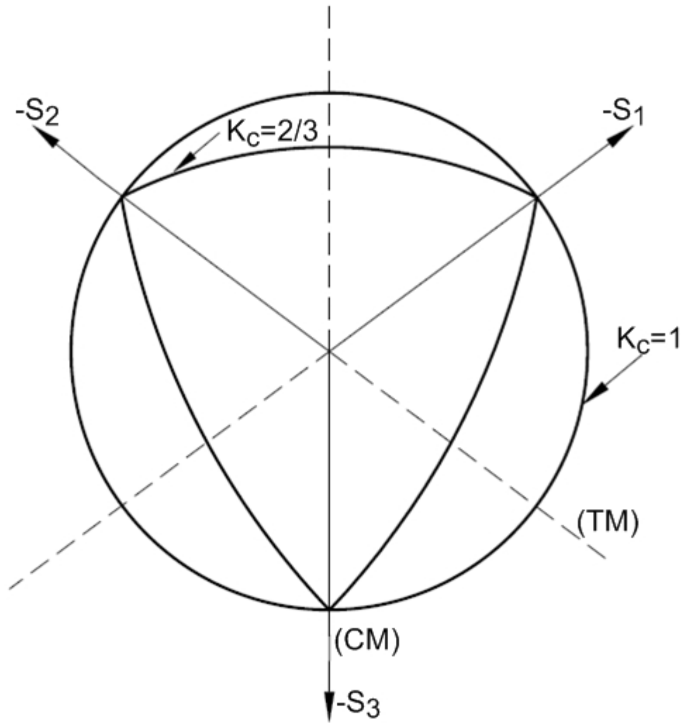

Figure 4-1 Failure surface on the deviatoric plane. Adapted from [1]

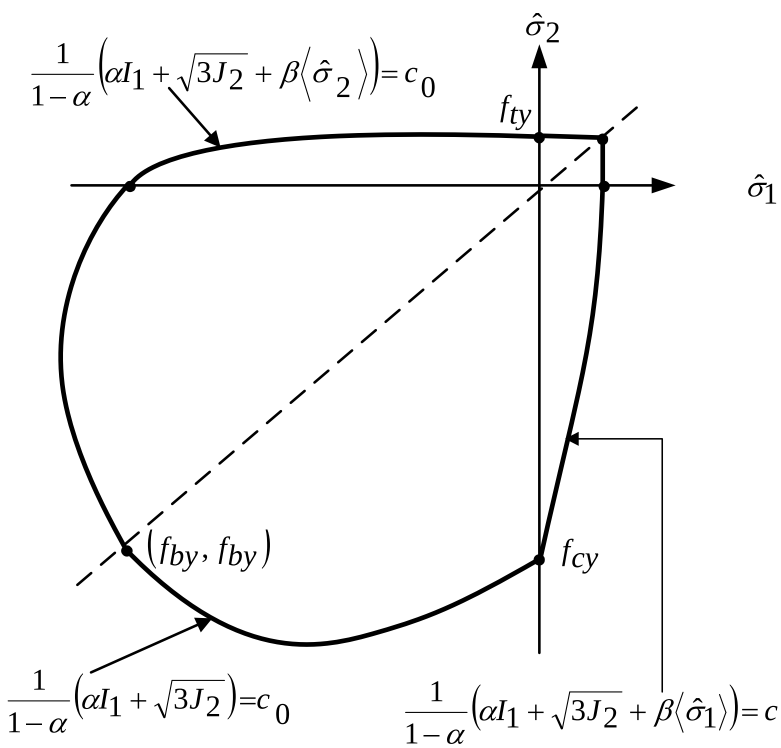

Figure 4-2 Proposed yield surface in the stress space by Lubliner (1989). Adapted from [15]

The flow potential G chosen for the concrete plasticity model is the Drucker-Prager hyperbolic function and this is shown in Equation 4-7.

$$G = \sqrt{\left(\in \sigma_{t0} \tan\psi\right)^2 + \bar{q}^2} - \bar{p}\tan\psi \qquad \textbf{Equation 4-7}$$

In Equation 4-7, ψ is the dilation angle measured in the $p-q$ plane at high confining pressure; σ_{t0} is the uniaxial tensile stress at failure; and $\in$ is a parameter related to the eccentricity that defines the rate at which the function moves toward the asymptote (see Figure 4-3a) [1]. Figure 4-3a and Figure 4-3b show the response of the concrete under uniaxial loading in tension and compression, respectively.

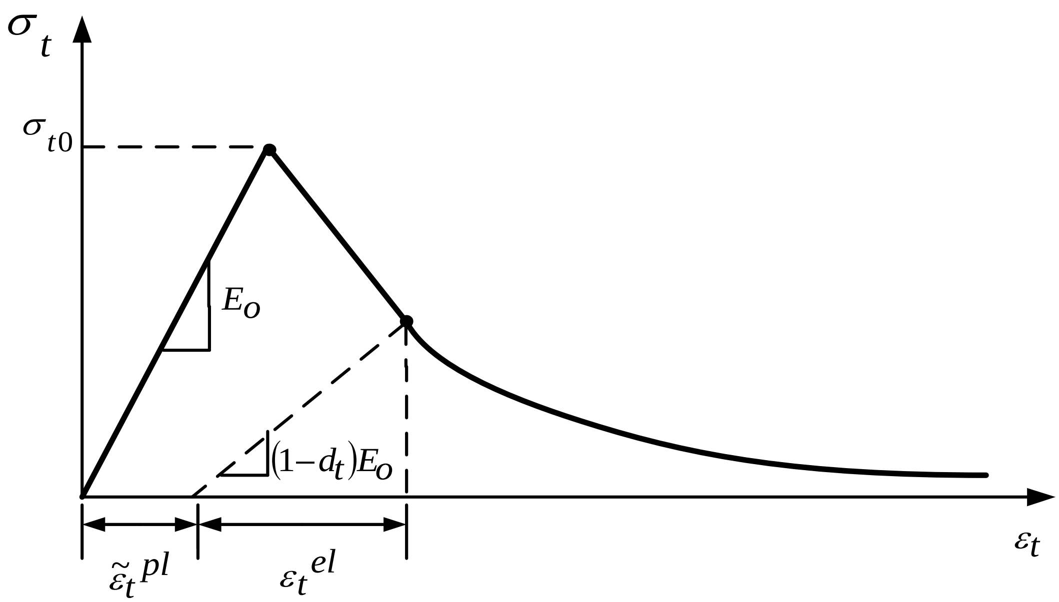

a) Tension Response

Figure 4-3 Response of the concrete under uniaxial loading. Adapted from [1]

Figure 4-3 cont'd.

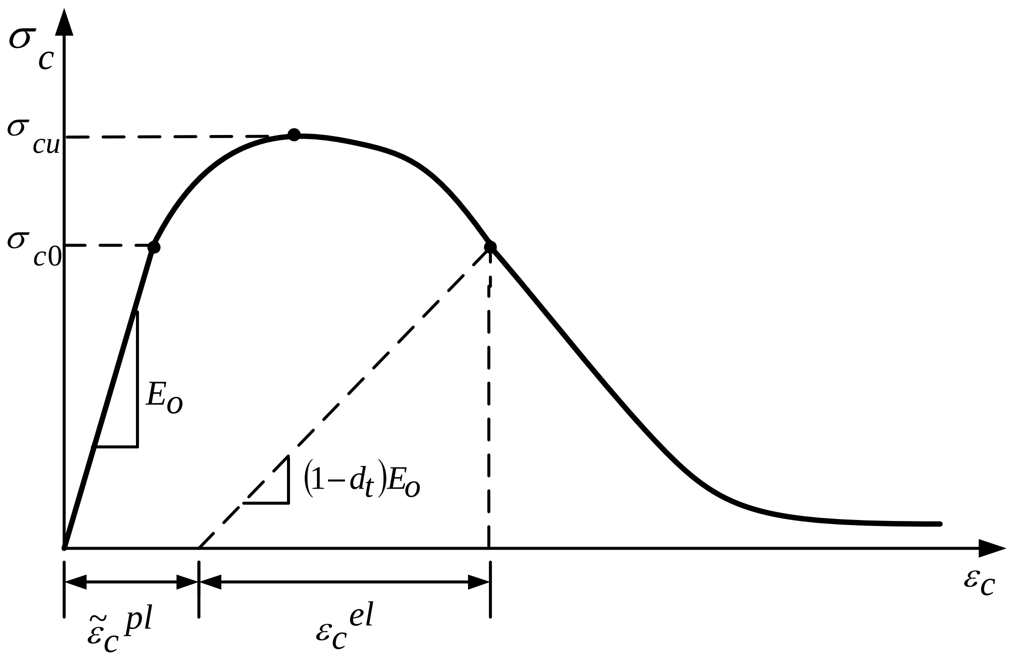

b) Compression

Under uniaxial tension, the stress-strain curve exhibits a linear-elastic response until the value of the failure stress, σ_{t0}, is reached (see Figure 4-3a). In this study, σ_{t0} corresponds to the modulus of rupture of the concrete, $f_r = 7.5\lambda\sqrt{f'_{ci}}$, where $\lambda = 1.0$ for normal weight concrete [3]. The failure stress corresponds to the initiation of micro-cracking in the concrete. If the concrete is subjected to uniaxial compression, the material behaves linear-elastically until the value of initial yielding σ_{c0} reached (see Figure 4-3b). In the plastic state, the compressive response of the concrete is usually identified by stress hardening followed by strain softening beyond the ultimate stress, σ_{cu} (see Figure 4-3b) [1]. If the concrete is subjected to high compressive loads, the propagation of cracks is reduced since cracks run parallel to the loading direction. Nonetheless, the effective load-carrying area is significantly reduced after substantial crushing of the concrete has taken place. The effective uniaxial cohesion stresses, $\bar{\sigma}_t$ and $\bar{\sigma}_c$, can be determined using Equation 4-8 and Equation 4-9, respectively.

$$\bar{\sigma}_t = E_o\left(\varepsilon_t - \tilde{\varepsilon}_t{}^{pl}\right) \qquad \textbf{Equation 4-8}$$

$$\bar{\sigma}_c = E_o\left(\varepsilon_c - \tilde{\varepsilon}_c{}^{pl}\right) \qquad \textbf{Equation 4-9}$$

4.2.1 Parameters and Assumptions on the CDP Model

In order to incorporate the concrete damaged plasticity (CDP) model in the numerical simulations for this research, plasticity parameters need to be defined. The values of the variables can be found from experiments or the default values available in ABAQUS [1] can be preliminary used. A summary of the parameters that need to be defined is presented in the following.

- Dilation angle, ψ, in the $p-q$ plane. The value needs to be entered in degrees.
- Eccentricity, ∈, which is a small positive number that defines the rate at which the hyperbolic flow potential approaches its asymptote. The default value in ABAQUS is 0.1.
- The ratio of initial equibiaxial compressive yield stress (σ_{b0}) to initial uniaxial compressive yield stress (σ_{c0}), f_{b0}/f_{c0}. Experimental values of f_{b0}/f_{c0} range from 1.10 to 1.16 [18]. The default value in ABAQUS is 1.16.
- K_c is the ratio of the second stress invariant on the tensile meridian, $q(TM)$, to that on the compressive meridian, $q(CM)$, at initial yield for any given value of the pressure

invariant p. The following condition must bet satisfy: $0.5 < K_c \le 1.0$. The default value in ABAQUS is 2/3.

- Viscosity Parameter, μ, use for the visco-plastic regularization of the concrete constitutive equations [1]. This value was selected by trial and error procedure and chosen to be 0.02. The viscosity parameter must be kept as small as possible for accurate results.

The compressive stress data is to be provided as a tabular function of inelastic (crushing) strain, $\tilde{\varepsilon}_c^{in}$. Positive (absolute) values shall be given for the compressive and tensile stress and strain curves. The stress-strain curve can be defined beyond the ultimate stress into the strain-softening state [1].

4.3 Description of the Contact Interaction Friction Model in ABAQUS

Surfaces in contact can transmit shear and normal forces. The relationship between these two types of forces is known as friction, which is usually expressed in terms of the stress at the interface of the surfaces in contact as shown in Figure 4-4-a.

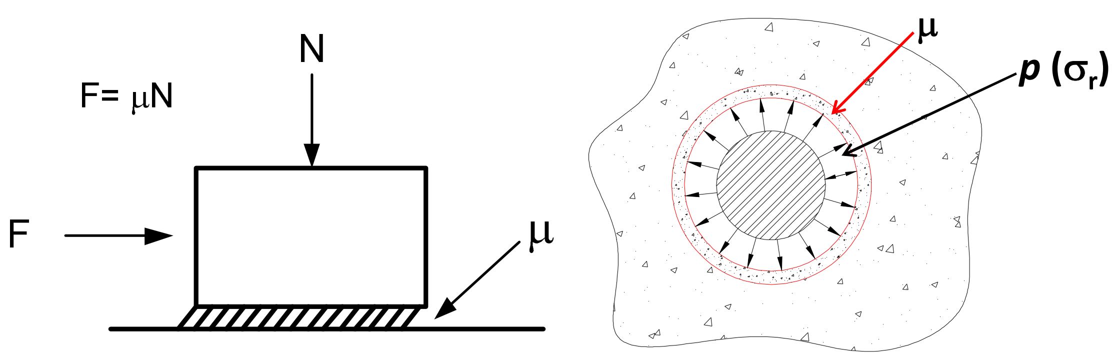

a) Classical Coulomb friction model **b) Schematic of the strand dilation**

Figure 4-4 Schematic of the basic Coulomb friction model and radial pressure due to dilation of strand upon release

The friction model available in ABAQUS [1] gives the option of defining static and kinetic coefficients of friction with a smooth transition zone defined by a decay curve. The critical shear stress, $\bar{\tau}_{crit}$, is the stress at which sliding of the surfaces in contact begins as a fraction of the contact pressure (p) between surfaces, $\bar{\tau}_{crit} = \mu * p$, μ is the coefficient of friction. This critical shear stress can be defined using the classical Coulomb friction model (see Figure 4-4-a). A static coefficient of friction can be defined for the friction model and this is known as the "stiffness (penalty) method" [1]. Once the maximum shear stress is exceeded, sliding of the surfaces with respect to each other will occur. In the real case of the strand in contact with concrete, the normal behavior (N as shown in Figure 4-4a) is developed by the radial pressure exerted to the concrete as the strand dilates upon release (see Figure 4-4-b). Longitudinal friction forces are developed by the mechanical interlock mechanism and friction between the two surfaces creating the tangential interaction between the strand and the surrounding concrete. This behavior is simulated by the aforementioned normal and tangential models and is referred herein as a nonlinear friction model.

In ABAQUS [1], the stick/slip calculations determine when a point changes from sticking to slipping or vice versa. The maximum shear stress $\bar{\tau}_{\max}$ can be specified when using the friction model [1]. An acceptable upper bound for estimating the value of $\bar{\tau}_{\max}$ is $\sigma_y / \sqrt{3}$, where σ_y is the Von Mises yield stress of the material adjacent to the surface. Figure 4-5 shows the sticking and slipping frictional states of the friction model. As it can be seen, the slope of the curve is related to the sticking-friction state (linear-elastic region). The slipping friction state is related to the plastic regime, and this takes place when $\bar{\tau}_{crit}$ is reached [1]. The response shown in Figure 4-5 is comparable to the behavior of an elasto-plastic material without hardening where κ would correspond to the elastic modulus and τ_{crit} represents the yield stress.

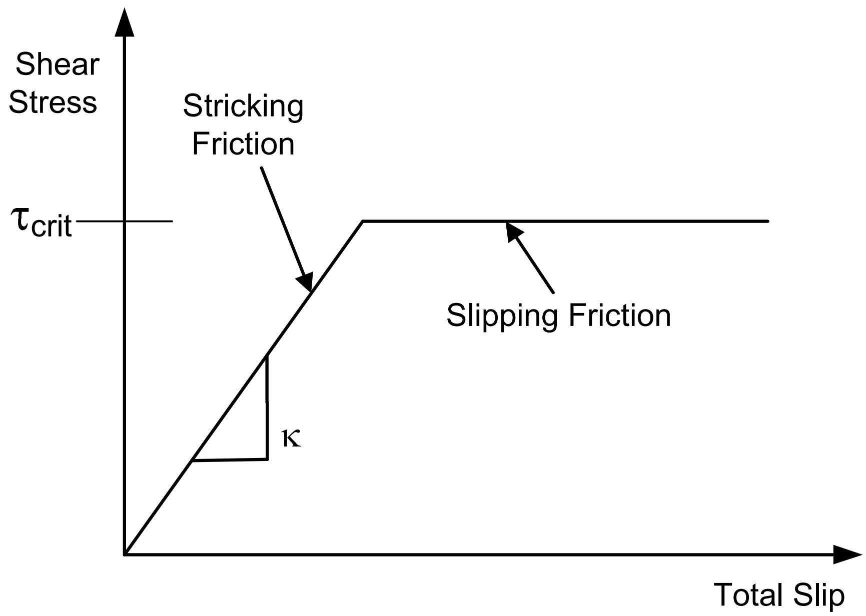

Figure 4-5 Sticking and slipping friction. Adapted from [1]

The nonlinear friction model is implemented in ABAQUS by using a contact constraint and such a constraint is activated in the finite element model when the distance separating two node surfaces defined with the possibility to be in contact becomes zero. If the contact pressure between the surfaces in contact becomes zero or negative, the constraint is removed and the surfaces separate. This behavior is referred to as “hard contact” and it is the default contact behavior in ABAQUS [1].

4.4 Modeling of Prestress Bond Transfer in 2-D and 3-D Models

According the goal of the investigation, prestress bond transfer can be modeled using different approaches. Mirza and Tawfik [19] developed a one-dimensional (1D) model to study the restraint effect in beam end-cracking and valuable contributions were obtained from this model, namely, that the short free length of the uncut strands can lead to high stresses in the end region. Kannel et al. [13] developed 3D numerical models to study the stress distribution in the end region of pretensioned concrete girders. The strand was modeled as truss elements embedded in the concrete and the prestressing force was transferred into the concrete at nodes where the truss elements were connected to the concrete region, as shown in Figure 4-6. The models by Kannel et al. were developed to show the effect of strand release sequence on the stress state in anchorage zones. Another modeling technique using 1D elements is to connect the truss elements to the concrete elements (2D or 3D) by means of springs. This technique allows for distinct modeling of tensile and compressive stress transfer behavior.

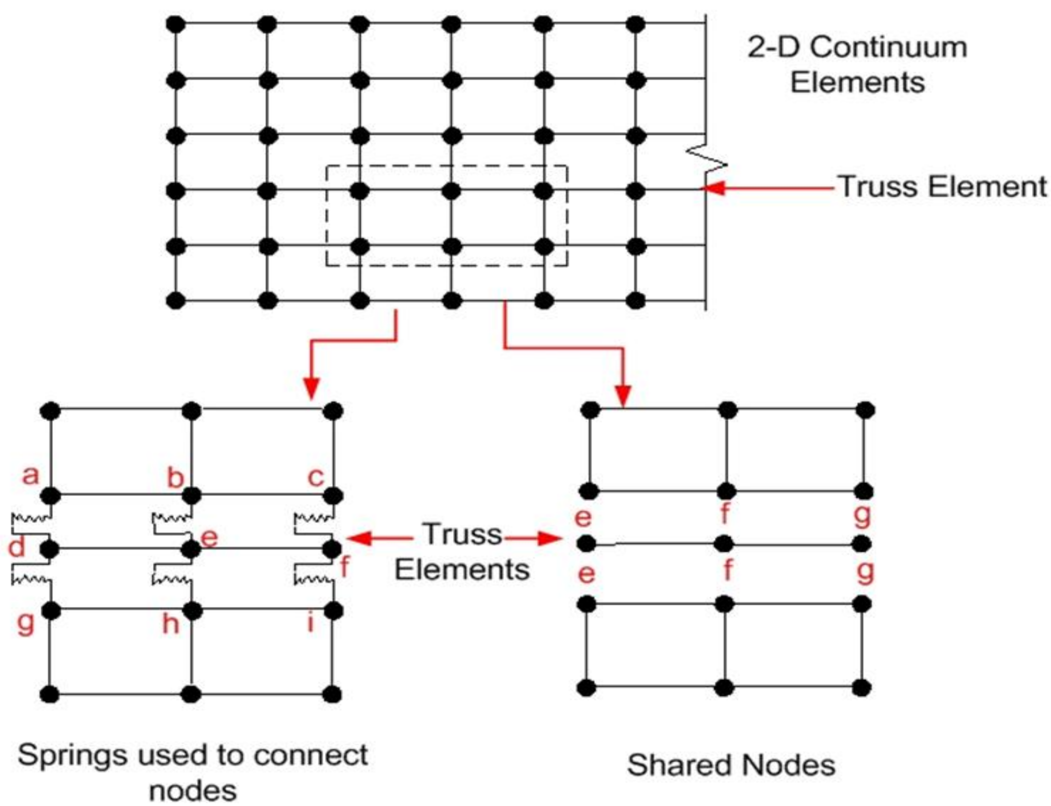

Figure 4-6 Prestress bond transfer in 2D

The use of truss elements in a simulation model does not allow for capturing the dilation of the strand due to the Poisson's effect from detensioning. One of the goals of this study was to investigate the stress state in the beam end regions due to the dilation of the partially debonded strand upon detensioning and the effects that this may have in beam-end cracking. Thus, modeling of the strand using three-dimensional continuum elements was needed. Figure 4-7 shows an isometric view of a beam and the strand indicating the surfaces to be in contact. In this figure, the strand was modeled as a simplified circular rod since this facilitated computational demand and the simulation of prestress bond transfer using surface contact interaction definitions, as described in Section 4.3.

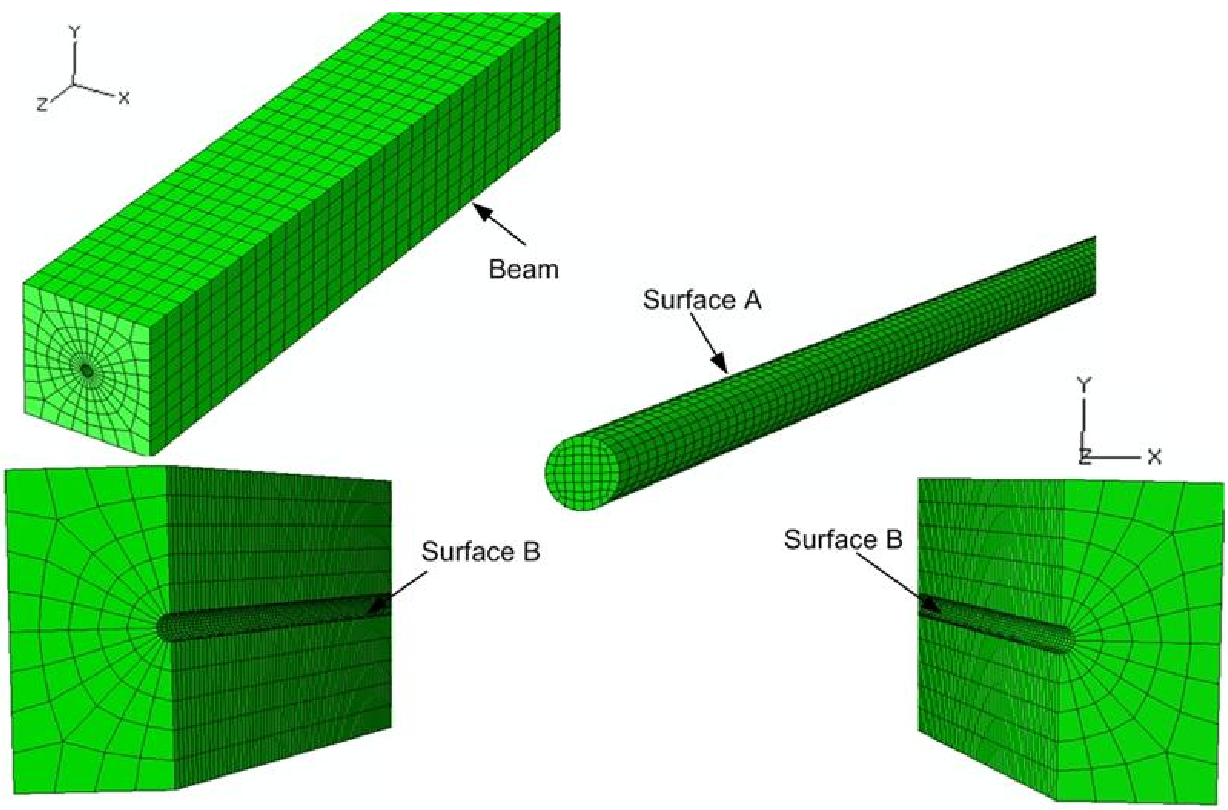

Figure 4-7 3D Modeling of prestress bond transfer using contact interaction definitions

4.5 Numerical Modeling of Laboratory-Scale Beams

Three-dimensional (3D) nonlinear finite element (FE) models that replicated the beams in the experimental study presented in Section 3.6 were created and analyzed to emulate the bond stress transfer behavior using the program ABAQUS [1]. The FE models incorporated inelastic behavior and damage to the concrete material using the built-in material models in ABAQUS. The high-fidelity three-dimensional models considered surface interaction definitions (see Section 4.3) between the strand and concrete to model the stress transfer between the two. The main parameter for the definition of the surface interaction model was the coefficient of friction. Use of the "hard-contact" surface interaction model in ABAQUS[1] requires the definition of tangential and normal behaviors. For the tangential behavior, a nonlinear friction formulation and a coefficient of friction were defined. For the normal behavior, a contact constraint was applied when the distance separating two surfaces in contact becomes zero such that radial stresses develop as the strand tries to expand and the two surfaces cannot penetrate each other.

The aim of this simulation was to model bond stress transfer behavior to obtain basic numerical parameters that control the surface interaction definitions needed to model realistic bond behavior of prestressing strand in concrete beams. The FE beam models were calibrated by comparing the numerically calculated and the experimentally measured concrete surface strain profiles along the beam length. The calibrated parameter was the coefficient of friction, which controls the nonlinear-friction model. The value of the coefficient of friction obtained from the calibration was used the case study presented in Chapter 5.

4.5.1 Description of the FE Beam Model

The characteristic finite element model developed for this task is shown in Figure 4-8 and Figure 4-9. The beam had a cross section of 6”x6” (150 mm x 150 mm), as the tested laboratory-scale beams (see Section 3.6). One half of the beam was modeled due to symmetry along the Z-axis, 120” (3050 mm). Eleven FE beam models were created and analyzed. The models followed the experimental test matrix given in Figure 3-23. Four models had a concentric fully bonded strand and the rest had a concentric partially debonded strand. The unbonded length was 24 in. (610 mm) and a tight-fit was provided along the debonded length to simulate the flexible slit sheathing. With a tight fit between the strand and the surrounding concrete, radial stresses develop upon release. The strand was modeled as a cylindrical rod with a diameter of 0.5268” (13.4 mm), which was determined to match the area of the prestressing 0.6-in. (15.2 mm) diameter strand (0.218 in.^{2} [140 mm^2]). The strand was stressed using the initial stress condition [1]. The input stress values were those obtained from the experimental program (see Table 3-6 and Table 3-7). The model had just one loading step in which the prestressing force was transmitted into the concrete member. For the normal behavior of the friction model the overclosure pressure was defined as “hard contact” or as impenetrable surfaces. For the nonlinear friction model, the tangential behavior was defined as penalty, and the coefficient of friction was the parameter to be calibrated. The maximum shear stress value was not specified. The coefficient of friction influences the transfer length and the stress transfer rate; however, the coefficient of friction in these models was an artificial parameter that was used/calibrated to account for the mechanical interlock and friction bond mechanisms. The coefficient of friction was changed by trial and error until the transfer length from the numerical model closely matched (± 1 in. [25.4 mm]) the values experimentally obtained.

For the partially debonded beam models, the coefficient of friction along the debonded length was defined as 4.5 percent of the coefficient of friction given along the fully bonded region. This followed the experimental observations that a small level of prestressing force was transferred along the debonded region. The value of 4.5 percent was obtained from the wall-like block results (see Section 3.5.3) by calculating the ratio of the average maximum pull-out force for the debonded strand group to the average peak pull-out load for the group of fully bonded strand, group which was found to be 0.045

Continuum three-dimensional, C3D8 (eight-node linear brick), elements were used for the concrete and the strand parts in the FE model. The mesh size for the beam was approximately 1”x1”x1” (25.4 mm x 25.4 mm x 25.4 mm), and the elements of the strand varied in cross section and their length was 1 in. (25.4 mm [see Figure 4-9]). The concrete damaged plasticity (CDP) model (see Section 4.2) was used in the numerical models. The linear-elastic material properties of the concrete and the plasticity parameters for the normally-consolidated concrete and self-consolidated concrete sets of beams are shown in Table 4-1 and Table 4-2, respectively. For the strand, linear-elastic material properties were defined. The value of the Young’s modulus was defined as 29,000 ksi (200 GPa) and the Poisson’s ratio was set equal to 0.3. An overview of the beam model is shown in Figure 4-8 to Figure 4-11, and the end-region of the model is shown in Figure 4-9. Some of the plasticity parameters shown in Table 4-1 and Table 4-2 were obtained from the literature. The value of the dilation angle was obtained from Jankowiak and Lodygowsky [11]. The remaining values were based on the default values recommendations from ABAQUS [1]. The viscosity parameter was selected by trial and error.

.

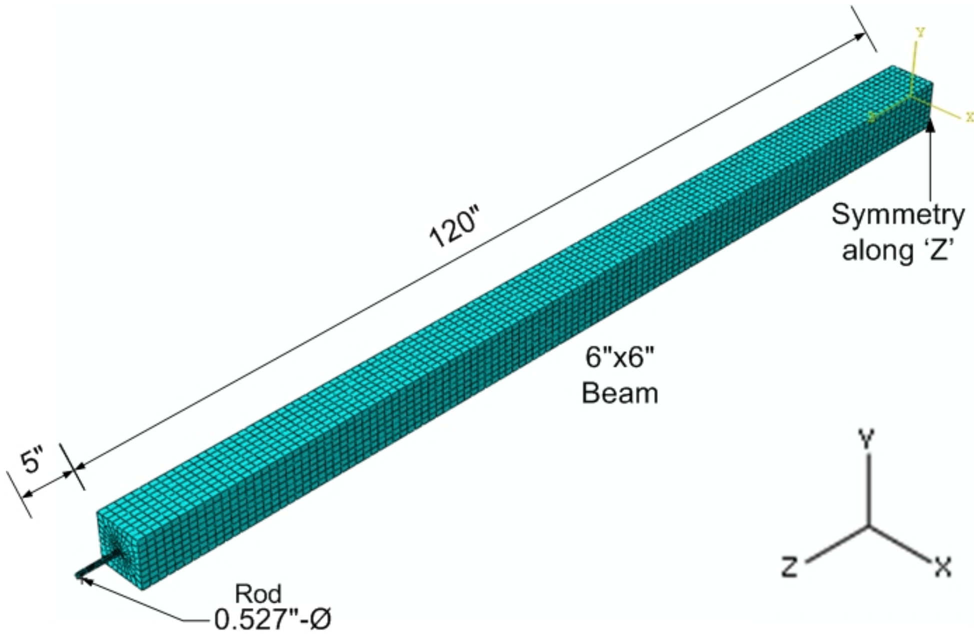

Figure 4-8 Geometry of the numerical beam model

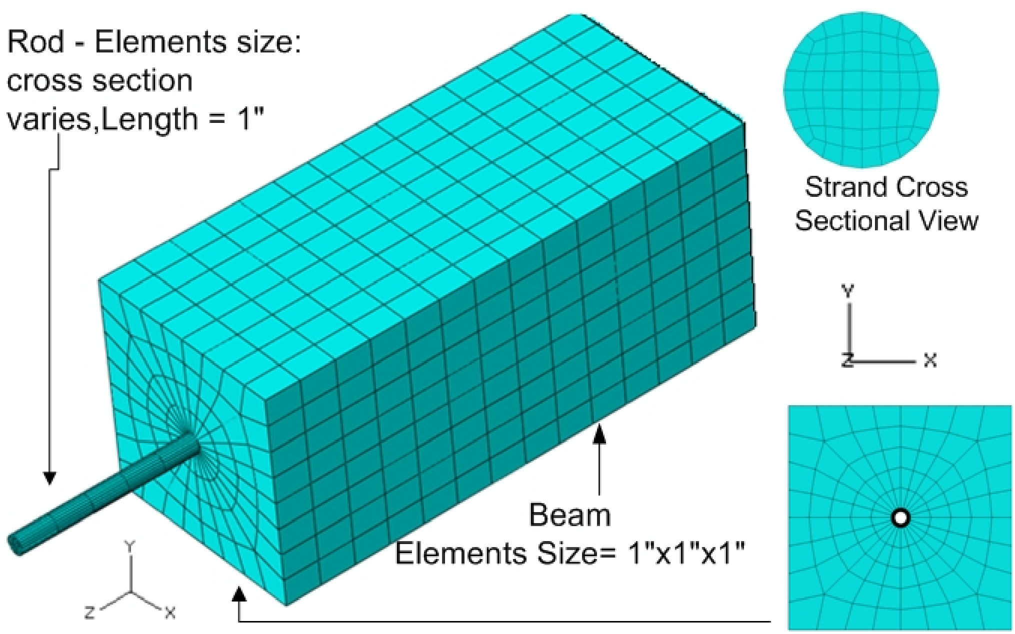

Figure 4-9 End region of the FE beam model

When the theoretical and experimental concrete strain levels due to the prestress release were first compared, it was found that the experimental values were higher than the calculated ones. Further inspection indicated that this was due to creep and shrinkage effects (see Section 3.6). To account for those effects in the numerical models, temperature load was applied to the beam to simulate the additional creep and shrinkage effects. The thermal expansion coefficient was fixed to one, and temperature was gradually applied along the transfer length and fully applied beyond the transfer region (see Figure 4-10 and Figure 4-11). The maximum temperature value that was applied to each beam was obtained from the difference between the maximum longitudinal strain value of obtained from the FE beam model before applying temperature and the 100% AMS experimental value obtained for that specific beam (see Section 3.6). Temperature load was applied along the transfer zone in increments of 10 percent. Representative results from the calibrated FE small-scale beam models are shown in Section 4.5.2.

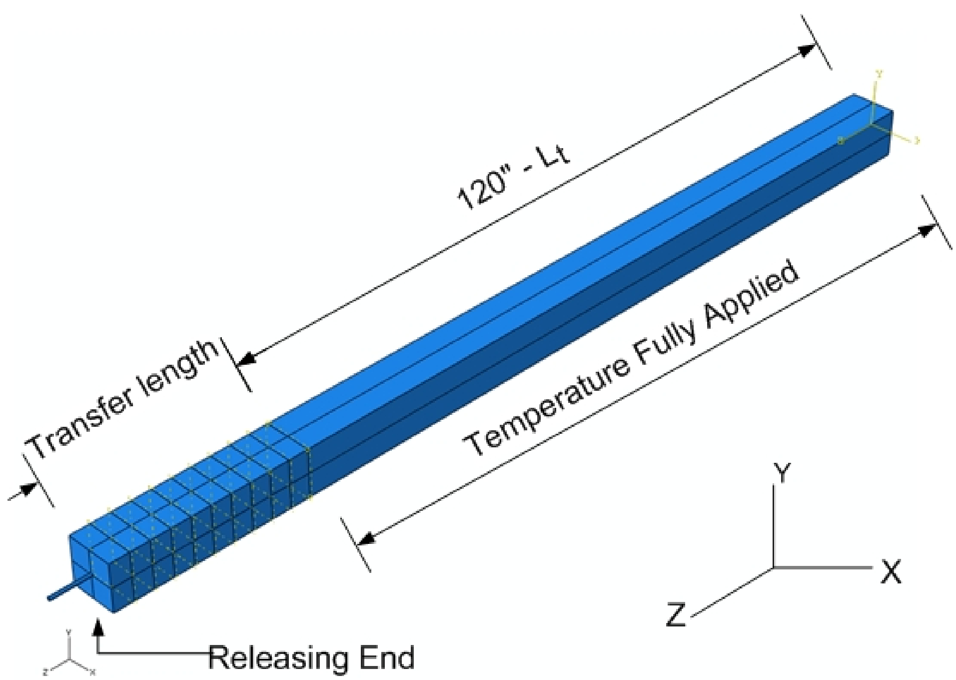

Figure 4-10 Fully bonded beam model

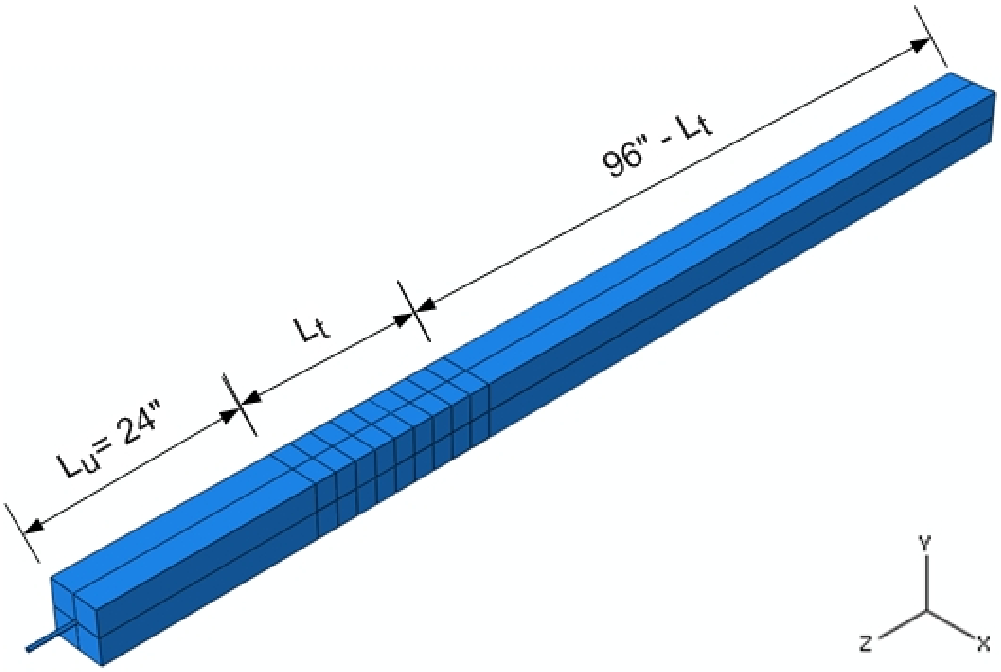

Figure 4-11 Typical debonded beam model

Table 4-1 Concrete damaged plasticity model parameters for NCC FE models

Concrete parameters	**f'_{ci}=7300 psi**	**Parameters for CDP model**	
		Dilation Angle	38°
Concrete Elasticity		Eccentricity	0.1
E_c (ksi)	4870	fb0/fc0	1.16
ν	0.2	K_c	0.67
		Viscosity parameter	0.02
Concrete compression hardening		**Concrete tension stiffening**	
Stress (psi)	Crushing strain	Stress (psi)	Cracking Strain
1209.0	0	640	0
4710.1	0.000026	375	0.000868
6480.7	0.000160	288	0.002868
7195.5	0.000512	248	0.004868
5733.8	0.001314	198	0.009868
3652.1	0.002245		
1281.6	0.003735		
625.8	0.004621		
274.3	0.005693		
160.5	0.006467		

1 MPa= 145 psi

Table 4-2 Concrete damaged plasticity model parameters for SCC FE models

Concrete parameters	**f'_{ci}=9400 psi**	**Parameters for CDP model**	
		Dilation Angle, ψ	38°
Concrete Elasticity		Eccentricity, Є	0.1
E_c (ksi)	5526	fb0/fc0	1.16
ν	0.2	K_c	0.67
		Viscosity parameter	0.02
Concrete compression hardening		**Concrete tension stiffening**	
Stress (psi)	Crushing strain	Stress (psi)	Cracking Strain
1381.6	0	727	0
5482.2	0.000008	364	0.001868
7885.7	0.000073	291	0.004368
9287.0	0.000320	242	0.007868
9134.3	0.000597	225	0.009868
5557.8	0.001744		
1556.4	0.003218		
442.0	0.004170		
147.9	0.004973		
24.8	0.006496		

1 MPa= 145 psi

4.5.2 Results of Simulations on Bond Transfer on Prestressed Concrete Beams

Representative results of the calibrated beam models are presented herein. Concrete surface strain profiles were obtained from each beam model along the longitudinal direction. In addition, plot contours from each model were obtained to illustrate the longitudinal forces and axial and transverse stress/strain from the strand's Poisson effect. A complete set of results obtained from the FE models is given in Appendix C.

The naming convention for stress and strains output from ABAQUS is as follows. The X, Y, and Z axes are represented by numbers 1, 2, and 3, respectively. The letter E represents strain, and the letter S means stress [1]. Figure 4-12 shows the normal and shear stresses in a differential element.

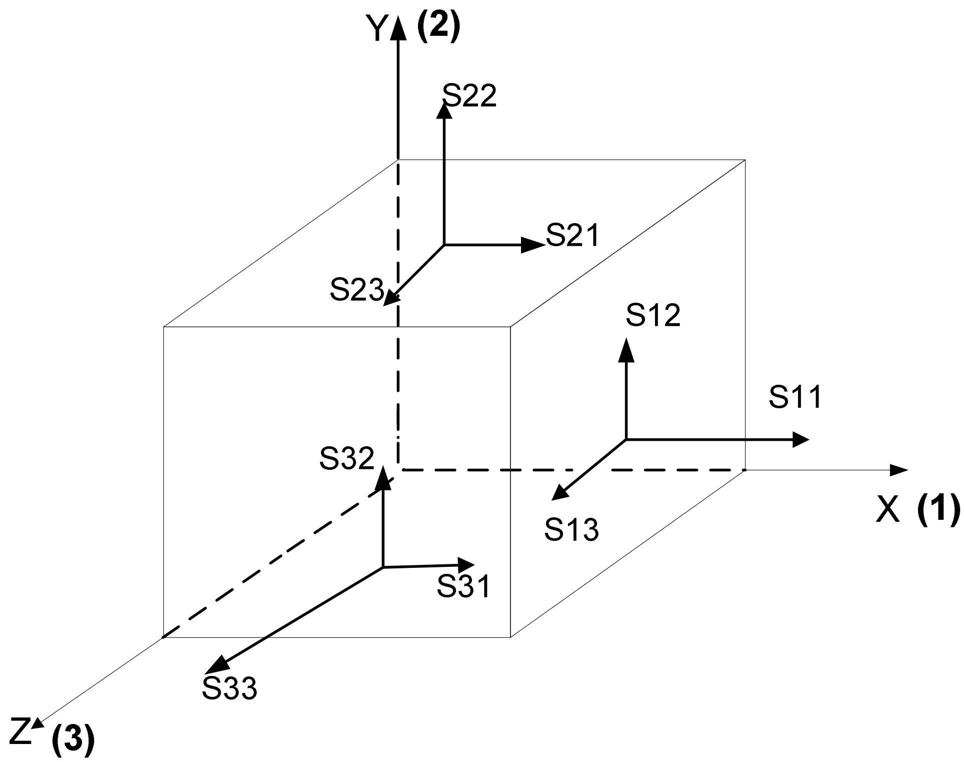

Figure 4-12 Differential element subjected to normal and shear stresses

a) Concrete Surface Strain Profile Curves

The concrete surface strain (CSS) profile curve obtained from each model was closely matched to their respective experimental CSS curves (see Section 3.6). It is well-known that transfer length increases with time. One of the main contributors to this time-dependent change is creep. Therefore, it was needed to normalize the coefficients of friction obtained from each beam model to a common time at which the longitudinal strain measurements were taken during the tests. The chosen time was six hours after the release of the first strand line. Equation 4-10 shows the expression used to normalize the coefficients of friction,

$$\mu_{norm} = \frac{\mu * (\varepsilon_{cbeam})}{\varepsilon_{c\,NCC}}$$ **Equation 4-10**

where, μ represents the static coefficient of friction for a specific beam model; ε_{cbeam} is the creep strain value calculated according to the time at which longitudinal strain measurements were taken for that specific beam; and, ε_{cNCC} is the creep strain value calculated at a time of six hours after releasing the first strand. The latter was a common value for all six numerical beam models for the normally-consolidated concrete (NCC) set of beams. The creep strain value was different for the SCC set of FE beam models since the compressive strength at release for both groups was not the same. For the NCC set of beams, the creep strain value was found to be 135 μs, and for the SCC group it was equal to 100 μs. A summary of the coefficients of friction obtained for each beam model, the time at which measurements were taken during the tests, and the normalized coefficients of friction are shown in Table 4-3.

Table 4-3 Summary of coefficient of friction used in calibration of models

Beam ID	Coefficient of friction	Time @ measurement (minutes)	Normalized coefficient of friction based on creep strain at 6 hours
NCFBC	0.65	180	0.53
NCFBU	0.55	300	0.51
NCD1C	0.65	380	0.66
NCD1U	0.55	360	0.54
NCD2C	0.7	30	-
NCD2U	0.45	435	0.47
SCFBC	0.5	210	0.43
SCFBU	0.75	300	0.71
SCD1C	0.85	280	0.78
SCD1U	0.8	378	0.79
SCD2U	0.5	540	0.56

The purpose of normalizing the coefficients of friction was to obtain an average value with a lower standard deviation and account for the variation on the experimentally obtained transfer lengths due to creep effects. The coefficients of friction obtained from each beam model (see fourth column in Table 4-3) were further normalized based on a release strength of 8,000 psi (55 MPa) and an initial prestressing force, f_{si}, of 202.5 ksi (1396 MPa) using Equation 4-11. The final values are shown in Table 4-4.

$$\mu'(f_{si}) = \frac{\mu_{norm} * \sqrt{8}(ksi)}{\sqrt{f'_{ci}}(ksi)} * \frac{f_{pi}(ksi)}{202.5(ksi)} \qquad \textbf{Equation 4-11}$$

In Equation 4-11, f_{pi} is the initial prestressing force after sitting losses, and f'_{ci} is the compressive strength at release. A compressive strength of 8 ksi (55 MPa) and an initial prestressing force equal to 202.5 ksi (1396 MPa) were selected to normalize the values of the coefficient of friction since these values were used for the case study presented in Chapter 5. The coefficients of friction presented in Table 4-3 (last column – right side) were also normalized based on the above mentioned release strength and on an effective prestressing force, f_{se}, of 189.5 ksi (1,307 MPa) using Equation 4-12, and this value was obtained assuming 13 ksi (89.6 MPa) in instantaneous prestress losses, which was the average value obtained from the FE beam models.

$$\mu'(f_{se}) = \frac{\mu_{norm} * \sqrt{8}(ksi)}{\sqrt{f'_{ci}}(ksi)} * \frac{f_{se}(ksi)}{189.5(ksi)} \qquad \textbf{Equation 4-12}$$

Table 4-4 Normalized coefficients of friction based on f'$_{ci}$= 8 ksi and on f_{si} = 202.5 ksi

Beam ID	Values normalized based on f_{si} = 202.5 ksi		Statistics on Normalized Coef. Of Friction		
	Normalized Coef. of Friction	f'$_{ci}$ (ksi)	Mean	Standard Deviation	Coef. of Variation (COV)
NCD1C	0.690	7.3	0.69	0.0585	0.0851
NCD1U	0.604	7.3			
SCD1C	0.724	9.4			
SCD1U	0.731	9.4			
NCFBU	0.545	7.3	0.60	0.08	0.1330
SCFBU	0.658	9.4			

1 ksi = 6.89 MPa

Table 4-5 Coefficients of friction normalized on f_{se} = 189.5 ksi and f'$_{ci}$=8 ksi

Beam ID	Values normalized based on f_{se} = 189.5 ksi		Statistics on Normalized Coef. Of Friction		
	Normalized Coef. of Friction	f'$_{ci}$ (ksi)	Mean	Standard Deviation	Coef. of Variation (COV)
NCD1C	0.602	7.3	0.60	0.068	0.1129
NCD1U	0.507	7.3			
SCD1C	0.645	9.4			
SCD1U	0.657	9.4			
NCFBU	0.52	7.3	**0.59**	0.1103	0.1845
SCFBU	0.676	9.4			

1 ksi = 6.89 MPa

It can be seen from Table 4-4 and Table 4-5 that the mean value of the coefficient of friction based on a compressive strength at release of 8,000 psi (55 MPa) was 0.59. This value was used for the case study presented in Chapter 5. After applying temperature on the concrete and releasing the prestressing force, the concrete surface strain (CSS) profile curves for the models were obtained by creating a longitudinal path at mid-height of the beam-part (same location as the experimentally measured CSS) as shown in Figure 4-13.

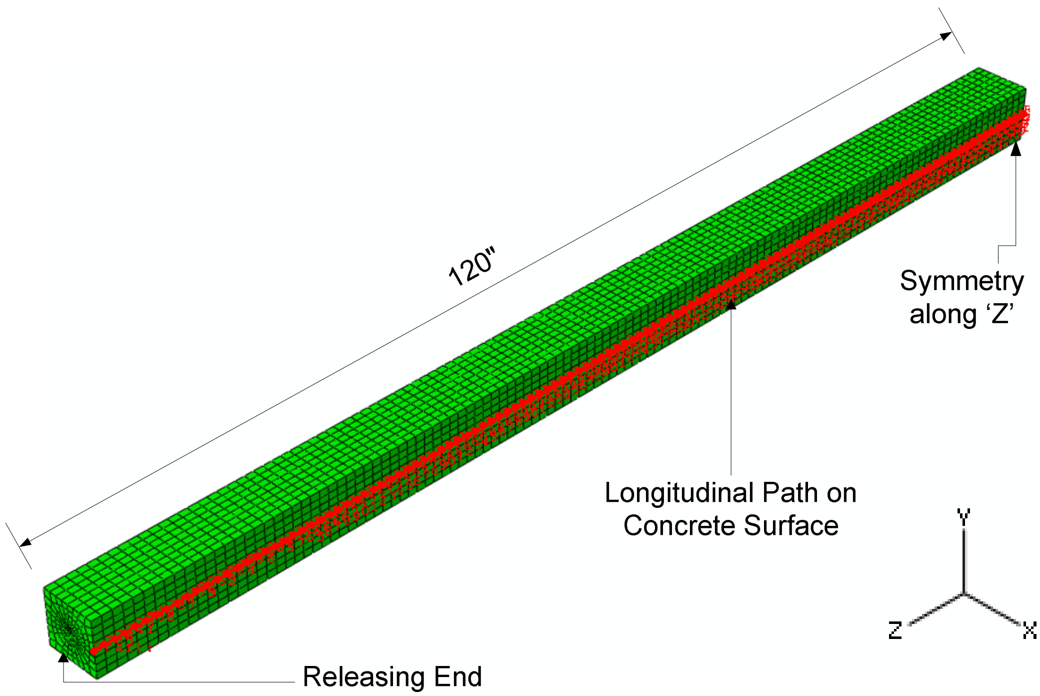

Figure 4-13 Longitudinal path along the FE beam models

Figure 4-14 and Figure 4-15 show the concrete surface strain profiles for two FE beam models versus the corresponding experimental CSS traces. It can be seen that the FE and experimental CSS traces match each other well. Calibration of the self-consolidated concrete (SCC) beams is shown in Figure 4-16 and Figure 4-17.

Figure 4-16 shows the calibrated FE response and the experimentally measured concrete surface strain profiles for the SCFBU beam. The CDP model was not used in this particular model due to numerical problems (lack of convergence) attributed to the high compressive strength and coefficient of friction needed to match the experimental transfer length. Because of this issue, the results in Figure 4-16 were obtained from a linear-elastic analysis. The differences between a linear-elastic and an inelastic analysis in terms of stress and strain values are discussed in Section 4.7. However, it was verified that material behavior of the concrete does not affect transfer length in the FE models.

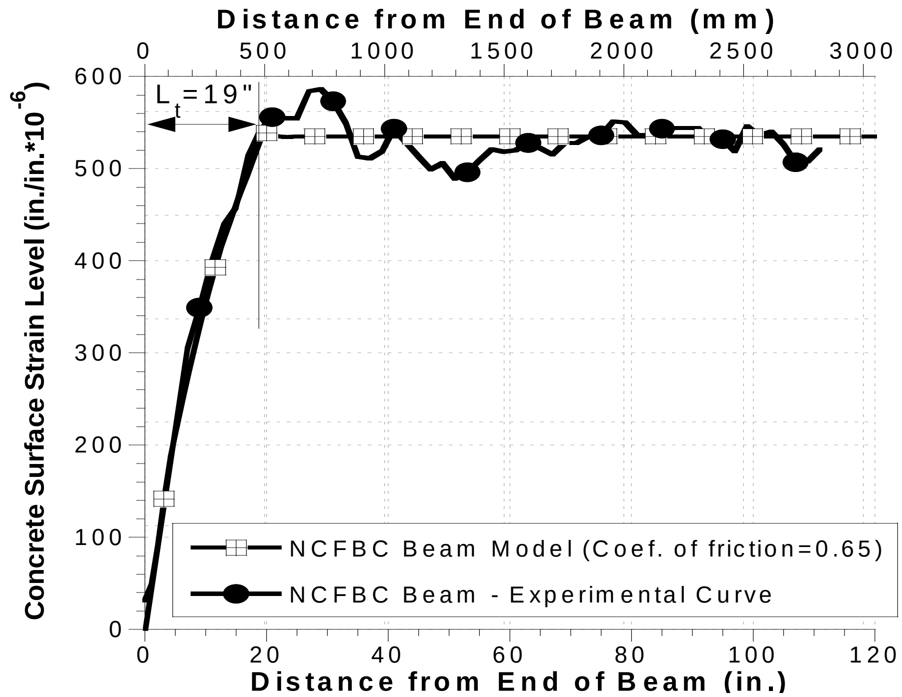

Figure 4-14 NCFBC beam model vs. experimental data

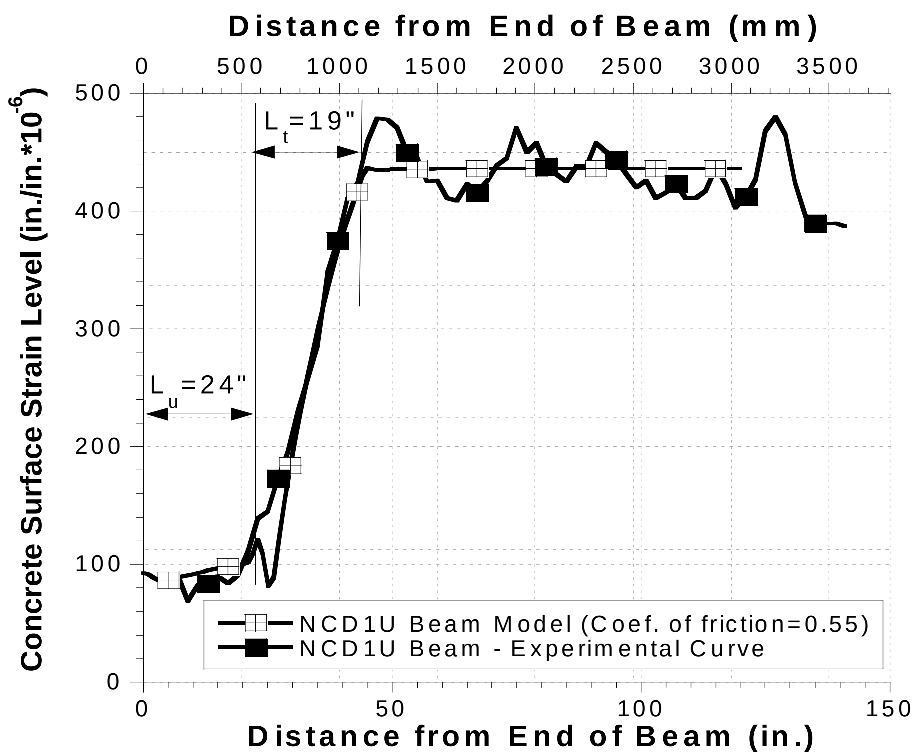

Figure 4-15 NCD1U model vs. experimental data

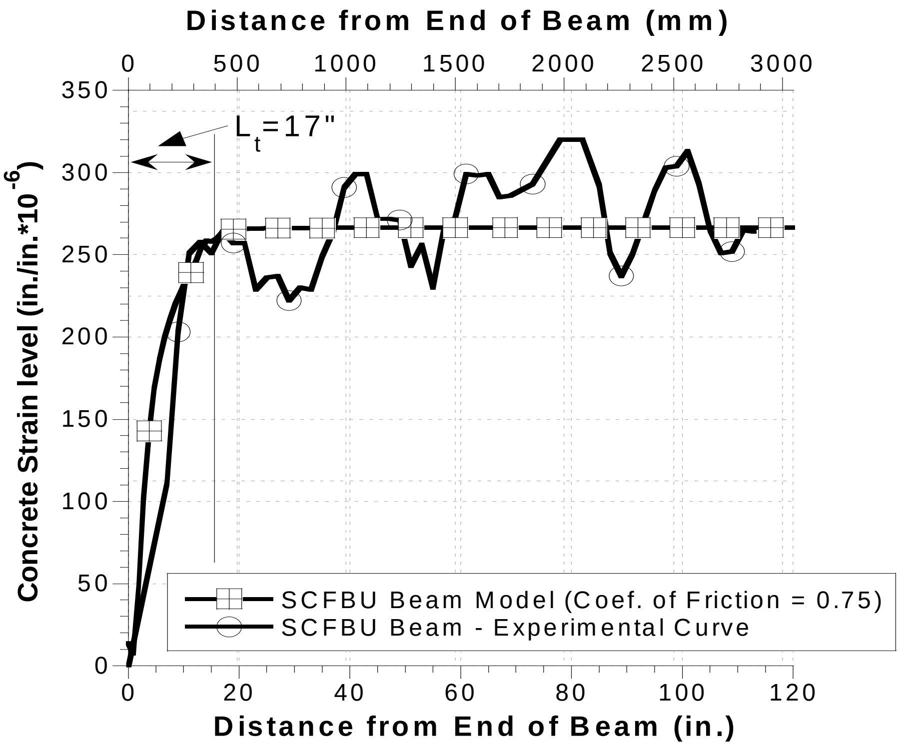

Figure 4-16 SCFBU beam model vs. experimental data

As it can be seen from the results in Figure 4-14 to Figure 4-17, the numerical models were successfully calibrated. It shall be kept in mind that the calibrated parameter was the coefficient of friction because this variable controls the transfer length. Further, the calibration process was done by simple comparison of the numerically predicted vs. experimental transfer length value.

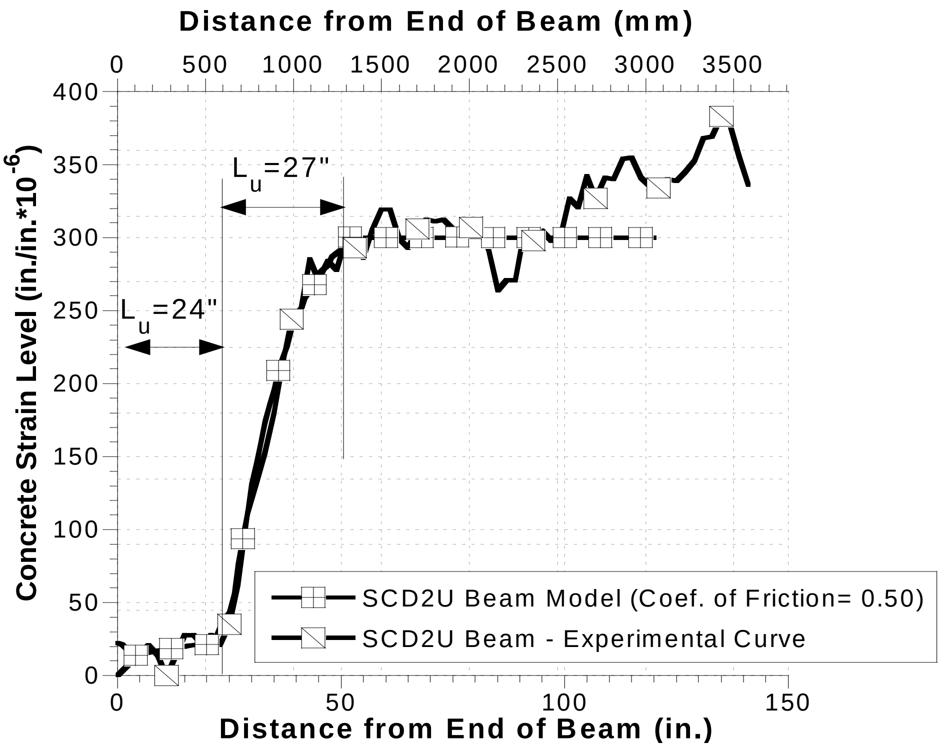

Figure 4-17 SCD2U beam model vs. experimental data

b) Stress and Strain Paths and Plot Contours

The stress and strain values along the cross section at the releasing end of each beam model were obtained to assess the level of stress and deformation induced by the prestressing force in the concrete member. A path along the cross section of the beam was selected to obtain stress and strain levels at the releasing end. In order to understand how the stresses and strains on the cross section at the releasing end of the beam model can be affected when the strand is fully bonded or partially debonded with tight fit sheathing, the maximum principal strain, axial and transverse stress levels are shown in the following. Figure 4-18 shows the maximum principal strains on the cross-section of the beam at the releasing end for all the NCC numerical models.

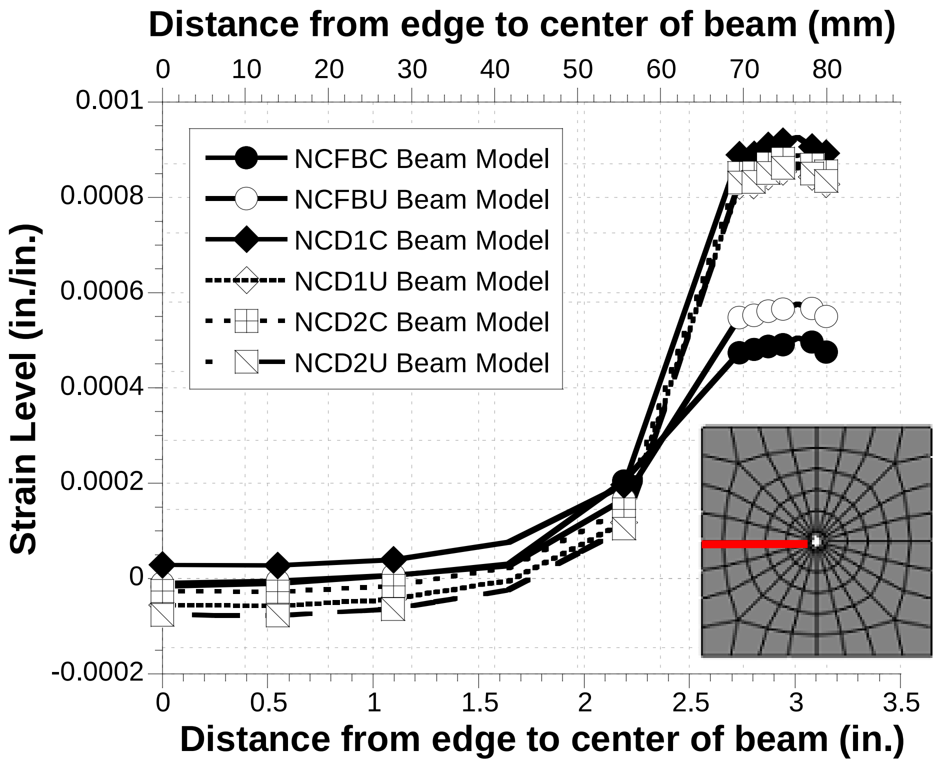

Figure 4-18 Maximum principal strain levels along cross section - NCC beams

Representative results of stress and strain contours are discussed next. In the following figures, positive values denote tension, and negative values mean compression. In addition, the red color denotes the highest tension value and darkest blue color refers to the largest compressive value. In order to carry out a better comparison from the simulation, the maximum and minimum contour values were fixed to the minimum value in tension and in compression for each group of beams, NCC and SCC, respectively. Thus, the light gray color denotes the tensile force above the defined tension-limit value, and the dark gray color represents compressive values beyond the maximum compression-limit established. See Appendix C for supplementary plot-contour results obtained from each beam model.

To compare the stress and strain levels along the debonded/transfer zone after the prestressing force was transferred into the concrete member, contour plots comparing a beam with partially debonded and fully bonded strand are compared in the following. Figure 4-19-a and Figure 4-19-b show the axial strain contours for the NCD1C and NCFBC beam models, respectively. During the experimental phase the two beams were placed in the same strand line, thus having the same initial prestressing force. The transverse strain E22 contour plots for the NCD1U and NCFBU beam models are shown in Figure 4-20-a and Figure 4-20-b, respectively. The two beams were subjected to the same initial prestressing force of 198 ksi (1365 MPa). The maximum principal strain contour plots for the NCD1C and NCFBC beam models are shown in Figure 4-21-a and in Figure 4-21-b, respectively.

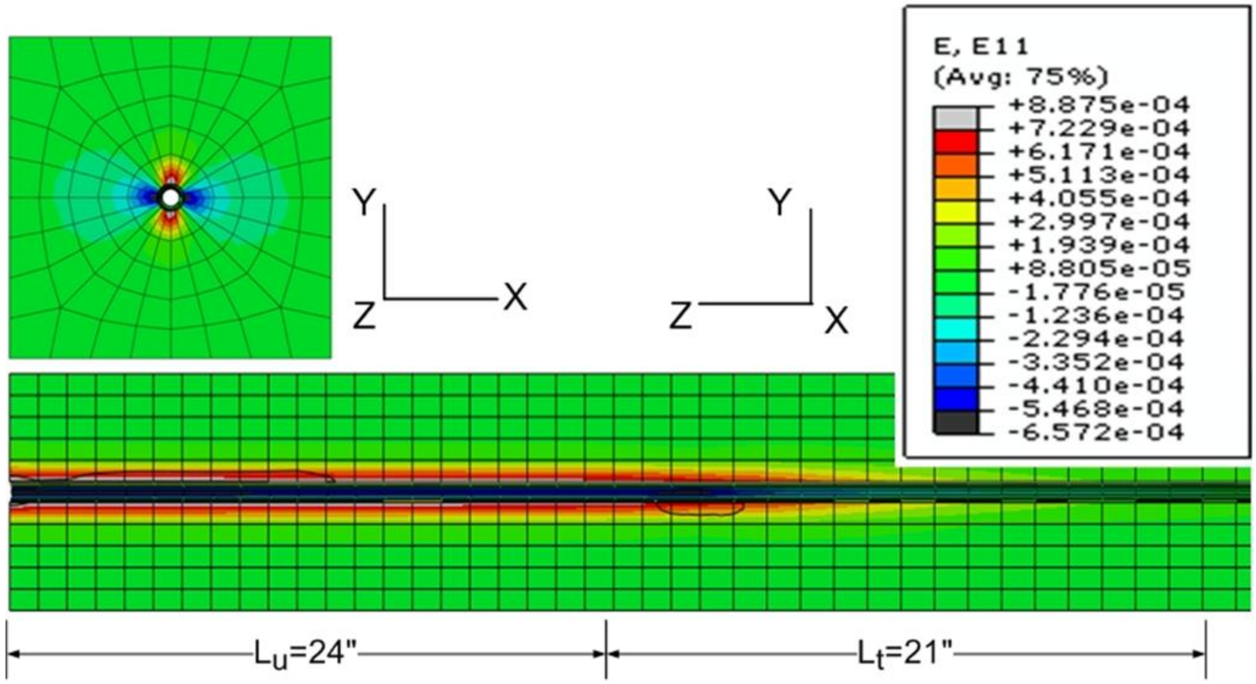

a) NCD1C beam model

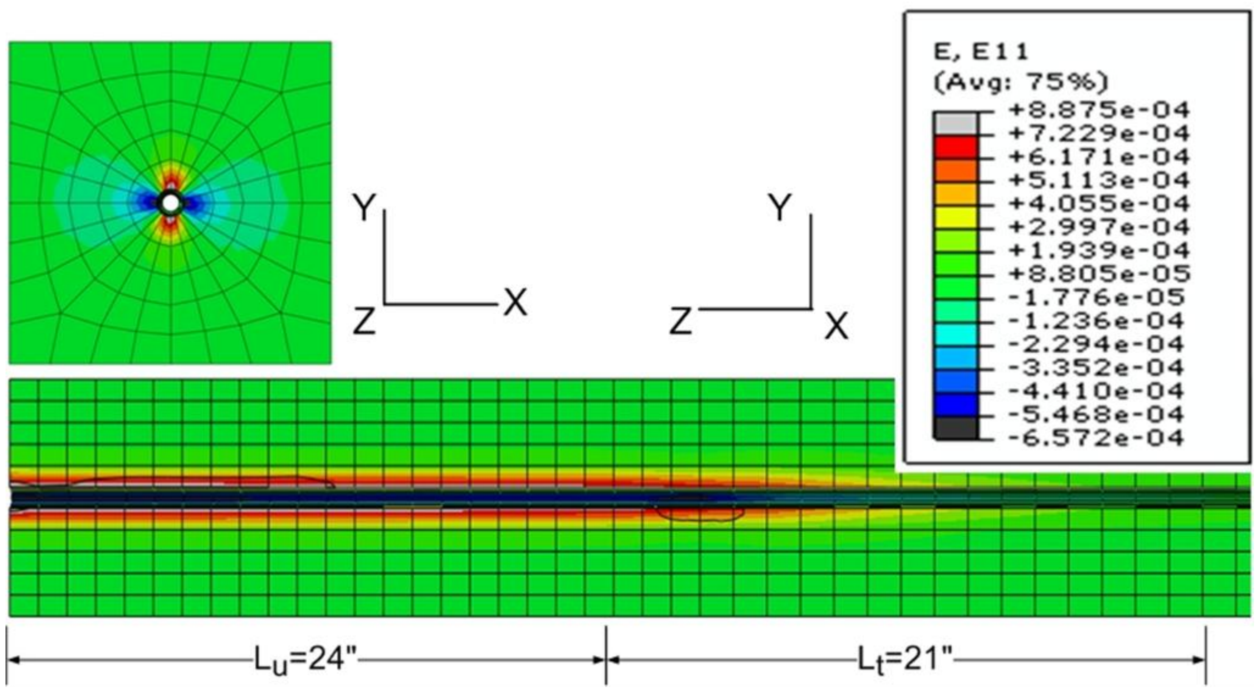

b) NCFBC beam model

Figure 4-19 Axial strain contour plots

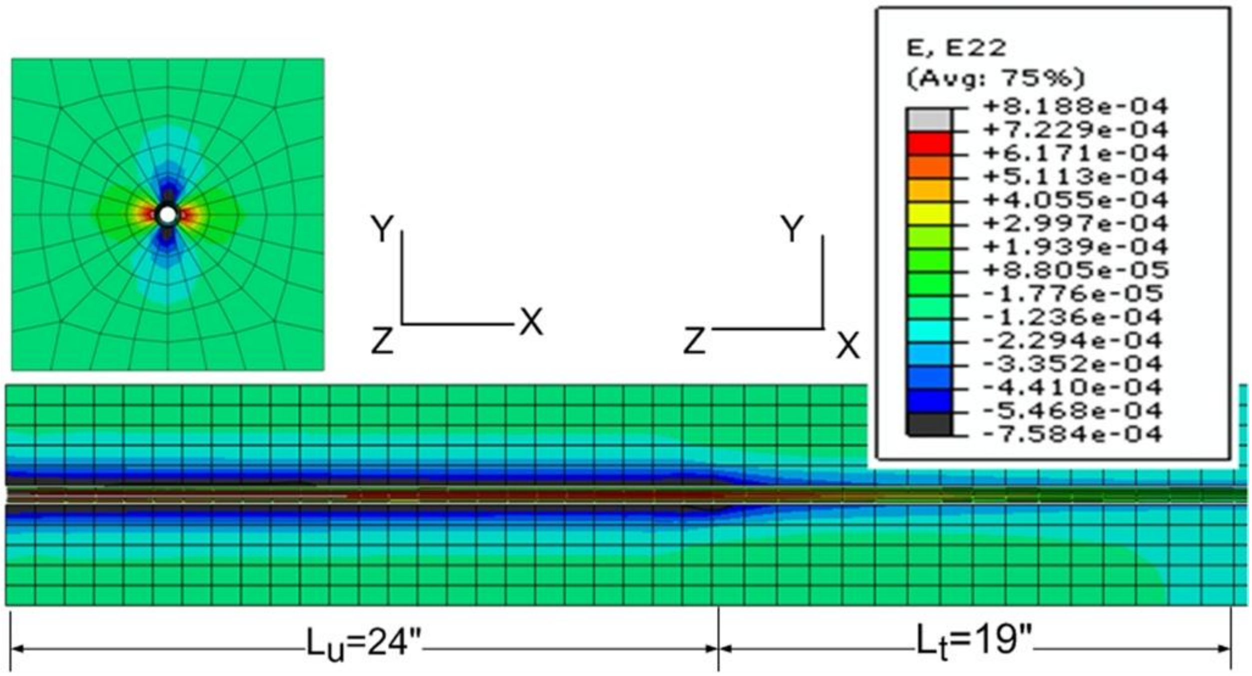

a) NCD1U beam model

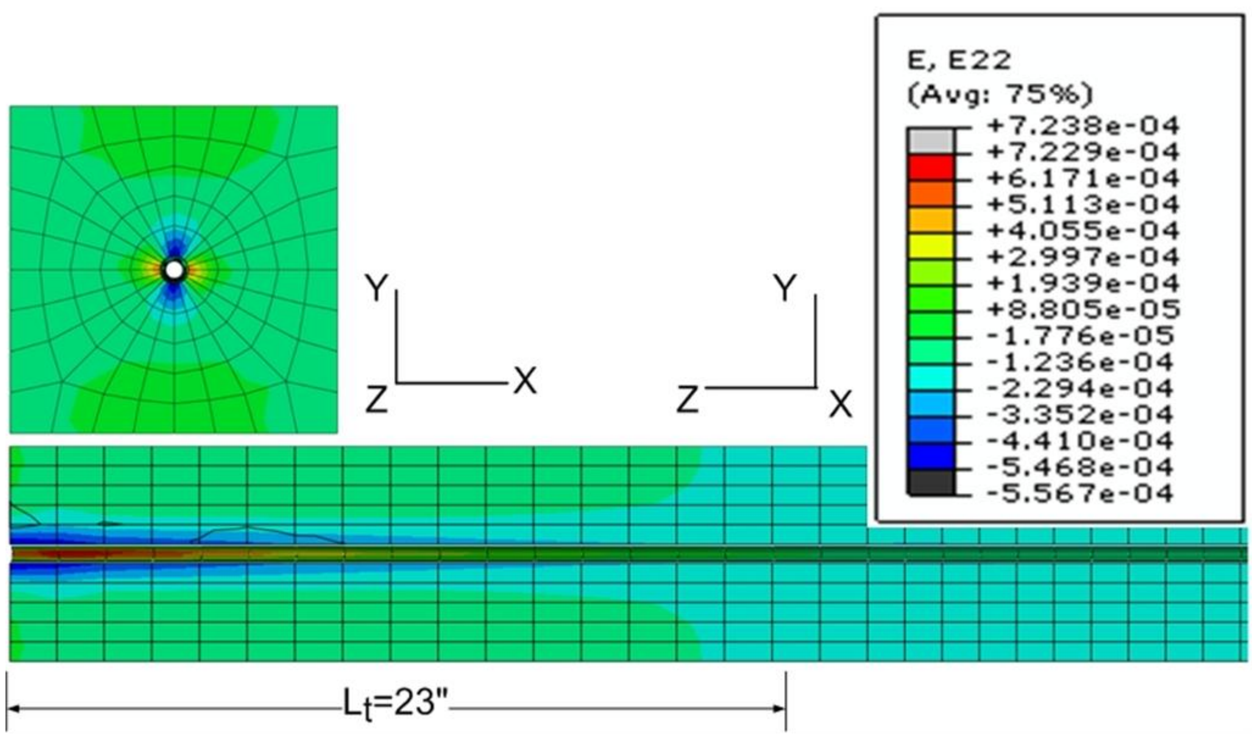

b) NCFBU Beam Model

Figure 4-20 Transverse strains contour plots: front and side views

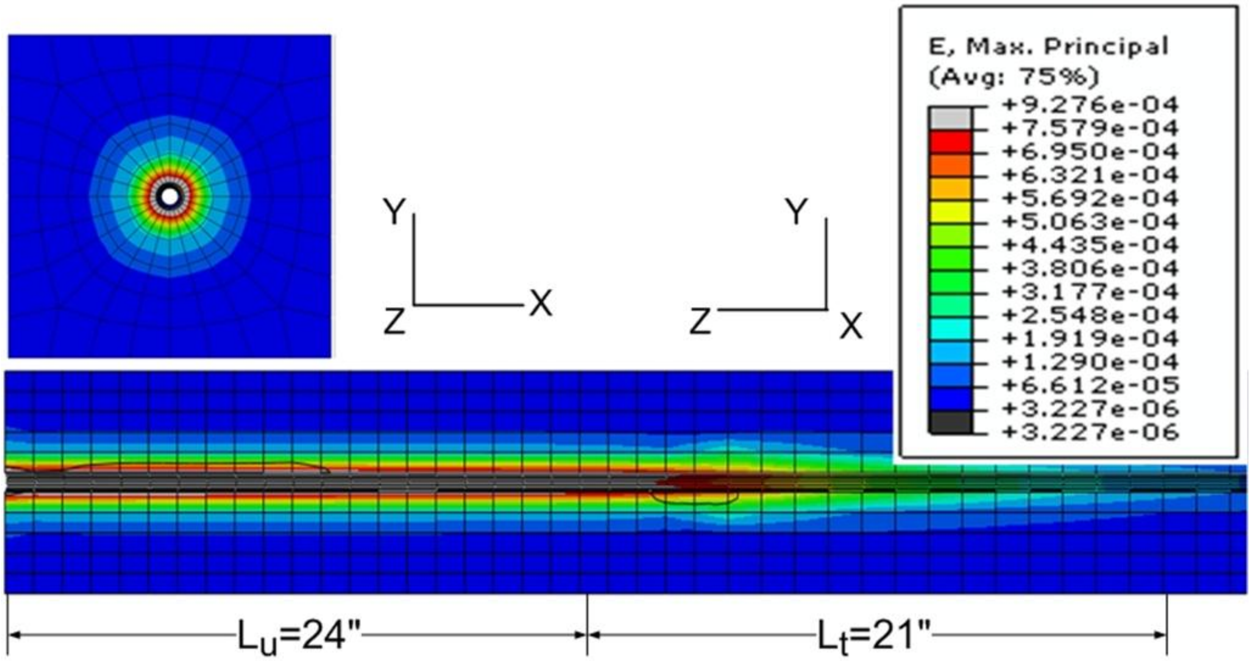

a) NCD1C beam model

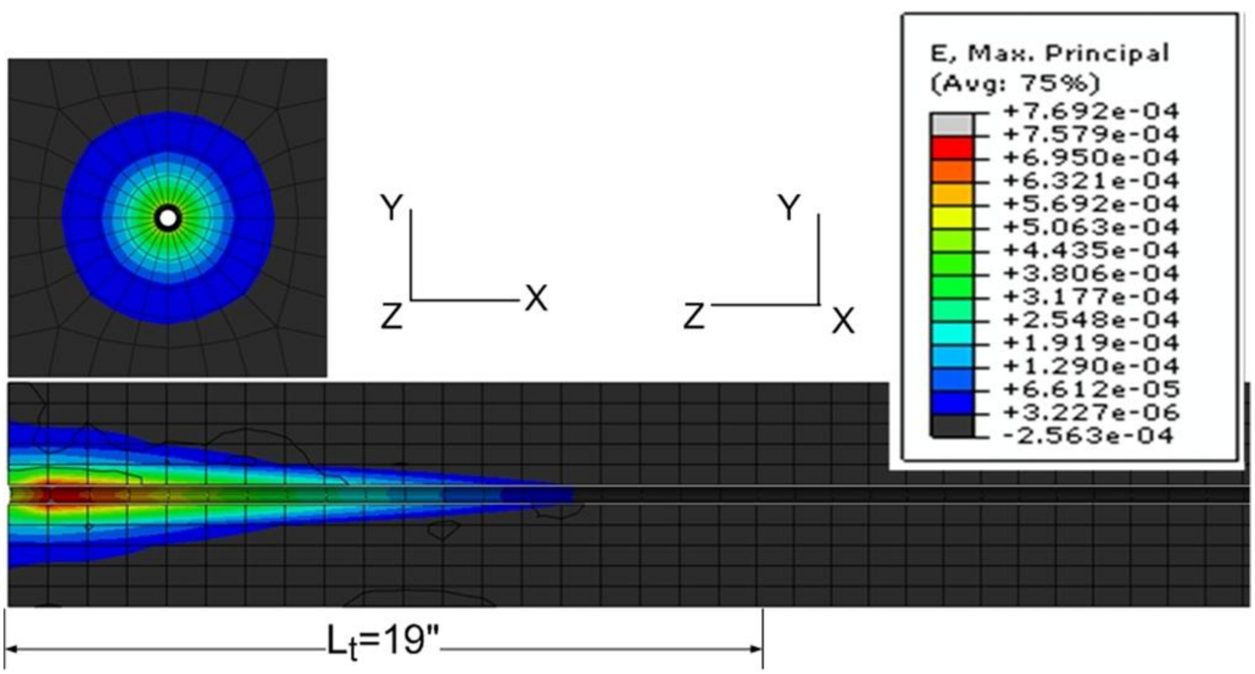

b) NCFBC beam model

Figure 4-21 Maximum principal strain contour plots: side and front views

As it can be seen from Figure 4-19-a, the axial strain values along the debonded zone were high and somewhat constant, which indicates that with a tight fit (flexible slit sheathing), high radial stresses develop at the interface of the two materials. This phenomenon is also observed in Figure 4-20-a and Figure 4-21-a. On the other hand, for the beam models with a fully bonded strand, NCFBC and NCFBU models, and the strain values were high close to the release end and decrease at about 10 in. (250 mm) measured from the releasing end.

The transverse stresses, S22, for the NCD1U and NCFBU beam models are shown in Figure 4-22-a and Figure 4-22-b, respectively. The maximum principal stresses are shown in Figure 4-23-a for the NCD2C beam model, and Figure 4-23-b shows the same type of stresses obtained from the NCFBC beam model. The entire length of the beam is not shown in order to present a closer view to the stresses and strains distribution on the anchorage zone and along the transfer region. The maximum principal strain values at the release end were numerically found to be higher for the models with a partially debonded strand than the ones containing a fully bonded strand. Since there was nominal friction between the strand and the surrounding concrete along the debonded zone of the beam models, the radial stresses caused by the dilation of the unbonded strand were higher as is explained in Figure 4-24.

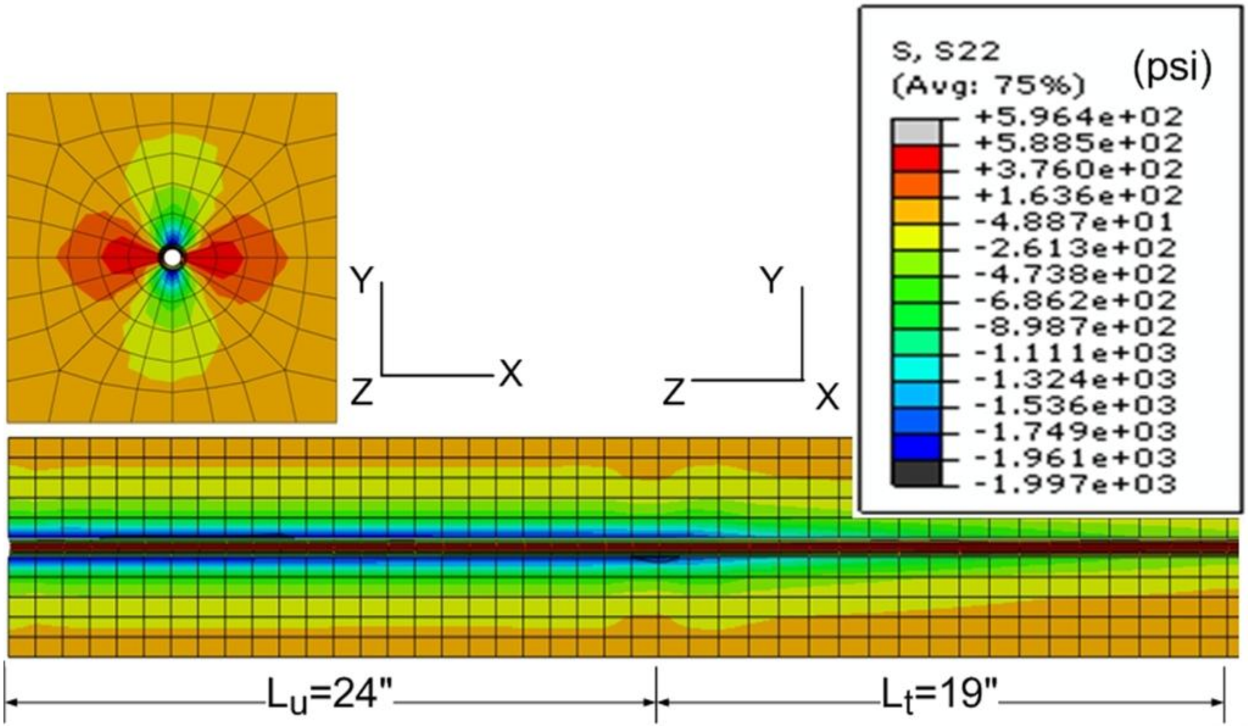

a) NCD1U beam model

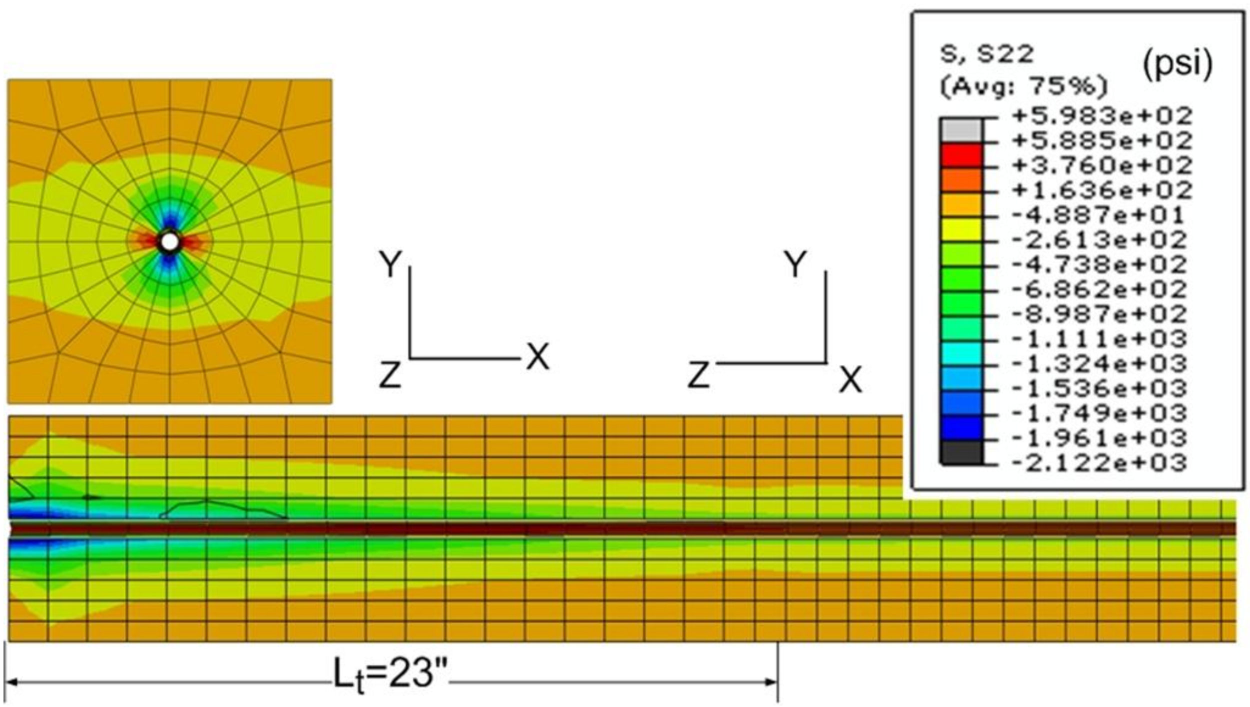

b) NCFBU beam model

Figure 4-22 Transverse stresses: side view and cross section at release end

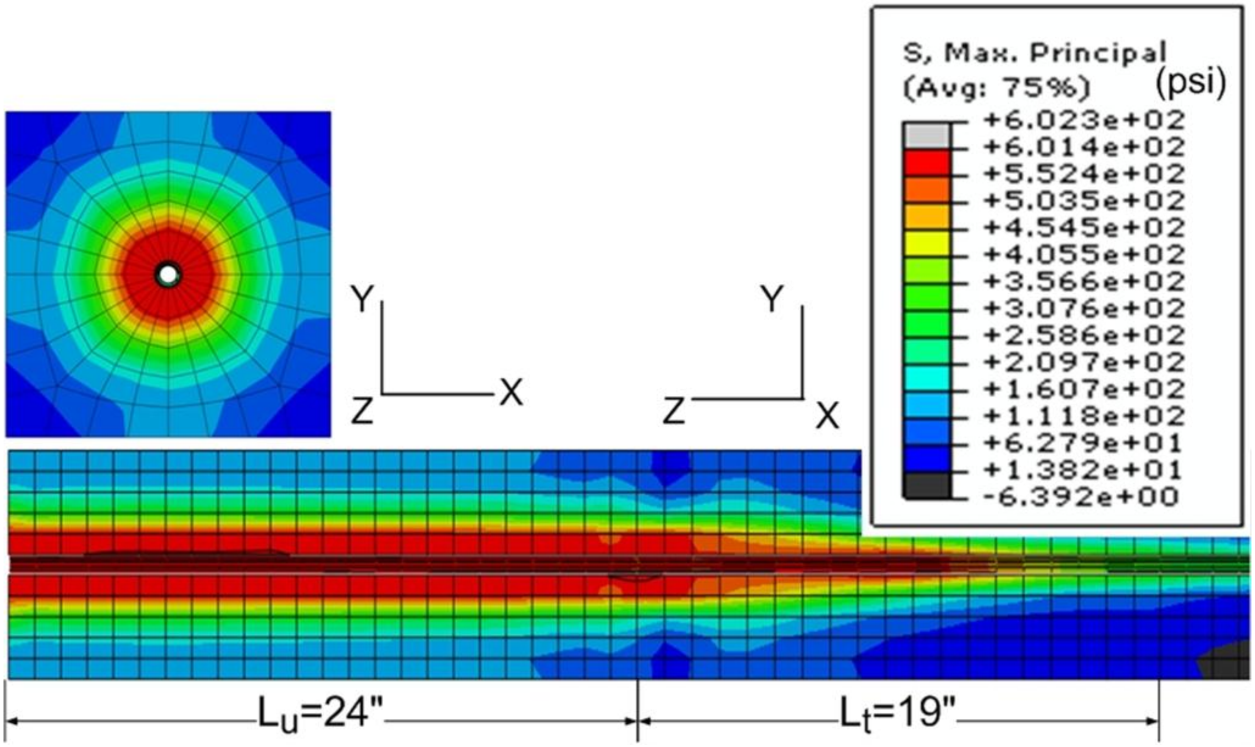

a) NCD2C beam model

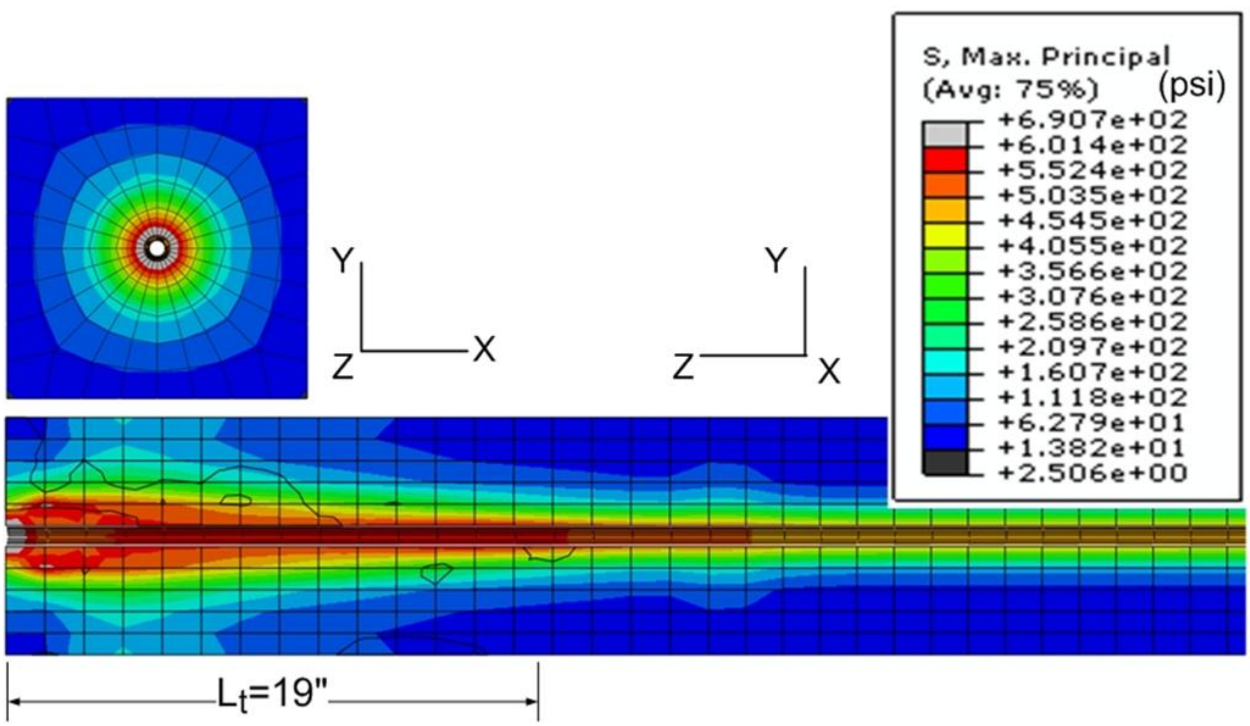

b) NCFBC beam model

Figure 4-23 Maximum principal stresses contour plots: front and side views

The transverse and maximum principal stress contours shown in Figure 4-22-a and Figure 4-23-a also show high values along the unbonded zone. Figure 4-24 is presented as an aid to explain the phenomenon observed when a tight fit is provided between the partially debonded strand and the surrounding concrete. At time zero, prior releasing the prestressing force into the concrete member, the stress in the strand σ_s is equal along the entire prestressed steel and the concrete has not been precompressed yet. As the prestressing force F_s is released into the concrete radial stresses σ_r develop due to the dilation of the prestressing strand. If the strand is fully bonded longitudinal bond stresses σ_b ($\mu\sigma_n$) develop. The axial strains ε_x can be related to radial strains ε_r by the Poisson's ratio υ. The prestressing force in the strand is reduced by a fixed amount ΔF_s, which is composed of the bonding force F_b (σ_b/A) and the axial force F_x (σ_x/A). Thus, as the friction between the strand and the concrete decreases the radial stresses at the interface increase.

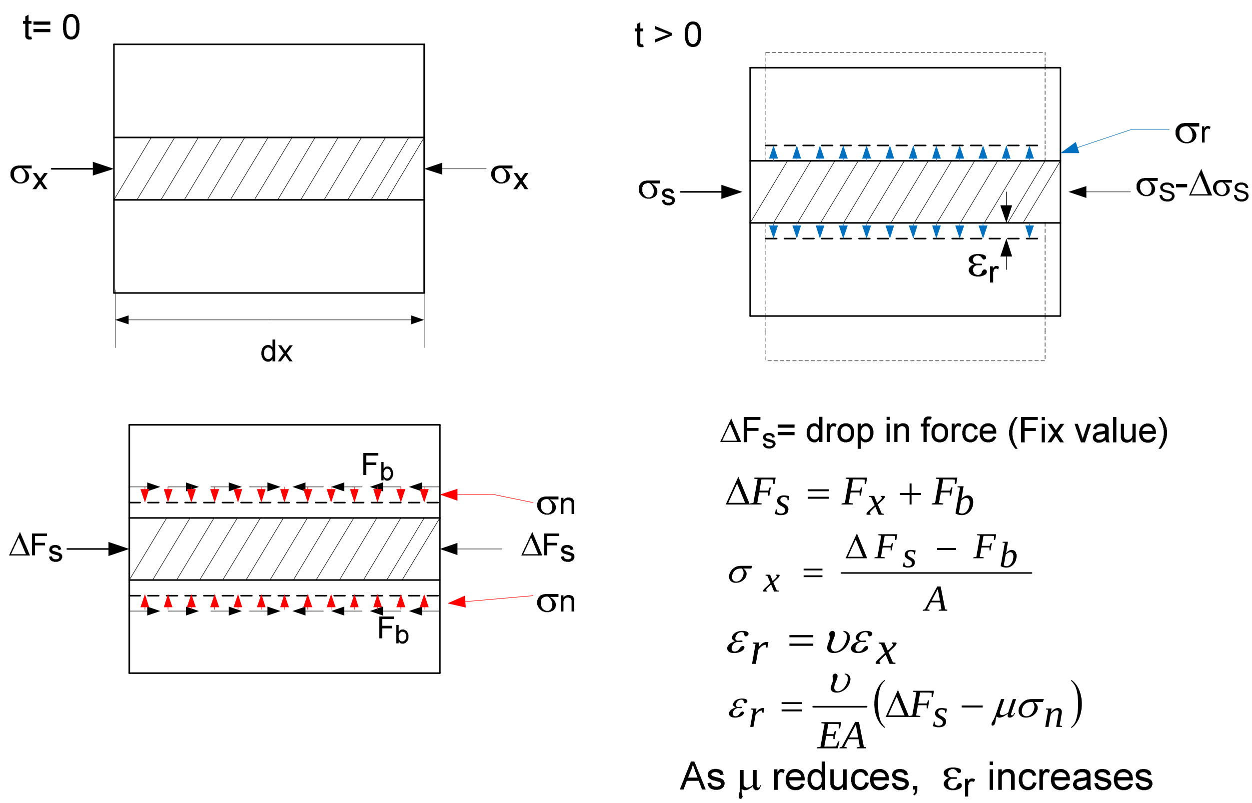

Figure 4-24 Schematic illustrating of high stresses along debonded zone

4.6 Influence of Confinement Reinforcement on Transfer Zone Stress State

The distribution of stresses in the end zone of a prestressed concrete member depends on strand location, the magnitude of prestressing force, the degree of bond between strands and the surrounding concrete, the amount of draped strands in the end zone, the geometry of the girder, the compressive strength of the concrete, etc. [33]. Vertical stirrups in the end zone of pretensioned concrete girders become effective once horizontal cracks develop. Thus, the use of confinement in the anchorage region could minimize the high stresses cause by the releasing of the prestressing force. The provision of transverse and confining reinforcement has thus been recommended to delay bond failure [29]. Confining and transverse reinforcement is a detailing requirement in the design of pretensioned concrete members since it is the only mechanism that could prevent bursting and spalling cracks in the end zone upon release [27]. The provision of confinement reinforcement was studied through numerical simulations along the transfer and debonded zone to investigate the stress state in the end-region upon release, as is presented next.

4.6.1 Numerical Evaluation of Confinement in Prestressed Concrete Beams

The effect of confinement reinforcement in the beam-end region was evaluated through numerical simulations on beams with single concentric strands. Circular stirrups were placed along the transfer zone in the case of the beam model containing a concentric fully bonded strand, and along the debonded region for the beam model containing a concentric partially debonded strand. Different bar sizes and spiral diameters were considered for the confinement reinforcement. Two of the eleven FE beam models were considered for this investigation, namely, the NCFBC and NCD1C beam models. The description for each model is presented next.

a) NCFBC Beam Model

Numerical analyses were carried out to study the effect of confinement in the end region of one the laboratory-scale beams containing a concentric fully bonded strand. The NCFBC beam model was modeled using different confinement conditions. Circular hoops with bar sizes of #3, 4 and 5 (No. 10, 13, and 16) were considered for this study, and the diameter of the hoops were 1.5, 3.0, and 4.0 inches (35, 75, and 100 mm). Thus, the NCFBC beam model was run nine times with the different confinement conditions. Inelastic behavior of the concrete was incorporated. The results to be shown in this section are the ones obtained from the numerical model with circular hoops with a 1.5 in. (35 mm) diameter and using #3, 4, and 5 (No. 10, 13, and 16) reinforcing bars. The minimum realistic diameter that was considered was 1.5 in. (35 mm) since the diameter of the strand is 0.6 in. (15.2 mm), leaving only 0.45 in. (11.4 mm) for the concrete to flow between the strand and the stirrup. The hoops were concentrically placed around the strand along the transfer region (see Figure 4-25) and spaced at every 2 in. (50 mm) from center-to-center. The first stirrup was placed at 1 in. (25 mm) from the beam end.

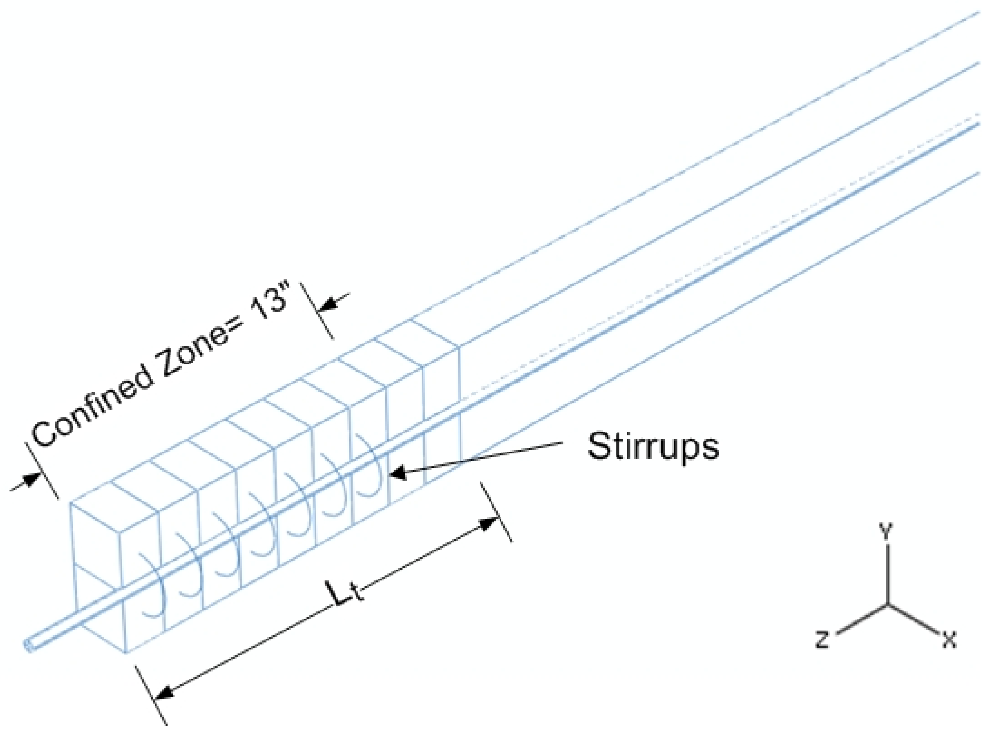

Figure 4-25 NCFBC beam model: close view of the end-zone

b) NCD1C Beam Model

Modeling for the NCD1C (see Figure 3-23) was similar to the one presented in Section 4.5. The dilation of debonded strands upon release can cause transverse stresses along the debonded length when using soft sheathing (see Figure A-10). In this case, the circular stirrups were placed along the debonded region to assess if the use of confinement reinforcement in the end-region helped minimize radial stresses along the debonded zone. The confinement reinforcement options were the same ones considered for the NCFBC beam model (see Section 4.6.1-a). The results presented here are those obtained for the NCD1C beam model containing #3, 4 and 5 (No. 10, 13, and 16) hoops and diameter equal to 1.5 in. (35 mm). These cases seemed to be the most effective in reducing high tensile stresses along the transfer length as seen from the results obtained from the NCFBC beam model with confinement reinforcement. Figure 4-26 shows the NCD1C beam model.

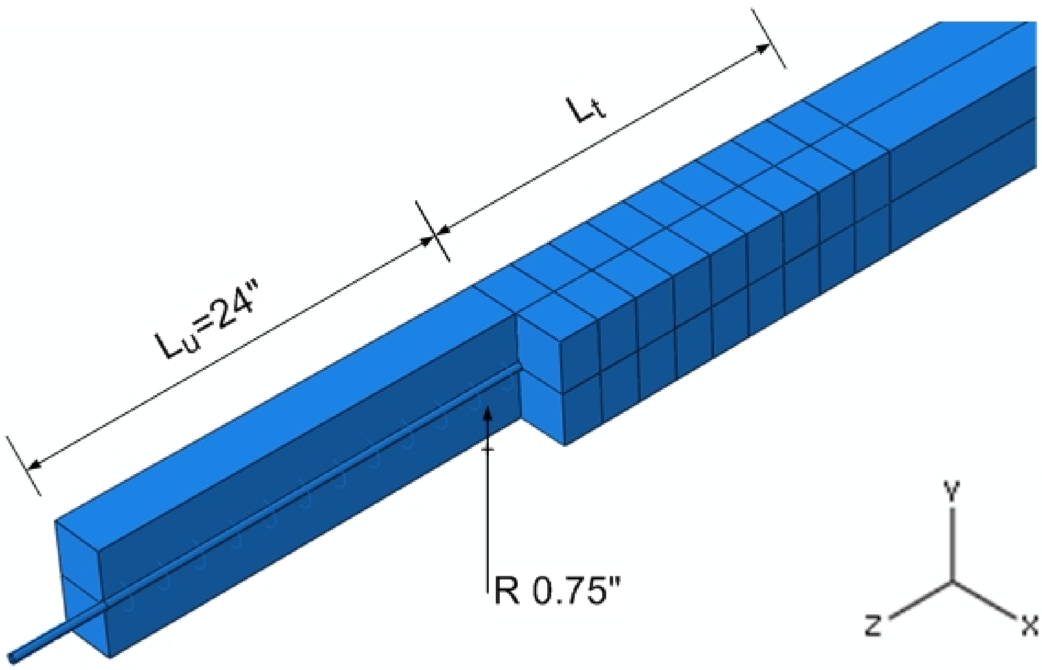

Figure 4-26 NCD1C beam model with circular stirrups along debonded zone

4.6.2 Results

a) **NCFBC FE Beam Model**

Representative results obtained from the NCFBC beam model with confinement reinforcement consisting of 1.5” (35 mm) diameter hoops with #3, 4, and 5 (No. 10, 13, and 16) bar sizes are presented the following. Results along two paths were studied: one along the cross section of the beam at about 4” (100 mm) from the beam end, and another one at the top-center of the beam along the first 35” (900 mm) from the beam end. Figure 4-27 shows the maximum principal stresses along the cross-sectional path. The axial strains (E11) along the same cross-sectional path are shown in Figure 4-28, and the transverse stresses (S22) are shown in Figure 4-29. The maximum principal stresses along the top-center path are shown in Figure 4-30.

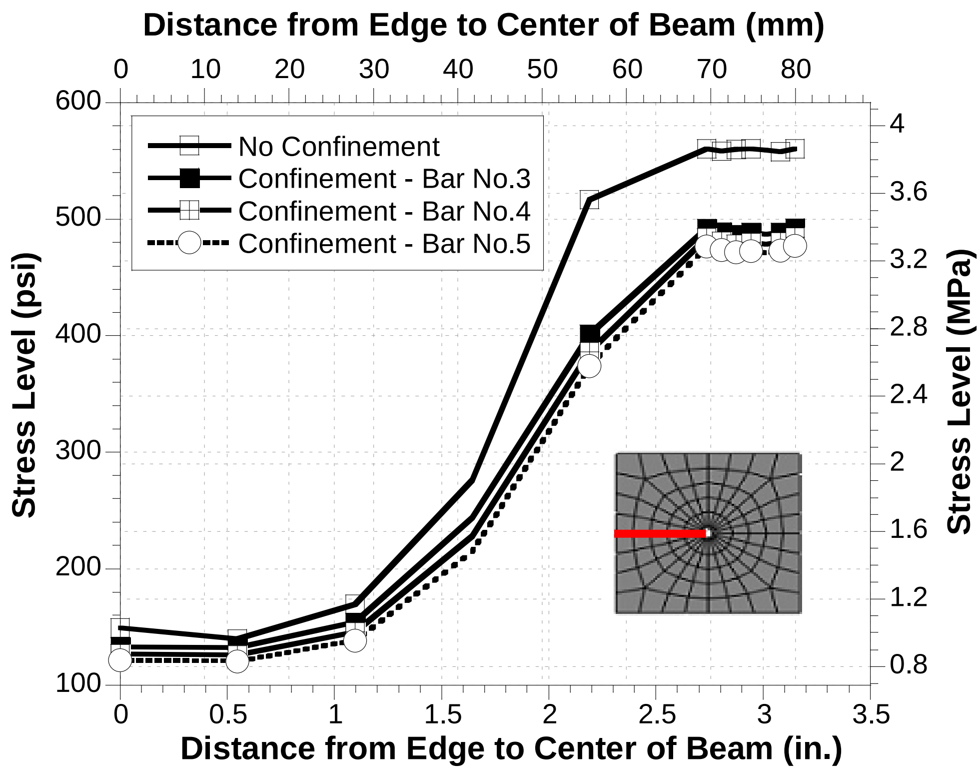

Figure 4-27 Maximum principal stress: NCFBC beam model - cross-sectional path

As it was to be expected, the models with the highest confinement level – smallest diameter and largest bar size - performed better. At the same time, the differences between the FE beam model without confinement and the one having the highest confinement level was not significant. The highest difference in stress value obtained from the model with confinement (1.5 in. [35 mm] diameter hoops with #5 [No. 16]) to that without confinement was about 100 psi, obtained from the maximum principal stress plot at the cross section of the beam at the releasing end. However, the minimum spacing between prestressing strands established in codes such as the AASHTO Bridge Design Specifications [2] and ACI-318 [3] is 2 in. (50 mm). If circular stirrups are used in girders to reduce the high tensile stresses in the anchorage region, the 1.5-in. (35 mm) diameter stirrups may not be possible to use for girders containing 0.6-in-diameter strands.

The axial strain (E11) and transverse strain (E22) levels obtained from the beam model with high confinement (#5 [No. 16] bar and hoop diameter of 1.5 in.[35 mm]) seemed to reduce the stress values by about 2.5 times compared to the model without confinement. In terms of maximum principal stresses along the top-center of the NCFBC beam model (see Figure 4-30), the stresses decreased about 50 psi (345 kPa) compared to those obtained from the NCFBC beam model without confinement and the one with confinement using a #5 (No. 16) and a hoop diameter of 1.5 in. (35 mm)

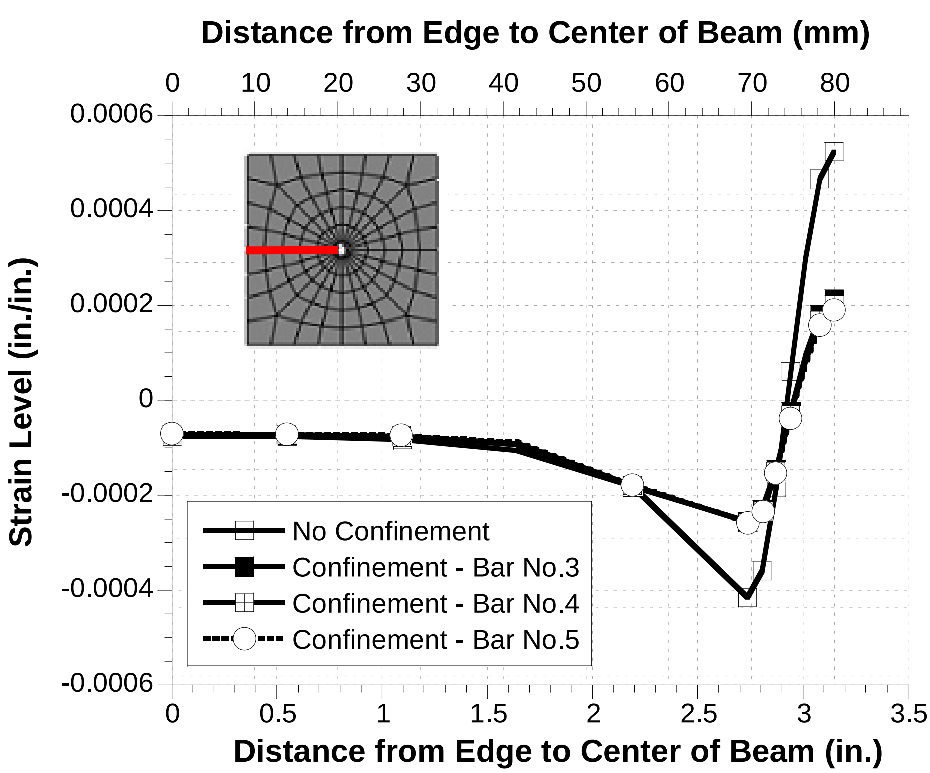

Figure 4-28 Axial strains: NCFBC model

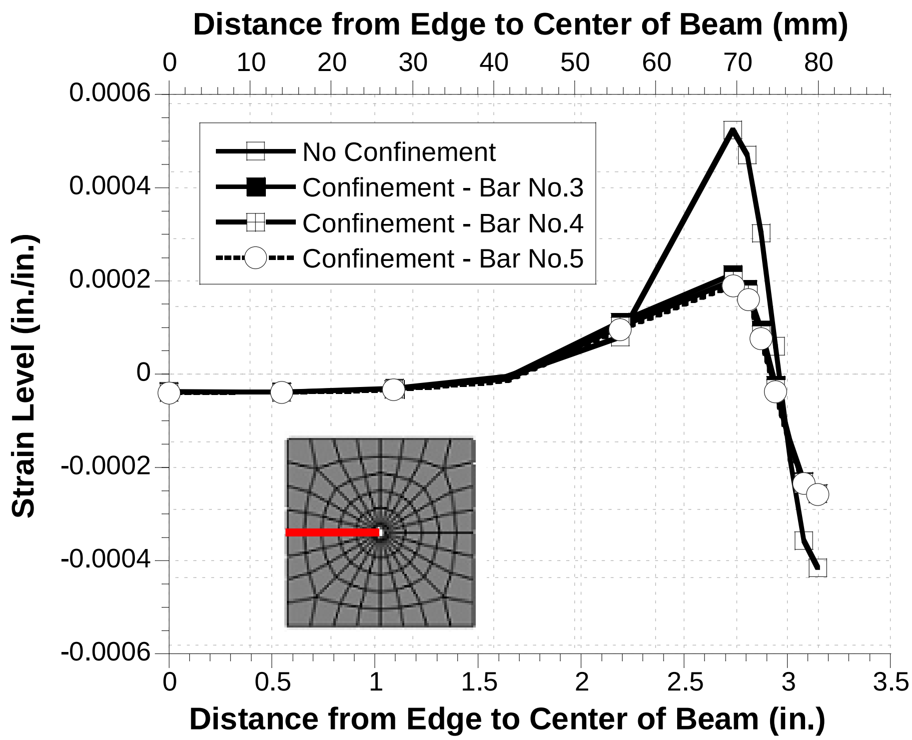

Figure 4-29 Transverse strains: NCFBC beam model – path along cross section

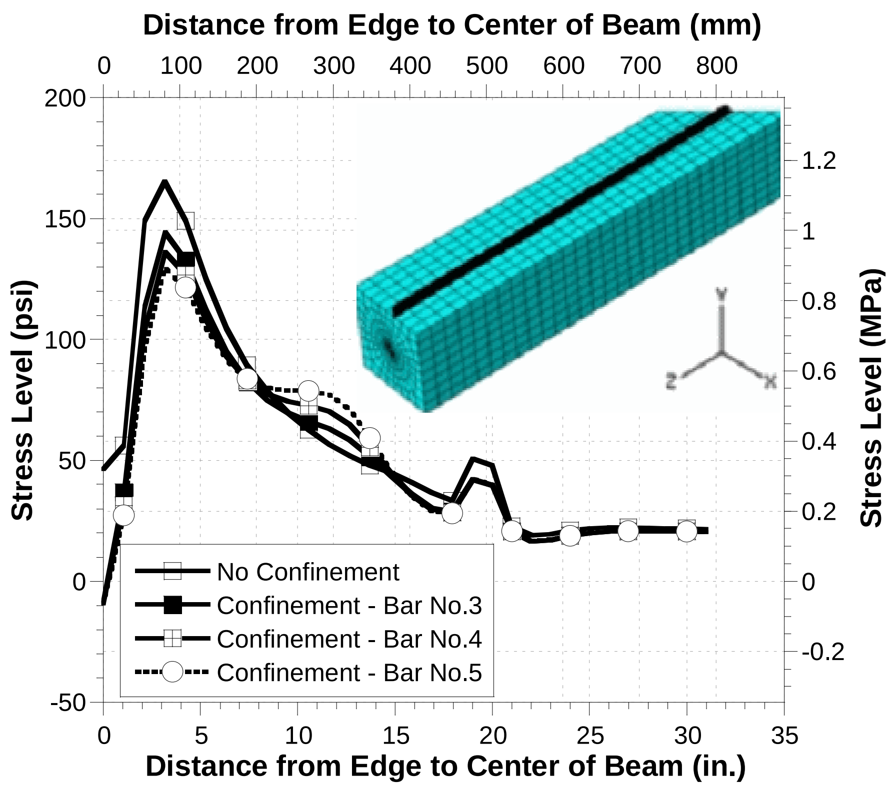

Figure 4-30 Maximum principal stresses: NCFBC beam model – path along top beam center

b) **NCD1C Beam Model**

From the results obtained from the NCFBC beam model, it was observed that the circular #5 (No. 16) bar hoops performed slightly better than the other two. Thus, only the results obtained from the beam model with a 1.5 in. (35 mm) diameter hoop with #5 (No. 16) bars are presented for the NCD1C model. Maximum principal stress values along top-center of the beam (see Figure 4-31) and equivalent plastic strain in uniaxial tension (PEEQT [see Figure 4-32]) are shown to compare how the values can decrease when confinement is provided along the debonded zone to reduce high stresses/strains produced by the dilation of the strand as it tries to recover its original diameter. As it is shown in Figure 4-24, if tight fit is provided between the debonded strand and the surrounding concrete the radial stresses increase along the blanketed region. It can be seen from these figures that the maximum principal stresses along the top-center of the beam reduced ~10% with the use of confinement (#5 [No.16] hoops), and the PEEQT values along the cross section at 4 in. (100 mm) from the releasing end only decreased 13% when using the same type of confinement. Thus, the use of confinement did not significantly affect the high stress/strain values along the unbonded zone; yet, the values seemed to decrease about 11% in average.

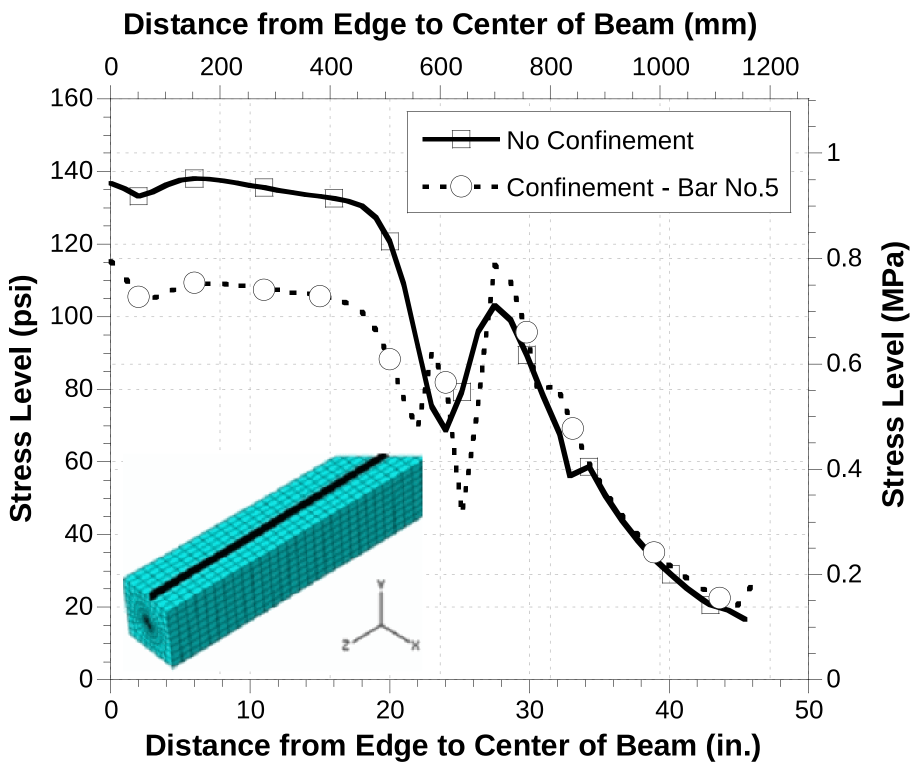

Figure 4-31 NCD1C model: Maximum principal stress along top-beam path

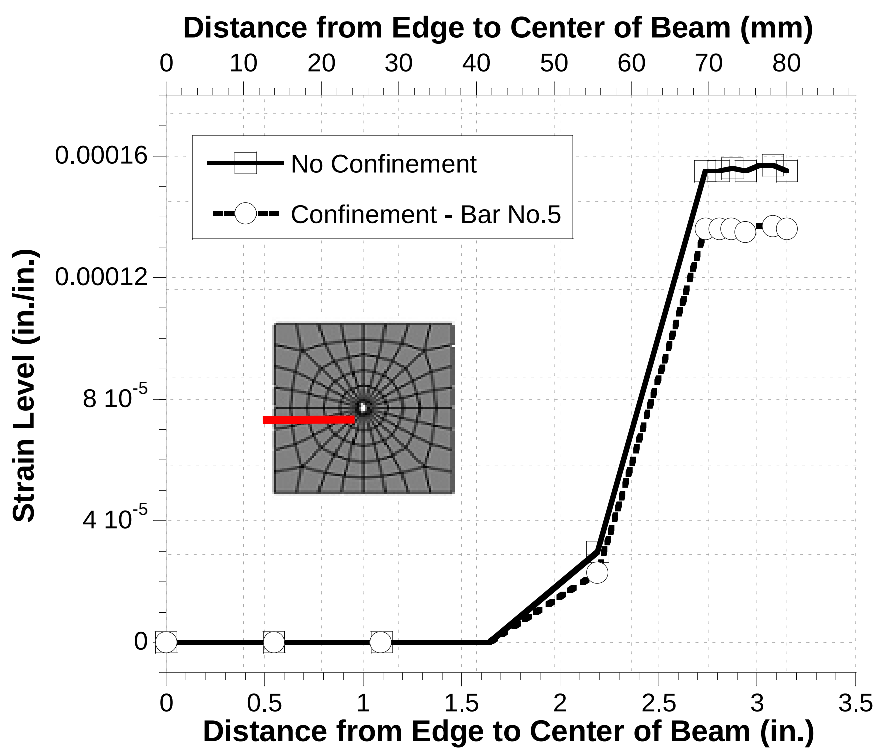

Figure 4-32 Equivalent plastic strain in uniaxial tension (PEEQT) along cross section (at 4 in. [100 mm] from the releasing end)

4.7 Linear-Elastic vs. Concrete Damaged Plasticity FE Models

A comparison between the linear-elastic and inelastic analyses is presented here since one of the eleven beam models was not calibrated using the concrete damaged plasticity (CDP) model due to numerical problems. One of the reasons for the problems was because of the high coefficient of friction needed to calibrate the model and the high compressive strength at release. The model did converge when using linear-elastic material properties for the concrete part. The concrete material properties are shown in Table 4-1.

The NCFBU beam model was selected for the comparison since the numerical model that did not converge was the SCFBU for the above-mentioned reasons. Hence, the NCFBU beam model was run using the same value for the static coefficient of friction, applying the same level of temperature to the beam (to simulate creep and shrinkage effects), but one was modeled with linear-elastic concrete material properties and the other one using the CDP model. Representative results are shown in the next section.

4.7.1 Results: NCFBU Linear-elastic vs. NCFBU Inelastic FE Beam Models

The representative results shown next were obtained from a path along the beam cross-section at the releasing end and a path on the top-center of the beam along the longitudinal direction. Other results were also plotted and they are provided in Appendix C. Figure 4-33 shows the transverse stresses (S22) along the cross section of the beam at the releasing end. The maximum principal stress values are shown in Figure 4-34 and the maximum principal strain values on the cross section of the beam at the releasing end are shown in Figure 4-35.

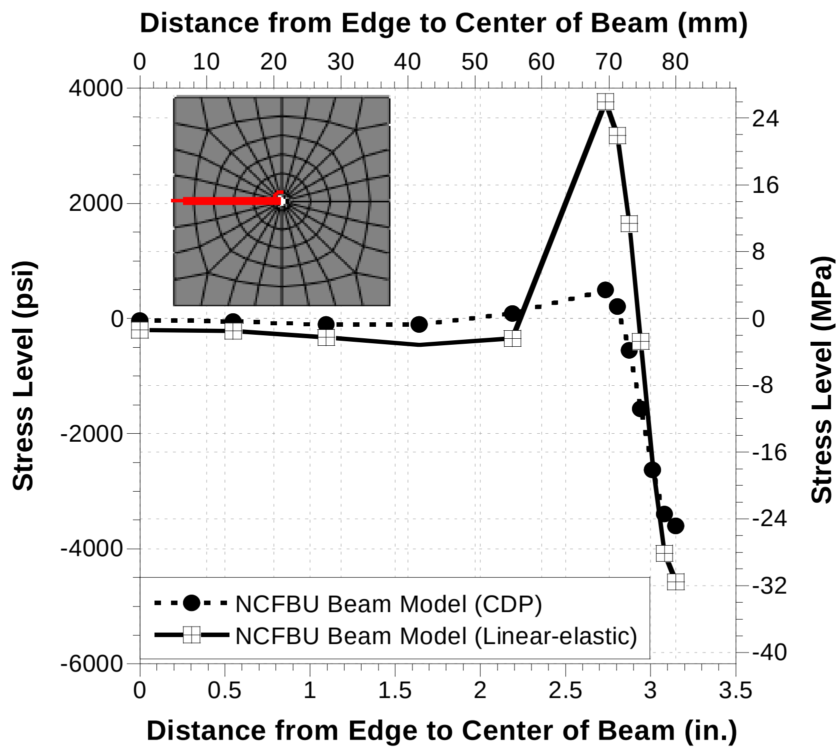

Figure 4-33 Transverse stresses – elastic vs. inelastic concrete behavior

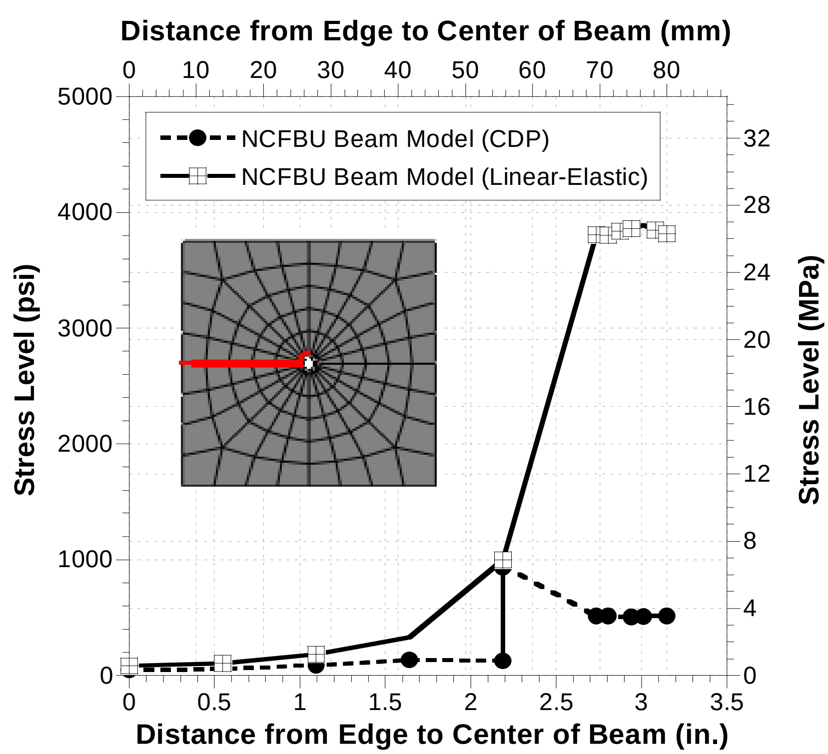

Figure 4-34 Maximum principal stress: cross sectional path

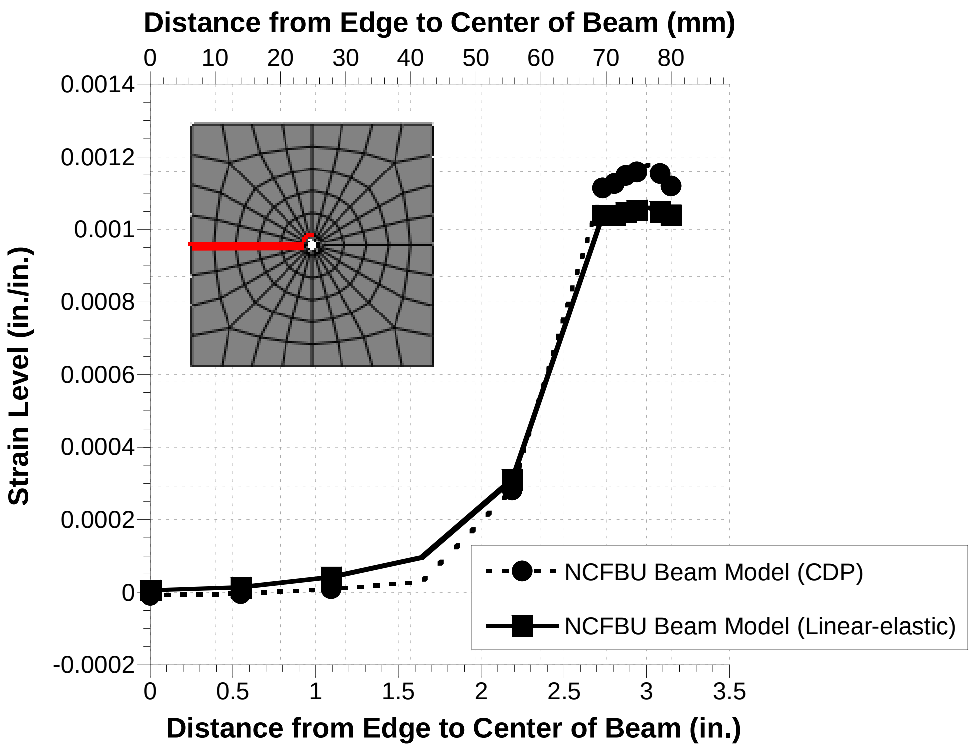

Figure 4-35 Maximum principal strain along front cross-section

The transverse stresses (S22) were obtained along the cross section at the releasing end and it can be observed from Figure 4-33 that the values from the linear-elastic NCFBU beam model are significantly higher than the ones obtained when using the CDP model. It shall be mentioned that the maximum principal stress values were obtained to have a global comparison in terms of stresses. The maximum value obtained from the linear-elastic analysis was about 3500 psi (24MPa), about 700% greater than the largest value obtained from the analysis incorporating material nonlinearity for the concrete part.

4.8 Findings

The following summarizes the findings from the numerical simulations of laboratory-scale beams presented in this Chapter.

- The laboratory-scale beam models were successfully calibrated with experimental data so as to obtain a coefficient of friction parameter to be used for the simulations of large-scale beam models to study the stress state in the end-regions of pre-tensioned concrete girders upon release.
- Results from the beam models with partially debonded strand showed high stress values along the debonded length and this can be attributed to the dilation of the strand as it tries to recover original diameter upon release causing high radial stresses (i.e., it is Poisson's effect). These high stresses can continue along the unbonded length because the debonding mechanism is effective. Thus, this observation can explain the concrete surface strain levels experimentally measured along the debonded zone of the laboratory-scale beam units.
- The use of confinement reinforcement along the debonded/transfer zones does not seem to reduce the high stresses in the end regions. However, confinement and transverse reinforcement must be provided in detailing pre-tensioned girders as these are essential elements that can prevent bursting and splitting cracks upon strand detensioning.

CHAPTER 5 NUMERICAL SIMULATIONS: STRESS ANALYSES OF ANCHORAGE REGIONS

5.1 Introduction

In order to evaluate the variables affecting end-cracking in full-size bridge girders containing partially debonded strands, nonlinear three-dimensional numerical models were developed using the general purpose FE program ABAQUS [1]. The variables incorporated in the numerical simulations were the type of sheathing material, flexible (tight fit) or rigid (oversized), and strand debonding distribution. A skew U-type bridge girder, which contained partially debonded strands, was chosen as case study because damage attributed to the debonding of strands was observed during production. The numerical models incorporated inelastic concrete material behavior and surface contact interaction definitions to model prestress load transfer. Four models were created incorporating the use of flexible or rigid debonding and a staggered debonded strand distribution. A description of the theory behind the concrete-inelastic behavior and contact interaction models was presented in Chapter 4, and the description of the U-beam models and results are presented in this chapter. It should be noted, however, that the intent of this study was to obtain qualitative information on the causes behind the observed damage and assess the role of strand debonding in this behavior. Thus, the aim was not to quantify the stress state or exactly match the cracking/damage pattern, which is not possible since the number of parameters involved are too complex and unknown since the only information available on the damaged girder is a qualitative (photograph) pattern of damage.

5.2 Case Study: Skew U-Beam Unit

A skew U-type bridge girder produced for the Indiana Department of Transportation (INDOT), for which evidence of end cracking believed to be caused by strand release, exists, was selected as a case study [8][23]. Figure 5-1 shows the damage seen on the U-beam girder upon release. The dimensions of the U-beam are 56 in. (1420 mm) wide in the bottom flange, 99.5 in. (2525 mm) wide at the top, 61.5 in. (1560 mm) void-wide in the upper part, and 54 in. (1370 mm) depth, with a skew angle of 18 degrees at both ends. The cross section of the U-beam girder is shown in Figure 1-6 and Figure 5-2; the region of interest is shown in the same figure. The length of the U-beam unit is 116’-5” (35.5 m) with a span length of 114’-11.5” (35 m).

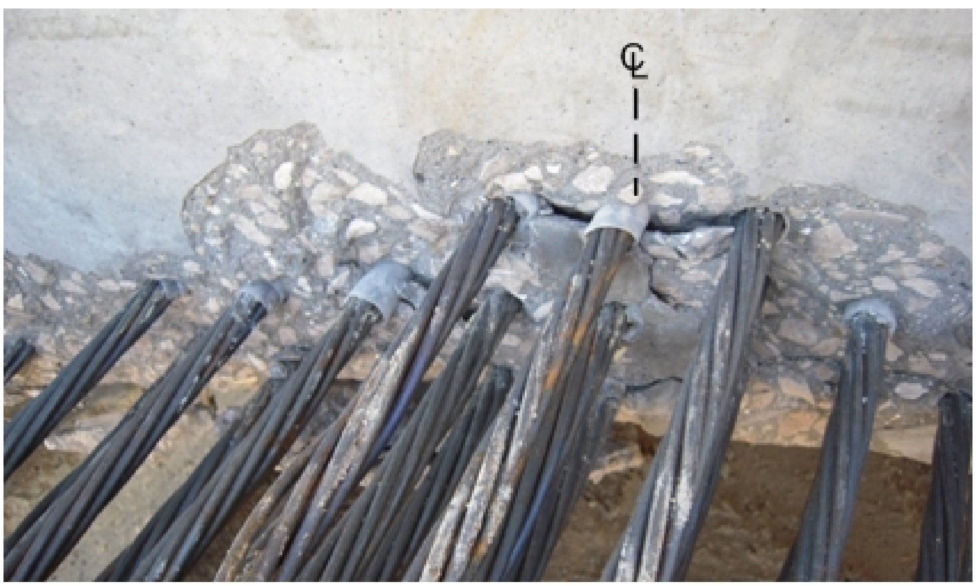

Figure 5-1 Damaged observed on skew U-beam during production at beam end [8][23]

The U-beam girder had ninety-three (93) 0.6-in. (15.2 mm) diameter Grade 270 (1860 MPa) strands: 57 straight strands in the bottom flange, and 36 draped strands in the sides of the beam (see Figure 1-4.) Twenty-one (21) of the 57 strands in the bottom flange were debonded using flexible (tight fit) slit sheathing. Thus, 37% of the strands were debonded in total and all the shielded strands were placed in the center-bottom flange of the beam (see Figure 1-4 and Figure 5-2.) The percentage of debonded strands was: 20% in row 1, 43% in row 2, and 43% in row 3. Such design exceeds limits established in the AASHTO LRFD Bridge Design Specifications [2] (see Section 2.5.1-a). Thirty-three (33) percent of the unbonded strands had the same unbonded length, which was less than the 40% limit in the AASHTO Specifications. The number (ID) below each symbol as shown in Figure 5-3 corresponds to the unbonded lengths in the U-girder unit as shown in Table 5-1. The symbol without number corresponds to the fully bonded strands. The concrete compressive strength at release was 8,000 psi (55.2 MPa) and the initial strand prestressing level was 0.75 f_{pu} (202.5 ksi [1396 MPa]).

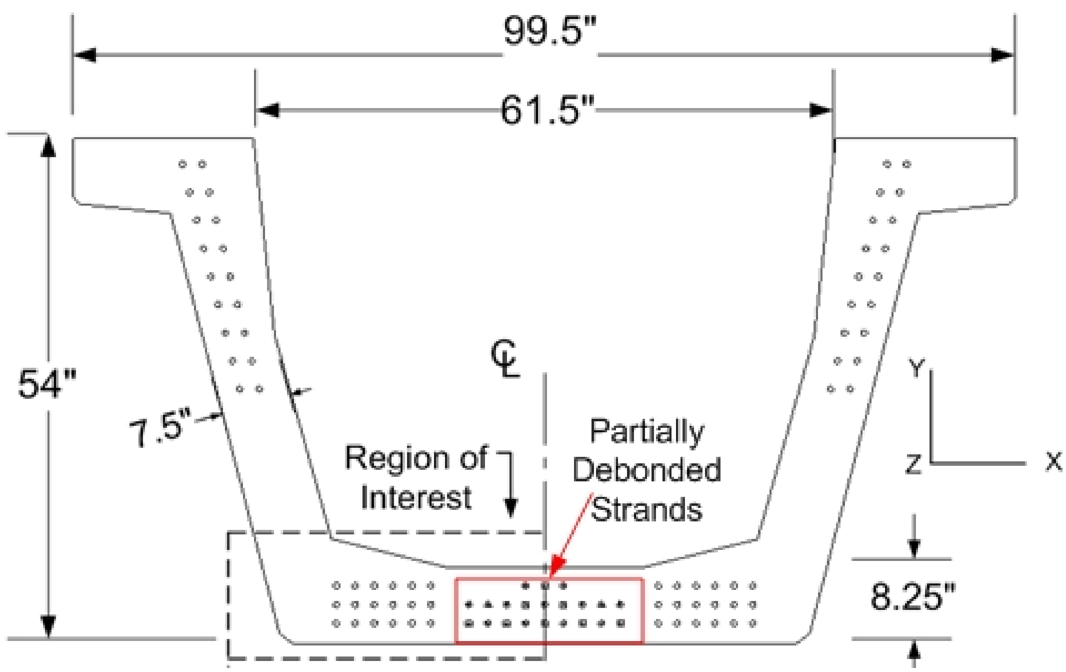

Figure 5-2 U-beam cross section. Adapted from [8] [23]

5.3 Simulation Case Studies

Nonlinear program ABAQUS [1] to investigate the effects of debonded strands and sheathing material in the damage seen in the U-beam girder during production (see Figure 5-1). As earlier mentioned, duplicating the exact observed damage is nearly impossible. Thus, the intent of this study is rather to gain insight into the role that strand debonding mechanisms and patterns may have on the observed damage and as potential source of cracking at beam ends in a qualitative manner.

The study considered the use of soft (tight fitting) sheathing and rigid (oversized hole) debonding. In addition, the arrangement, or distribution, of debonded strands in the beam cross section was also evaluated. Four FE models under different conditions were created and analyzed to study the above-mentioned parameters. The four models were classified as case studies and are described below:

- **Case 1**: As-built U-beam model with tight fitting. This model included all the features of the U-beam unit featuring flexible slit sheathing.
- **Case 2**: Model with staggered debonding arrangement for the unbonded strands with flexible (tight fitting) sheathing.
- **Case 3**: Model with rigid (oversized) sheathing for the debonded strands with the original (“as-built”) debonded strand arrangement. Rigid debonding was simulated by providing oversized holes in the concrete part along the strand unbonded (shielded) length.
- **Case 4**: Model with a staggered debonding distribution for the unbonded strands with rigid (oversized) sheathing.

The front view of the region of interest and debonding strand configuration for Case 1 and Case 3 is shown in Figure 5-3. The strand unbonded length for Cases 1 and 3 is given in Table 5-1 and for Cases 2 and 4 is one quarter (1/4) of those shown in Table 5-1. The debonded length for Cases 2 and 4 was reduced to improve computational efficiency and achieve convergence in the solution of the model. The arrangement of the partially debonded strands for Cases 2 and 4 is shown in Figure 5-4.

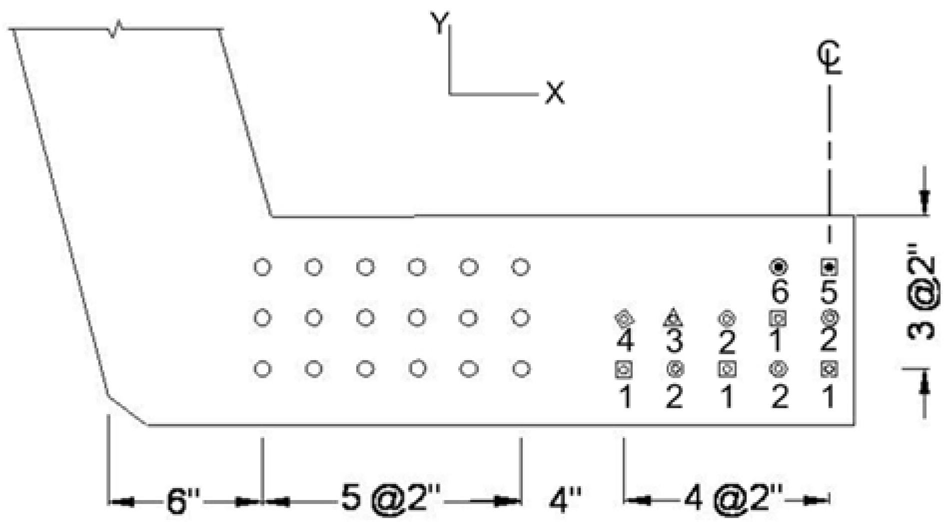

Figure 5-3 View of the region of interest and debonding strand numbering: Cases 1 and 3

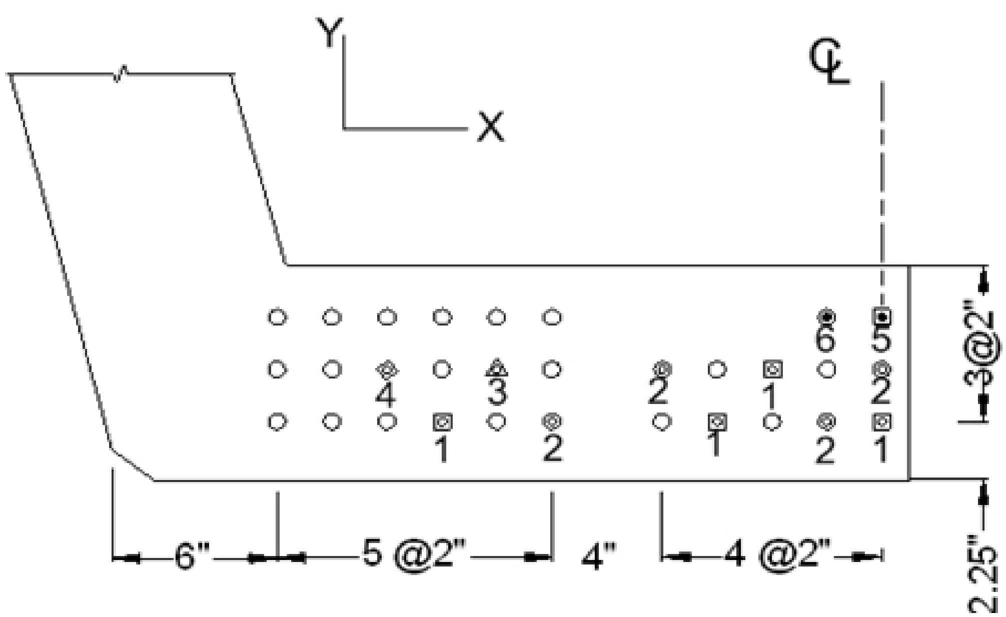

Figure 5-4 Partially debonding strand numbering: Cases 2 and 4

Table 5-1 Debonded strand length in U beam [8]

Unbonded Length (ft)			
ID	Length	ID	Length
1	12.0	4	18.0
2	9.0	5	21.0
3	15.0	6	24.0

1 ft = 0.3049 m

5.4 Case 1: As Built Condition

This case corresponds to the as-built condition, i.e., the U-beam unit for which evidence of damage exists (Figure 5-1) with some modeling assumptions/modifications. A tight constraint is provided to emulate the flexible slit sheathing debonding scheme. Details and schematics of the finite element model together with representative results are presented in the following

5.4.1 Model Geometry, Mesh, Material Properties and Contact Definition

The cross section of the region of interest was a rectangle at the corner of the cross section with dimensions of 28 in. (710 mm) by 8.25 in. (210 mm) as shown in Figure 5-2. As it can be seen from Figure 5-2, the cross section of the U-beam unit was slightly simplified. Since the strands are symmetrically distributed with respect to the center line of the beam (see Figure 1-4 and Figure 5-2), the high fidelity FE model was refined in a region of interest on one side of the beam. The U-beam FE model, which is shown in Figure 5-5, was 56 in. (1420 mm) wide, 54 in. (1370 mm) depth, and 58.33 ft long (17.8 m). The concrete parts were modeled using continuum solid elements (C3D8R: eight-node linear brick with reduced integration.) Half of the beam unit was modeled along the longitudinal direction (Z-axis) due to symmetry.

The end block (see Figure 5-6) was 56 in. (1420 mm) wide, 45.75 in. (1160 mm) in height, and 24 in. (610 mm) long (Z-axis). The side parts, region with embedded strands, of the beam were 7.5 in. (190 mm) wide, 45.75 in. (1160 mm) deep, and 56.3 ft. (17.2 m) long. These parts are inclined by 14.4° in respect with the vertical (Y-axis). The mesh for these concrete parts was 4.0 in. x 4.0 in. x 4.0 in. (100 mm x 100 mm x 100 mm).

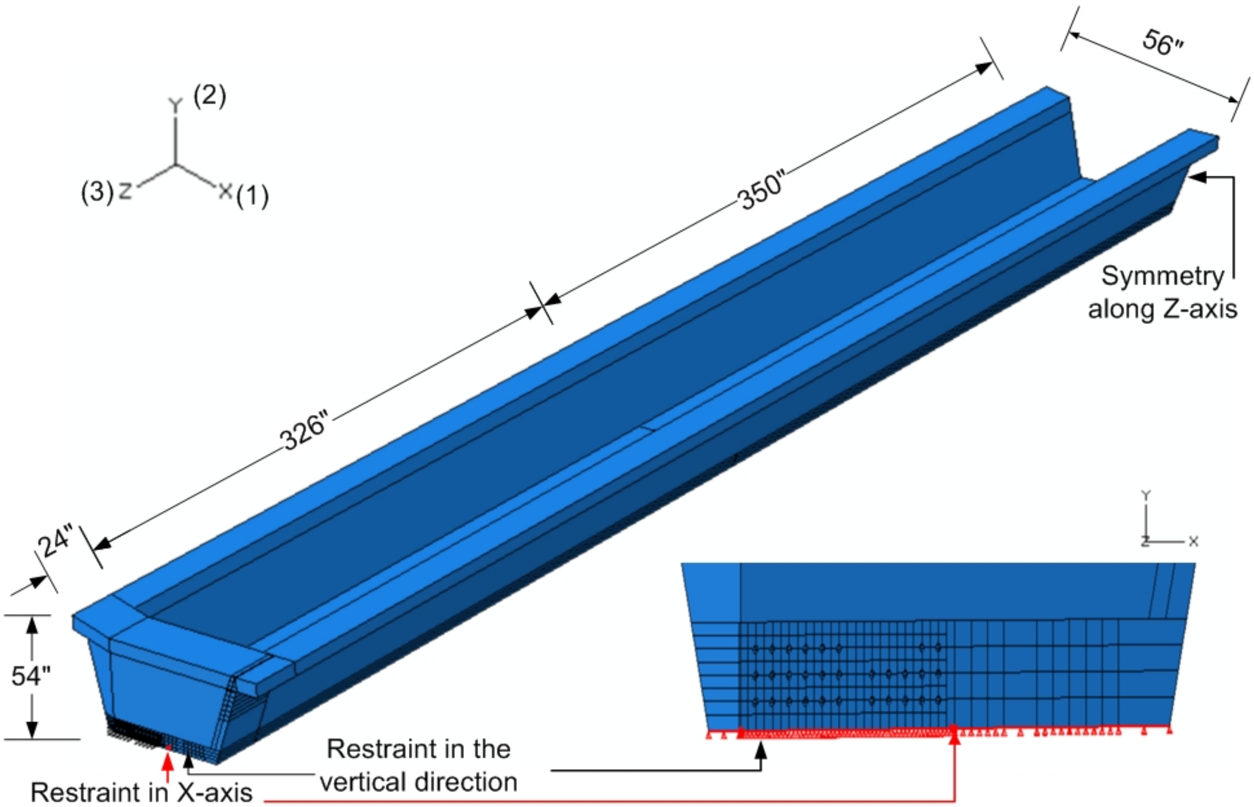

Figure 5-5 Overview of the U-beam girder as built condition model

The bottom flange was composed of three parts. The first, which was the region of interest (see Figure 5-2), was 28 in. (710 mm) wide, 8.25 in. (210 mm) deep, and 48 in. (1220 mm) long in the fully-bonded-strand region to allow transfer of the prestressing force, and 29.2 ft (8.9 m) long along the partially-debonded-strand region to accommodate the largest debonded length and additional length for transmission of the prestressing force. The size of the elements in the bottom flange along the region of interest varied in the cross section (see Figure 5-6) and had a length of approximately 4 in. (100 mm). Beyond the region of interest, the bottom flange was modeled with solid elements and the mesh size was 4 in. x 4 in. x 4 in. (100 mm x 100 mm x 100 mm). To the right of the region of interest (see Figure 5-5) the concrete part was modeled with a coarser mesh compared to the region of interest. The partially debonded strands along the unbonded zone were not accounted for in the model, and fully bonded strands and partially debonded strands along the fully bonded zone were modeled using discrete embedded truss elements.

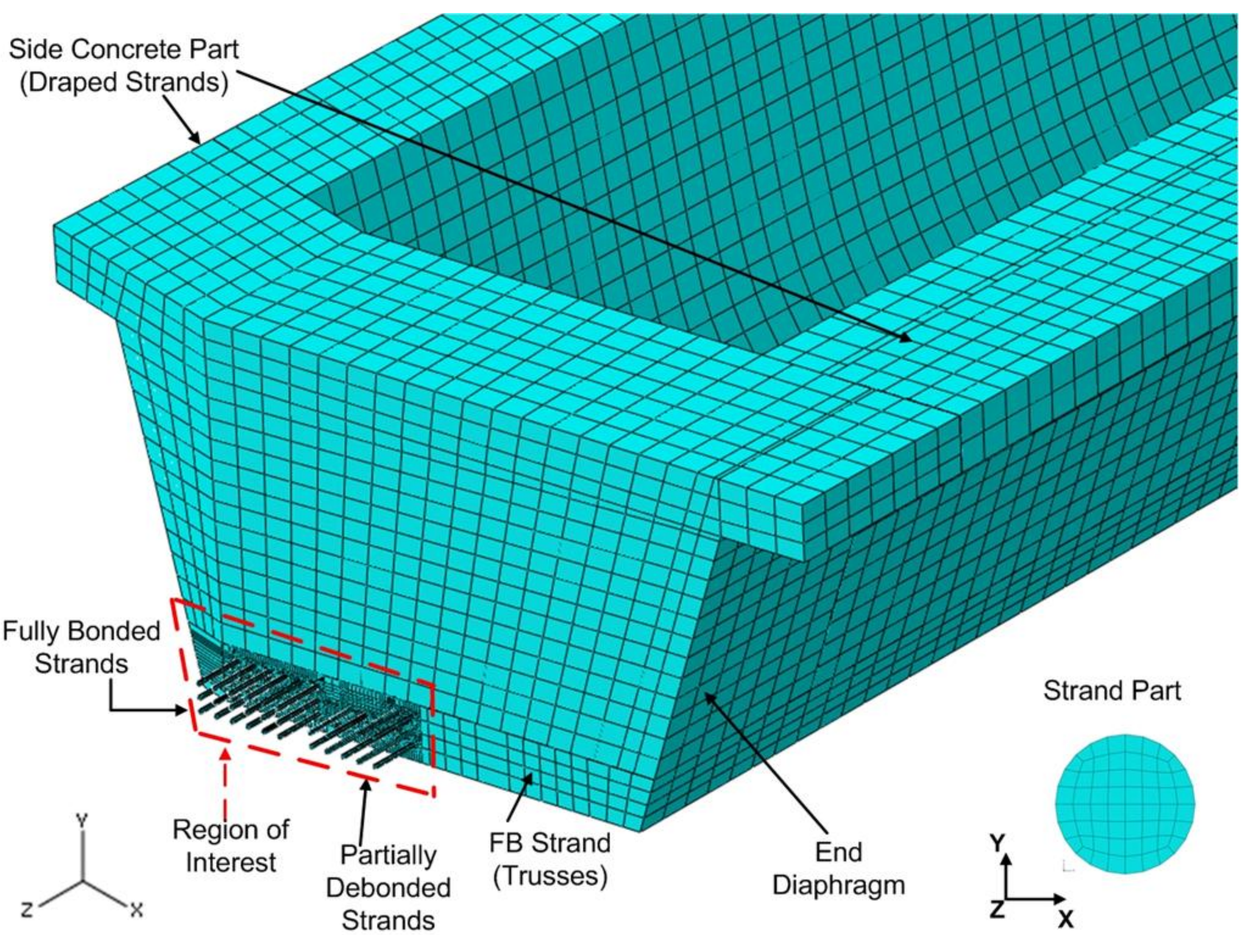

Figure 5-6 End region of the U-beam as built condition model

The strand in the region of interest was modeled as a 3-D cylindrical rod with an unstressed diameter of 0.5268 in. (13.4 mm). The diameter was calculated using the representative area of a 0.6-in.- (15.2 mm) diameter strand, which is 0.218 in^2 (144 mm^2). The fully bonded strands located in the bottom flange (see Figure 5-6) were modeled using continuum 3-D solid elements (C3D8R) elements up to 4 ft (1220 mm) from the beam end to accommodate the transmission length of the prestressing force at release. The partially debonded strands were modeled using C3D8R up to 29.2 ft (8.9 m) from the end of the beam to accommodate the largest debonded length and the respective transfer lengths. The mesh size varied on the cross section and was approximately 4 in. (100 mm) long. Beyond these noticed distances, the strands were modeled as discrete truss elements (T3D2) and the elements were embedded in the concrete (bottom flange). The draped strands located at the sides of the beam (see Figure 5-6) were modeled as discrete truss elements embedded in the concrete region as well, and the hold down point was located at about 47'-3.5" (14.4 m) from the releasing end (Z-axis).

The strand was modeled using linear elastic steel material properties. The elastic modulus was 29,000 ksi (200 GPa) and the Poisson's ratio was 0.3. The concrete was modeled using nonlinear-material behavior. The concrete damaged plasticity (CDP) model [1] was incorporated in the numerical simulation of the large-scale beams. A description of the CDP model is presented in Chapter 4. The compressive strength at release was 8,000 psi (55.2 MPa). The elastic modulus of the concrete was 5098 ksi (35.15 GPa), which was calculated using the expression, $57000\sqrt{f'_{ci}}\,(psi)$ [3]. The parameters used for the CDP model are shown in Table 5-2.

Regarding boundary conditions, the beam model was restrained from vertical displacement (U2) along the front-bottom edge (see Figure 5-5). Symmetry along the Z axis was defined and a center point at the back of the beam was restrained in rotation about the Z-axis (UR3) as shown in Figure 5-5. The model had just one step in which the prestressing force was transmitted into the concrete member. The initial prestressing force was 0.75 fpu, which corresponded to 202.5 ksi (1396.2 MPa). This value was obtained from the manufacturer construction plans [8].

Table 5-2 Concrete damaged plasticity parameters for U-beam model

Concrete parameters	**f'_{ci}=8000 psi**	**Parameters for CDP Model**	
		Dilation Angle, ψ	38°
Concrete Elasticity		Eccentricity, Є	0.1
E_c (ksi)	**5098**	fb0/fc0	1.16
ν	0.2	K_c	0.67
		Viscosity parameter	0.02
Concrete compression hardening		**Concrete tension stiffening**	
Stress (psi)	Crushing strain	Stress (psi)	Cracking Strain
1274	0	670	0
7028	0.00012	335	0.001868
7670	0.00025	260	0.004868
7976	0.00044	224	0.007868
7524	0.00077	207	0.009868
4949	0.00178		
2675	0.00273		
756	0.0041		
257	0.0052		
84	0.00648		

1 ksi = 6.89 MPa

The bond between the strand and the surrounding concrete was simulated using surface-based contact definitions as described in Section 4.3. The coefficient of friction used for the U-beam models was 0.59, which was obtained from the calibrated small-scale beam models (see Section 4.5.2). Along the unbonded zone, the coefficient of friction was defined as zero to eliminate the bond interaction between the strand and concrete due to the use of sheathing material. However, flexible (tight fitting) sheathing allows radial stresses to develop upon release because longitudinal shear stresses do not take place along the debonded length. Thus, normal interaction at the interface with the concrete is developed, as was explained in Section 4.5.2. All the concrete parts were interconnected using tie-constraint (surface-to-surface) interaction definitions. The solid strand and truss strand parts were connected by means of kinematic coupling constraints (U1, U2, and U3). The truss elements embedded in the concrete were connected to the concrete parts using embedded region constraints. Table 5-3 shows a summary of the interaction constraints used for the U-beam models.

Table 5-3 Interaction constraints in U-beam models

Part 1 (Master)	Part 2 (Slave)	Interaction-Definition
Concrete (solid)	Concrete (solid)	Tie-constraint
Strand (solid)	Concrete (solid)	Contact Friction Model
Strand (Truss)	Strand (solid)	Kinematic Coupling
Strand (truss)	Concrete (solid)	Embedded Region

5.4.2 Results

Representative results obtained from the as-built U-beam model, Case 1, are presented in this section. Contour plots on the cross section of the beam on the region of interest are used to show general trends that can be correlated to the observed damage on the U-girder unit during production. Additional contour plots and response traces along different paths at the interface of the partially debonded strands are shown in Appendix D. The value for the maximum tensile strength defined for the concrete for the damaged plasticity (CDP) model (see Table 5-2) corresponds to the value of the modulus of rupture, 670 psi (4.6 MPa), which was calculated as $7.5\sqrt{f'ci}\,(psi)$. Figure 5-7 shows the damaged observed during production of the U-beam unit and the maximum principal plastic strain contour plot on the cross section of the as-built condition model (Case 1) at the release end. It can be seen in Figure 5-7 that the as-built model with tight fit satisfactorily predicts, in a qualitative sense, the damaged observed upon detensioning.

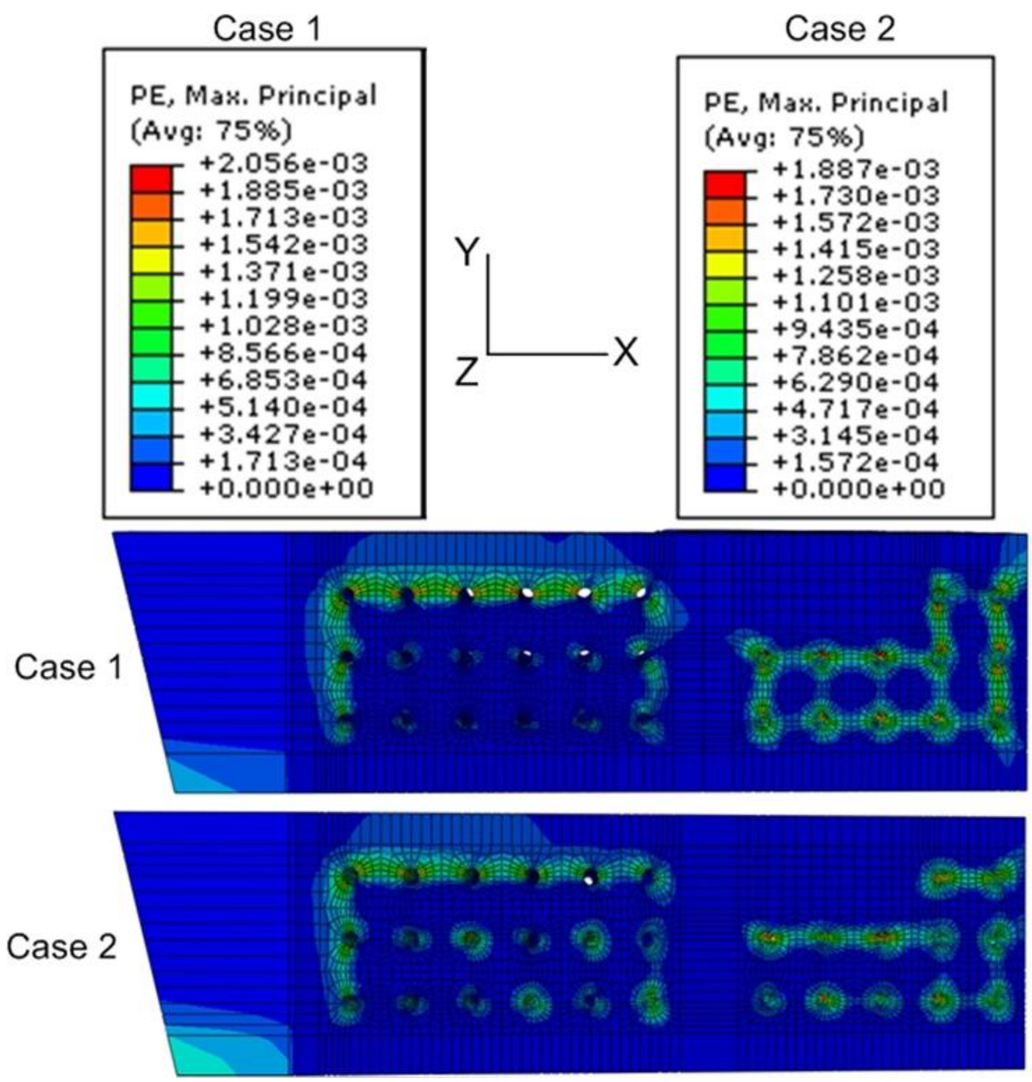

Figure 5-7 Damage seen during production of U-girder unit vs. maximum principal plastic strains: Case 1

The contour plot that shows the maximum principal stresses on the cross section at the release end of the as-built condition (Case 1) model is shown in Figure 5-8. Again, the maximum tensile strength in the CDP model was 670 psi (4.6 MPa). It can be seen from Figure 5-8 that the concrete elements surrounding the partially debonded strands had principal tensile stress values above 670 psi (4.6 MPa) indicating cracking of the concrete as it was observed in the picture of damage of the U beam (Figure 5-1).

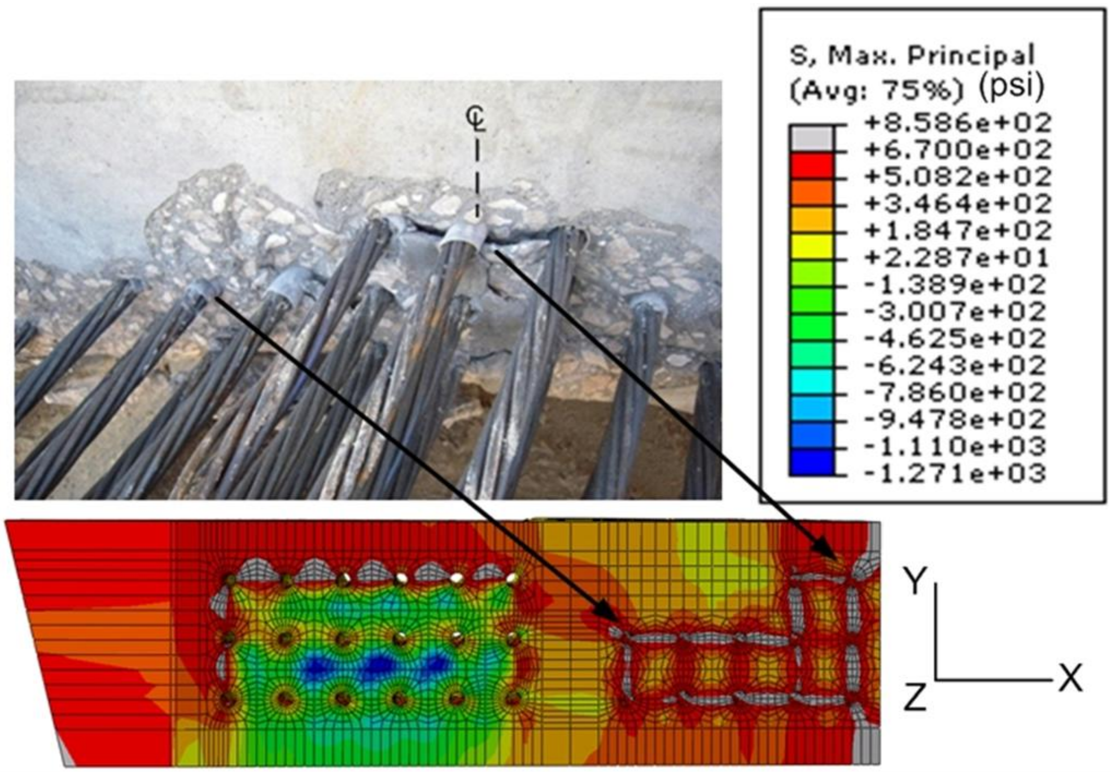

Figure 5-8 Maximum principal stresses: U-beam as-built condition (Case 1) model

It shall be mentioned that prediction of the exact cracking pattern is not possible with the CDP model since the concrete softness after the maximum tensile stress (i.e., damage) is reached. However, Figure 5-9 shows the regions that are beyond the linear-elastic regime of the concrete tension-response curve (see Figure 4-3-a). It can be observed in Figure 5-9 that the areas around the partially debonded strands are clearly beyond the elastic regime. Thus, the cracking and spalling off of the concrete observed at release during production of the U-beam correlates well to these results. Therefore, even though the exact cracking pattern cannot be duplicated with the modeling assumptions, the overall damage zone-observed during production of the U-beam girder was well captured by FE simulation (see Figure 5-7 - Figure 5-9).

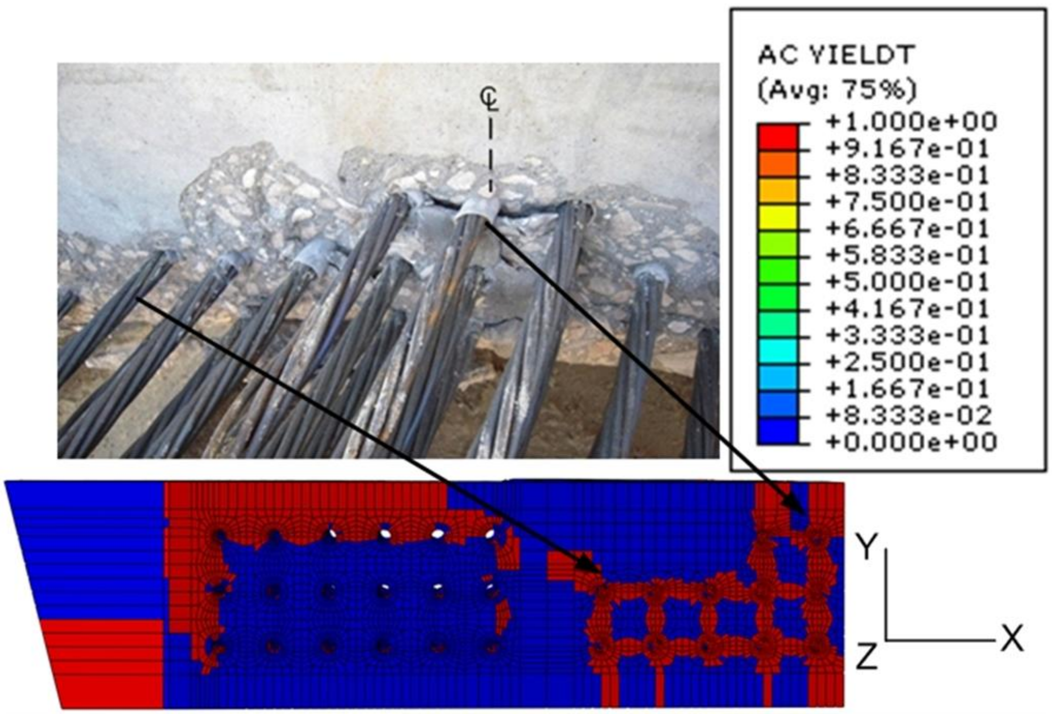

Figure 5-9 Active Yielding of the concrete at beam cross section at release end: Case 1

5.5 Case 2: Tight Fitting with Staggered Debonding Distribution

The simulation study in Case 2 had two distinct objectives. First, to investigate if a staggered unbonded distribution could help reduce the localized beam-end damage observed in the “as-built” model. The second aim was to assess the effect of the distribution of debonded strands in the beam cross section in terms of longitudinal shear stresses at the beam end. In the "as-built" configuration the partially debonded strands in the U-beam were placed in the center of the bottom flange, which could lead to high longitudinal shear stresses due to the large unbalance of forces along the section width. The use of a staggered debonding pattern is required in the bridge design guidelines of the Florida DOT [7], who recommended to evenly distribute the debonded strands such that, whenever possible, the shielded strands be separated in all directions by at least one fully bonded strand. However, the rationale behind the noted recommendation is not mentioned and could not be found in the available literature. A staggered strand debonding configuration was thus studied for the U-beam models using both flexible (tight fitting) sheathing and rigid (oversized) debonding, namely Case 2 and Case 4. The U-beam model with staggered debonding distribution and tight fit is referred to in this study as Case 2. The arrangement of the partially debonded strands is shown in Figure 5-4. The modeling details and representative results are presented next. Results from Case 2 are compared with those from Case 1 in Section 5.8.1.

5.5.1 Specific Modeling Details

The finite element model developed for Case 2 is similar to the one presented for Case 1 (see Figure 5-5 and Figure 5-6). However, there were two main differences. First, due to the staggered distribution of the partially debonded strands, the length of the fully bonded strands was equal to the length of the unbonded strands in the region of interest. Secondly, in order to maximize computational efficiency, the length of the region of interest was reduced from 29.2 ft-long (8.9 m) to 9.3 ft-long (2.85 m). The unbonded lengths were reduced to one-quarter of the original debonded lengths (see Table 5-1). The region of interest is shown in Figure 5-10 and as it can be observed from this figure, the strands in the region of interest (both fully bonded and partially debonded) were modeled as cylindrical rods (solid elements – C3D8R) up to 112” (2845 mm) from the releasing end. The other parts of the model remain similar to the geometry showed for Case 1 (see Figure 5-5 and Figure 5-6). Material properties, boundary conditions, and interaction constraints were also similar to those presented in Section 5.4.1. Symmetry along the Z-axis was also defined for this U-beam model (Case 2).

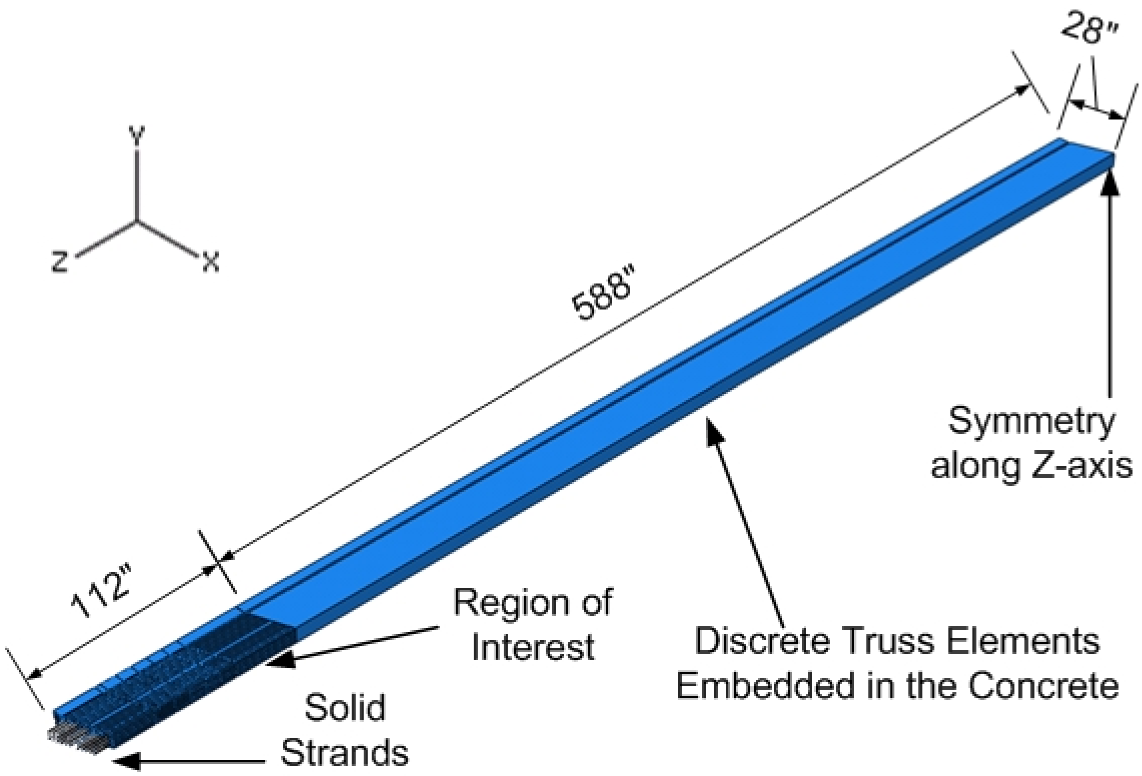

Figure 5-10 U-beam Bottom Flange for Case 2: Half-region along X-axis

5.5.2 Results

Representative results for Case 2 in the form of stress and strain contour plots are presented herein. The maximum principal plastic strains contour plot are compared to the cracking and spalling damage observed for the U-beam girder in Figure 5-11. From this figure, it can be seen that the simulation predicts a reduced level of damages if one fully bonded strand is located between partially debonded strands, except for the first column from left to right (front view) since those three strands were kept as the original distribution for being the center strands. The strain contour plot in Figure 5-11 shows high strains in the bottom-left region. This behavior is due to issues with the boundary conditions. The maximum principal stresses contour plot obtained from Case 2 is shown in Figure 5-12 and the results are also compared to the damage observed during production. As it is observed from this figure, the maximum principal stresses at the cross section of the beam model at the beam end are reduced compared to Case 1 (see Figure 5-8) when the partially debonded strands were staggered.

The results obtained from Case 1 and Case 2 are further compared in Section 5.8.1 for a better understanding of how the debonding strand pattern can minimize high stresses at the beam end and reduce longitudinal shear stresses.

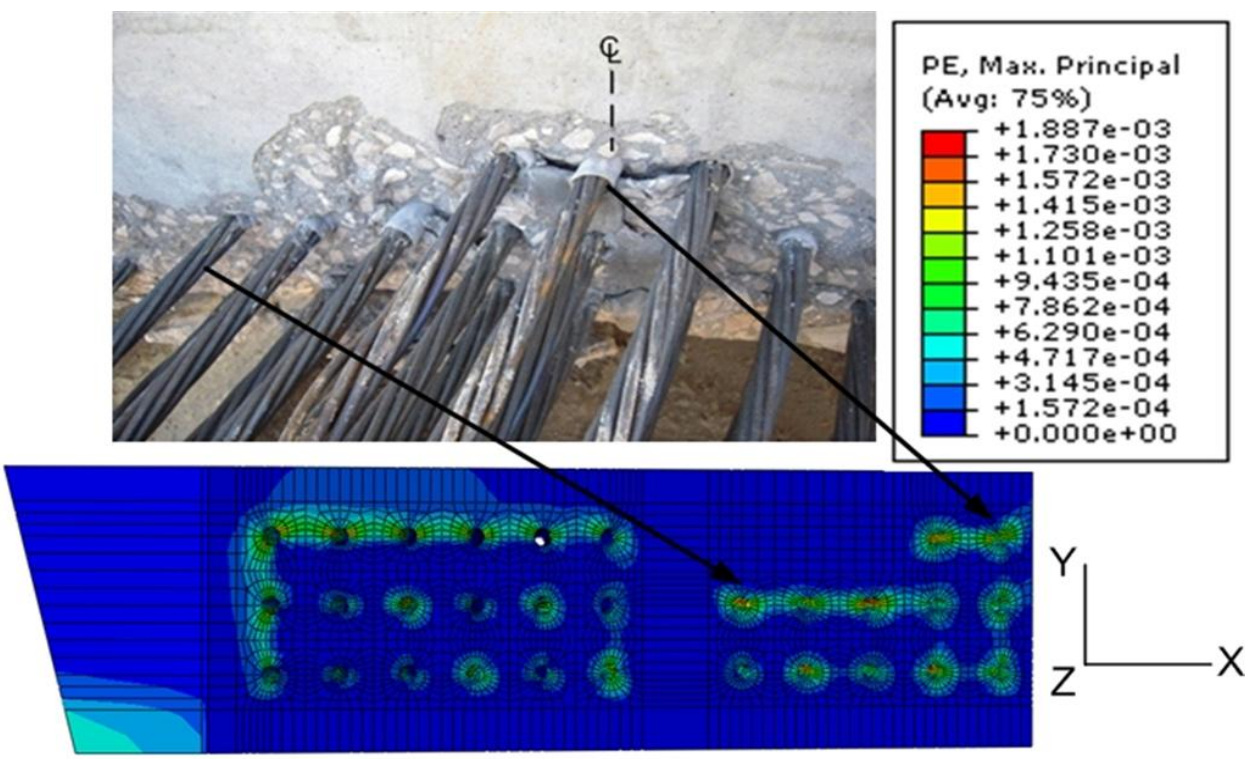

Figure 5-11 Maximum principal plastic strain vs. damage observed during production: Case 2

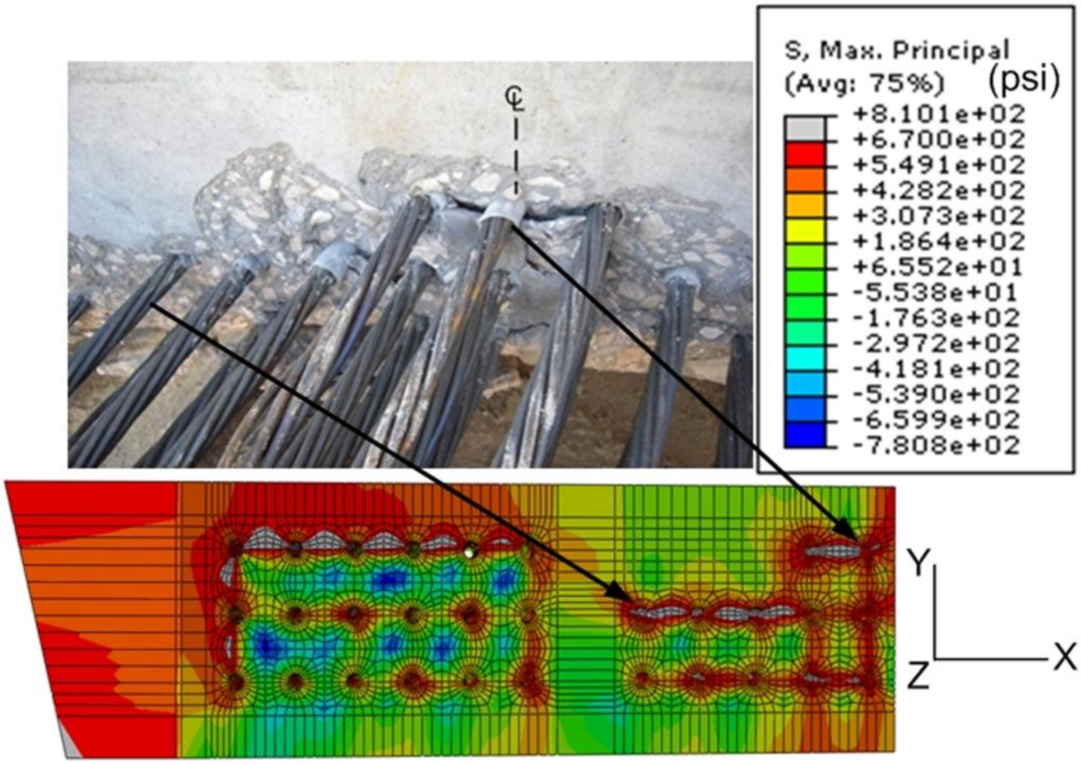

Figure 5-12 Case 2: Maximum principal strain vs. damage observed during production

5.6 Case 3: Oversized Debonding with Original Unbonded Strand Configuration

For Case 3 some modeling simplifications and assumptions had to be made due to numerical problems with the full-model (similar to Case 1) with rigid (oversized) debonding. To minimize computational demand, symmetry along the X-axis was assumed for this modeling case. This modeling simplification implies that the skew angle (18°) was considered small so that the beam was considered as straight. It is recognized that the assumption of lateral symmetry for the skew beam cross-section is not technically correct and that it has some drawbacks on the accuracy of the model results. These effects are addressed in Section 5.6.3. Geometric details of the model and relevant results are presented next.

5.6.1 Model, Geometry, Mesh, and Generalities

An oversized hole was defined in the concrete part of the model to simulate the rigid debonding material. The hole was 0.95 in. (24.1 mm) in diameter around the 3D cylindrical strand, which was greater than the diameter of the unstressed strand (0.5268 in. [13.4 mm]). Thus, the rigid sheathing was successfully simulated by fully decoupling the strand and the concrete parts. The size of the hole was selected so to not affect the elements in aspect ratio (i.e., cross-sectional area to length). The model developed for Case 3 is shown in Figure 5-13. The region of interest is similar to in Case 1 (see Figure 5-3). The main difference between Cases 1 and 3 is that in Case 3 symmetry was assumed along the X-axis. The total length of the model was 58.3 ft (17.8 m), half of the length of the U-beam girder, due to symmetry along the Z-axis.

The concrete part was modeled using solid elements (C3D8R) as it was described in Case 1, and the size of the elements was approximately 3.5”x3.5”x3.5” (90 mm x90 mm x 90 mm). The strand in the region of interest was modeled as a cylindrical rod with a diameter of 0.6-in (15.2 mm) as was previously described for Cases 1 and 2. However, for Cases 3 and 4, no strand elements were defined along the unbonded length to minimize computational demand. Rather, only about 6 in. (150 mm) of strand measured from the fully bonded zone toward the unbonded length were modeled using C3D8R elements to allow for the dilation and relative slip of the strand at the onset of the fully bonded zone upon release. The size of the elements for the strand (cylindrical rod) varied in cross section as it was earlier mentioned and the length of the elements was about 3.7” (94 mm). The elements in the strand part were given with a slightly higher mesh size because, as described in Table 5-3, the concrete part was defined as the slave surface, and this surface needs to be smaller or equal to the master surface (cylindrical strand part). The end-zone for the Case 3 is shown in Figure 5-14. As seen in this figure, no major changes were made between Cases 1 and Case 3 except for the symmetry definition along X-axis. The material properties and constraints are similar as described in Section 5.4.1.

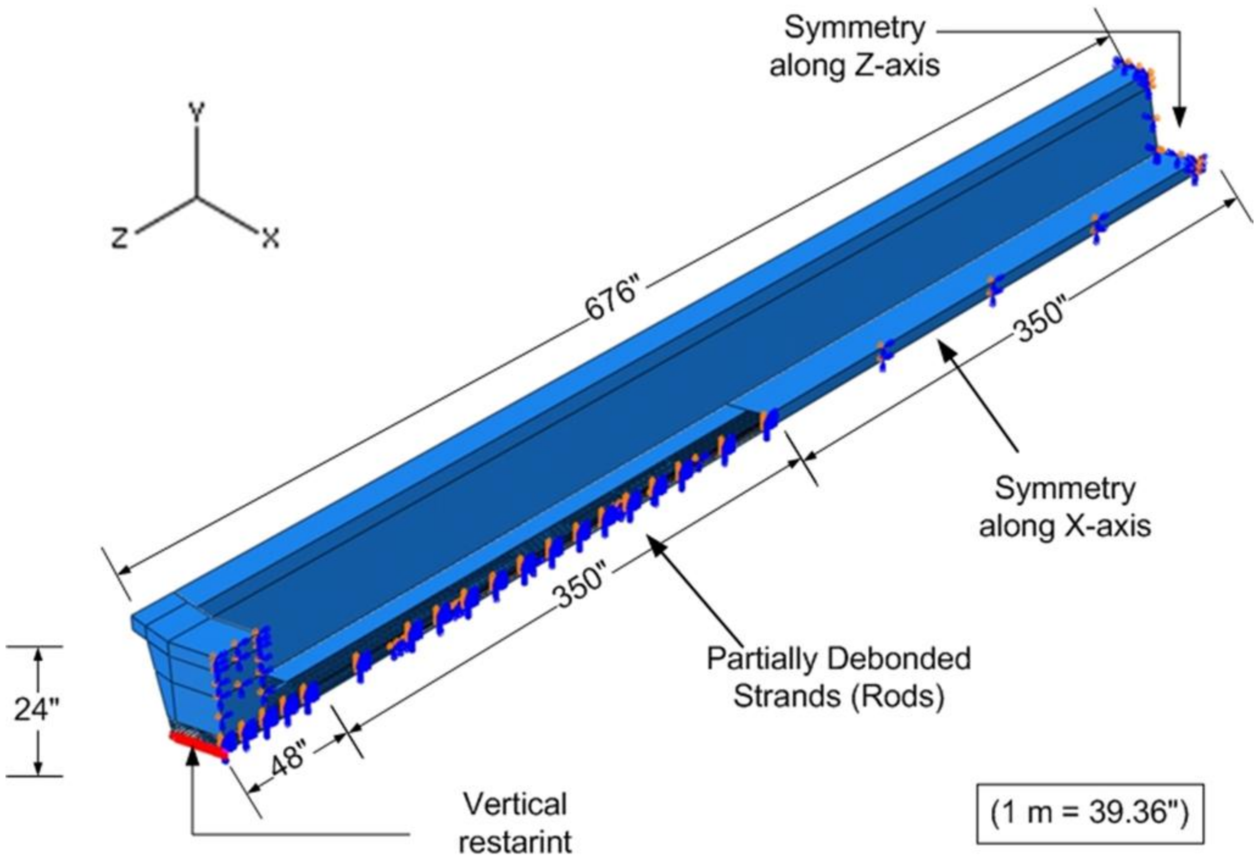

Figure 5-13 Skew U-beam model with oversized hole and original debonded distribution: Case 3

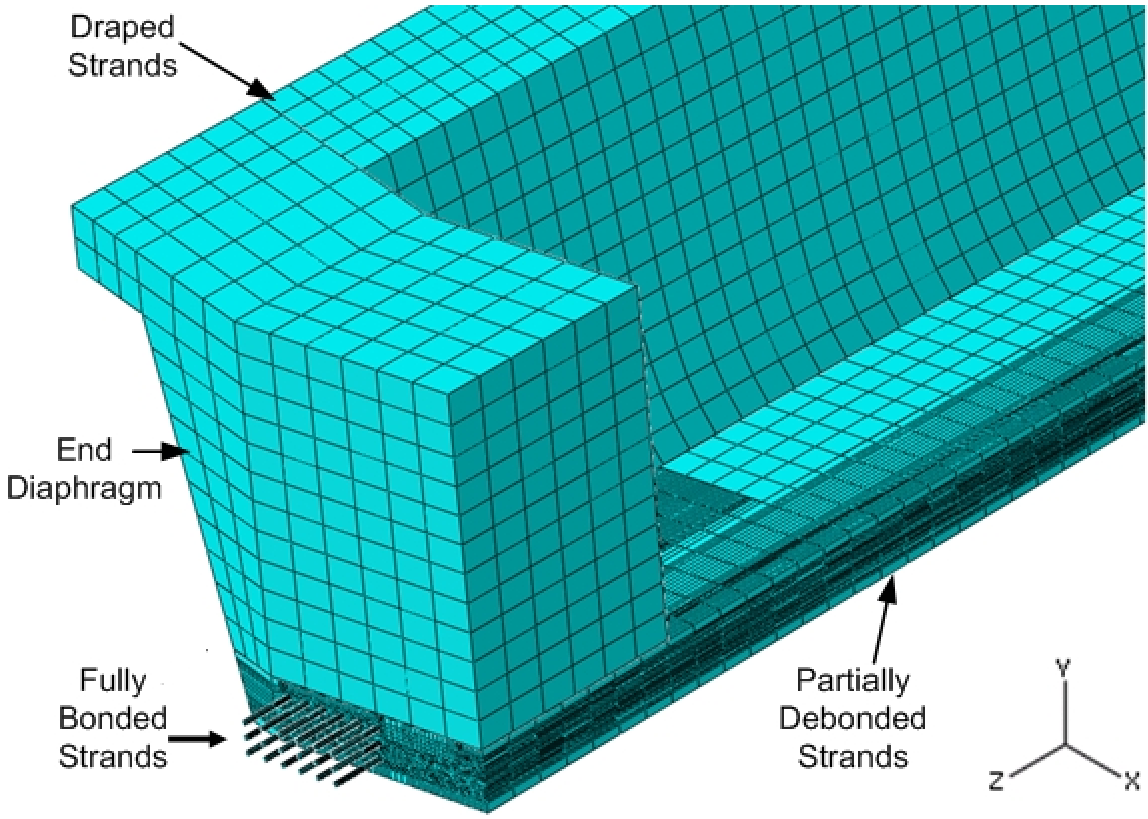

Figure 5-14 End-zone view: U-beam model – Case 3 (Half-model along X-axis)

5.6.2 Results

Contour plots that show results from Case 3 are presented herein. However, it should be noted that the assumption of symmetry along X-axis affected the accuracy of the results, especially at the beam end. This is addressed with detail in Section 5.6.3. Nonetheless, the results obtained from Case 3 gave valuable information on how the use of rigid (oversized) sheathing can help minimize high stresses in the end region of the U-beam girder upon detensioning. A detailed comparison of the results obtained from Case 1 and Case 3 are shown in Section 5.8.2.

The maximum principal strain contour plot at the beam end for Case 3 is shown in Figure 5-15. It is seen from this figure that at the bottom-right side (front view) of the U-beam model, shows a high concentration of strains. This is not a real effect and is attributed to issues with symmetric boundary condition defined along X-axis. This same issue is observed in the contour plots obtained for the equivalent plastic strain in uniaxial tension (PEEQT) shown in Figure 5-16. However, Figure 5-16 also shows that at a distance of 12 in. (300 mm) from the beam end the strain values significantly drop. The difference is attributed to the fact that at a distance of 1 ft. (300 mm) from the skew-end the effects of symmetry in X-axis are reduced. A top view of the end of the beam model is shown in Figure 5-17 for a better understanding of this issue.

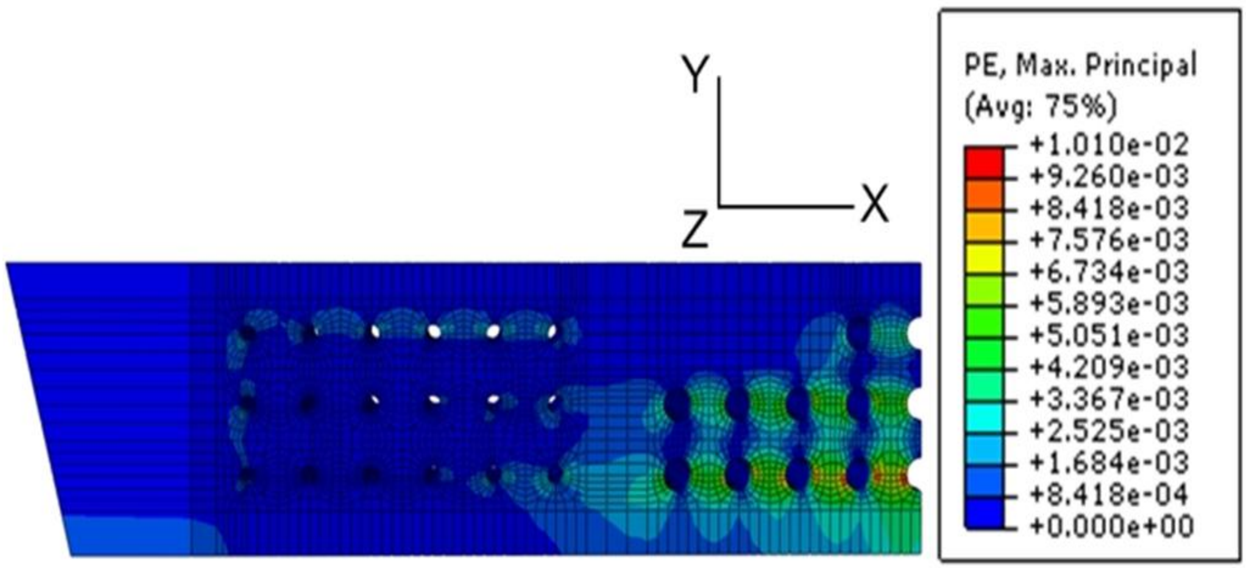

Figure 5-15 Case 3: Maximum principal plastic strain at release end

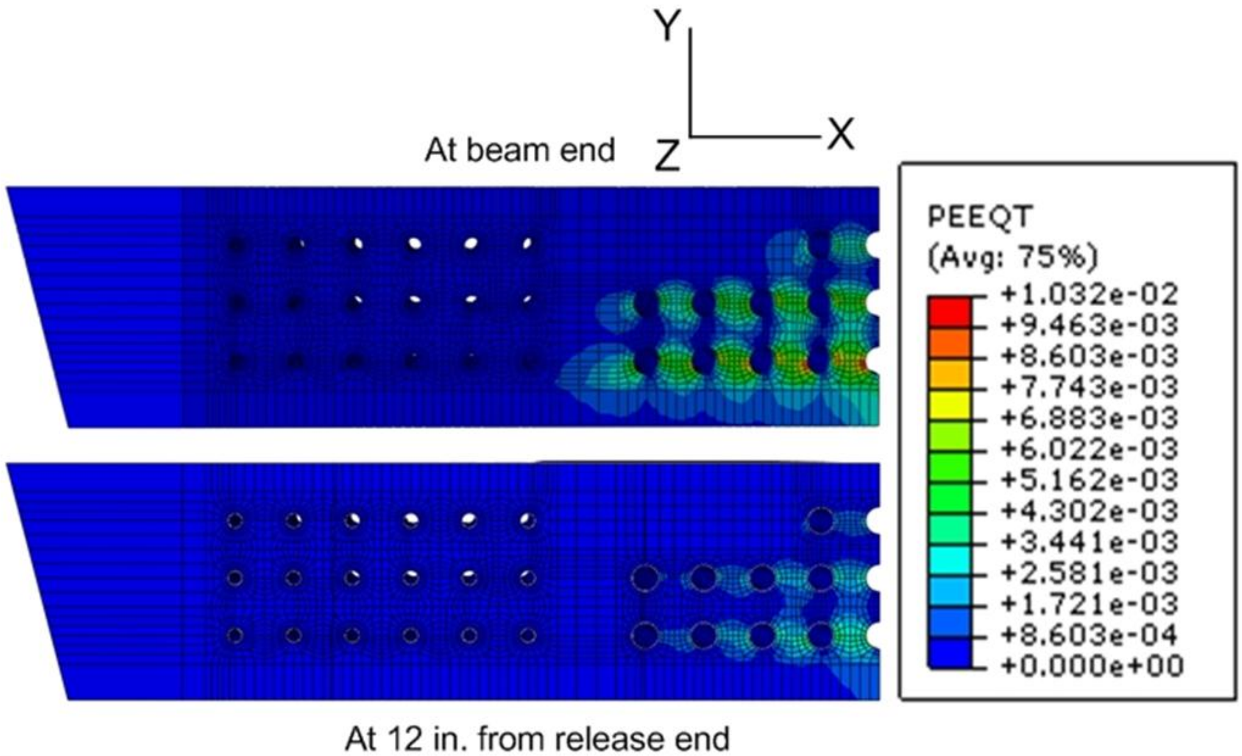

Figure 5-16 Case 3: Equivalent plastic strain in uniaxial tension

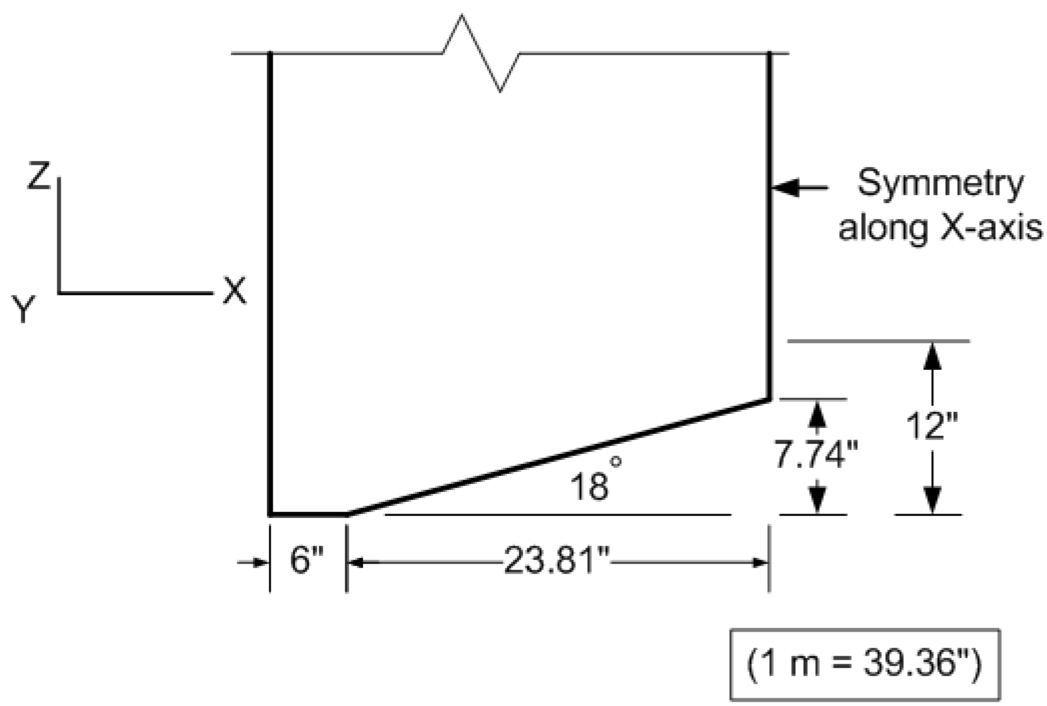

Figure 5-17 Top view of the end of the bottom flange of the beam model with symmetry along X-axis

5.6.3 Effects on Symmetry Assumptions

In order to evaluate the effects on symmetry along the X-axis made in the model for Case 3 model (see Figure 5-13), the results from a model similar to Case 1 but with symmetry along X-axis are compared to the results from the full model from Case 1 (see Section 5.4.1). Contour plots at the cross section from both models at the beam end are used as the basis for the comparison.

In Figure 5-18, the maximum principal plastic strain contours are shown for both models. It can be seen that the assumption on symmetry along the X-axis increased the plastic strain values, particularly around the location of the partially debonded strands.

Contour plots that show the equivalent plastic strains in uniaxial tension (PEEQT) are presented in Figure 5-20. The activated yielding flag on the concrete elements (tensile stresses beyond elastic regime) is shown in Figure 5-19. The maximum principal stresses for Case 1 and the skew beam model with symmetry along X-axis and tight fitting debonded strand is shown Figure 5-22. In

Figure 5-20, Figure 5-19, and Figure 5-22 similar results are obtained in terms of higher values due to the assumption of symmetry along X-axis for the skew-beam model. That is, the assumption of symmetry along the X-axis increases the stresses and strains at the end of the beam model especially toward the location of the partially debonded strands.

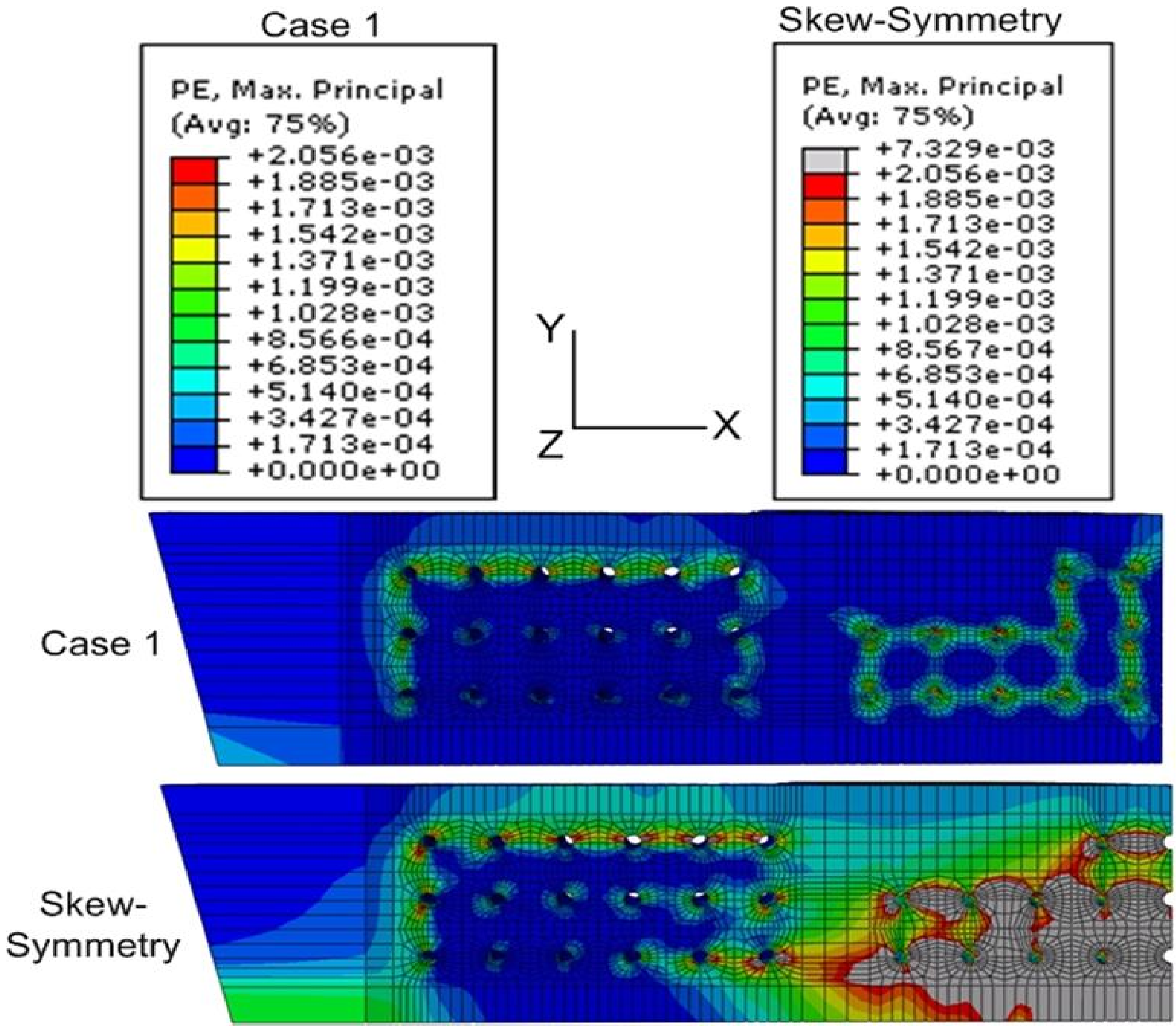

Figure 5-18 Maximum principal plastic strain: Case 1 vs. Skew- Symmetry Case 1

However, if contour plots are obtained at a small distance from the release end such as 12 in. (300 mm), where the beam becomes certainly straight (or where the effects due to symmetry along X-axis for a skew beam somewhat decrease) similar response is obtained from both models. This is shown in Figure 5-21.

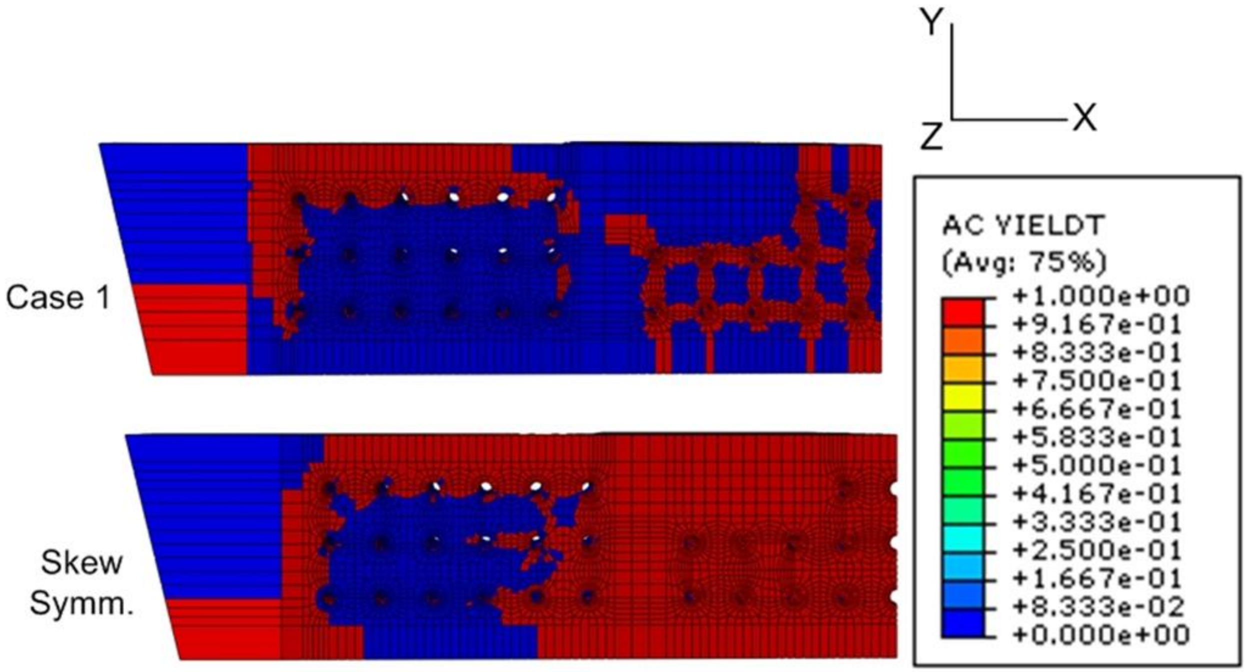

Figure 5-19 Effects on skew-symmetry boundary condition: Actively yielding

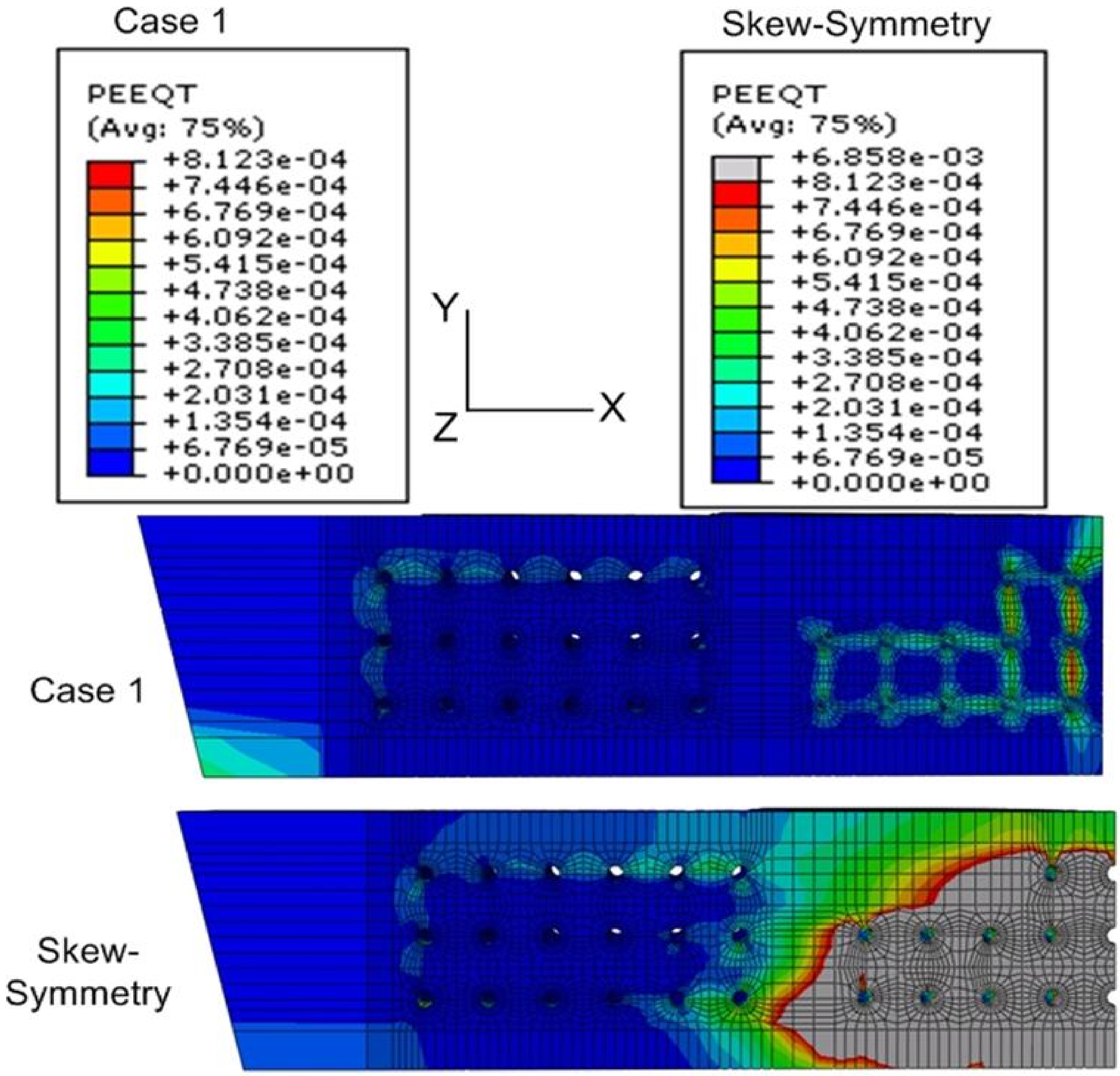

Figure 5-20 Case 1 vs. Skew-symmetry conditions: Equivalent plastic strain in uniaxial tension at beam end cross section

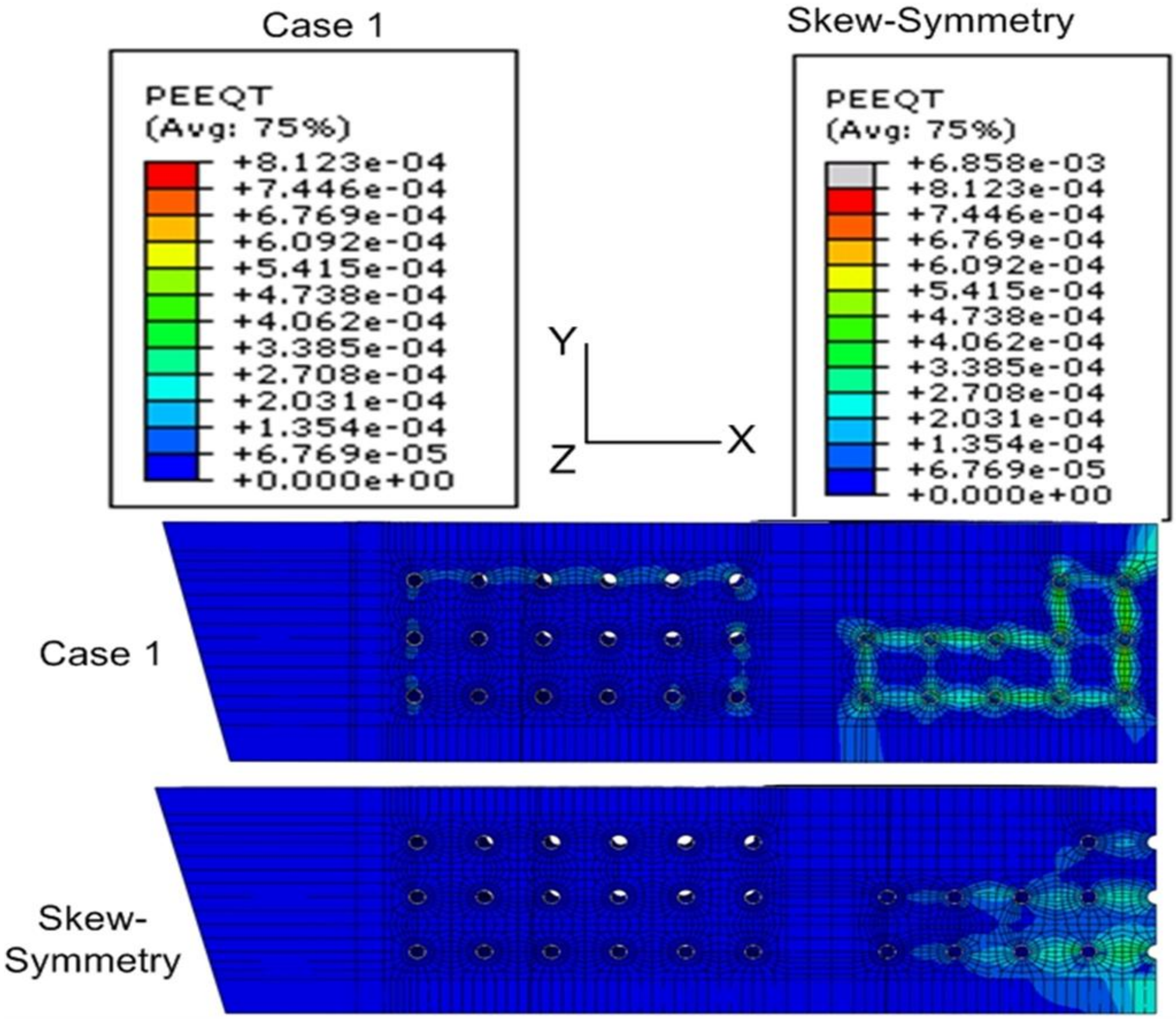

Figure 5-21 Equivalent plastic strain in uniaxial tension at 12 in. from release end

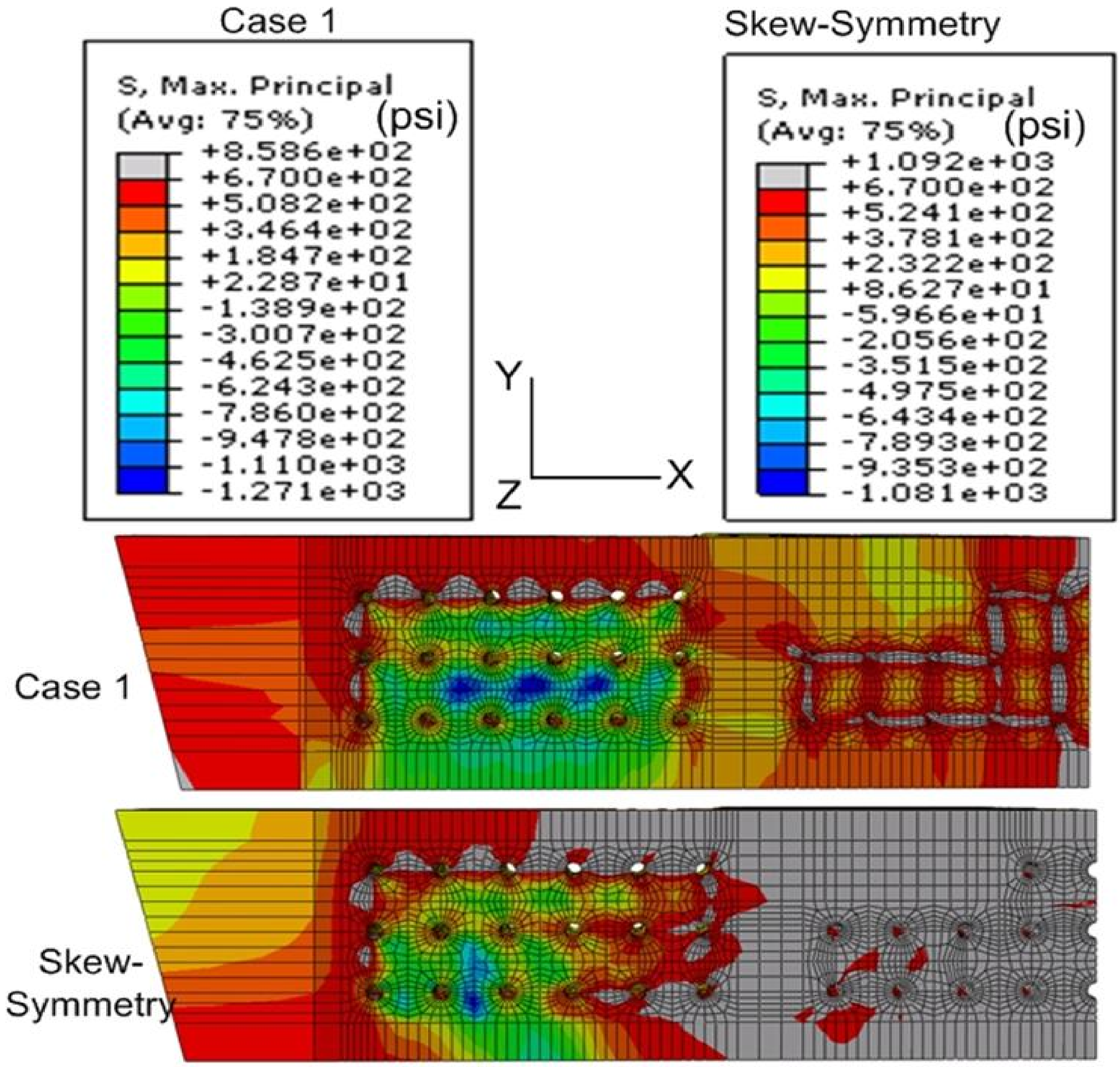

Figure 5-22 Maximum Principal Stresses: Case 1 vs. Skew-Symmetry

5.7 Case 4: Oversized Debonding with Staggered Unbonded Strand Distribution

In the case of the model with staggered debonding distribution and oversized hole, similar issues with convergence of the full numerical beam model (similar to Case 1) were encountered as described in Section 5.6 for Case 3. Therefore, the assumption of symmetry along the X-axis was also made for Case 4. A brief description of the model is following presented since the U-beam model developed for Case 4 has similarities to Cases 2 and 3.

5.7.1 Generalities of the Model

The model developed for Case 4 is similar to Case 2 in terms of the pattern distribution of the partially debonded strands (see Figure 5-4), and the dimensions of the region of interest are also similar to those presented in Section 5.5.1. On the other hand, Case 4 is comparable to the one in Case 3 since symmetry along X-axis was assumed. The impact of this assumption for a skew-beam was presented in Section 5.6.3. The geometry for Case 4 is shown in Figure 5-23.

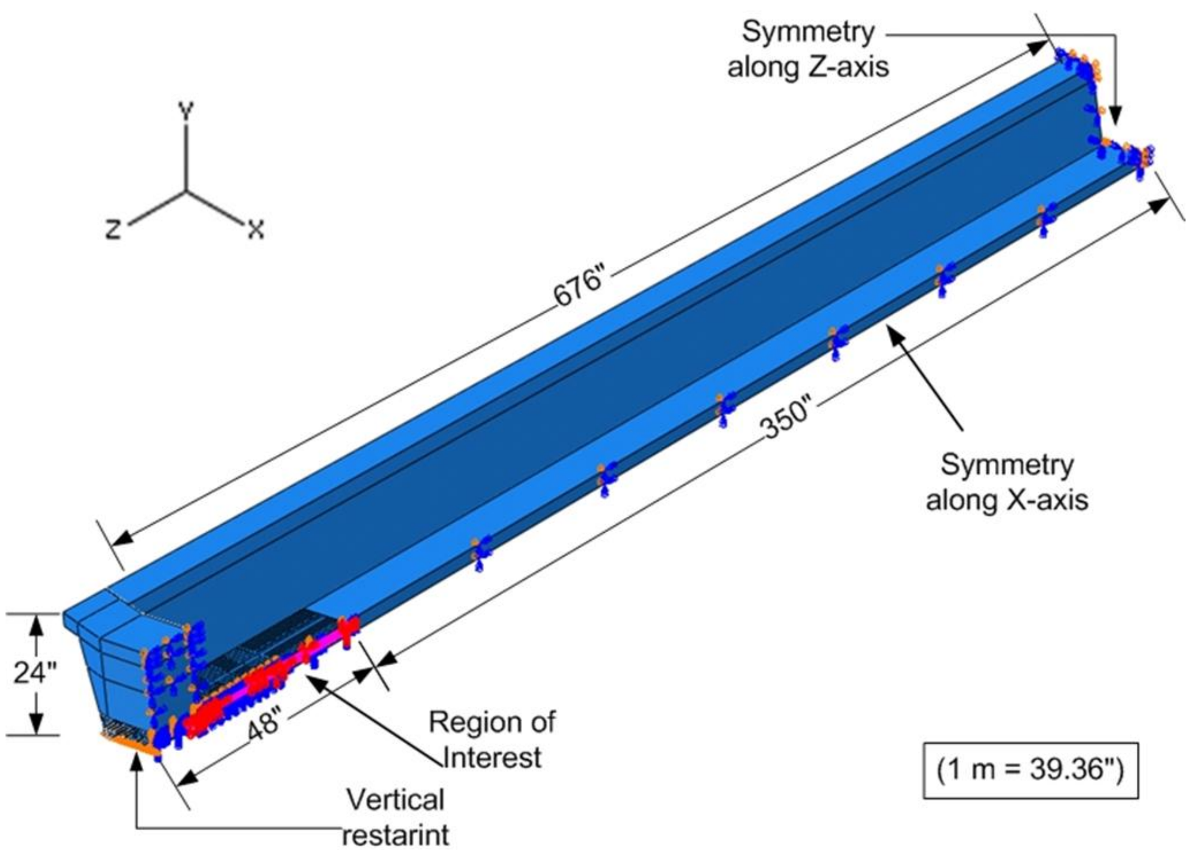

Figure 5-23 Overview of the model for Case 4

In Case 4 the fully bonded and partially debonded strands along the region of interest were modeled as 3-D cylindrical rods. However, along the unbonded zone, the strand part was almost eliminated; only about 6 in. (150 mm) [measured from the fully bonded zone toward the debonded zone] of cylindrical was rod was modeled as discussed in Section 5.6.1. All the concrete parts were modeled using continuum solid elements, and discrete embedded truss elements were used to modeled the strand beyond the region of interest and the draped strands located in the side part of the U-beam girder. As it can be seen from Figure 5-23, the model for Case 4 is similar to that of Case 2 (see Section 5.5) and Case 3 (see Section 5.6). Representative results from Case 4 are given next.

5.7.2 Results

Figure 5-24 shows the maximum principal plastic strain at the beam end and at a cross section 12 in. (300 mm) into the beam (see Figure 5-17). It is seen from Figure 5-24 that just few inches from the skew-release end the plastic strains decay quickly. This is also observed from the contour plots that show the equivalent plastic strain in uniaxial tension (PEEQT) in Figure 5-25. Thus, these two figures show that while the assumption of symmetry along X-axis leads to an increase on the response at the beam end, that this effect decreases rapidly into the beam. Thus, the simulation results are considered reliable in qualitatively shown that the use of a staggered debonding pattern and oversized strand sheathing decrease the high stresses in the end region upon release. This is further discussed in Section 5.8.2, where results from the four skew-beam models are compared to each other for a better understanding on the improvement on the results upon the use of a staggered debonding distribution and rigid (oversized) strand sheathing.

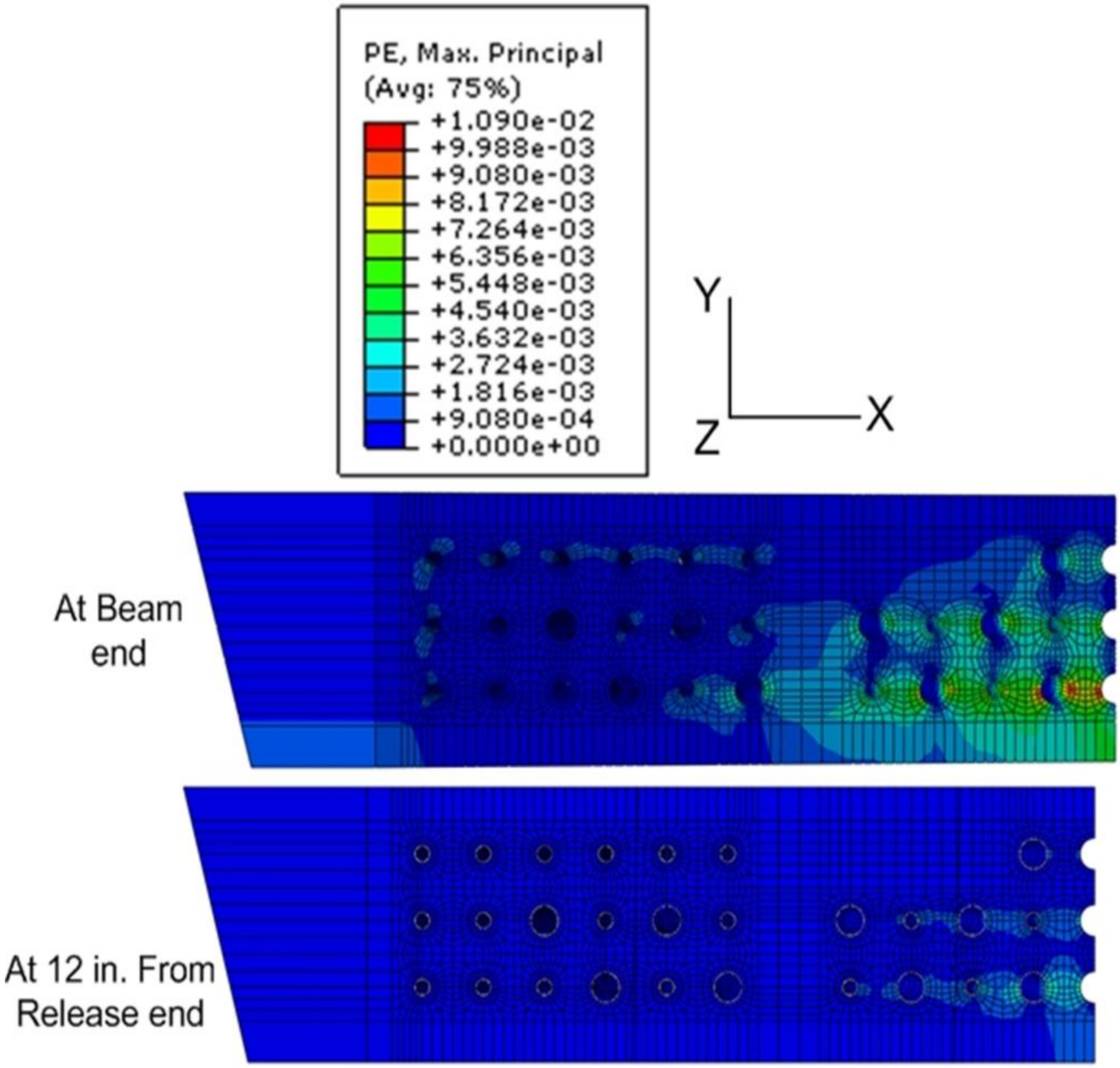

Figure 5-24 Results for Case 4: Maximum principal plastic strain

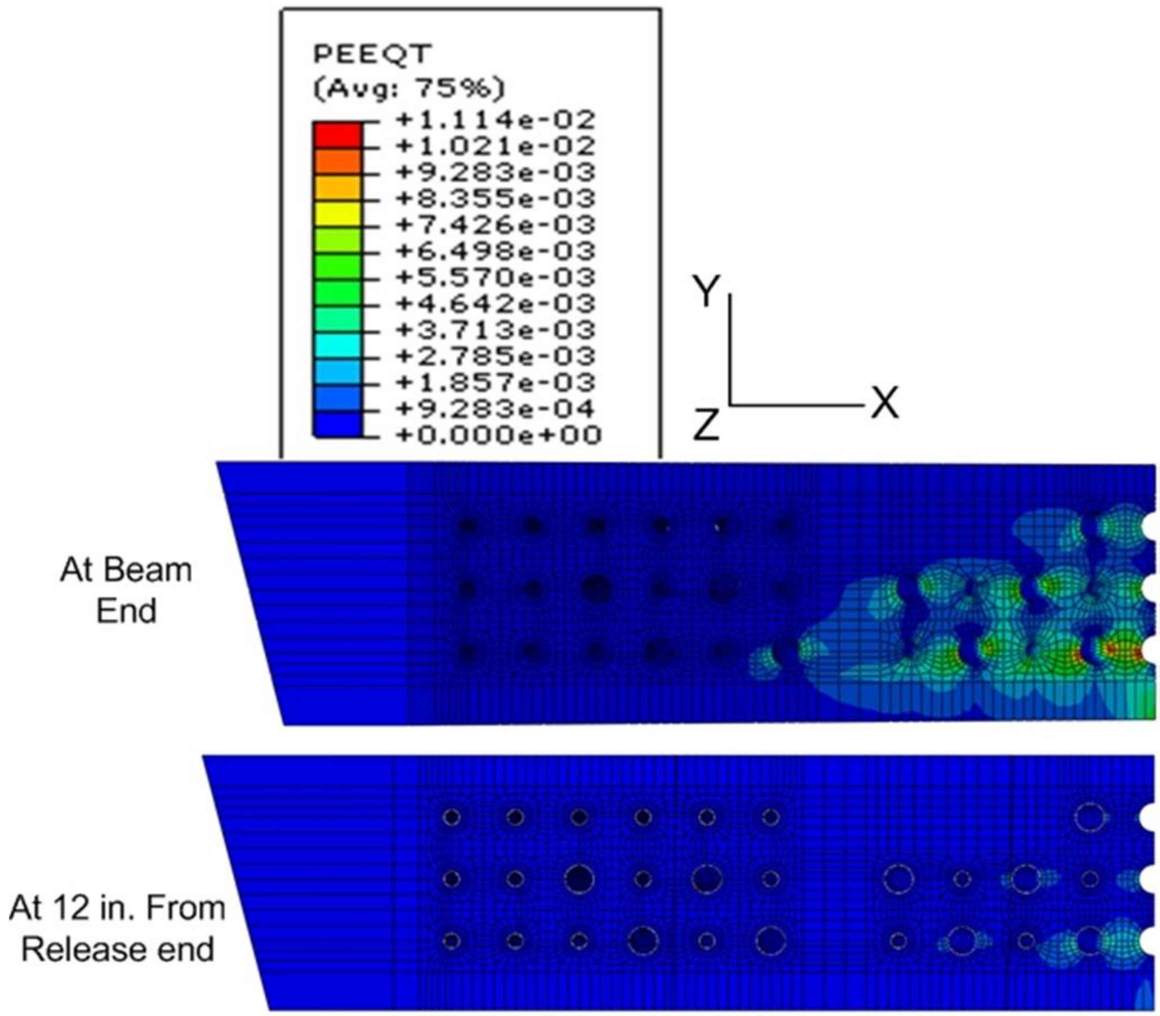

Figure 5-25 Equivalent plastic strain in uniaxial tension: Case 4

5.8 Comparison of Modeling Results

To better understand the results obtained from each of the numerical models just presented, the cases with common features are compared in the following sections. Case 1 and Case 2 are compared first because these two models had the same dimensions. Second, the four skew-beam models are compared using contour plots at the cross section and then response traces along different paths at the interface of partially debonded strands are compared according to the unbonded lengths in common, i.e., Case 1 vs. Case 3, and Case 2 vs. Case 4.

5.8.1 Case 1 vs. Case 2

It can be seen in Figure 5-26 that the use of a staggered distribution of debonded strand helps reduce the high stresses in the beam-end region upon release. In this particular case, a skew U-beam model, it is seen from the results obtained from Case 2 (see Figure 5-26) that the stresses at the cross section at the release end are still above the concrete modulus of rupture, 670 psi (4.6MPa), but the values are lower than those obtained from Case 1 (as-built condition model). Further, the high stress region is localized only at the beam end and decays rapidly.

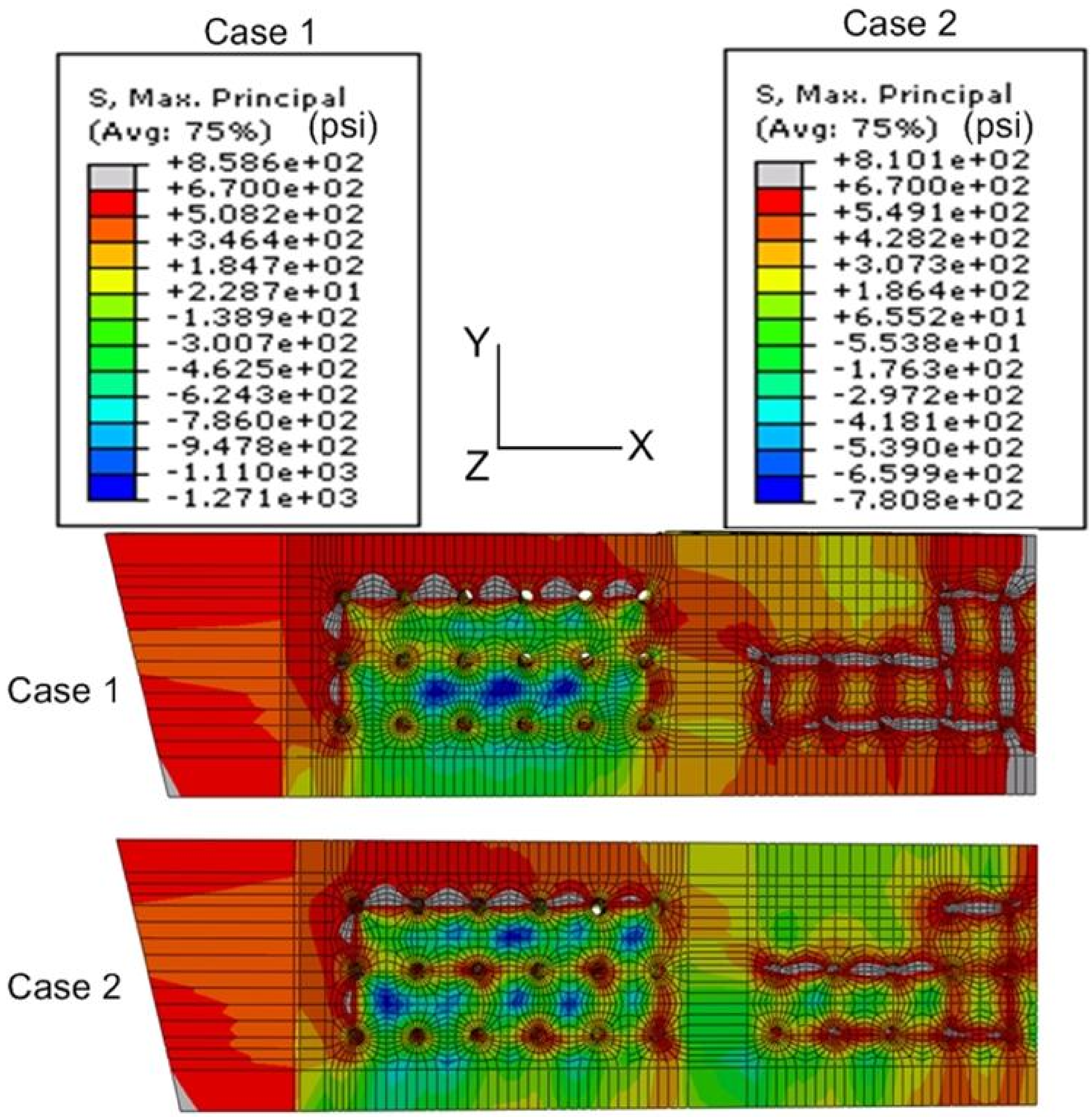

Figure 5-26 Maximum principal stresses: Case 1 vs. Case 2

The equivalent plastic strain in uniaxial tension (PEEQT) contour plots for Cases 1 and 2 are shown in Figure 5-27. In this Figure, Case 2 was divided in Case 2-a and Case 2-b because it was observed that the model had an spurious highly stressed zone in the bottom left corner due to boundary conditions. Since this effect does not affect the region of interest around the partially debonded strands, the highly stressed corner was removed from the results display as shown in Case 2-b. If Case 1 and Case 2-b are compared (see Figure 5-27), it can be observed that the use of a staggered debonding distribution noticeably decreases the high stresses in the end region upon release of the pretensioning force.

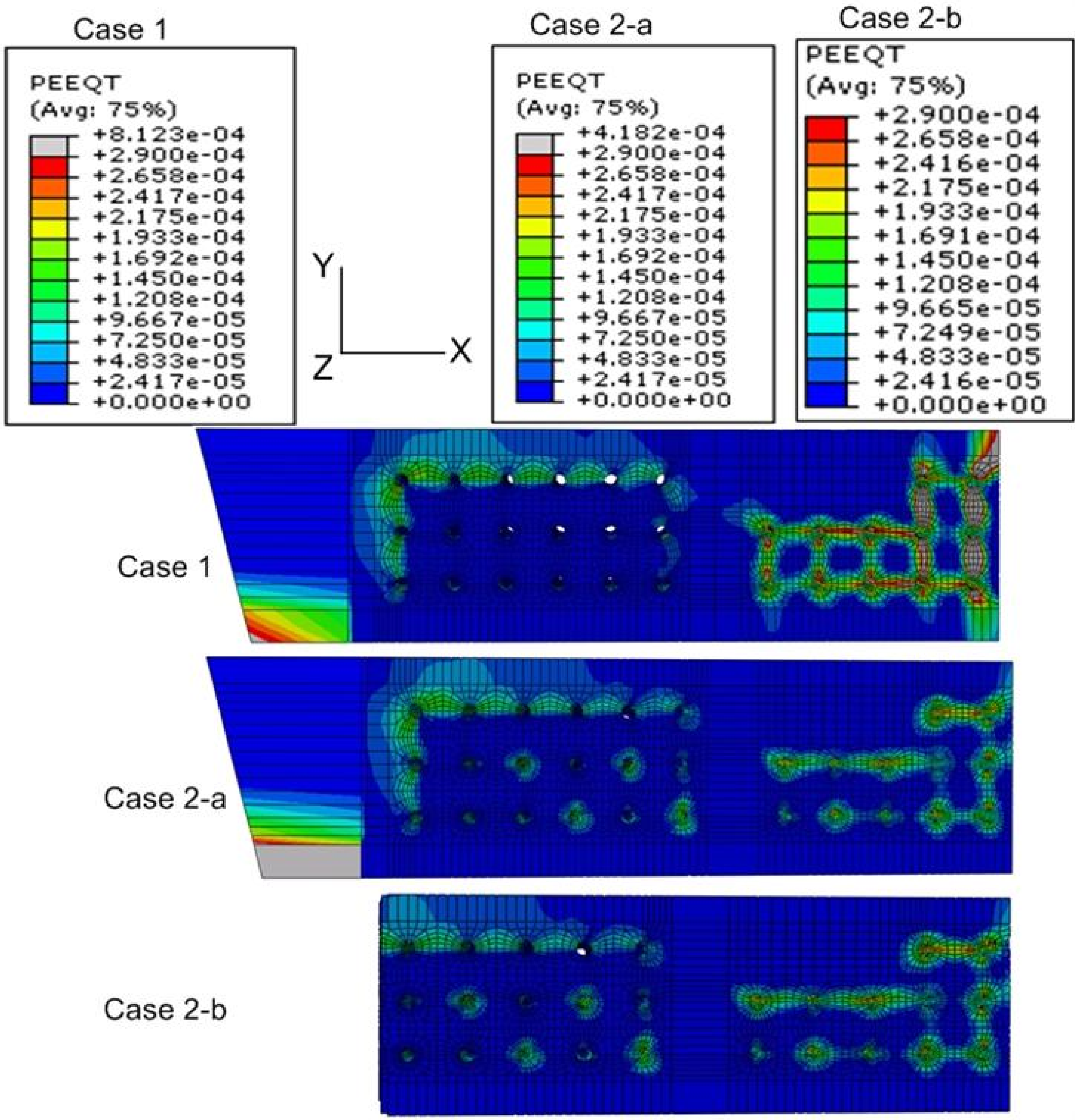

Figure 5-27 Equivalent plastic strain in uniaxial tension: Case 1 vs. Case2

The decrease in the high strain values is also seen by comparing the yielded concrete elements (those above the elastic state) as shown in Figure 5-28. Again, the spurious high stress region in the bottom corner needs to be neglected. While the staggered debonding pattern still indicates damage to the concrete, the number of affected elements is reduced and the yielded state decays much more rapidly into the beam for the Case 2 compared to Case 1.

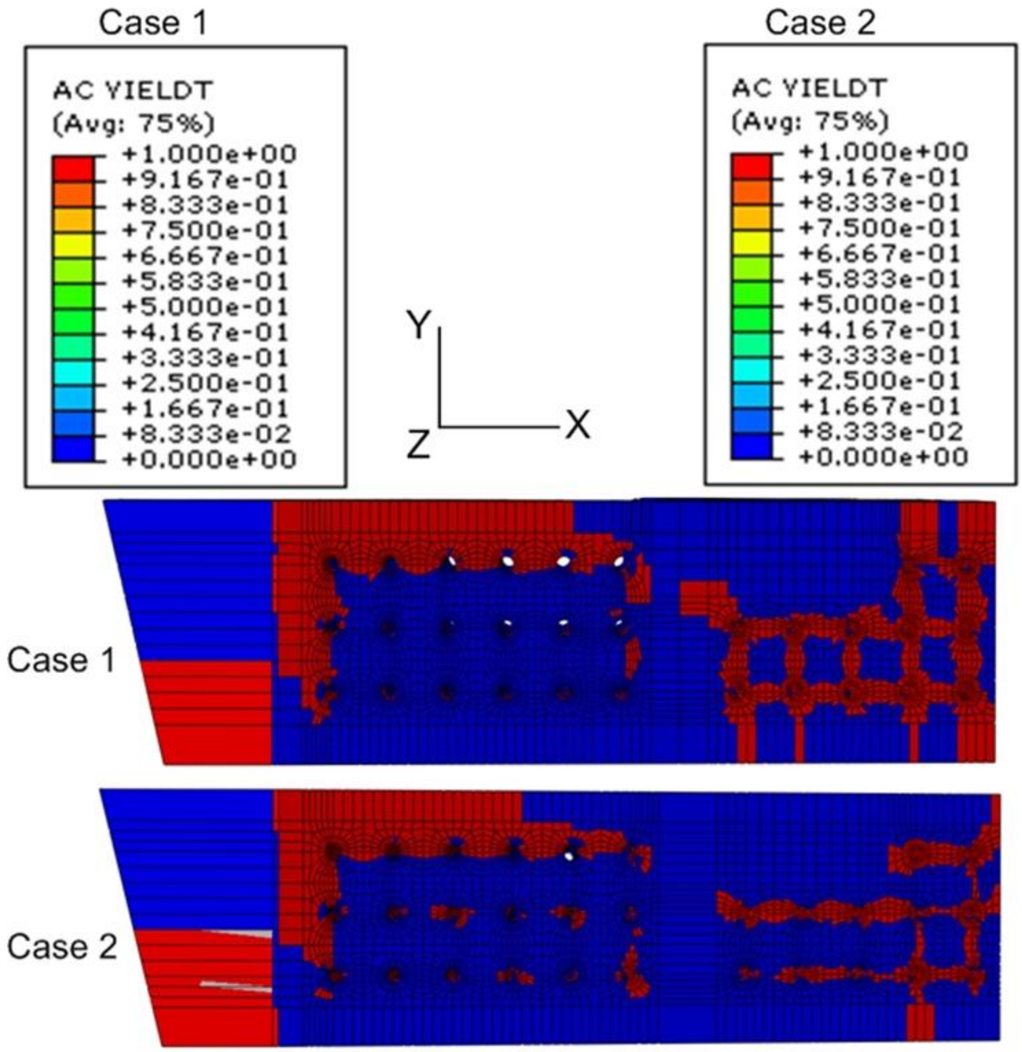

Figure 5-28 Yielding in concrete: Case 1 vs. Case 2

The effect of a staggered strand debonding pattern on the resulting longitudinal shear stresses was studied by examining the shear demands along an XZ plane located between the fully bonded and partially bonded strands in the "as-built condition" as shown in Figure 5-29. It is seen from this figure that the shear stresses are noticeably reduced in Case 2 (staggered debonded pattern) compared to the condition in Case 1 ("as-built.") This reduces the overall stress state in the anchorage region upon release, which can improve overall performance of the girder under service an ultimate demand. Therefore, the use of a staggered debonding distribution helps to control not only the high stresses in the beam-end region due to the dilation of the debonded strands, but also longitudinal shear stresses induced from strand force unbalance upon release.

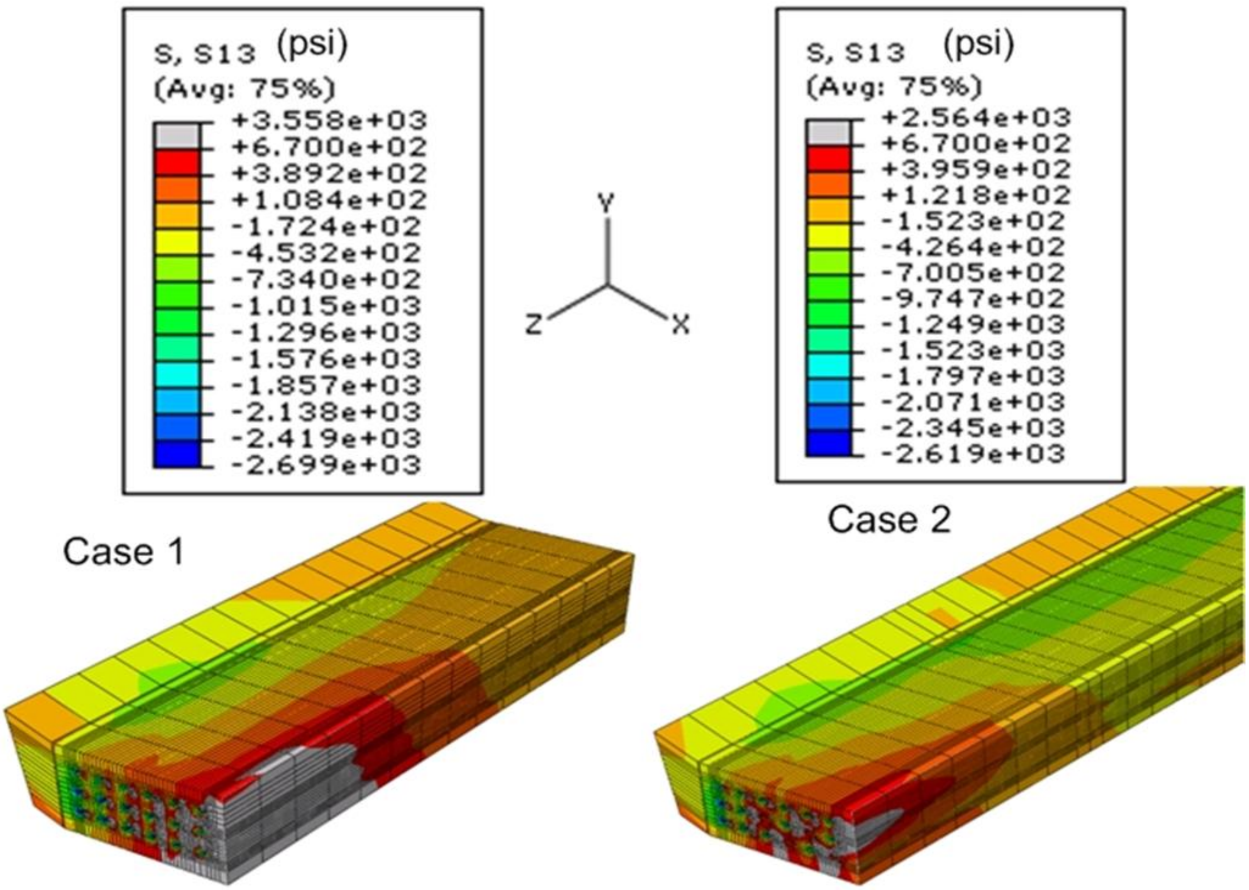

Figure 5-29 Shear Stresses on XZ Plane: Case 1 vs. Case 2

5.8.2 Four Skew-symmetry Beam Models

The four skew U-beam models with the assumption of symmetry along the ‘Z’ and ‘X’ axes are compared in this section. Contour plots at the beam-end cross section are compared as well as trances along three different partially debonded strands, #1, #9, and # 11 (see Figure 5-30).

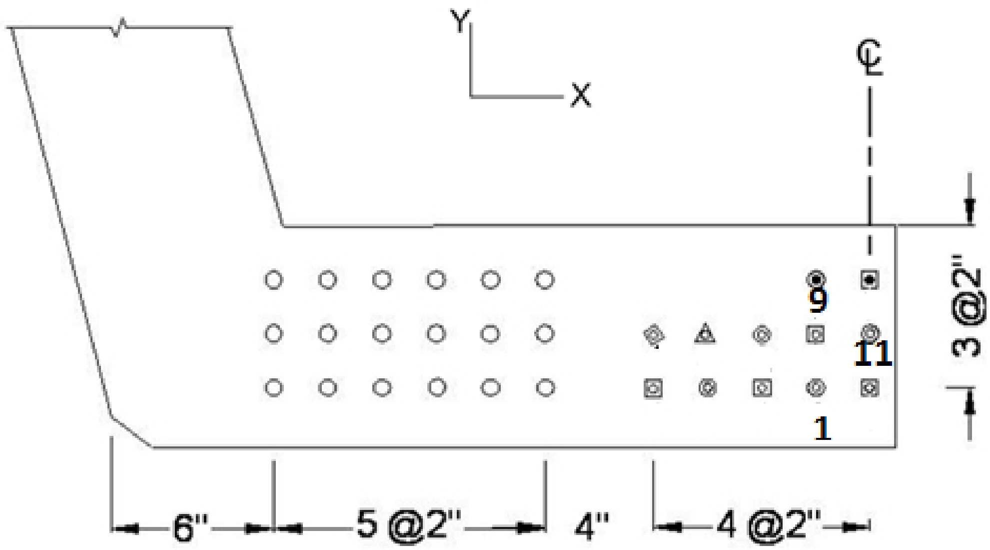

Figure 5-30 Partially debonded strands selected for response traces

5.8.2.1 Contour Plots at Beam-end: Four skew-symmetry U-beam models

Representative results comparing the stresses and strains at the beam-end cross section and at a distance of 12 in. (300 mm [see Figure 5-17]) into the beam are shown next. Figure 5-31 presents contour plots for the actively yielding concrete elements. This figure shows that the original strand configuration with rigid (oversized) strand sheathing (Case 3) presents the lowest “yielding” (demand beyond the elastic regime) among the four models.

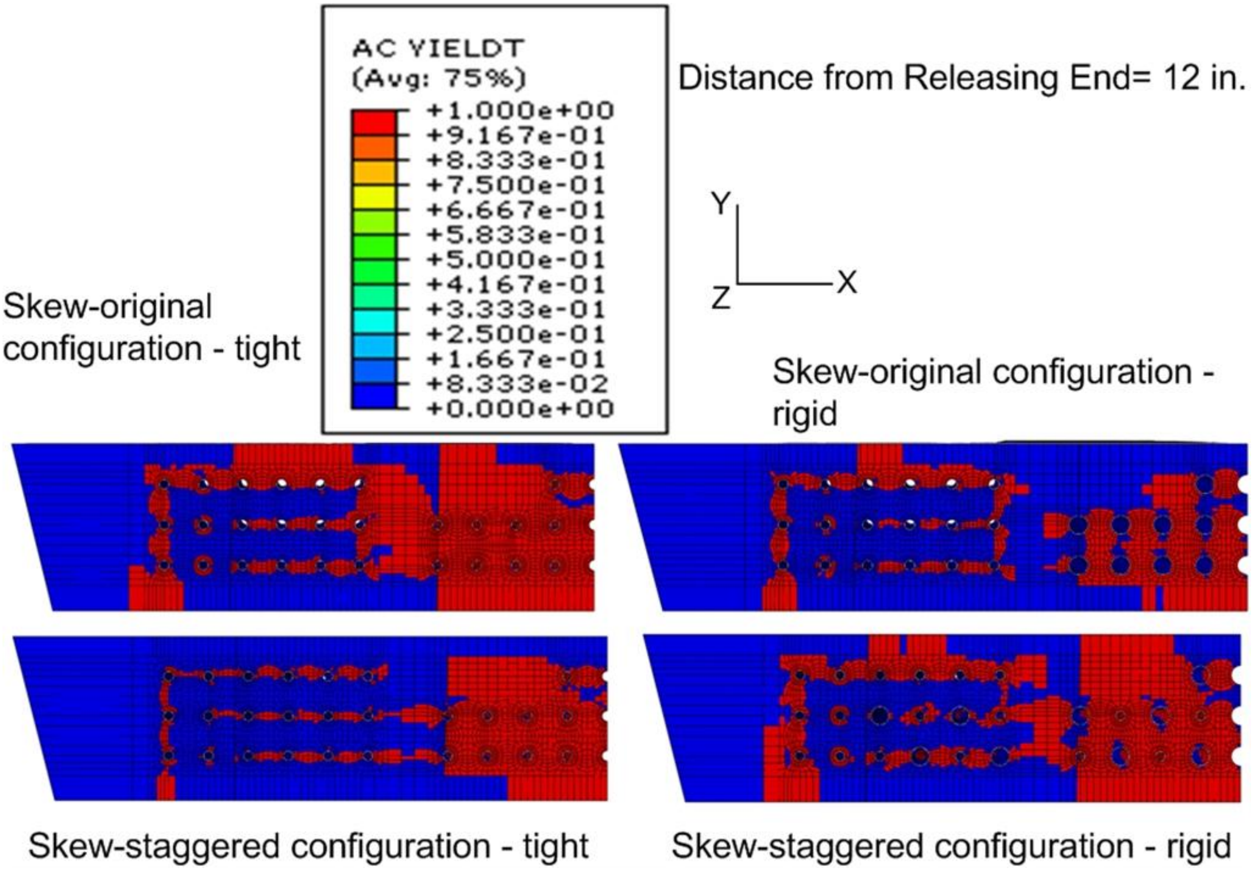

Figure 5-31 Actively yielding: Four skew U-beam models

Maximum principal strain contour plots at a distance of 12 in. (300 mm [see Figure 5-17]) from the release end are shown in Figure 5-32. It can be seen from this figure that the models with rigid (oversize) sheathing debonding had the lower strain demands compared to the models featuring tight fitting debonded strands. Similar results can be observed from the maximum principal stress contour plots shown in Figure 5-33. In addition, the longitudinal shear stresses contour plots for the four skew-symmetric U-beam models are compared in Figure 5-34.

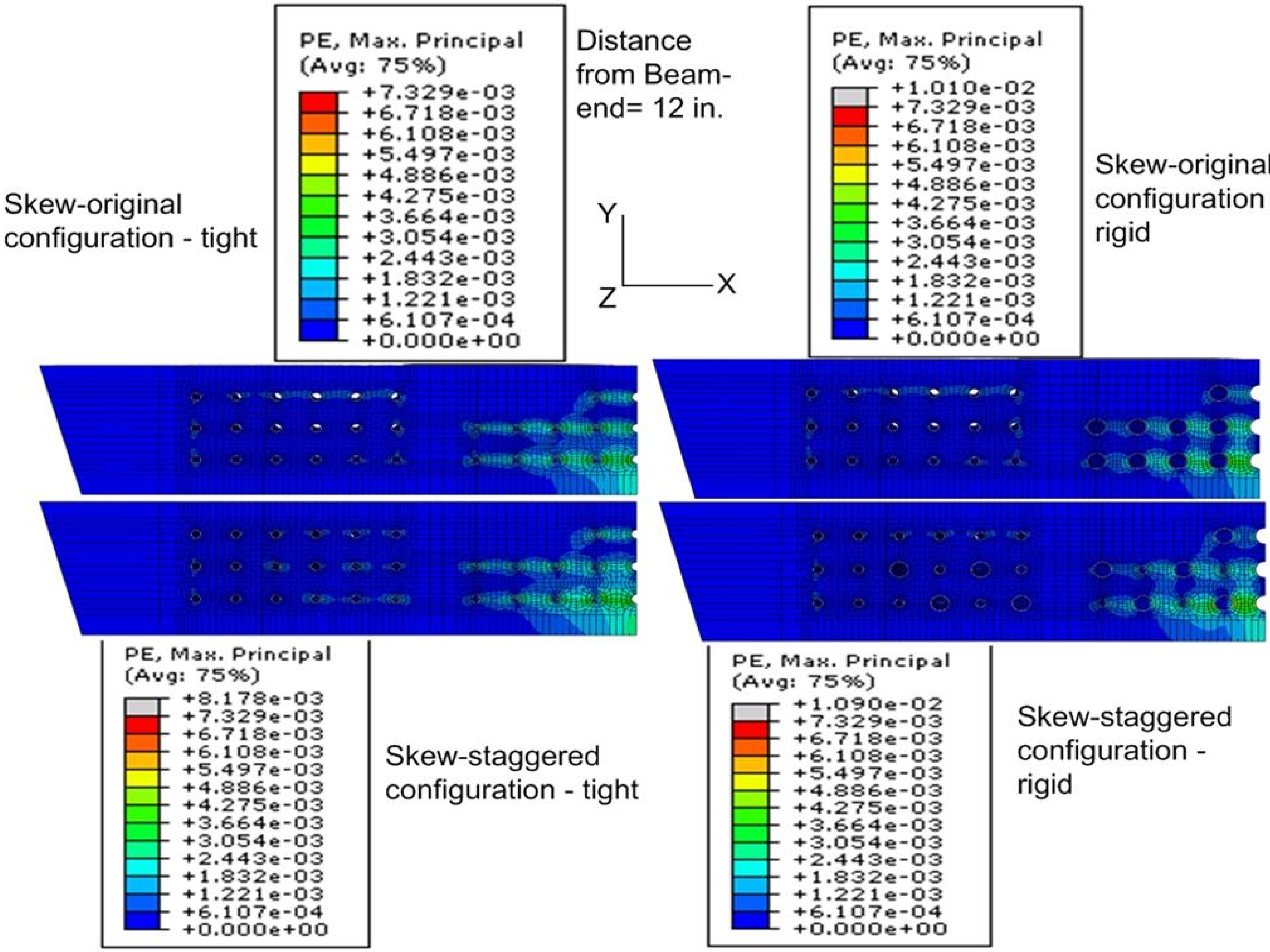

Figure 5-32 Skew U-beam models: Maximum principal plastic strain at 12 in. (300 mm) from release end

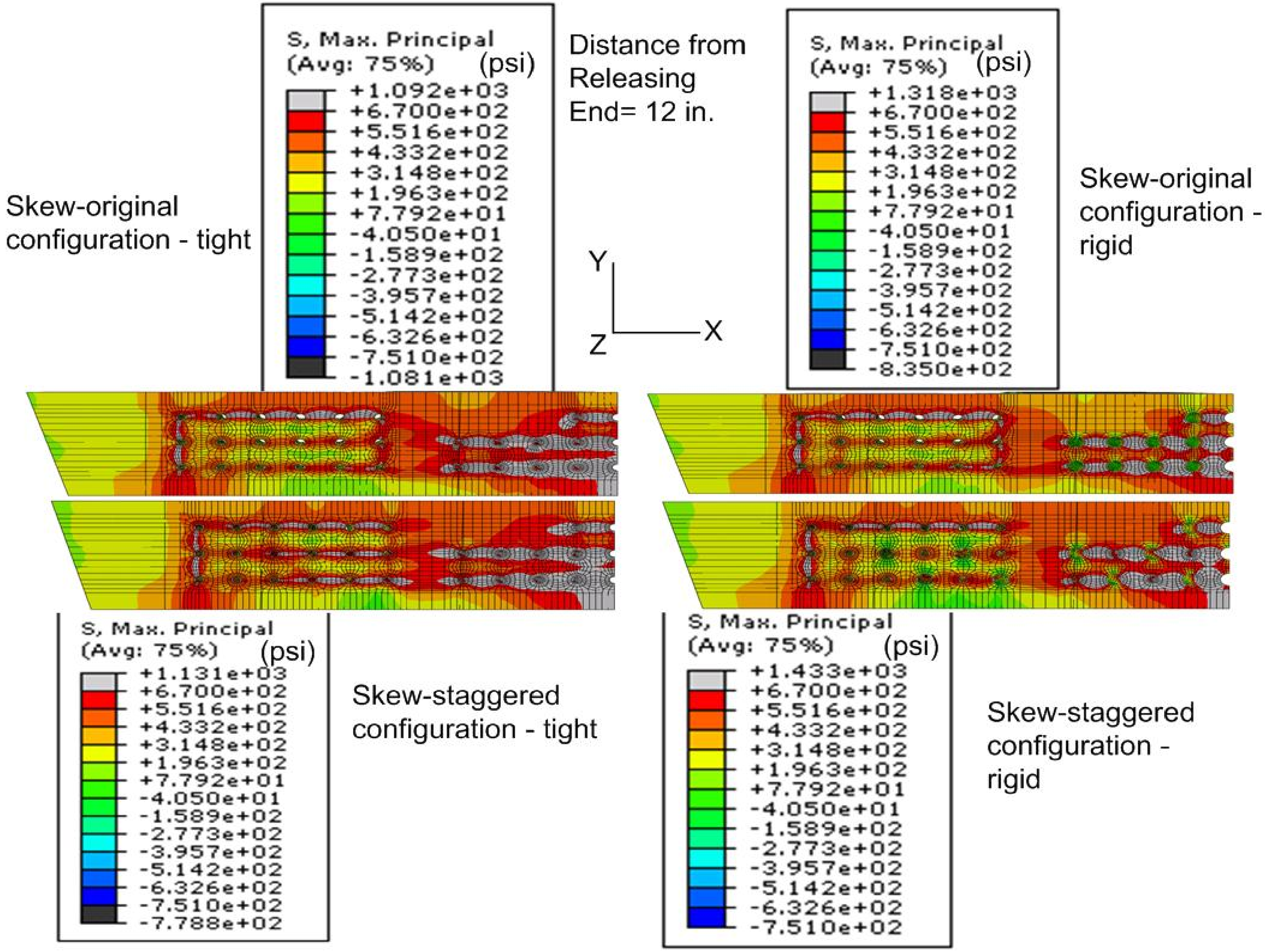

Figure 5-33 Maximum principal stresses at 12 in. (300 mm) from the release end

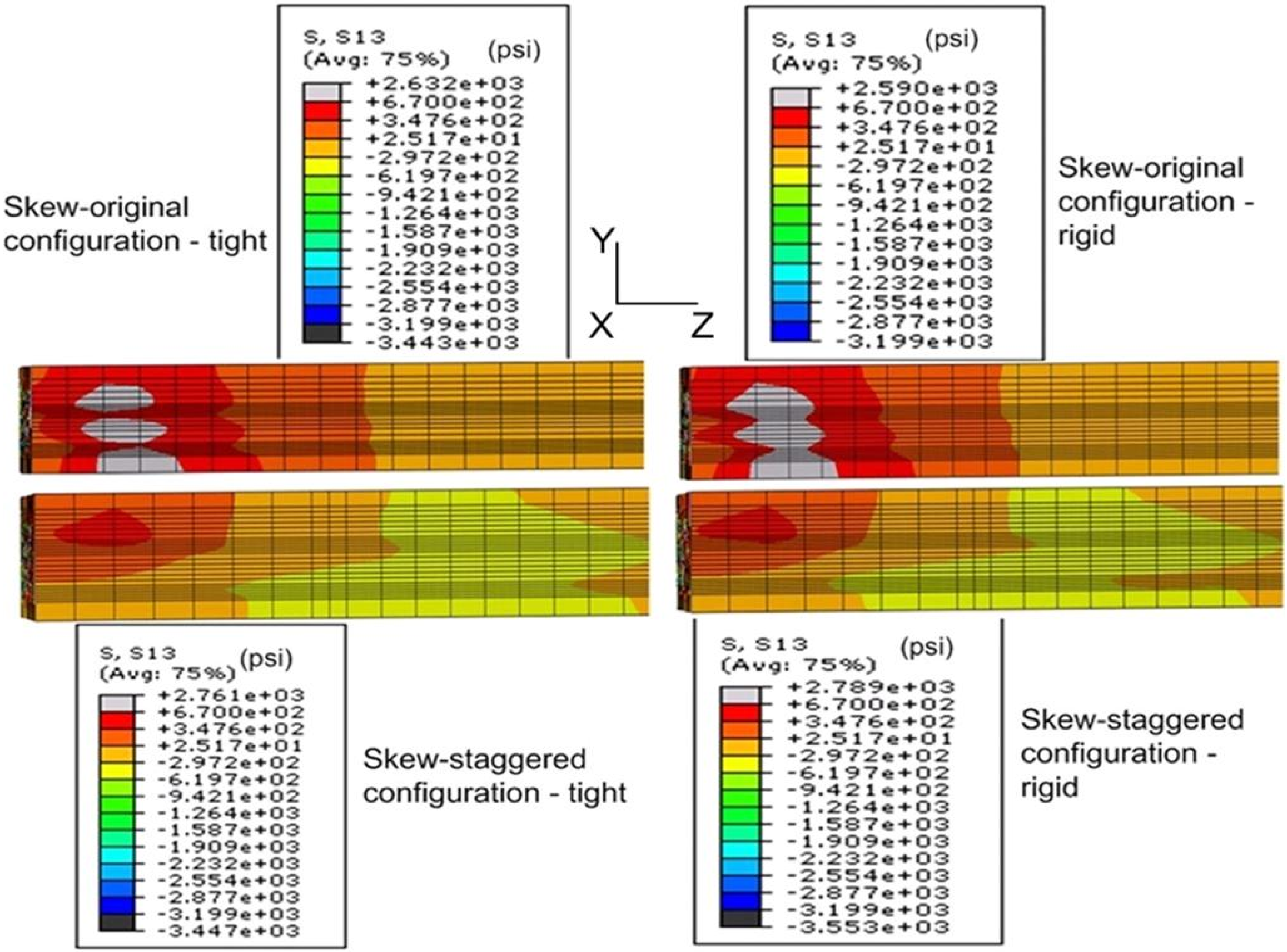

Figure 5-34 Shear stresses on the XZ Plane: Four skew-symmetry U-beam models

5.8.2.2 Paths along partially debonded Strands: Skew-symmetry beam with tight fit and original configuration vs. Case 3

Response traces along the interface of some partially debonded strands (No.1, No.9, and No.11 [see Figure 5-30]) comparing the results from the skew U-beam with X-symmetry, tight fitting debonding option, and original debonding configuration vs. Case 3 are presented herein. The maximum principal stresses along the interface of the partially debonded strand No.1 (see Figure 5-30) as shown in Figure 5-35. It can be observed from this Figure that the stresses along the debonded region for Case 3 are lower than the results obtained from the skew-symmetry model with tight fitting debonding material and original debonded strand pattern. However, at the release end the stresses are high for Case 3 and this can be attributed to boundary condition effects, that is, the X-symmetry definitions for the skew beam.

A similar pattern is observed from the response traces along partially debonded strand No.9, as shown in Figure 5-36. The maximum principal plastic strains (PE) are relatively constant and low along the unbonded/fully bonded region for Case 3, except for the response obtained close to the release end as previously mentioned. The maximum principal PEs from the model with symmetry along the X-axis with original debonded pattern decrease at the onset of the fully bonded zone, and the values are about the same level from those obtained for Case 3.

The response traces for the equivalent plastic strains in uniaxial tension (PEET) obtained at the interface of the partially debonded strand No.11 for the model with symmetry along X-axis, tight fitting debonding, and original debonding distribution and the results obtained from Case 3 are shown in Figure 5-37. The strain values obtained from both models at the release end are quite high; however, the response traces obtained from the Case 3 model are lower. The remaining of the response traces for these two beams models are presented in Appendix D.

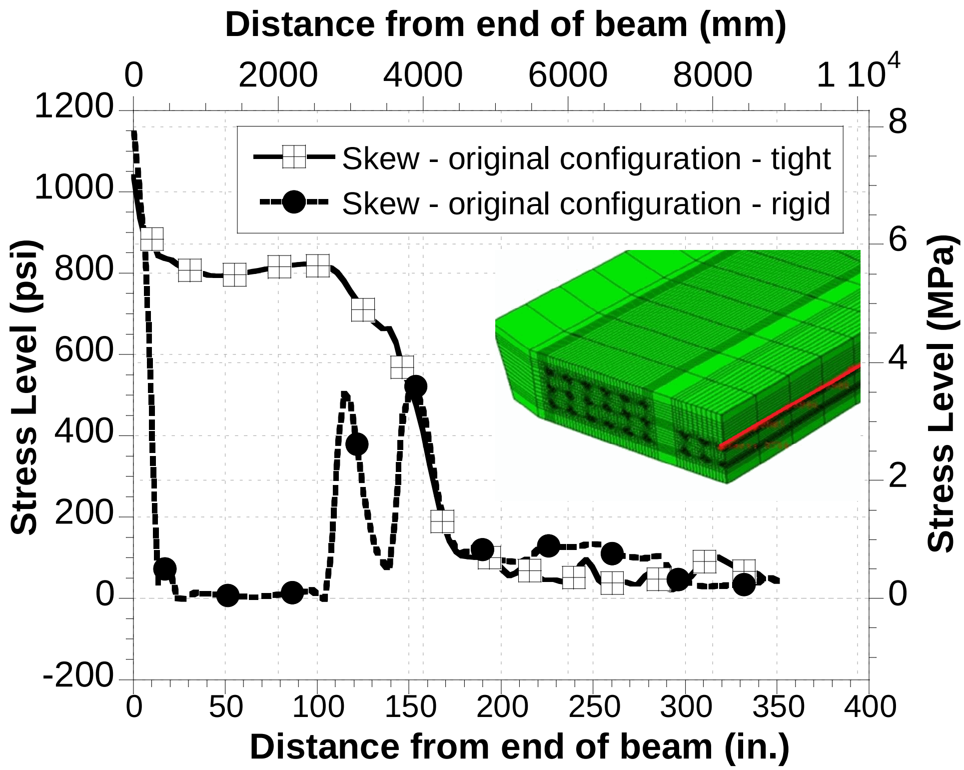

Figure 5-35 Longitudinal path along partially debonded strand 1: Maximum principal stresses – Skew-symmetry tight model vs. rigid and original configuration

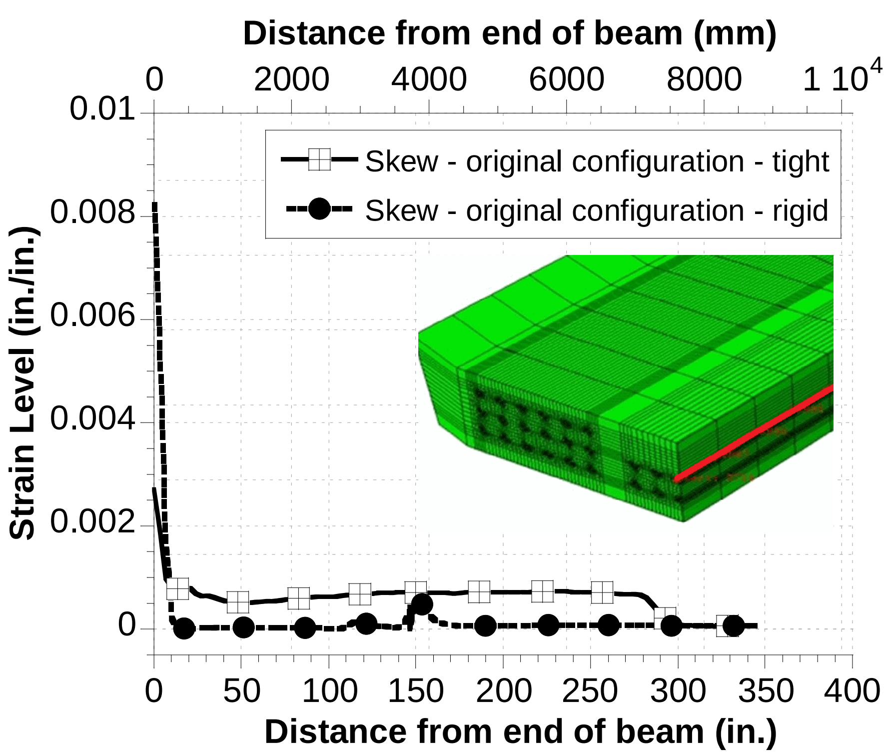

Figure 5-36 Response traces along partially debonded strand No.9: Maximum plastic strains – Skew-symmetry U-beam models tight vs. rigid with original configuration

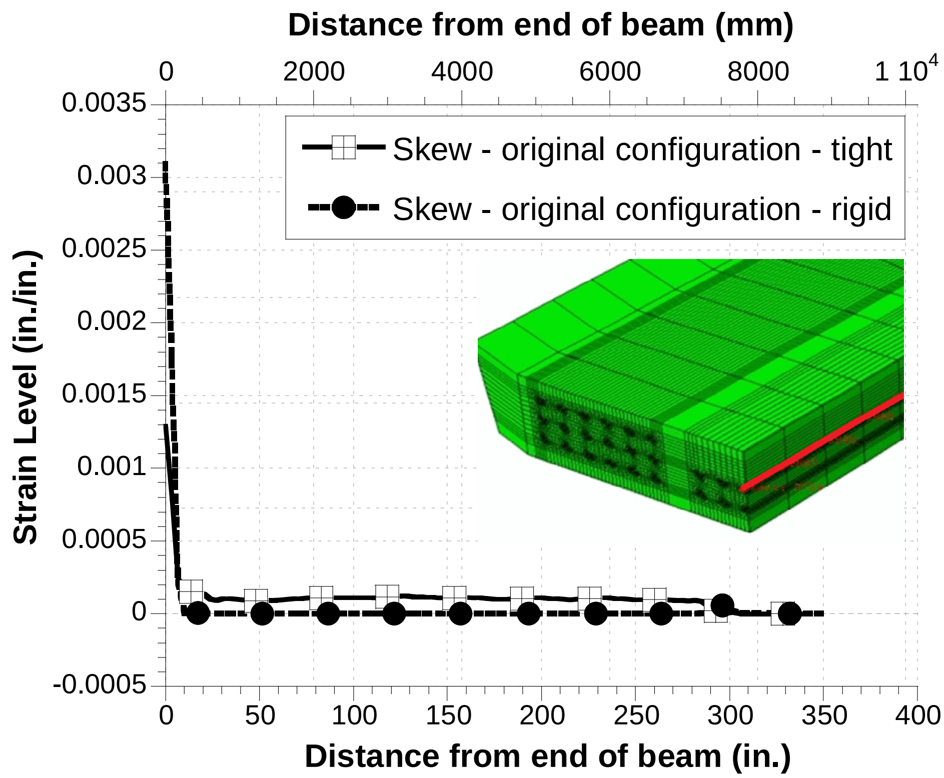

Figure 5-37 Longitudinal path along partially debonded strand No.11: Equivalent plastic strain in uniaxial tension – Skew-symmetry tight vs. rigid with original unbonded pattern

5.8.2.3 Longitudinal paths along partially debonded Strands: Skew U-beam model with tight fit and staggered debonding pattern vs. Case 4

Response traces along the interface of partially debonded strands No.1, No.9, and No. 11 (see Figure 5-30) for the beam model with symmetry along the X-axis, tight fitting strand debonding option, and staggered debonding distribution vs. Case 4 are presented in this section. In all the response traces, high values were observed from both models at the release end due boundary conditions effects. As previously mentioned, these are considered spurious effects from the symmetry boundary condition and are neglected in the interpretation of the results.

The maximum principal stress traces for the above-mentioned models are shown in Figure 5-38. The values observed in this Figure close to the release end are above 670 psi (4.6 MPa), which is the calculated concrete modulus of rupture for a compressive strength of 8,000 psi (55.2 MPa). However, as it is observed from Figure 5-35, Figure 5-36, and Figure 5-37, the values obtained from the model with rigid (oversized) debonding quickly decay into the beam, approximately 12 in. (300 mm) measured from the release end (see Figure 5-17 and Figure 5-38). The maximum principal stress values become somewhat similar for both models at the onset of the fully bonded region.

The maximum principal plastic strains and equivalent plastic strain in uniaxial tension response traces for Case 4 and the model with X-symmetry, tight fitting debonding, and staggered unbonded pattern are presented in Figure 5-39 and Figure 5-40. Both figures show similar trends, high values at the release end and a rapid decay further into the beam for the model with rigid (oversized) sheathing (Case 4).

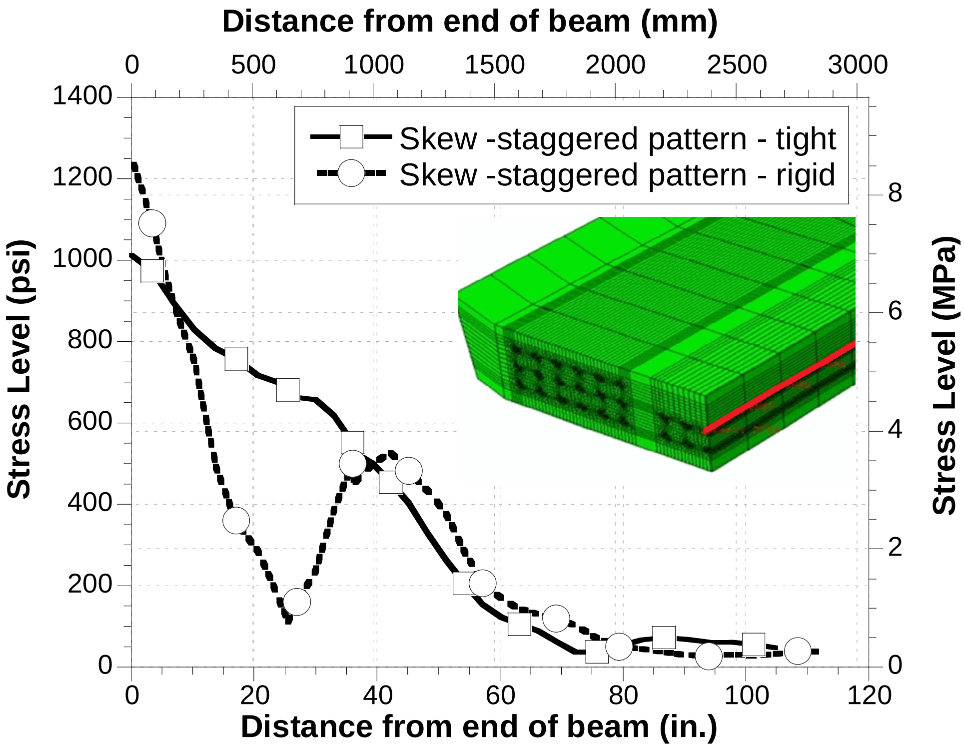

Figure 5-38 Maximum principal stresses: response trace along interface of partially debonded strand No.1 – skew-symmetry model tight vs. rigid with staggered pattern

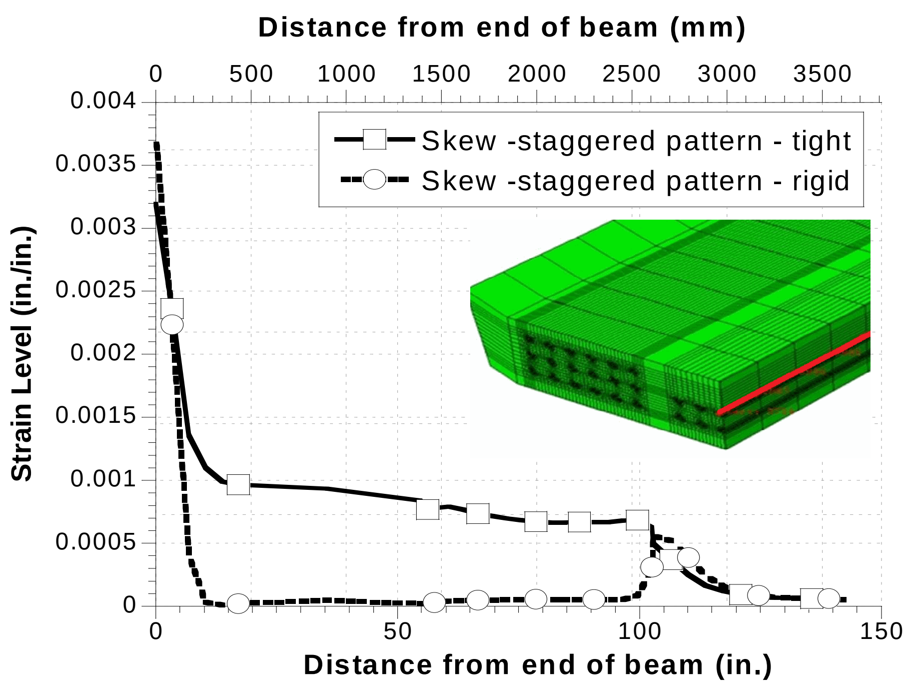

Figure 5-39 Maximum principal plastic strains along longitudinal path at the interface of partially debonded strand No.9

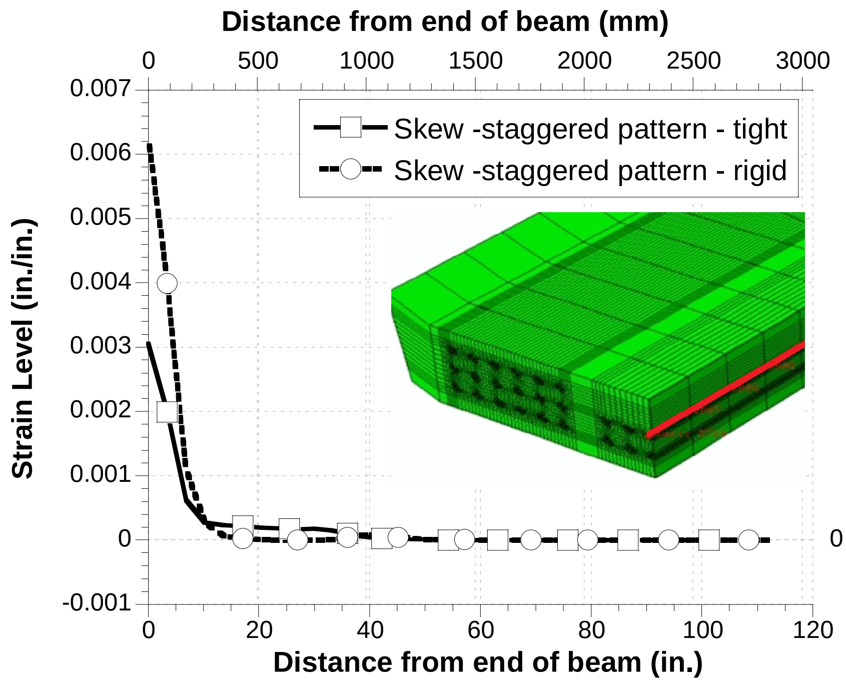

Figure 5-40 Equivalent plastic strain in uniaxial tension along longitudinal path at the interface of partially debonded strand No.11

5.8.3 Discussion

From the comparison of the results between Case 1 ("as-built" condition model) and Case 2 (skew U-beam model with a staggered debonding distribution and tight fitting debonding) it is seen that the use of a staggered unbonded pattern reduces the high stresses in the beam-end region created by the dilation of the debonded strand as shown in Figure 5-26, Figure 5-27, and Figure 5-28. In addition, the implementation of a staggered debonding distribution also decreases the longitudinal shear stresses (see Figure 5-29). To better understand how the longitudinal shear stresses are minimized with the use of a staggered debonding pattern, Figure 5-41 is presented as an aid. In this figure, a rectangular section of a beam is presented with four fully bonded strands, two at each side, and three partially debonded strands located in the center of the beam. The prestressing force in the fully bonded strands is immediately transmitted into the beam, at the onset of the release end until the end of the transfer length. However, the force in the partially debonded strands is transferred further into the beam, at the end of the debonded zone and along this unbonded region there are no (or very small) forces in the center of the beam to counteract the longitudinal shear stresses generated from the transmission of the prestressing force from the fully bonded strands. Thus, in the case study presented in this research, skew U-beam, the concentration of partially debonded strands in the center of the bottom flange of the beam leads to high (and probably) undesirable longitudinal shear stresses, as it is seen from comparing the results from Case 1 and Case 2.

On the other hand, it was observed from the results presented in Section 5.8 that the assumption of X-symmetry for the skew U-beam models had negative effects on the results obtained from the numerical models, especially at the beam end. However, the general trend that can be observed from these results seems obvious: that the use of rigid (oversized) strand debonding is beneficial to reduce the high stresses at the end region upon release. This general trend was observed from the response traces (see Section 5.8.2.1 and Section 5.8.2.2) at the interface of the partially debonded stands, and it was consistent with all the response traces obtained at the interface between the strands and concrete.

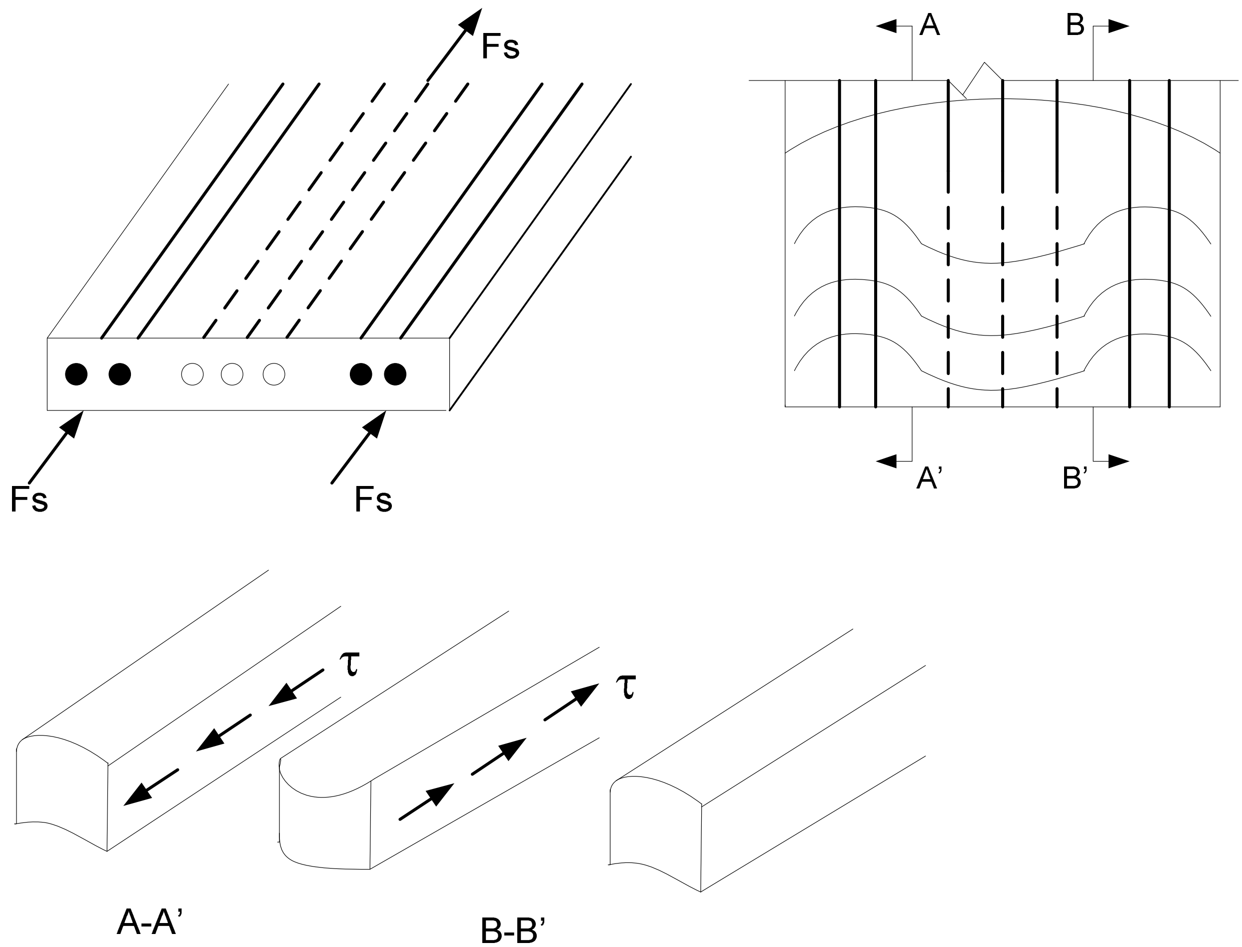

Figure 5-41 Discussion of un-balanced forces due to strand debonding distribution

5.9 Findings

It is recognized that the finite element models presented herein are far from reproducing the exact damage pattern observed during production of the U-beam girder in the presented case study. This follows from the following complex parameters involved in the problem, which include:

- Mechanical interlock bond resistance of the seven-wire twisted strand: in the models the strand was modeled as a smooth cylindrical rod with nonlinear friction interaction surface-to-surface with the surrounding concrete.
- Heterogeneity of concrete: in the FE models the concrete was simulated as a homogeneous material. This has an effect in the localization, initiation and propagation of cracking and the development of spalling regions.
- Construction procedure and release pattern: the prestressing force was released simultaneously and no interaction (i.e., friction) with the casting bed was simulated. Sole plates and other local reinforcement in the beam section were not considered.
- Concrete cracking and damage simulation: the concrete damage plasticity (CDP) model permits modeling the inelastic response of the concrete, but it does so in a homogeneous sense and damage is introduced by softening of the material and not discrete opening of cracks. This has an effect on the simulated damage propagation.
- Strand-concrete bond simulation and damage: strand bond was simulated through a friction model between the interacting surfaces of a smooth rod (strand) and concrete. Bond resistance thus depends on the normal pressure generated between the interacting surfaces. Upon damage the CDP model will soften the concrete elements, an action which in turn will minimize the constraint onto the expanding strand part and thus decrease the normal surfaces between the interacting surfaces and thus bond resistance. Such a decrease in bond resistance is likely not present in the mechanical interlock component of bond even if microcracks become present along the transfer region.

It follows from the points noted above that while the presented finite element models have many features (positive features) and allow a high degree of fidelity, they are not able to replicate the exact cracking and damage pattern seen in the case study. Thus, the stress and strain values presented in this chapter are to be used as qualitative measures for the choices on strand debonding options and distribution and not as exact predicted responses. Nonetheless, it is felt that the numerical models provide “enhance” qualitative data. Thus the following findings are presented:

- It was found from the results of Case 1 that the high stresses developed around the partially debonded strands upon release are comparable in general sense to the damage observed during production of the U-beam girder in the case study. Thus, the dilation resulting from the flexible slit sheathing debonding material and the concentration of strands in a group at the center of the section bottom flange are attributed as the cause of the damage.
- It is believed that the use of a staggered debonding pattern can decrease high stresses in the end region and longitudinal shear stresses into the beam depth as shown from the results from Case 2.
- The use of rigid (oversized) strand sheathing can minimize the high stresses (those intruded from the dilation of debonded strands with flexible slit sheathing) at the beam end and along the entire unbonded zone (across the section and along the debonded length) upon detensioning.
- The implementation of strand debonding with rigid oversized sheathing in a staggered distribution pattern provided the best option for reducing high dilation stresses at the beam end as well as longitudinal shear stresses due to unbalanced forces generated when the partially debonded strands are concentrated in the center of the beam.

CHAPTER 6 RECOMMENDATIONS AND CONCLUSION

6.1 Relevant Findings

Based on the experimental and numerical studies presented in this thesis, the following relevant findings are offered.

- Experimental results on pull-out tests on simple cylinders with a concentric partially debonded or fully bonded strand showed that confinement reinforcement had only a minor effect (~10 %) on bond strength.
- Flexible-slit sheathing, single or double layer, is an effective debonding mechanism based on experimental data from pull-out tests on cylinders and wall-like block with unstressed strands.
- The hydraulic head effect does not affect the debonding mechanism provided by the use of a single or double layer of flexible slit (tight fit) sheathing based on experimental results on pull-out tests on unstressed strands in wall-like blocks.
- Experimental results on laboratory-scale beam models with a concentric partially debonded strand using single or double layer slit sheathing indicated that flexible sheathing did not fully break the "bond" between strand and concrete since an average of 16% of prestressing force was transferred along the "unbonded" length. Numerical simulations on the same beams showed that the axial stress transfer follows from the wedge effect that develops as the blanketed strand dilates due to the lack of bond resistance, and it creates a wedging anchorage mechanism with the concrete due to the tight fit created with the soft (and collapsible) flexible sheathing.

6.2 CONCLUSION

- The use of flexible sheathing in either one or two layers seems to be an effective debonding mechanism on unstressed strands based on experimental data. Paste infiltration did not take place in debonded strands as the maximum pull-out load was close to zero.
- Concrete fluidity did not affect the effectiveness of slit sheathing on unstressed strands as the maximum pull-out load reached from wall-like blocks was significantly small compared to fully bonded strands.
- Experimental results on laboratory-scale beam models showed that a nominal amount of prestressing force was transferred along the debonded length when using a double slit sheathing. This is attributed to the strand's dilation from a Poisson's effect as the strand tries to expand and creates a wedging anchorage mechanism against the tight fitting concrete.
- Numerical studies on small-scale and large-scale beam models (U-beam model) showed that the use of flexible (tight fit) sheathing allows the development of high radial pressure at the interface of the strand and concrete and that these stresses continue along the debonded length decreasing only after the transfer zone. With the use of rigid (oversized) debonding the strand is fully debonded as the strand and concrete are not on contact upon release. Thus the use of rigid sheathing decreases the high stresses in the end-region of pretensioned concrete members upon detensioning.
- A staggered strand debonding configuration seems to reduce the shear stresses in the longitudinal direction of the beam upon strand release. It was observed that the use of a staggered debonded strand distribution and rigid (oversized) sheathing can decrease the

high tensile and shear stresses in the anchorage region of pretensioned concrete girders upon strand detensioning.

APPENDICES

APPENDIX A – Materials Testing and Concrete Mix Designs

The strand specifications and the mix designs used for both sets, normal-consolidated concrete and self-consolidated concrete, are presented in this section. In addition, the mix design used to cast the large block to verify the quality of the strand is also presented.

Strand Specifications

Table A-1 Seven-wire 0.6-in. (15.2 mm) diameter strand specifications

Ultimate breaking strength	60.13 kip (267 kN)
Load @ 1% Extension	54.14 kip (241 kN)
Ultimate elongation, %	7.4
Representative area	0.218 in2 (140.6 mm2)
Actual area	0.2175 in2 (140 mm2)
Average modulus of elasticity	29000 ksi (200 GPa)

Mix Design for the Large Block Pull-out

Table A-2Concrete Mix Design – Large Block

	Design
Type III cement	660 lbs/c.y.
Fine Aggregate (2NS sand)	1269 lbs/c.y.
Coarse Aggregate (#4 limestone)	1900 lbs/c.y.
Water	292 gal/c.y.
ASTM C-494 (Type A)	106 oz/c.y.
Water/Cement Ratio = 0.44	
Concrete Unit Weight = 146.3 PCF	

Normal Consolidated Concrete (NCC)

Table A-3 Concrete mix design - NCC

	Design
Type III cement	658 lbs/c.y.
Fine aggregate (2NS sand)	1356 lbs/c.y.
Coarse Aggregate (6AA limestone)	1779.6 lbs/c.y.
Water	16 gal/c.y.
HRWR	52.8 oz/c.y.
Air-entraining Admixture	2 oz/c.y.

Self-Consolidated Concrete (SCC)

Table A-4 Self-consolidating concrete mix design

	Design
Type III cement	658 lbs/c.y.
Fine Aggregate (2NS sand)	1511 lbs/c.y.
Coarse Aggregate (6AA limestone)	1463 lbs/c.y.
Water	31.6 gal/c.y.
HRWR	106 oz/c.y.
Delvo Type D	39.5 oz/c.y.
Rheomac VMA	9.9 oz/c.y.
Air-entraining Admixture	2.6 oz/c.y.
Water/Cement Ratio = 0.4	
Concrete Unit Weight = 143.8 PCF	
Total Air = 6.0% +/- 1.5	

APPENDIX B – Supplementary Results from Experimental Program:

Pull-out on Cylinders

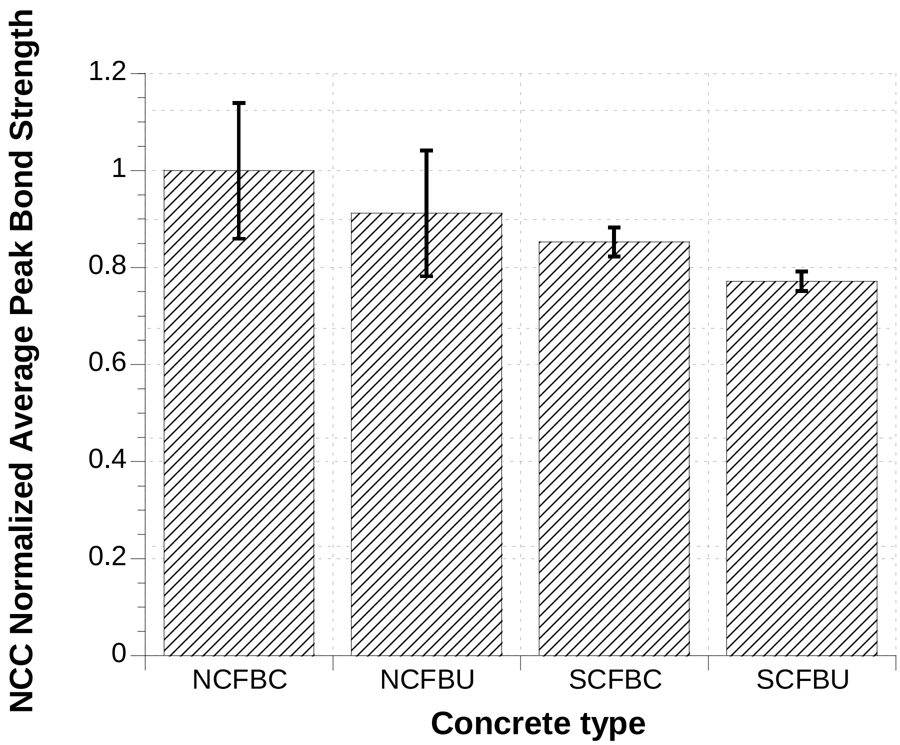

Figure A-1 Normalized average peak bond strength on pull-out cylinders

Pull-out on Wall-like Blocks

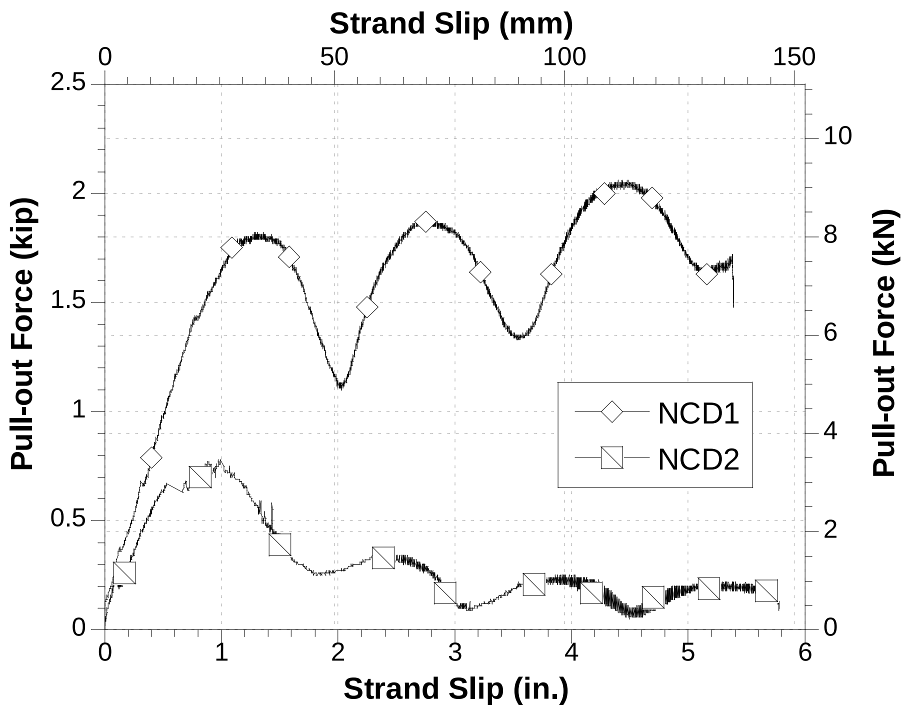

Figure A-2Response of debonded strands in wall-like block cast with NCC – 5th row

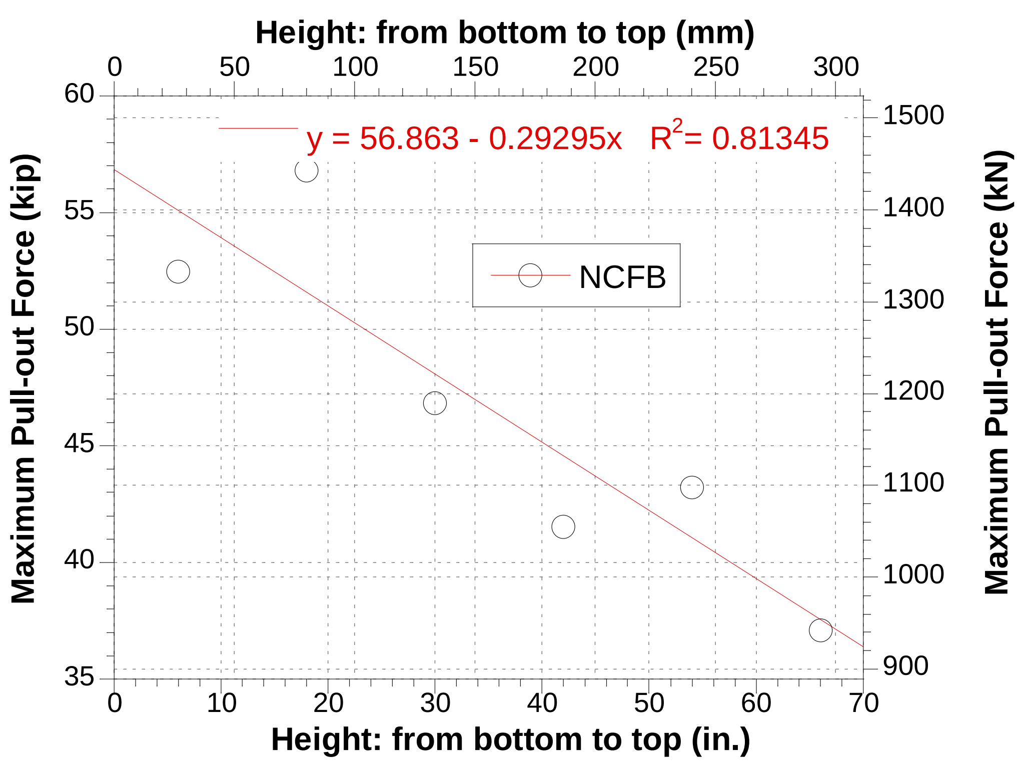

Figure A-3 Least square fit fully bonded strand in wall-like block cast with NC

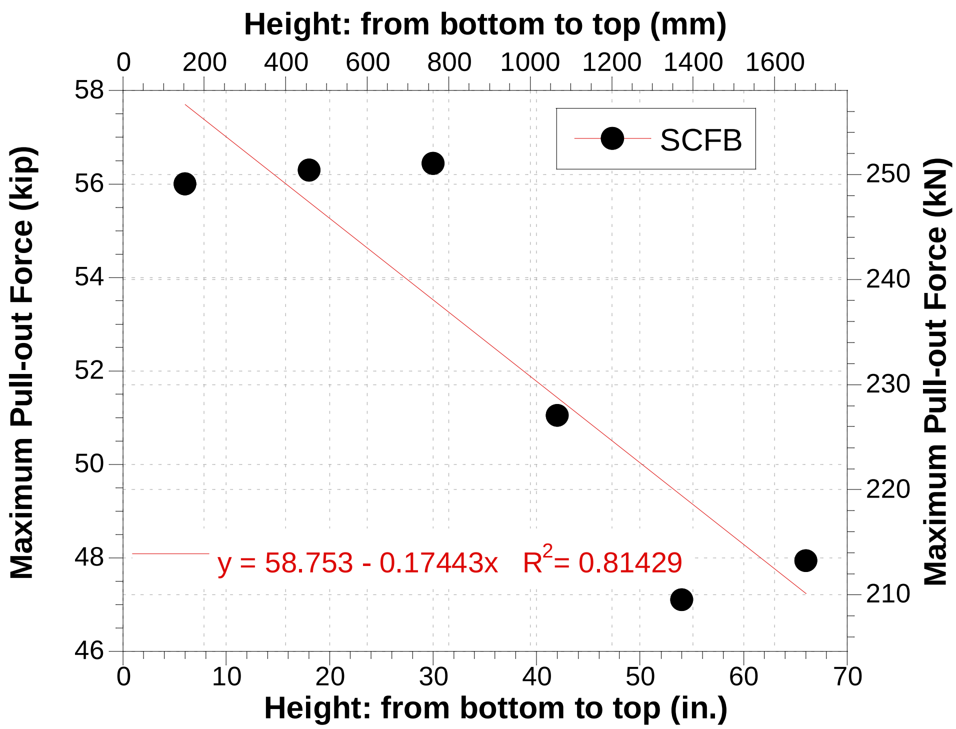

Figure A-4 Least square fit fully bonded strand: top-strand effect on wall-like block cast with SCC

APPENDIX C – Results from numerical small-scale beam models

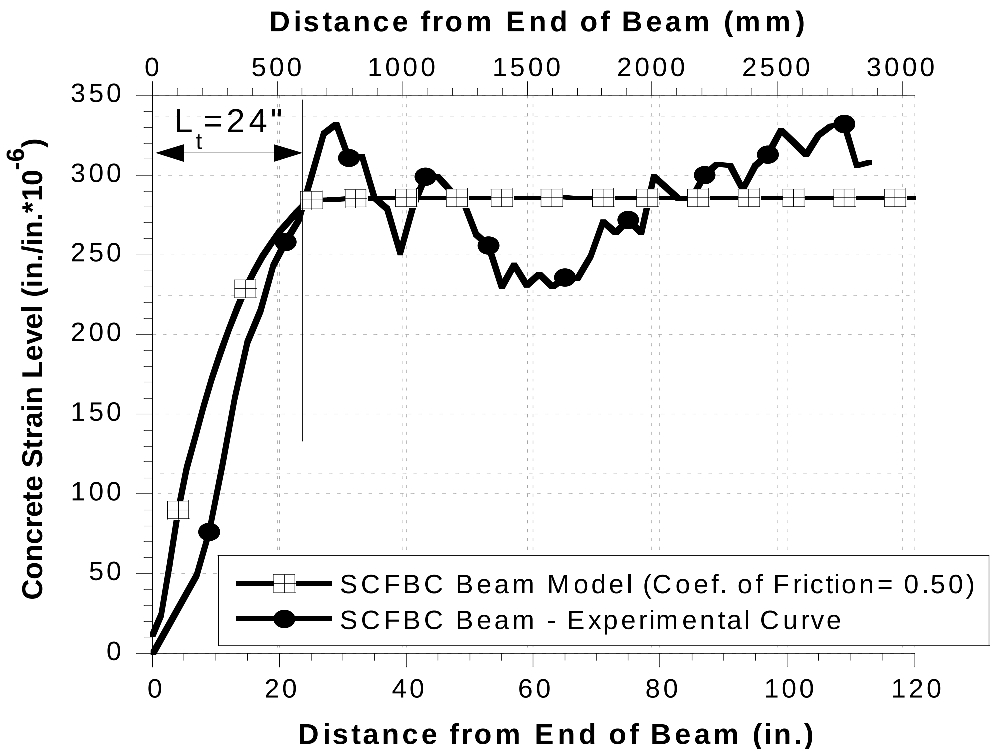

Figure A-5 SCFBC numerical model vs. experimental data

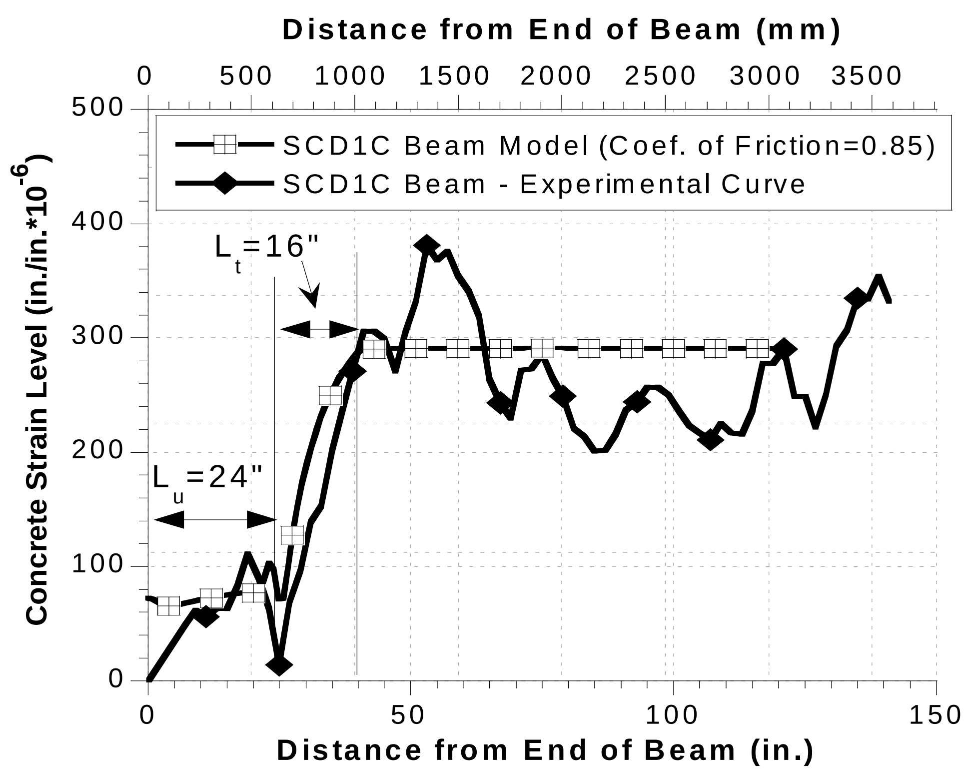

Figure A-6 SCD1C beam model vs. experimental results

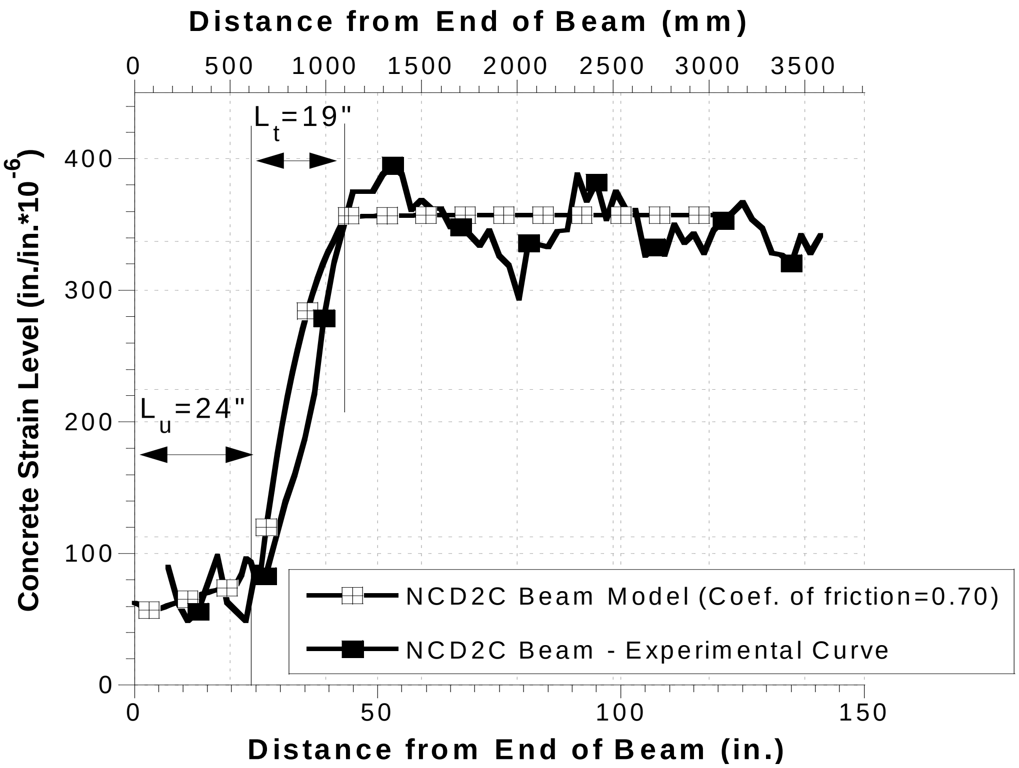

Figure A-7 NCD2C Beam Model vs. Experimental Data

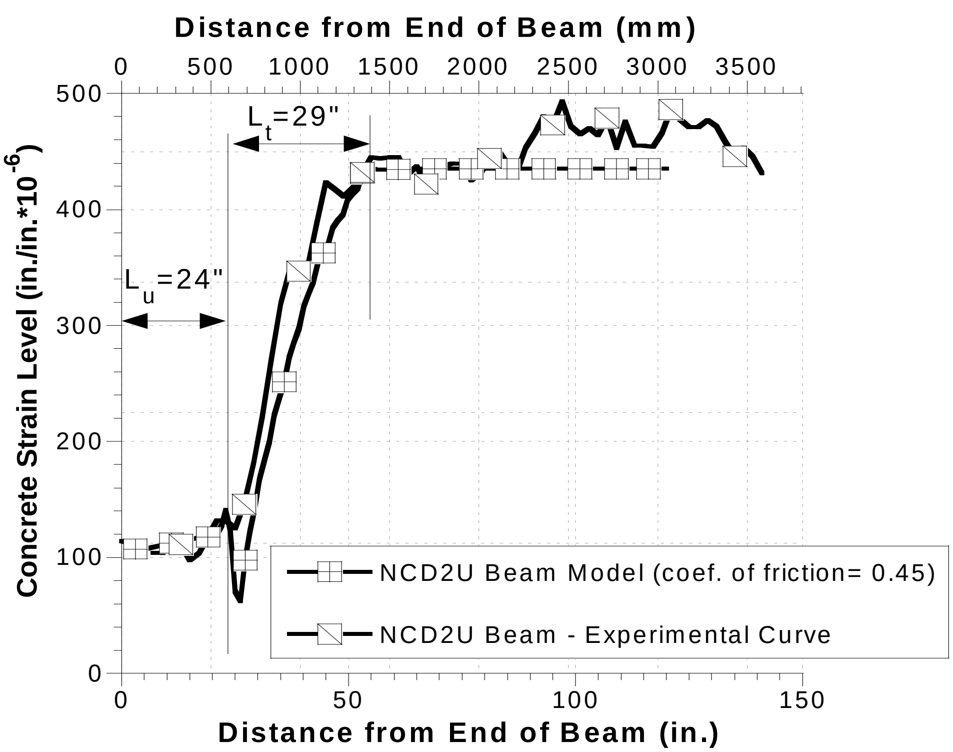

Figure A-8 NCD2U Beam model vs. experimental curve

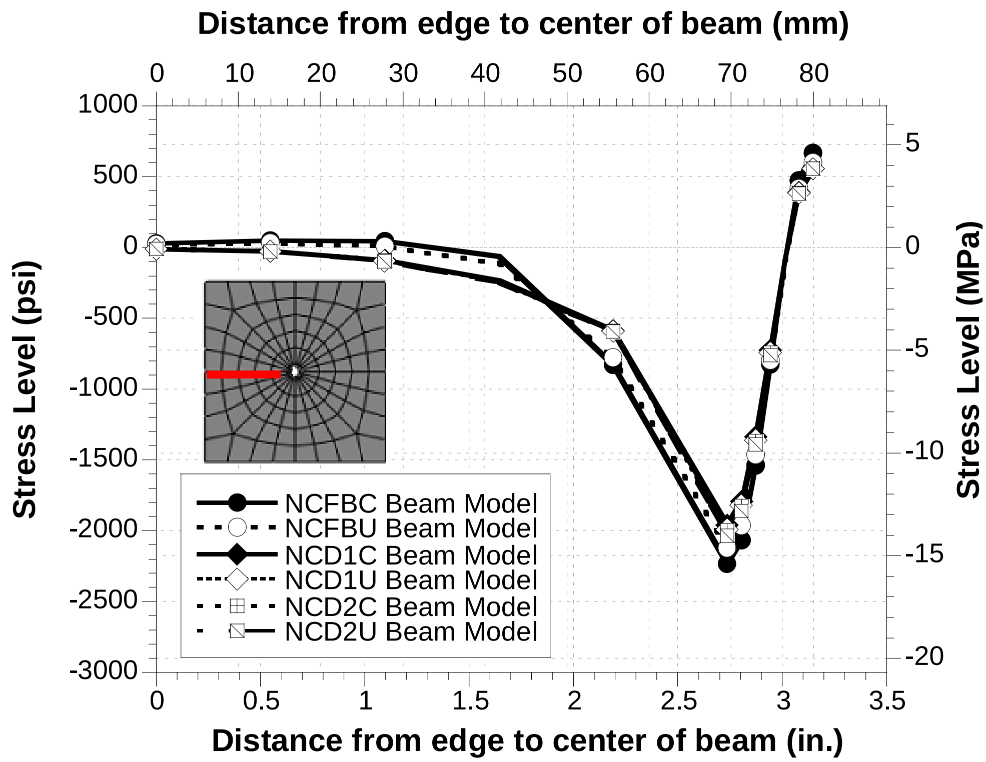

Figure A-9 Axial stresses along cross-section of beam at releasing end - NCC set

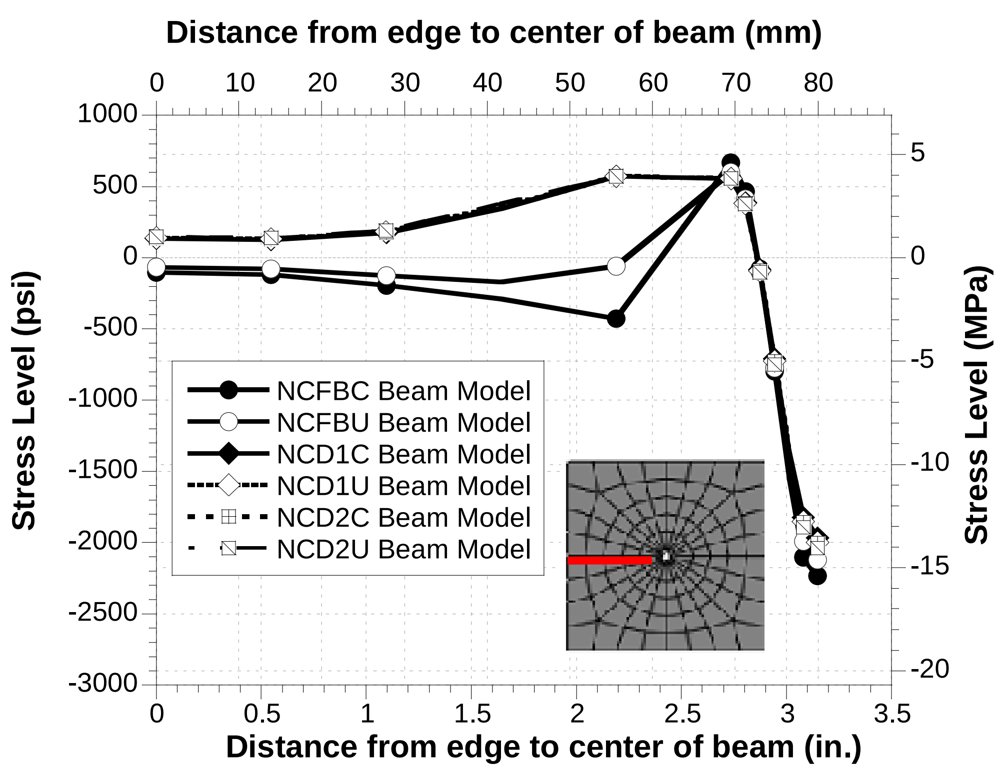

Figure A-10 Transverse stresses along cross-sectional Path: NCC set of beams

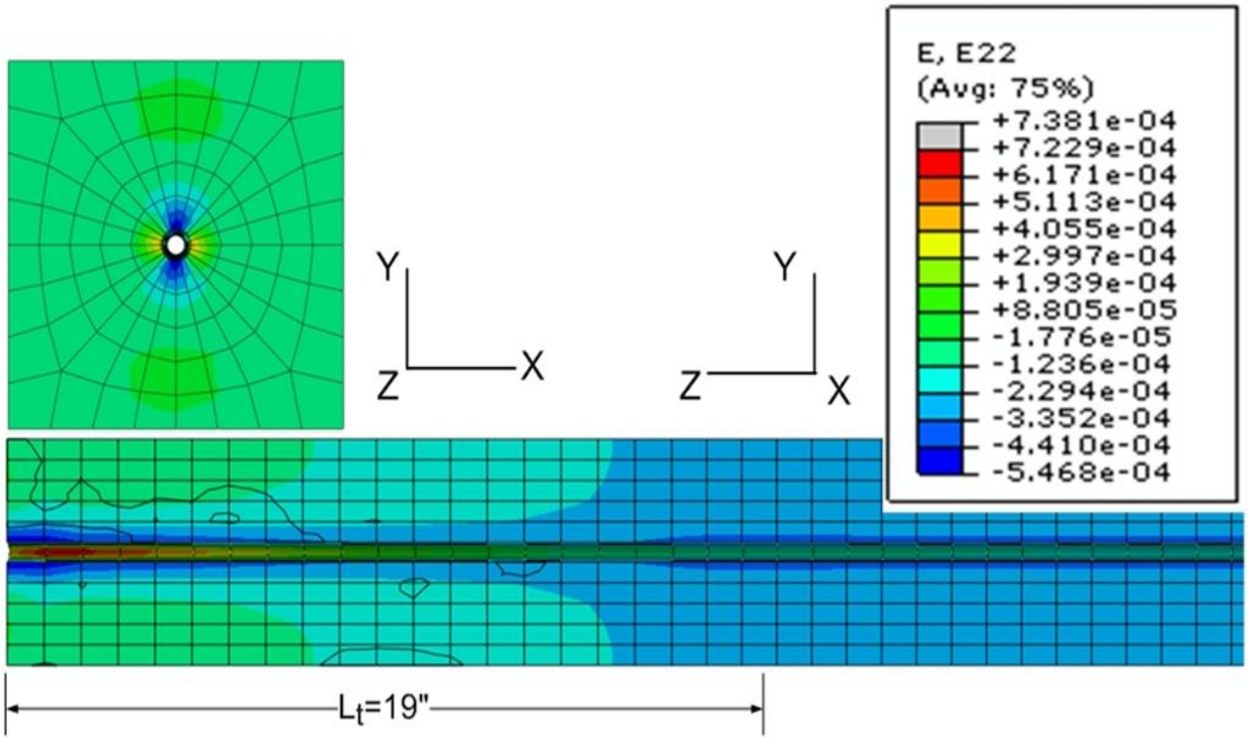

Figure A-11 NCFBC Beam Model: Transverse Strains

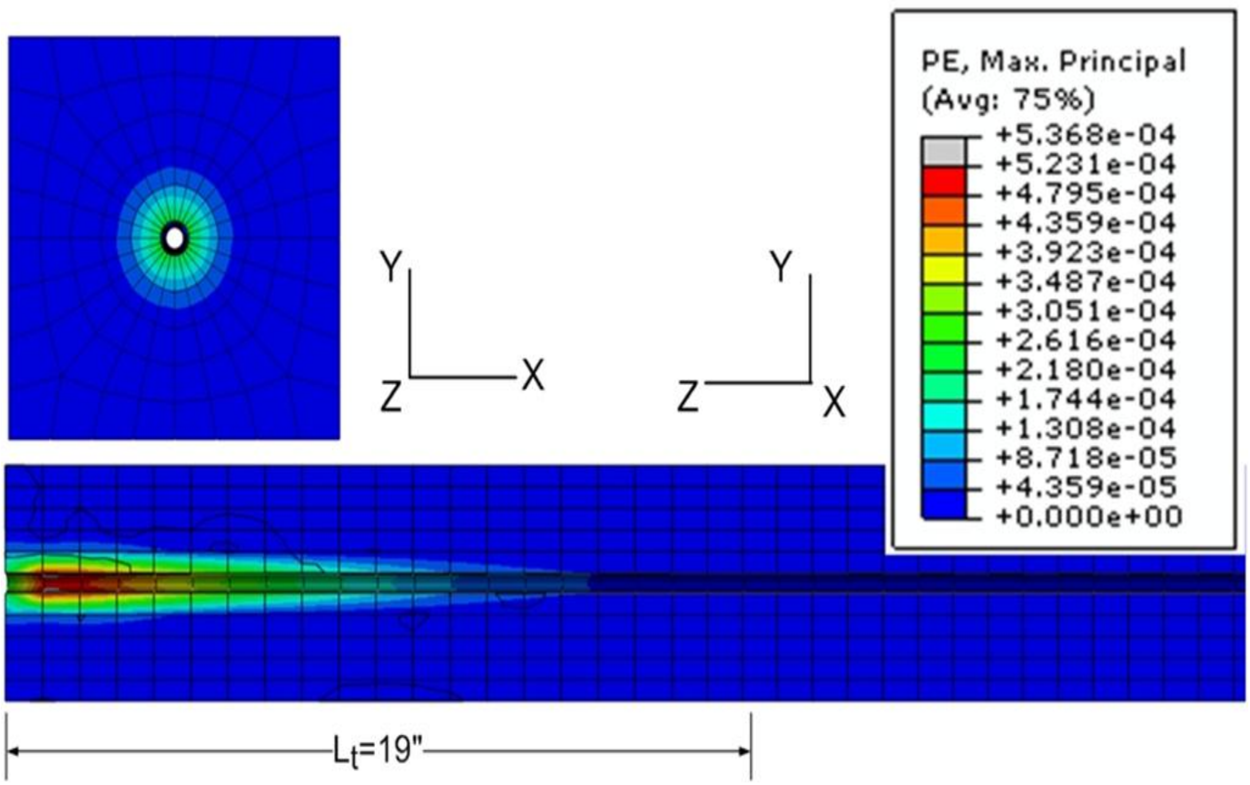

Figure A-12 NCFBC Beam Model: Maximum principal plastic strains

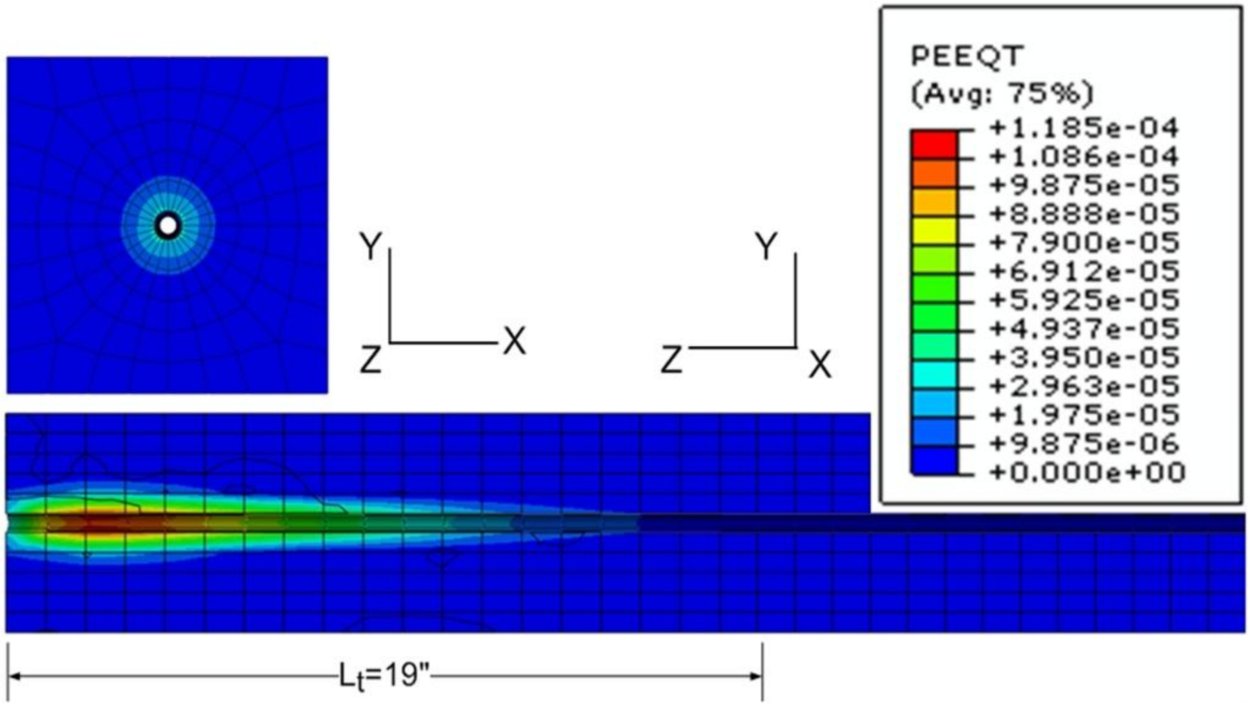

Figure A-13 NCFBC Beam Model: Equivalent plastic strain in uniaxial tension

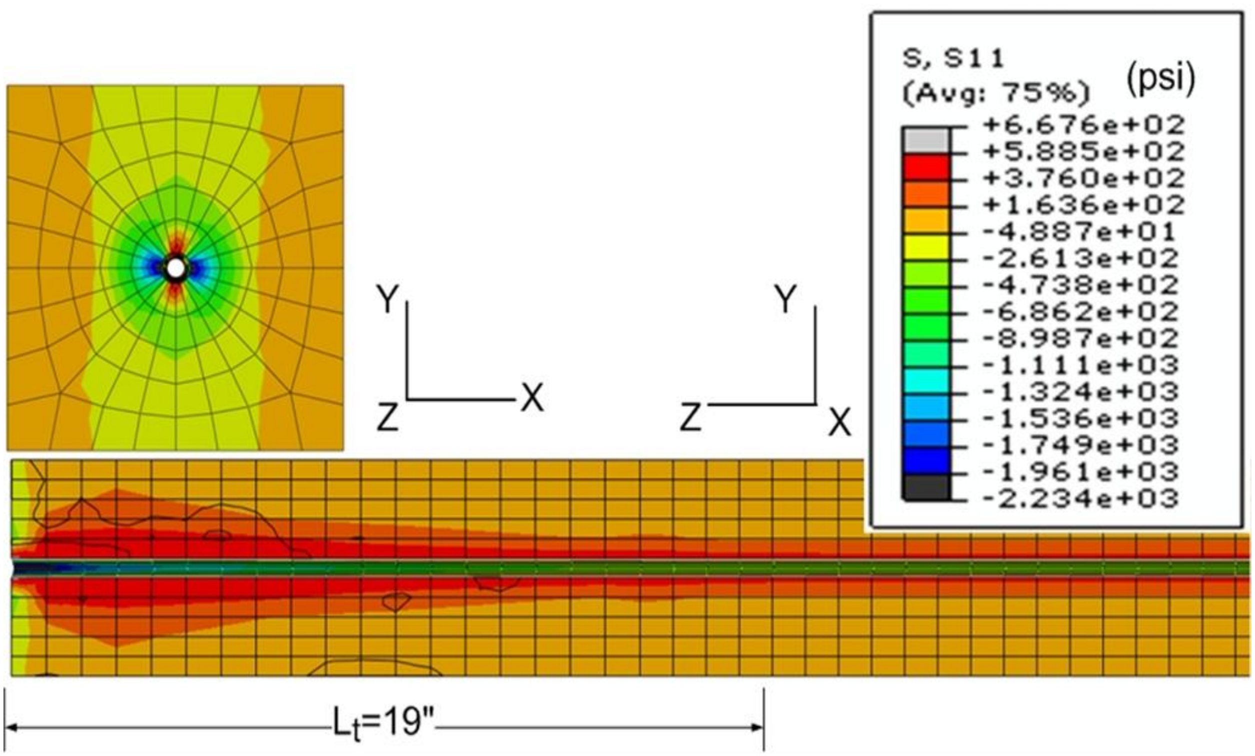

Figure A-14 NCFBC Beam Model: Axial stresses

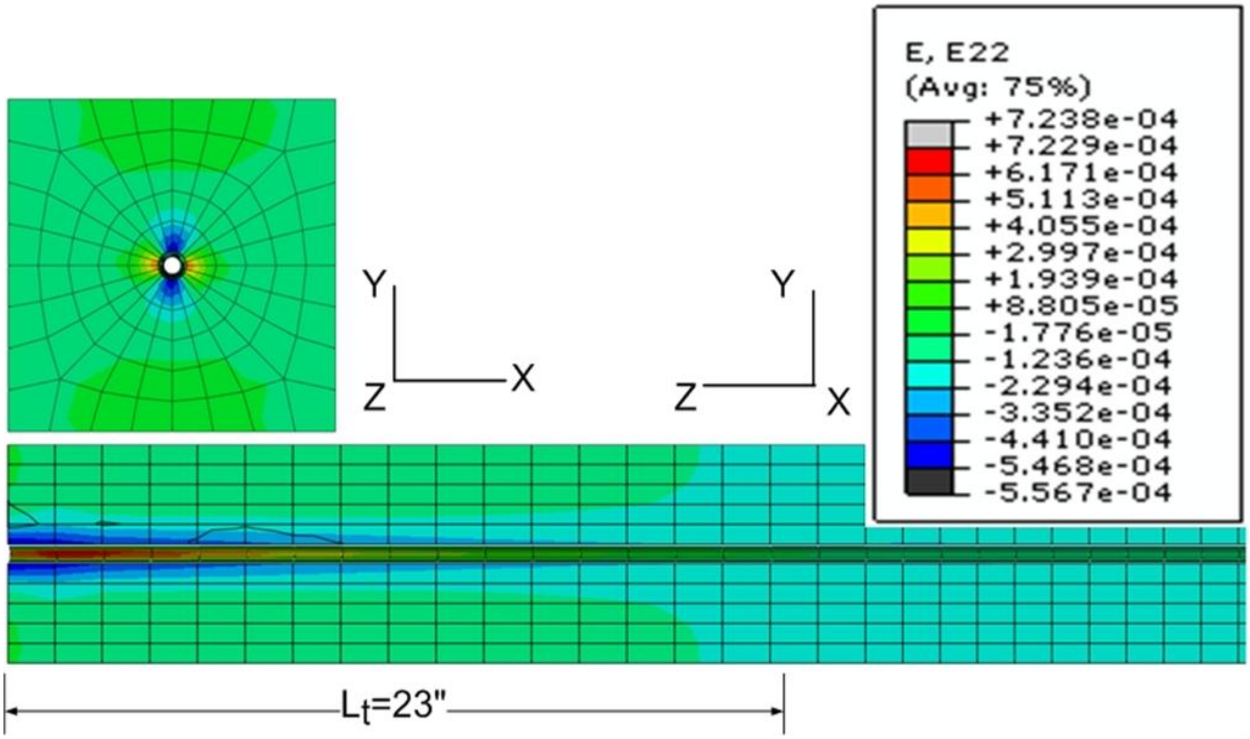

Figure A-15 NCFBU Beam Model: Transverse strain

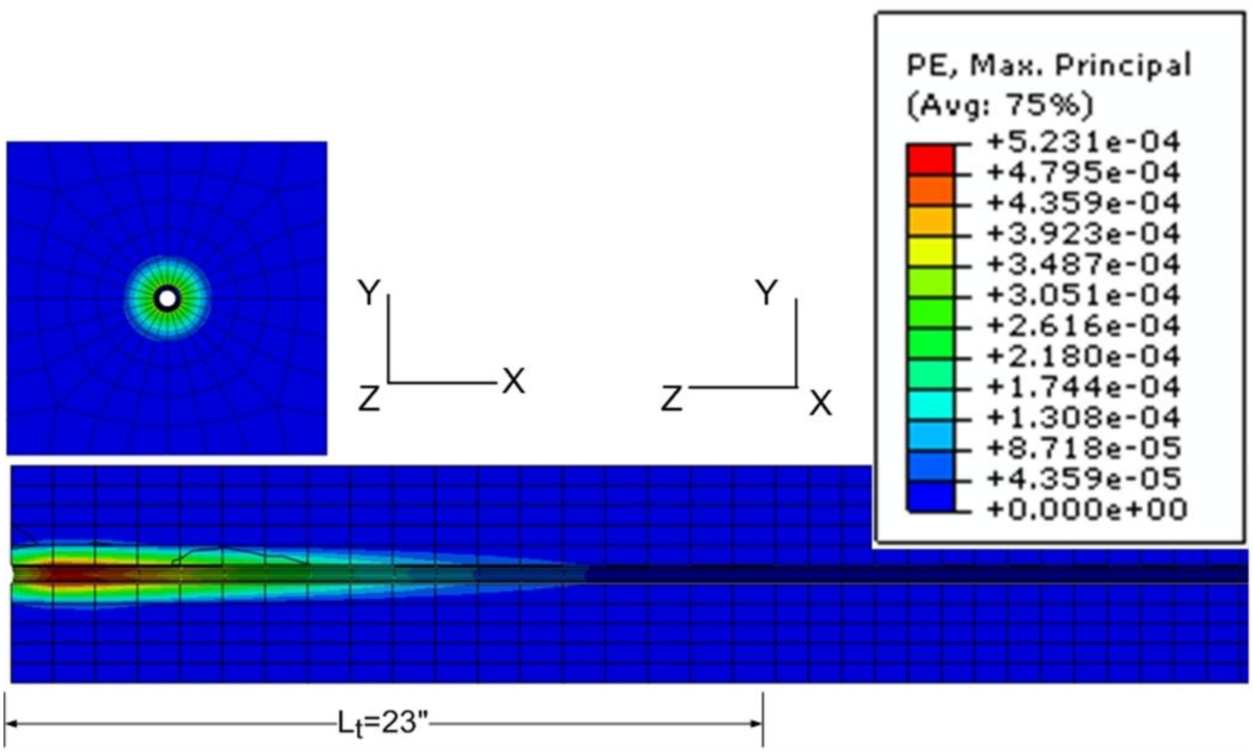

Figure A-16 NCFBU Beam Model: Maximum principal plastic strains

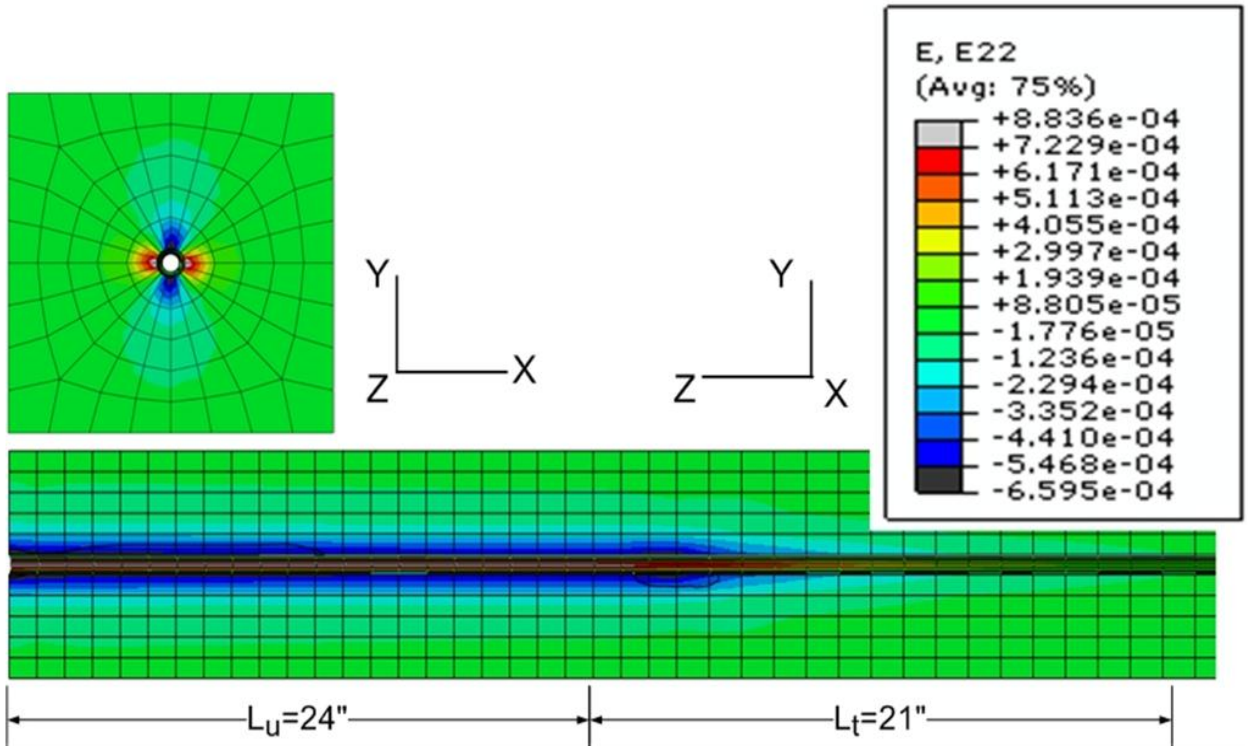

Figure A-17 NCD1C Beam Model: Transverse strain

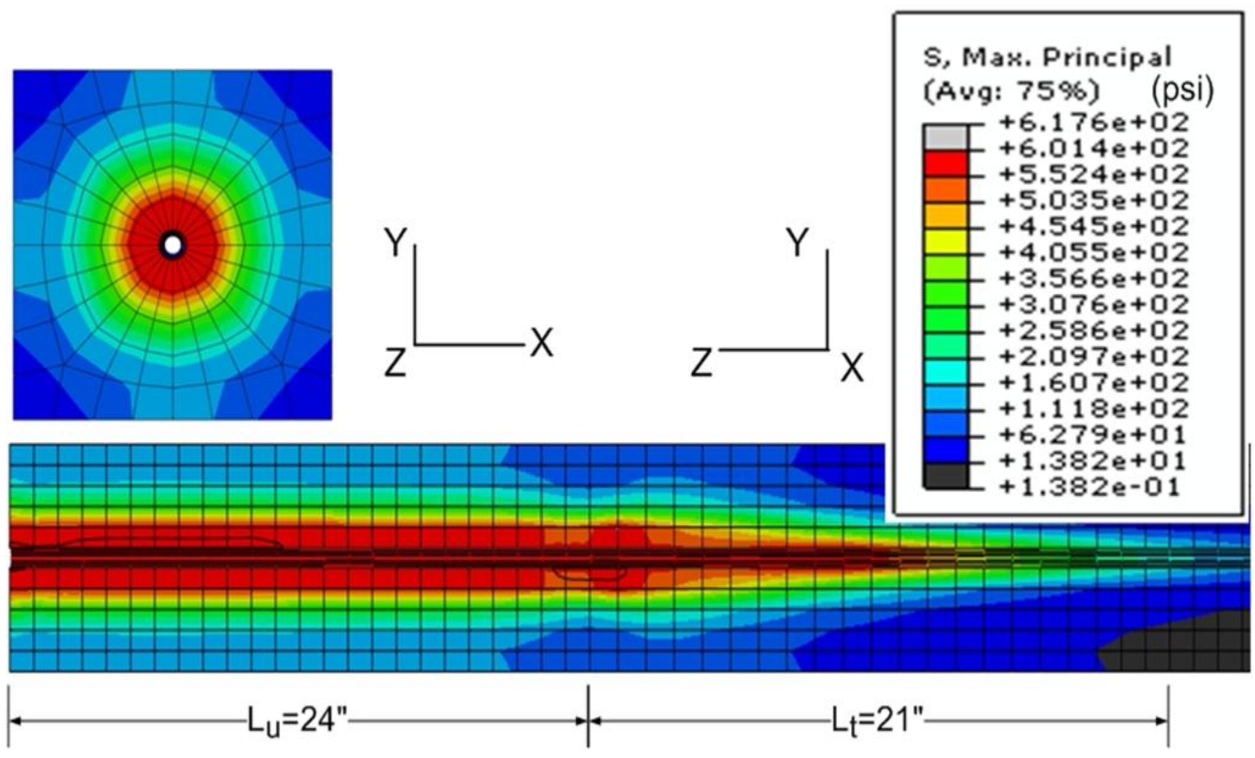

Figure A-18 NCD1C Beam Model: Maximum principal stresses

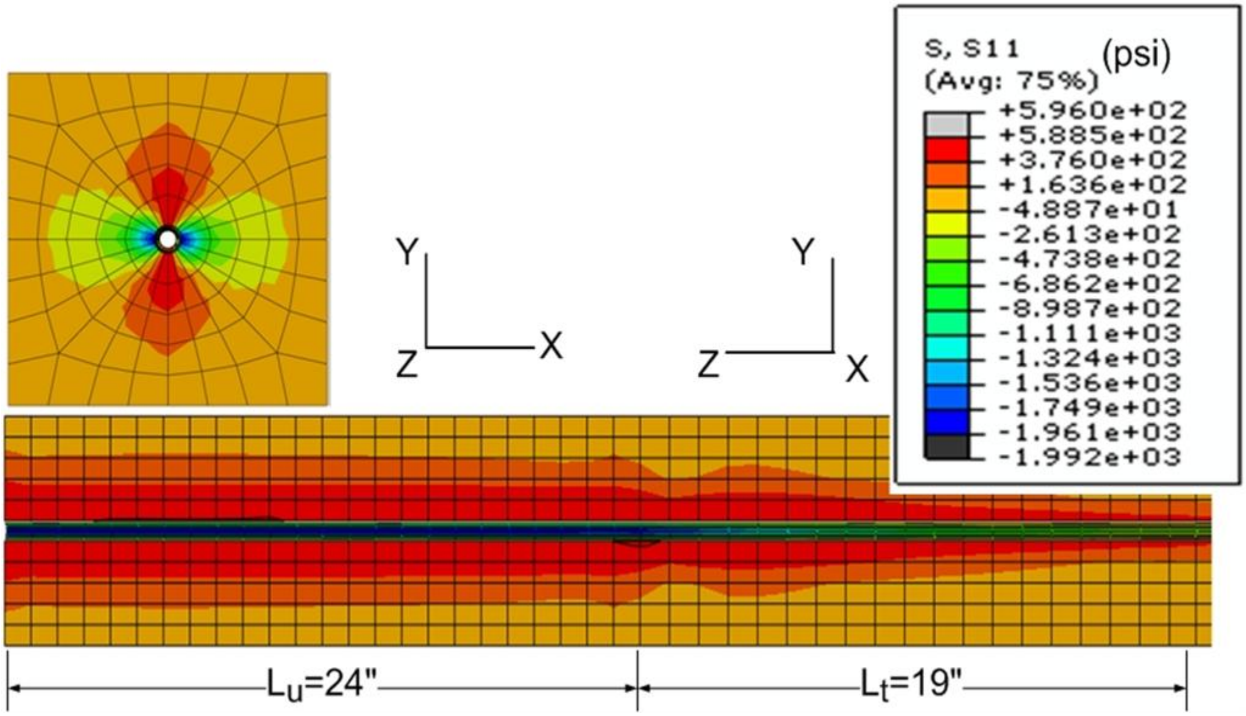

Figure A-19 NCD1U Beam Model: Axial stresses

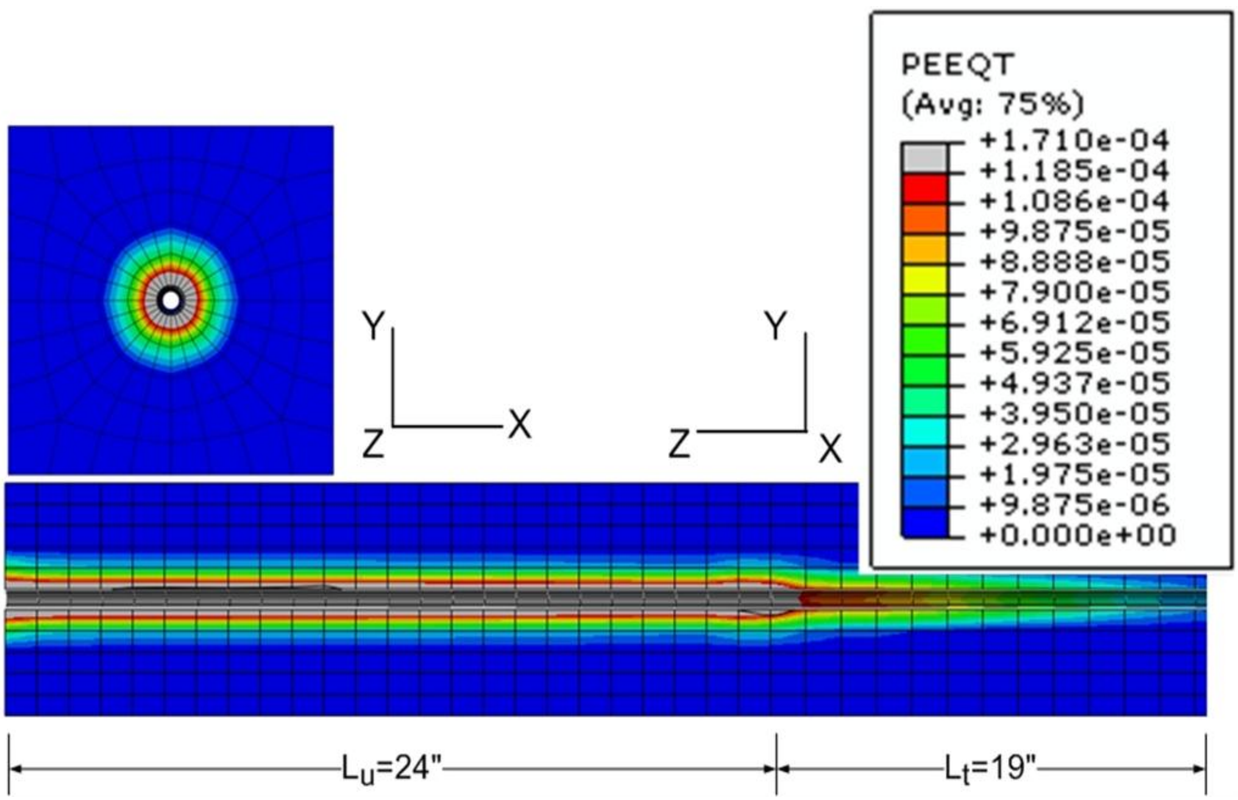

Figure A-20 NCD1U Beam Model: Equivalent plastic strain in uniaxial tension (PEEQT)

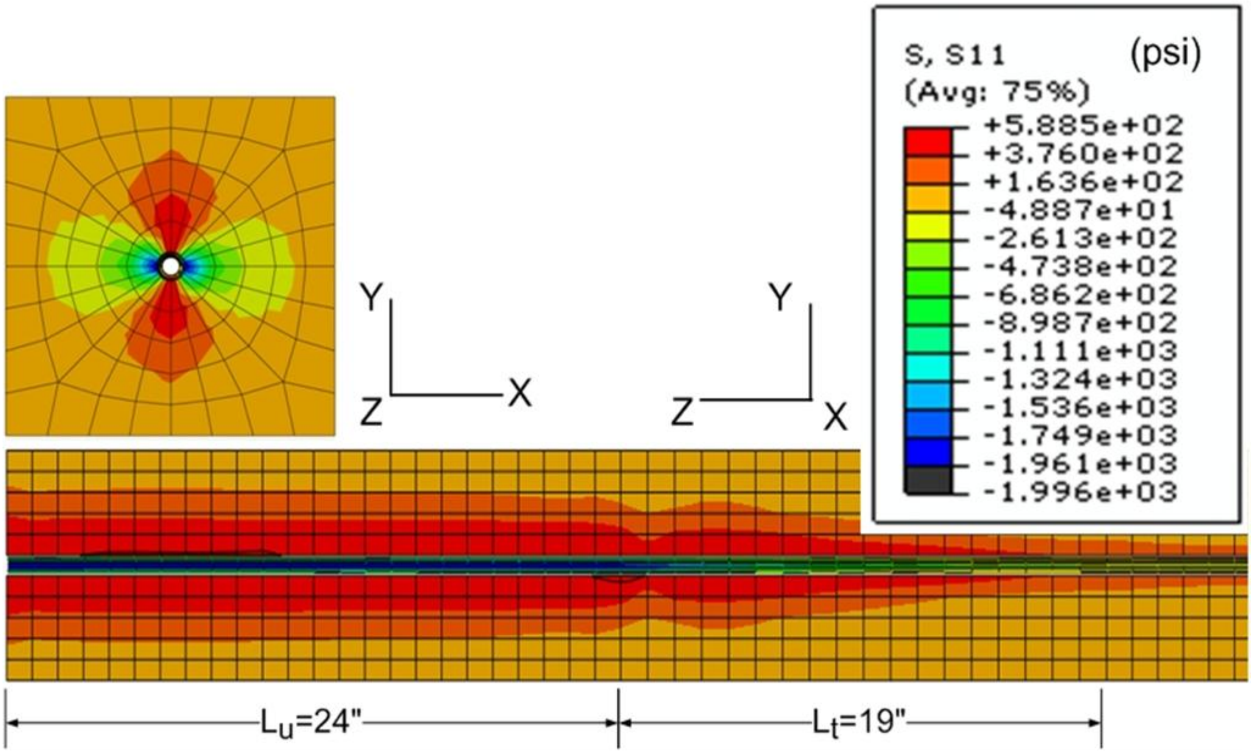

Figure A-21 NCD2C Beam Model: Axial stresses

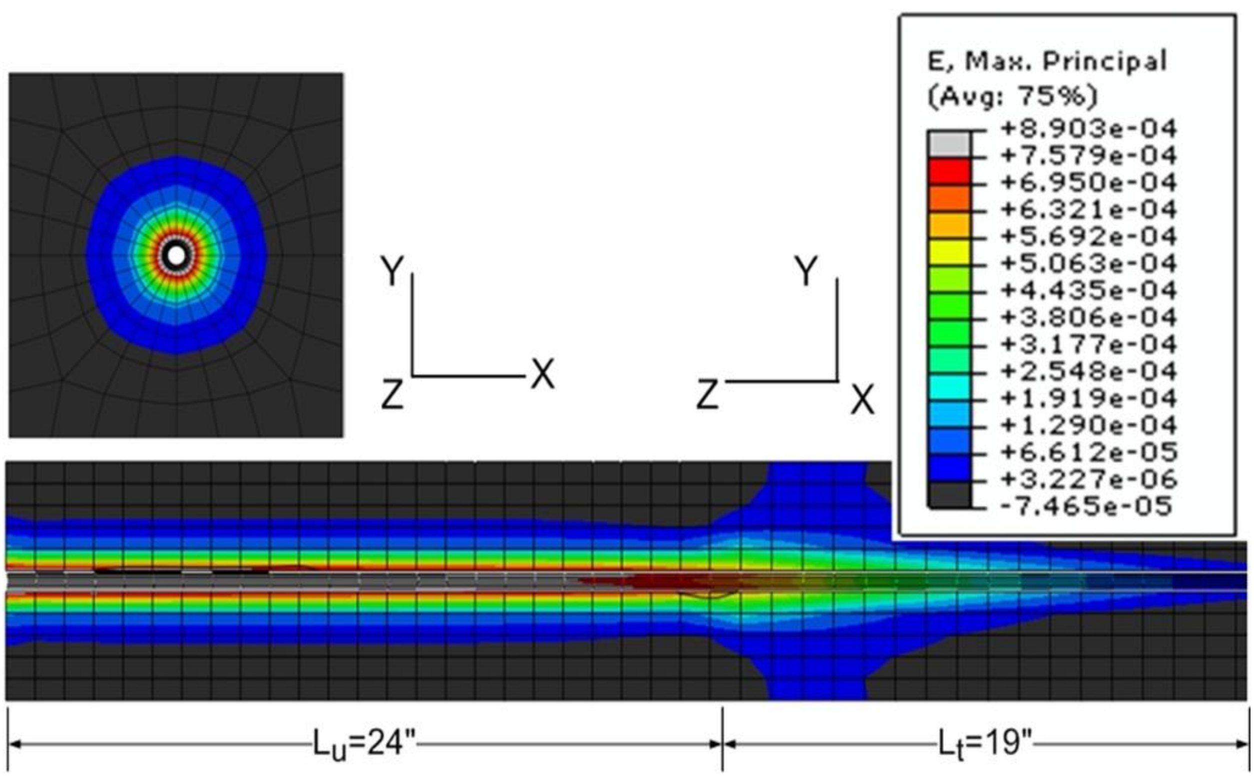

Figure A-22 NCD2C Beam Model: Maximum principal strain

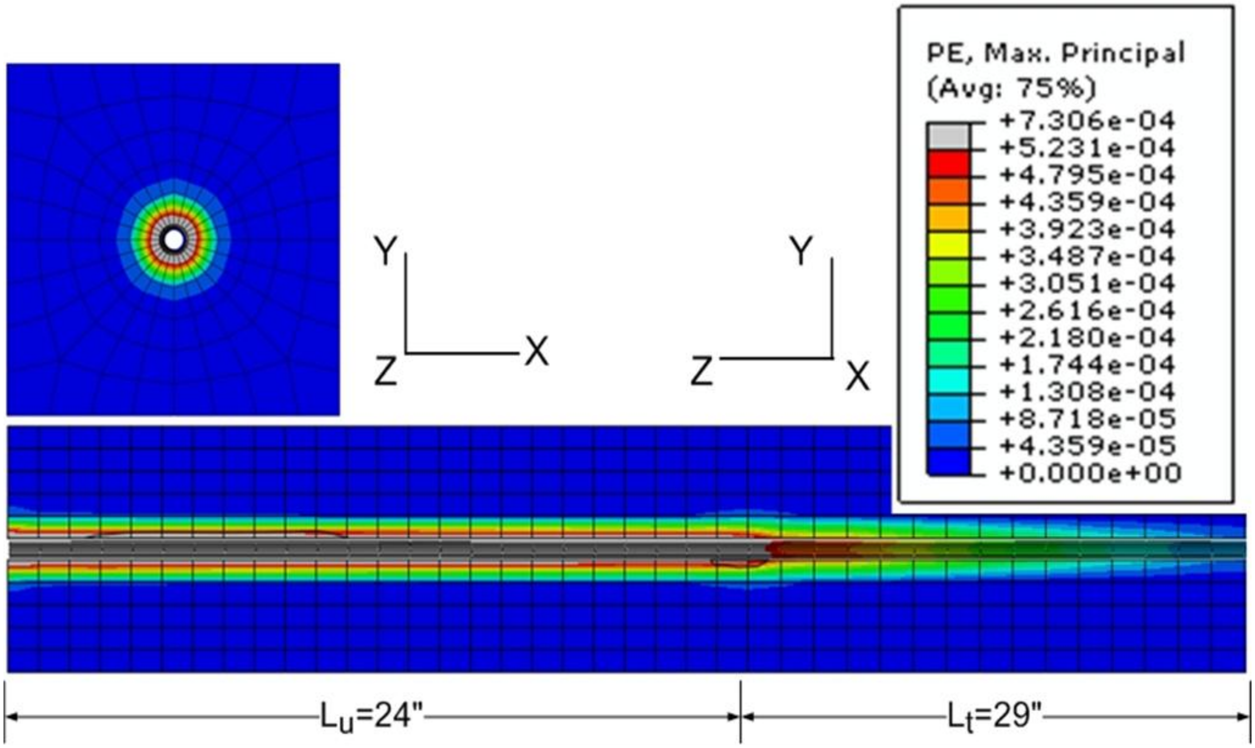

Figure A-23 NCD2U Beam Model: Maximum principal plastic strain

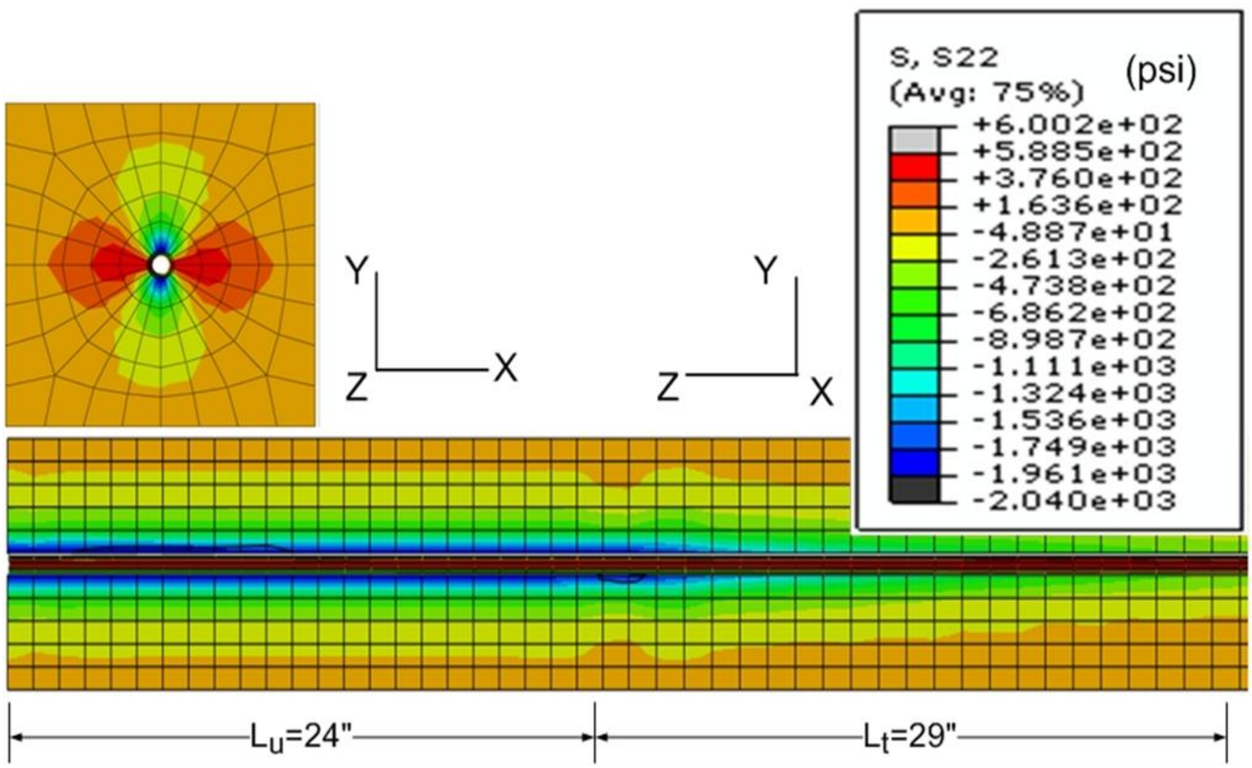

Figure A-24 NCD2U Beam Model: Transverse stresses

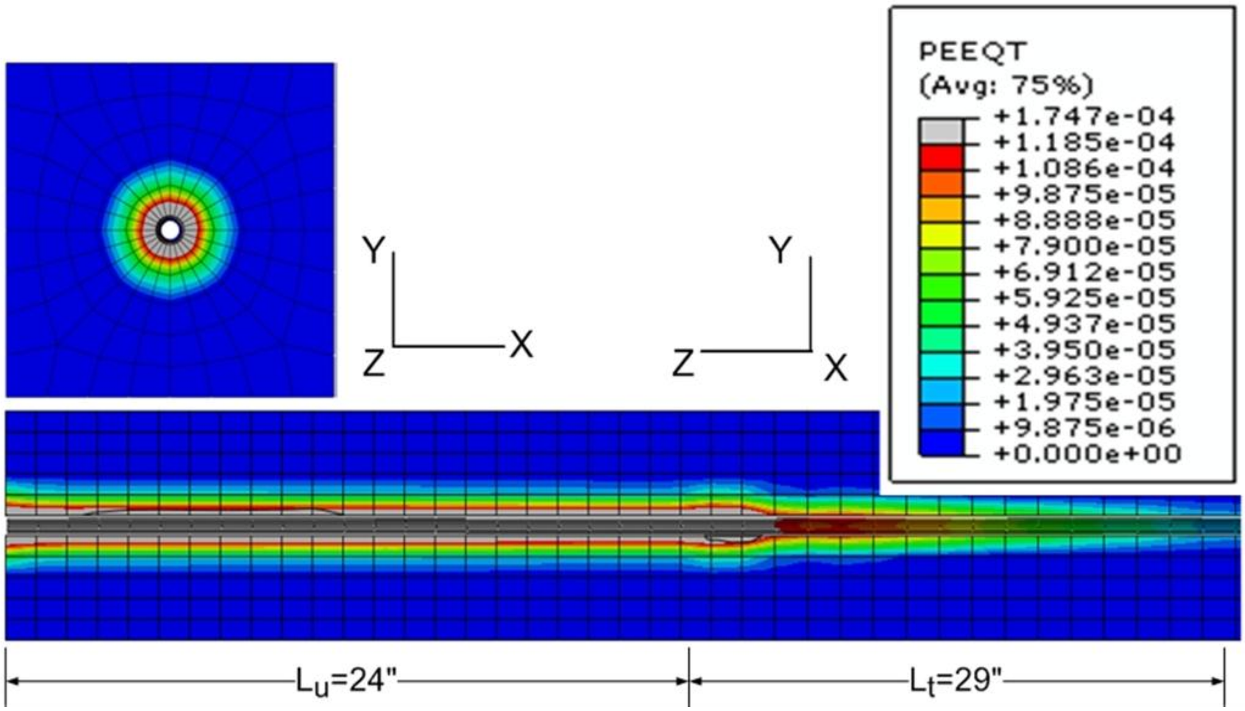

Figure A-25 NCD2U Beam Model: PEEQT

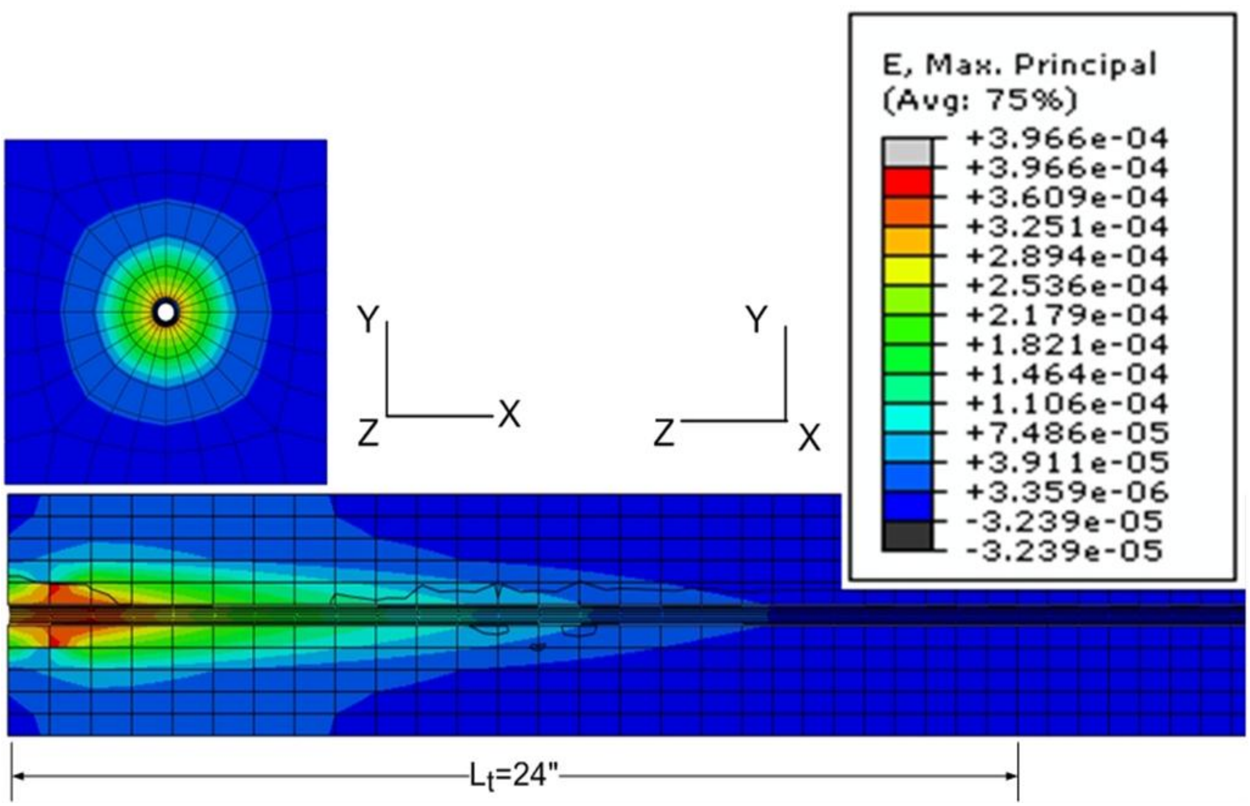

Figure A-26 SCFBC Beam Model: Maximum principal strains

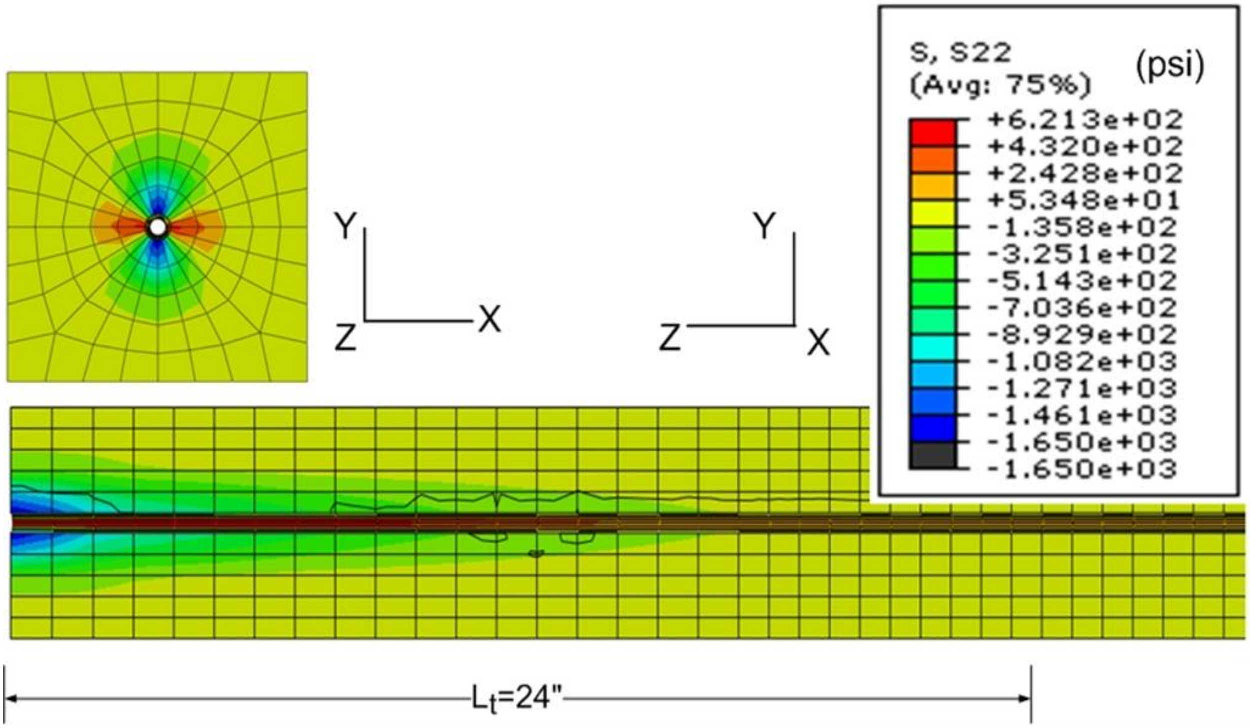

Figure A-27 SCFBC Beam Model: Transverse stresses

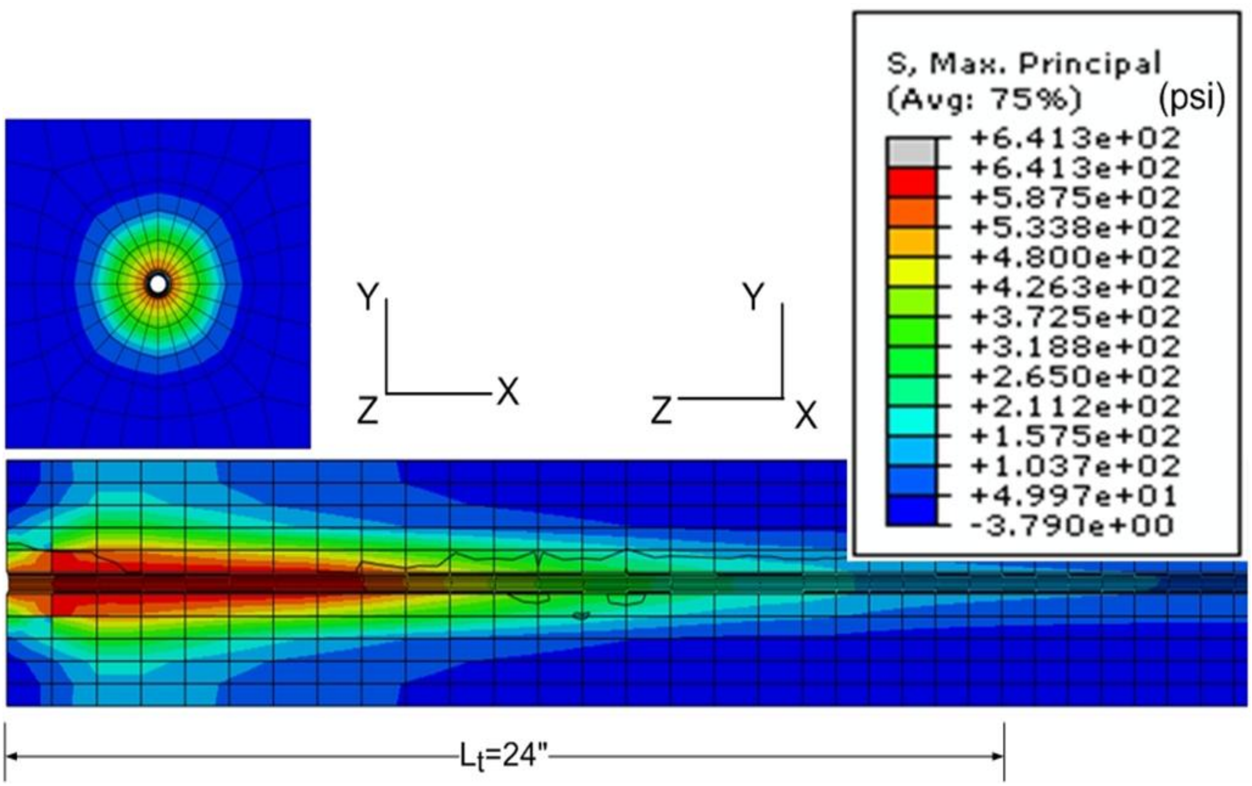

Figure A-28 SCFBC Beam Model: Maximum principal stresses

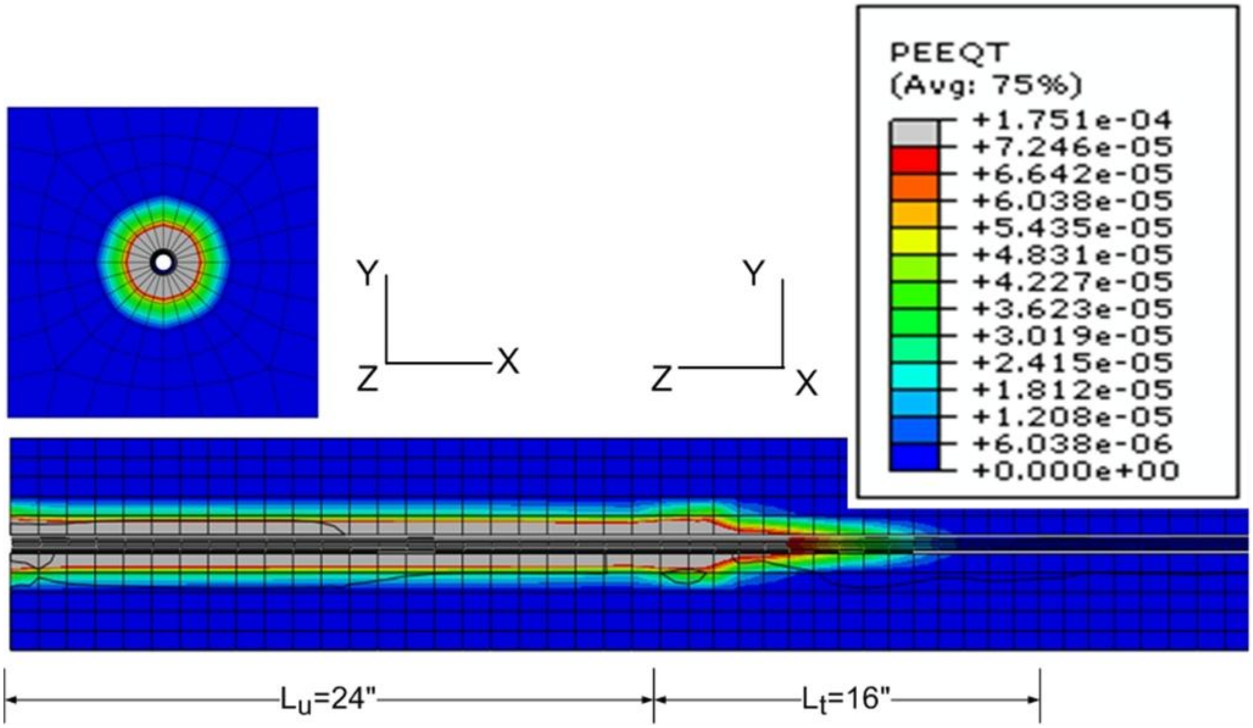

Figure A-29 SCD1C Beam Model: Equivalent plastic strain in uniaxial tension (PEEQT)

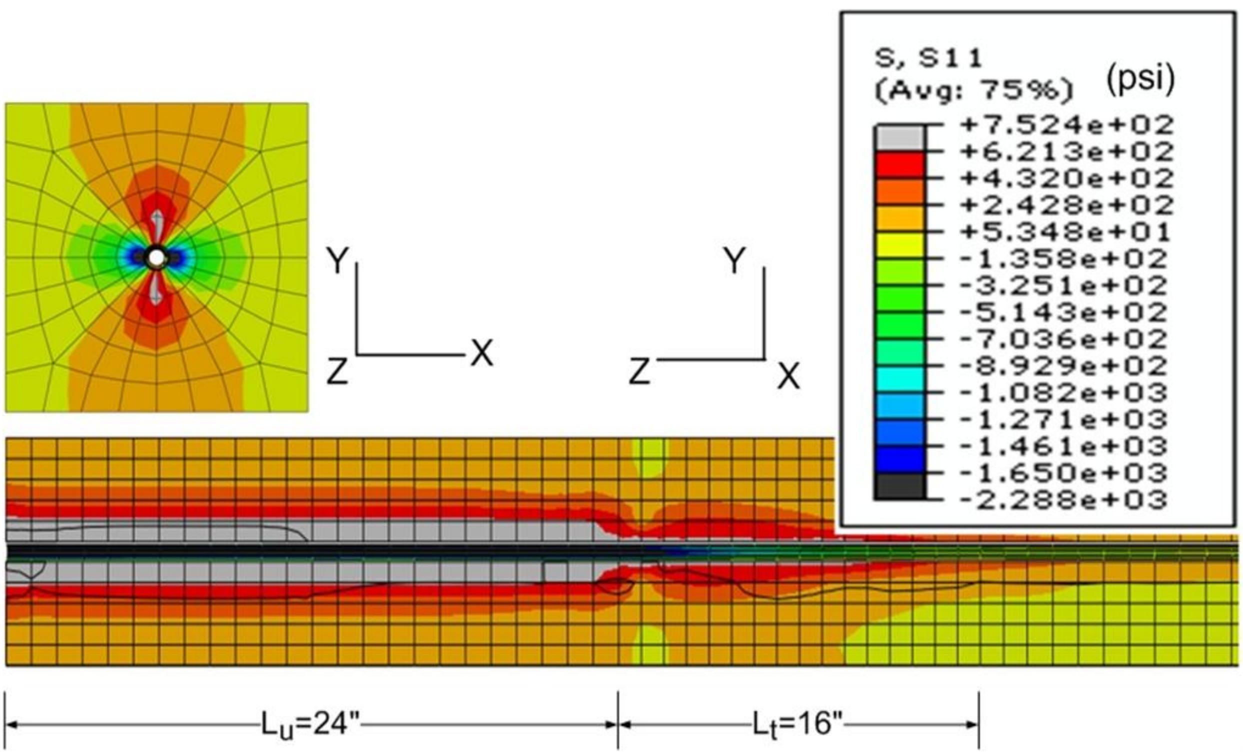

Figure A-30 SCD1C Beam Model: Axial stresses

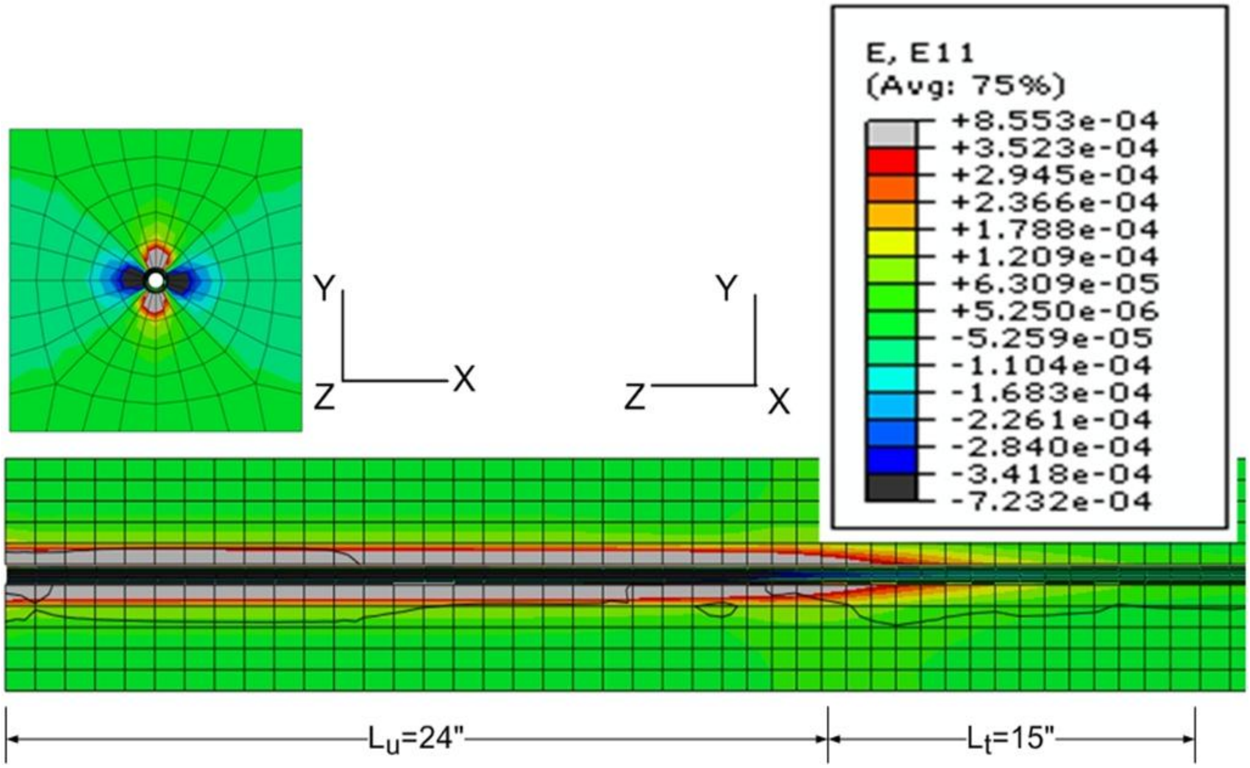

Figure A-31 SCD1U Beam Model: Axial strains

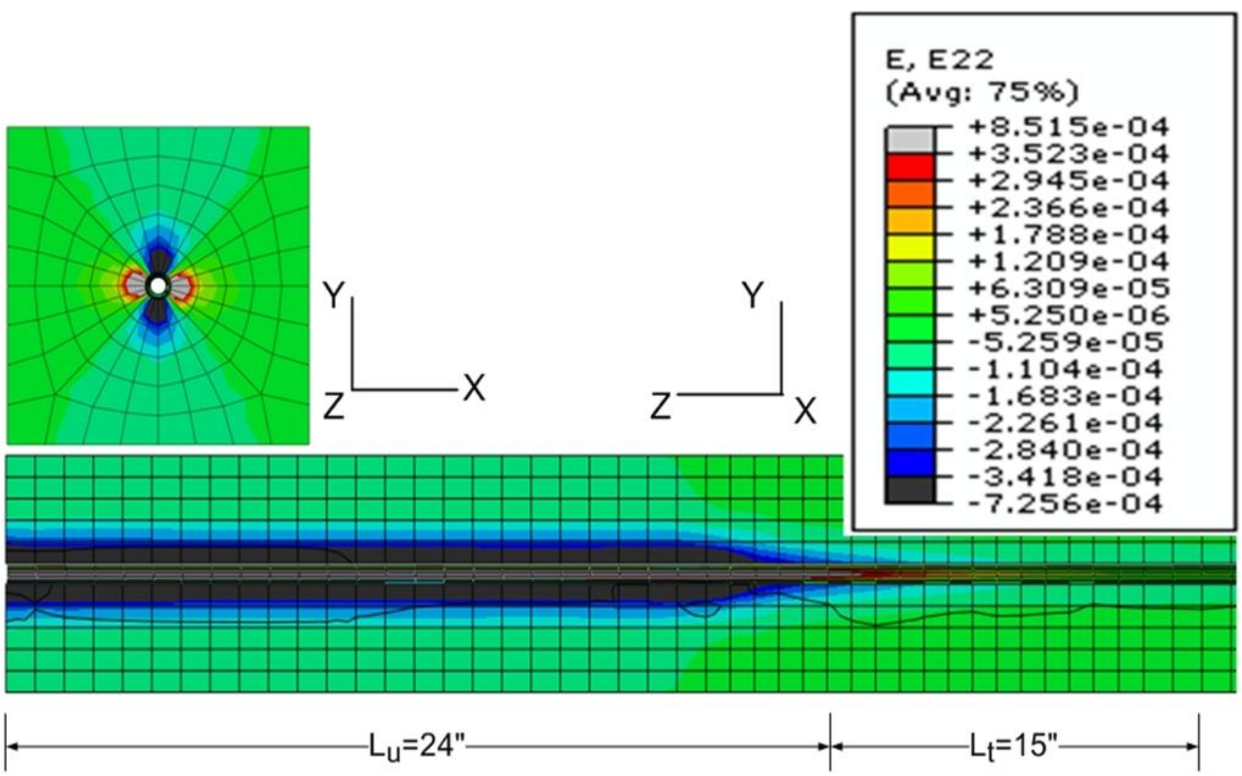

Figure A-32 SCD1U Beam Model: Transverse strains

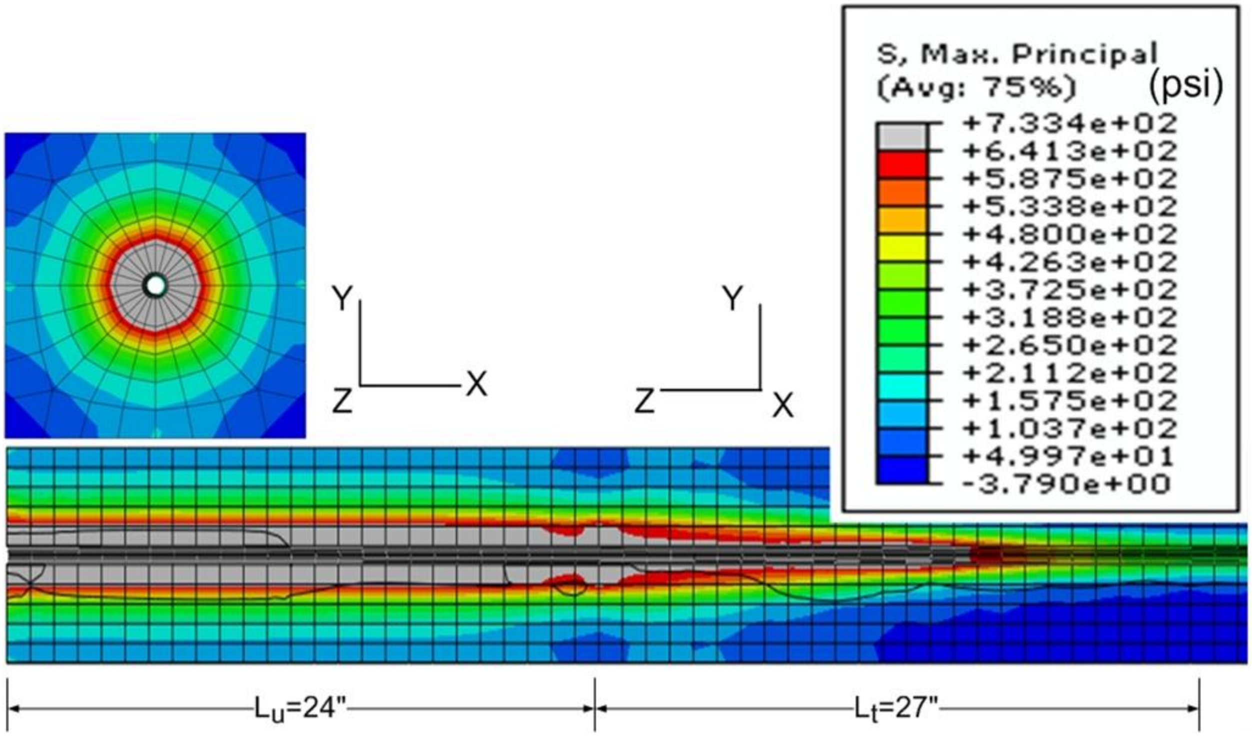

Figure A-33 SCD2U Beam Model: Maximum principal stresses

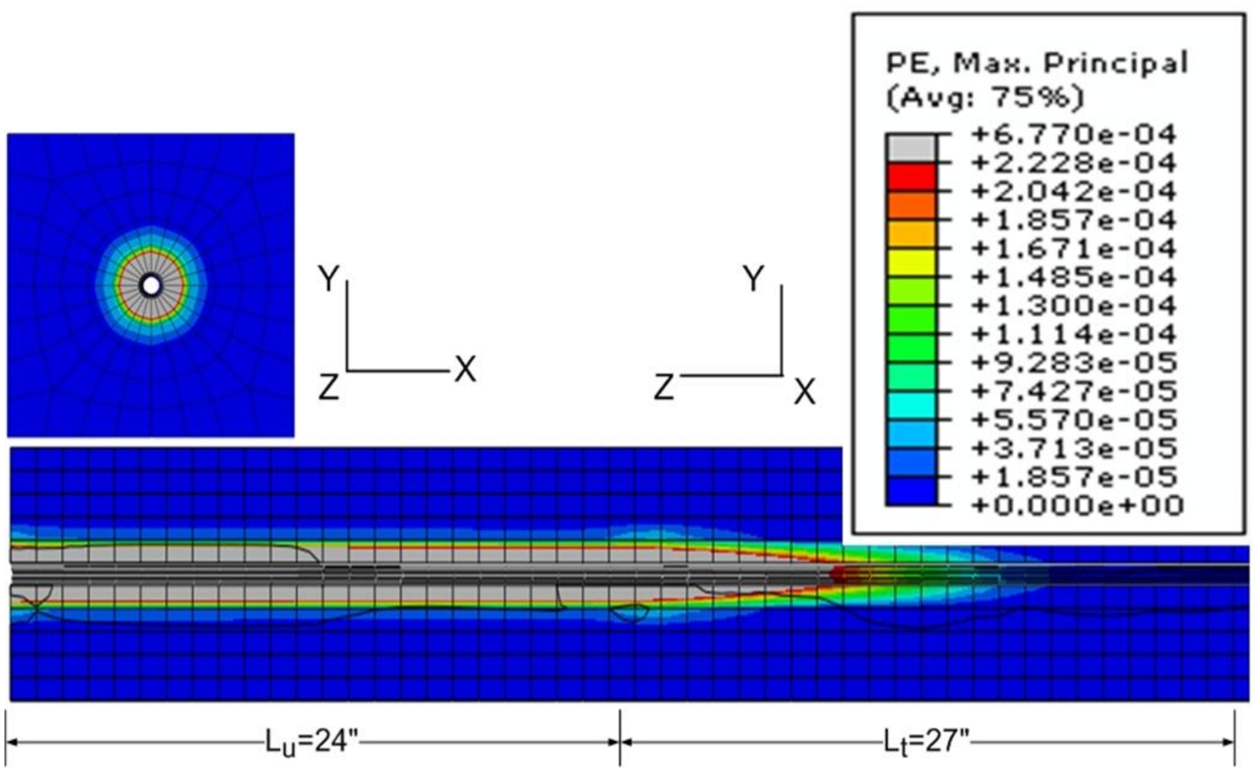

Figure A-34 SCD2U Beam Model: Maximum principal plastic strains

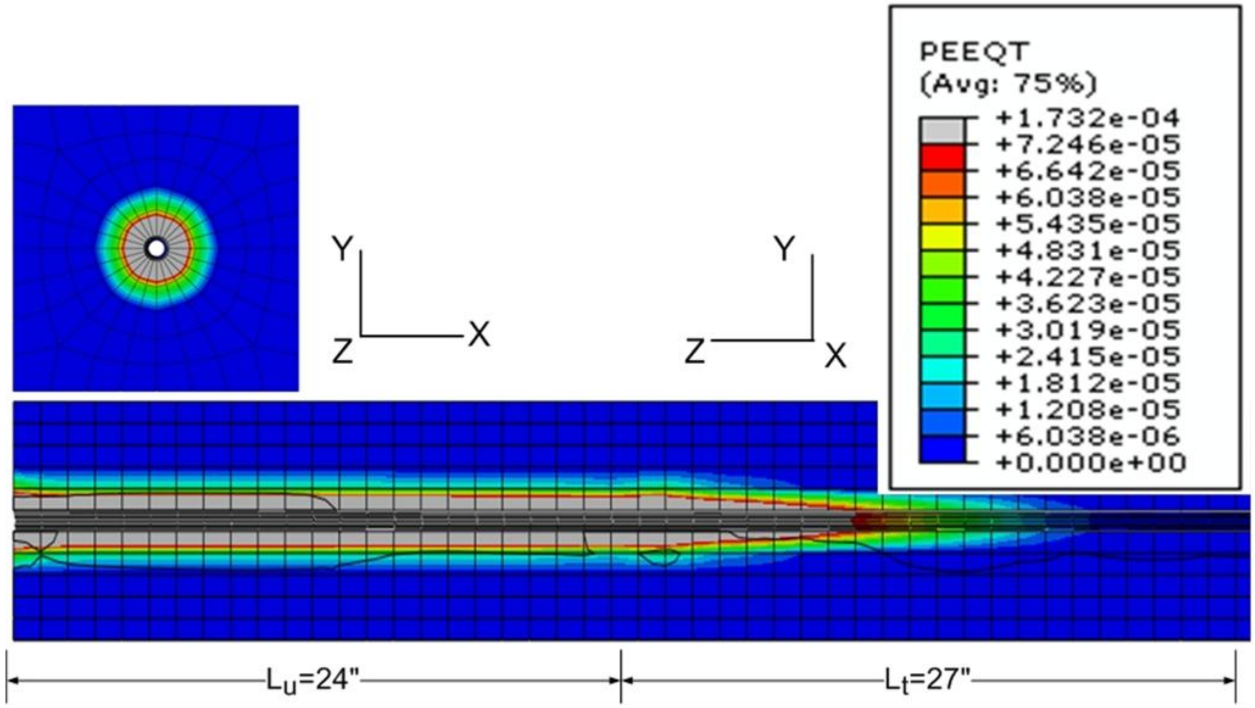

Figure A-35 SCD2U Beam Model: PEEQT

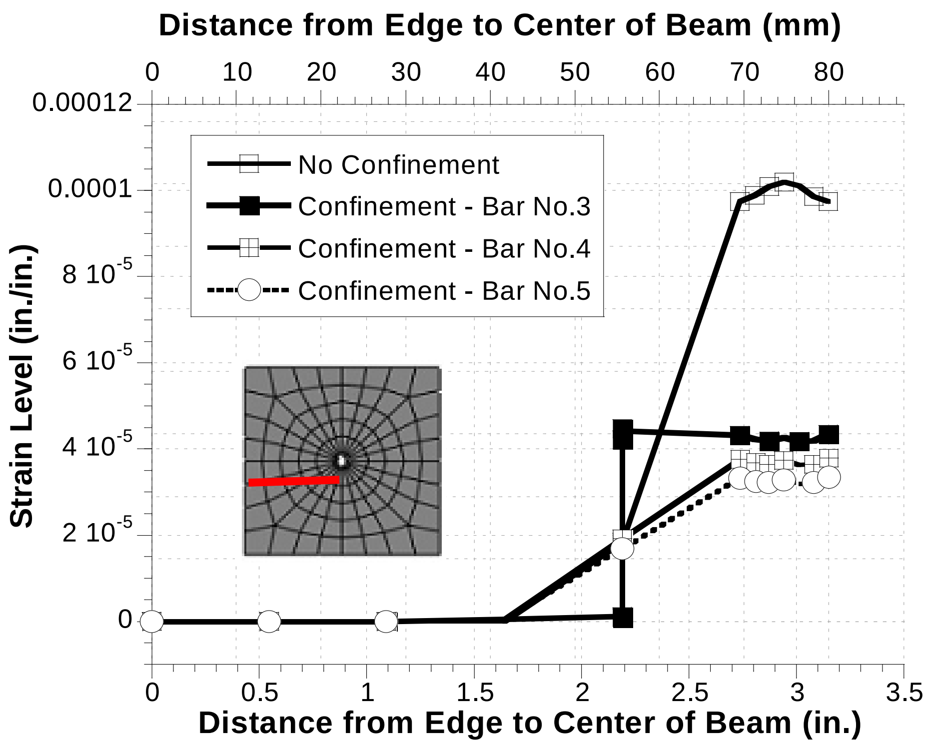

Figure A-36 PEEQT: NCFBC beam model – path along the cross section of the beam at 4 in. (200 mm) from releasing end

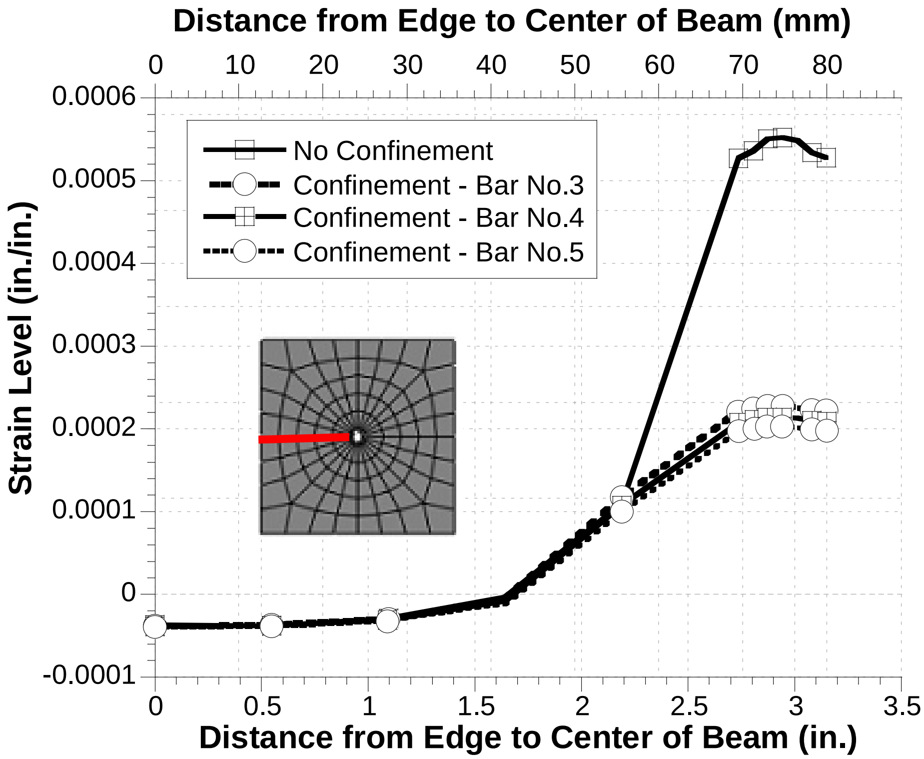

Figure A-37 Maximum Principal Strain – NCFBC Beam Model along cross section (4 in. [100 mm] from the releasing end)

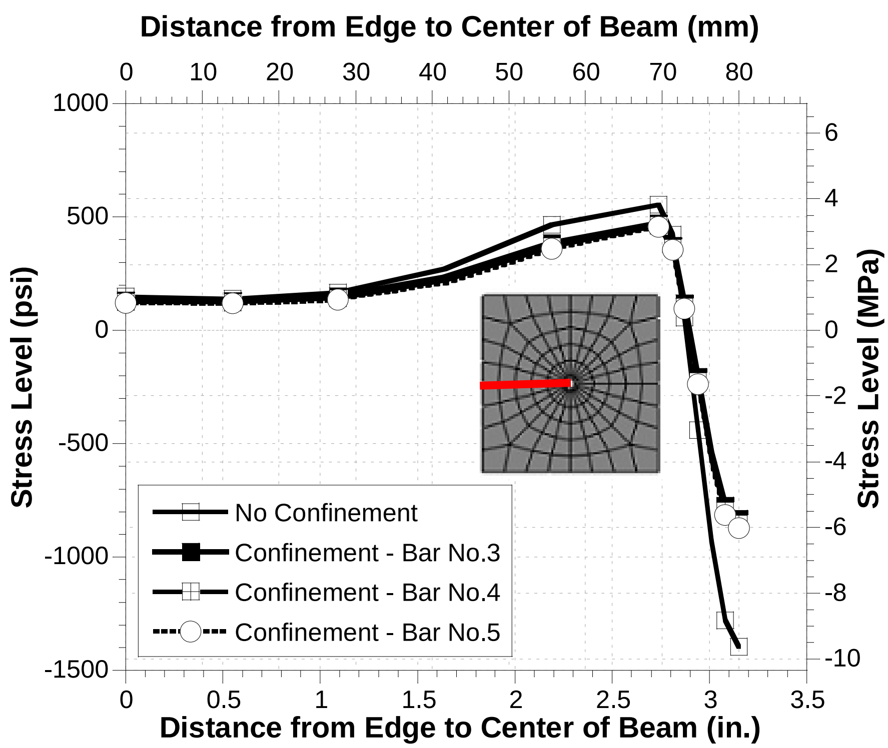

Figure A-38 NCFBC beam model – Transverse stresses along cross section (at 4 in. [100 mm] from releasing end)

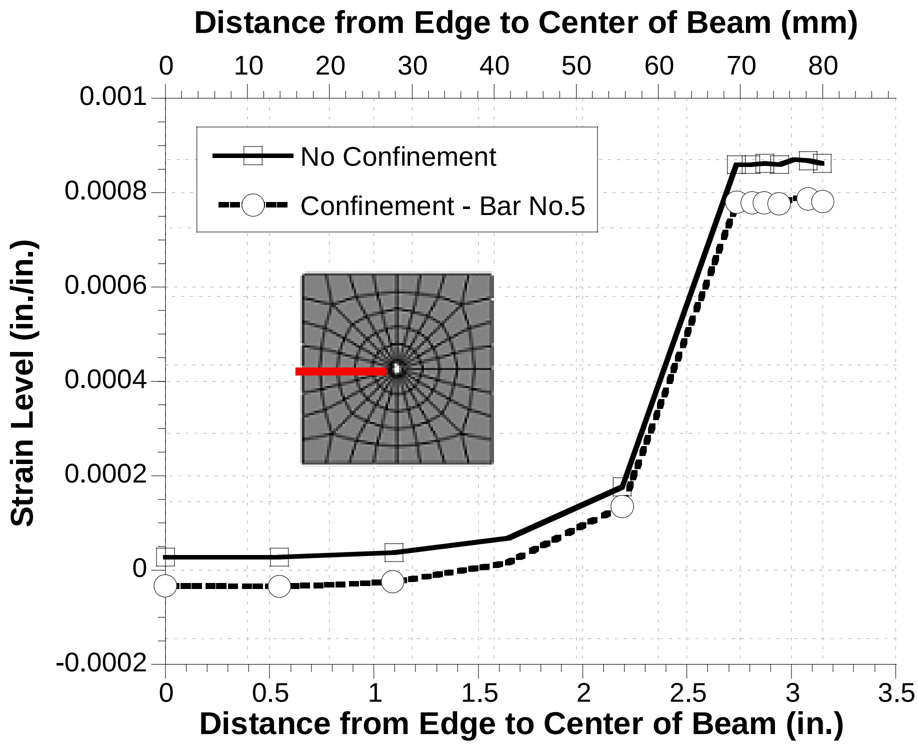

Figure A-39 NCD1C beam model – Maximum Principal Strain along cross section (at 4 in. [100 mm] from releasing end)

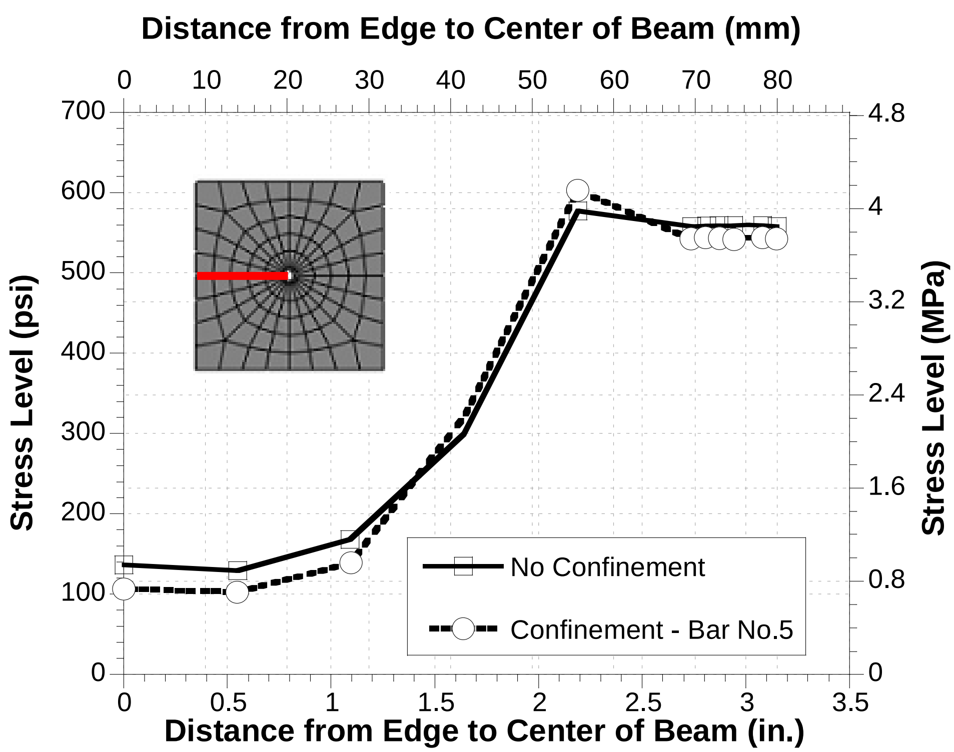

Figure A-40 Maximum principal stress along cross section – NCD1C beam model

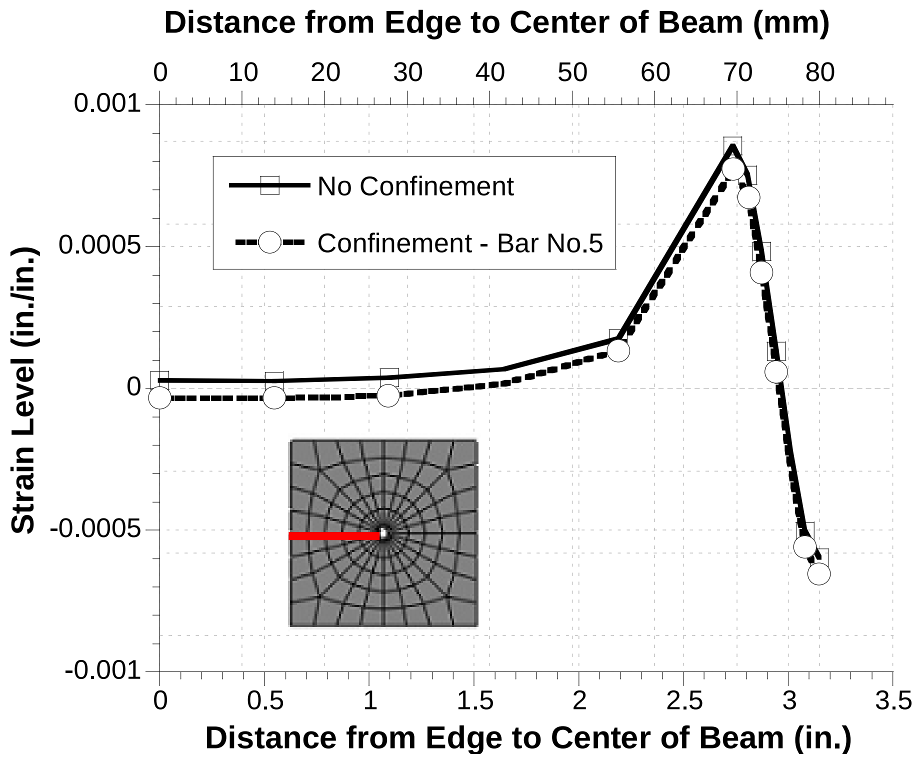

Figure A-41 NCD1C beam model – Transverse Strain along cross section

APPENDIX D –Results from Numerical Case Study: U-beam Models

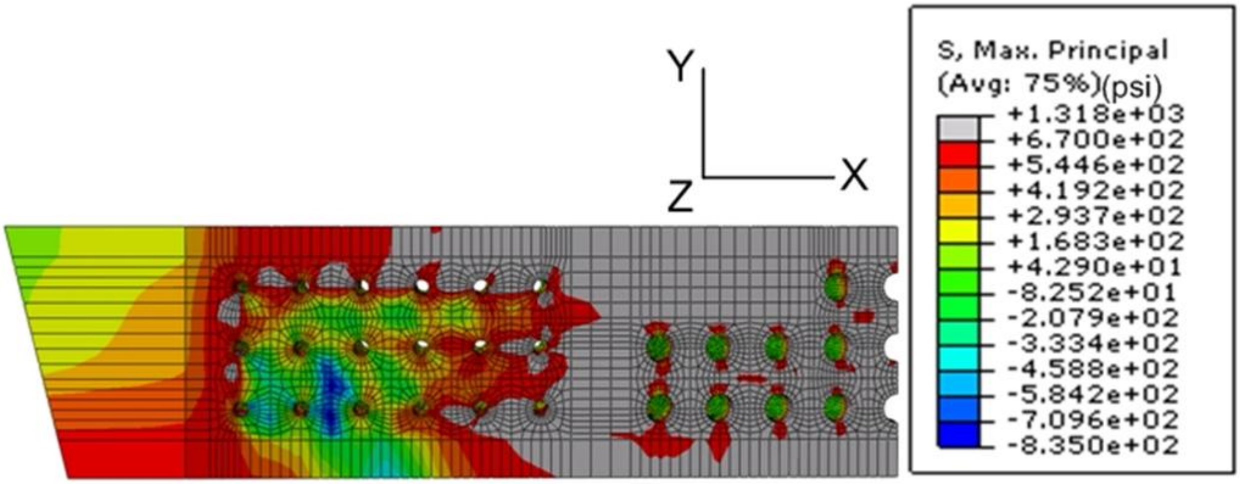

Figure A-42 Case 3: Maximum principal stresses at beam end

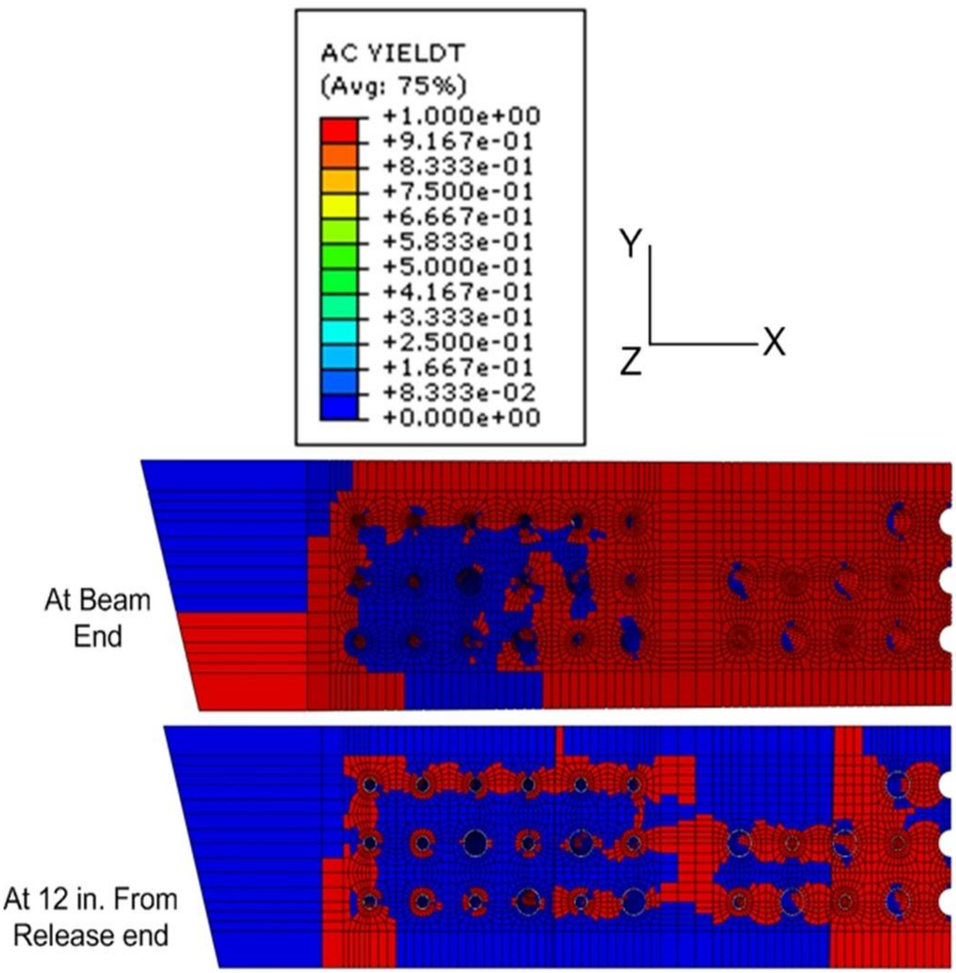

Figure A-43 Results for Case 4: Yielding of concrete elements at beam cross section

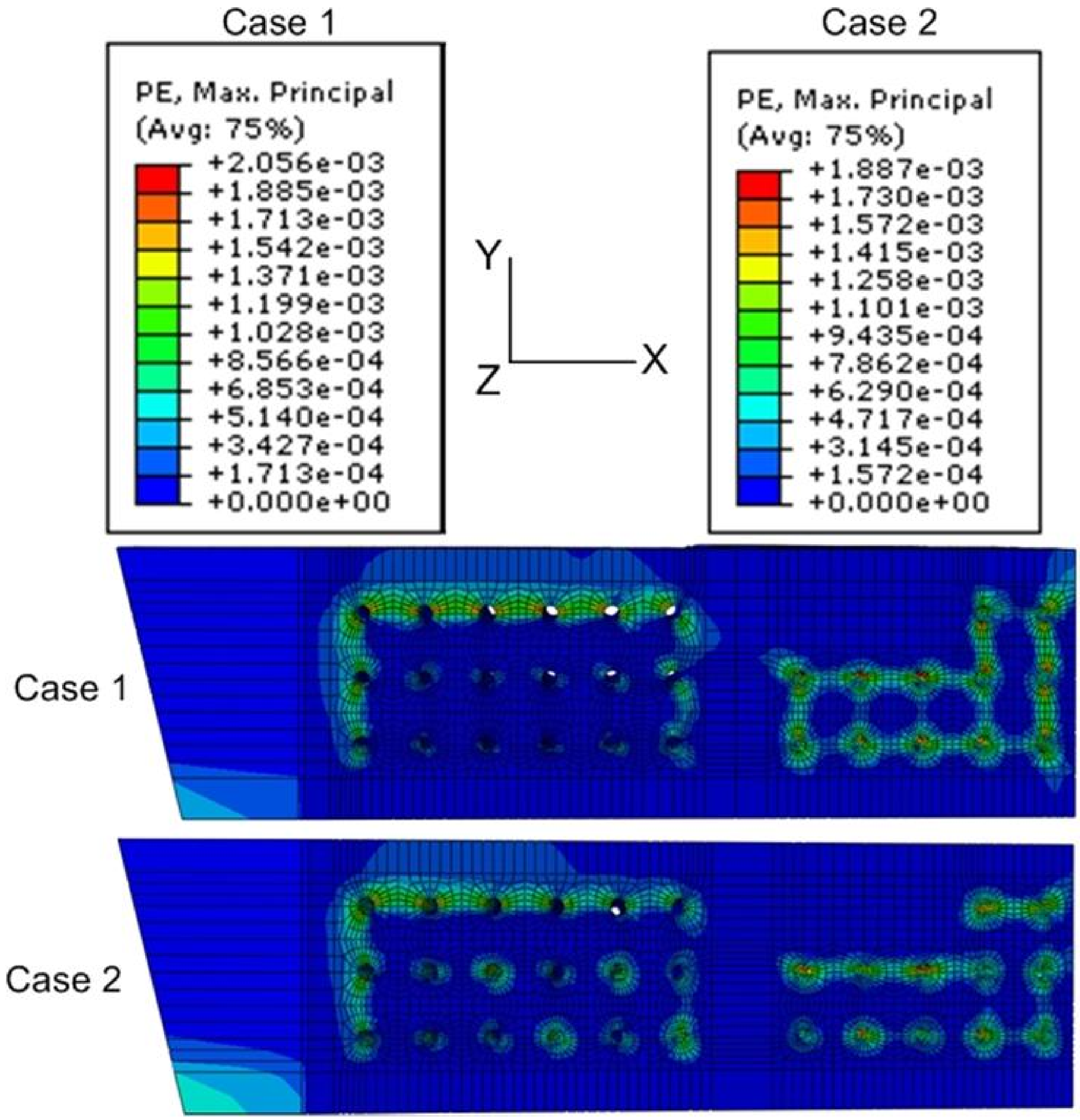

Figure A-44 PE Max Principal: Case 1 vs. Case 2 at beam end

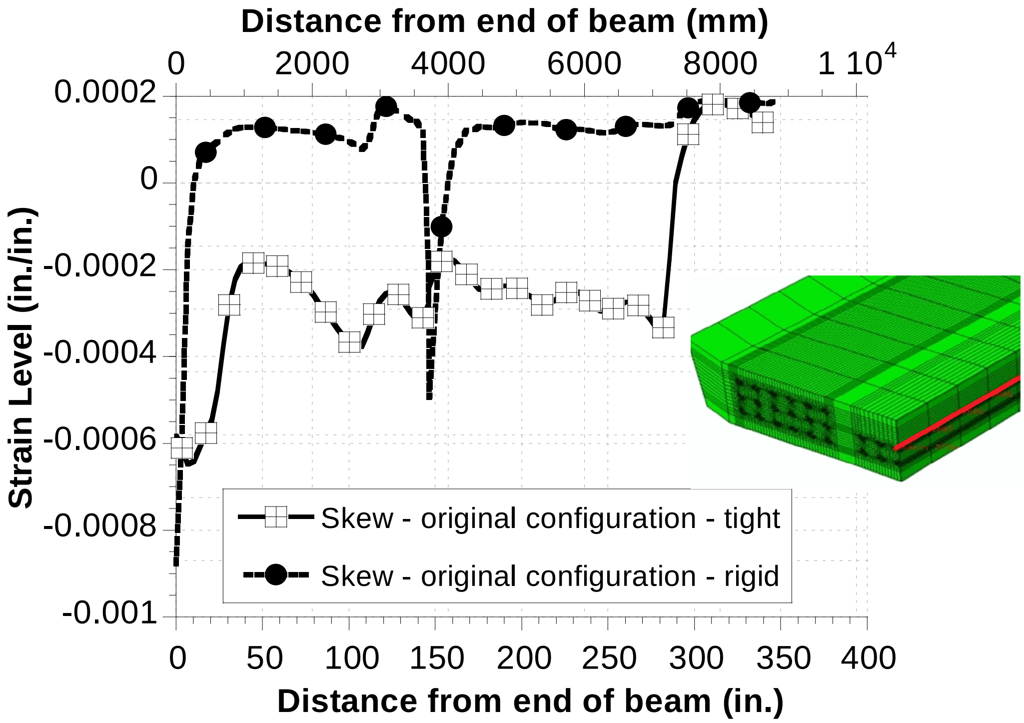

Figure A-45 Response traces along partially debonded strand No.9: Axial strains – Skew-symmetry U-beam models tight vs. rigid with original configuration

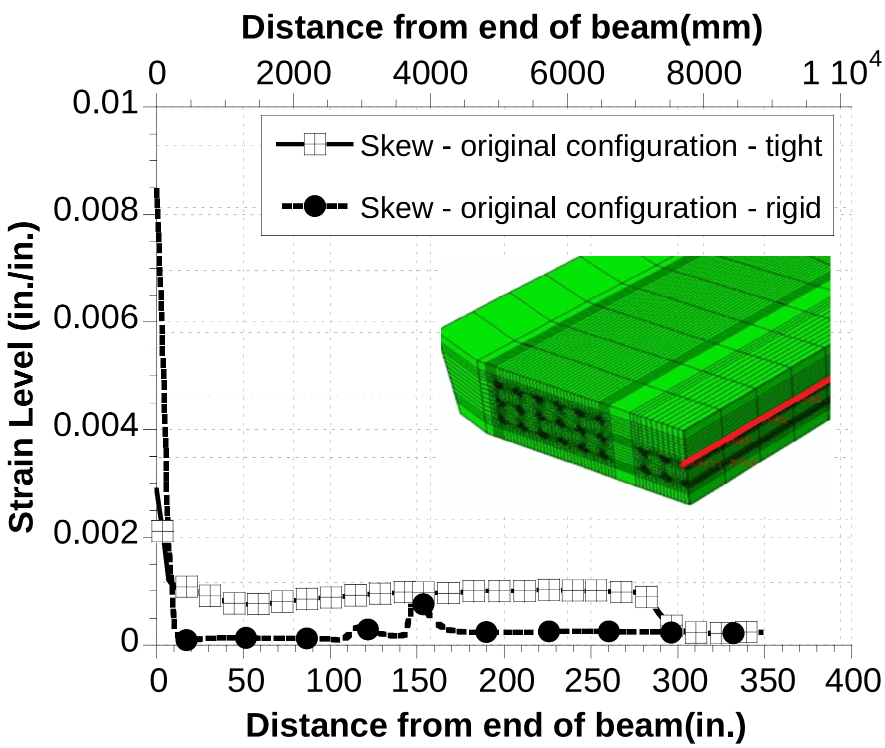

Figure A-46 Response traces along partially debonded strand No.9: Maximum principal strains – Skew-symmetry U-beam models tight vs. rigid with original configuration

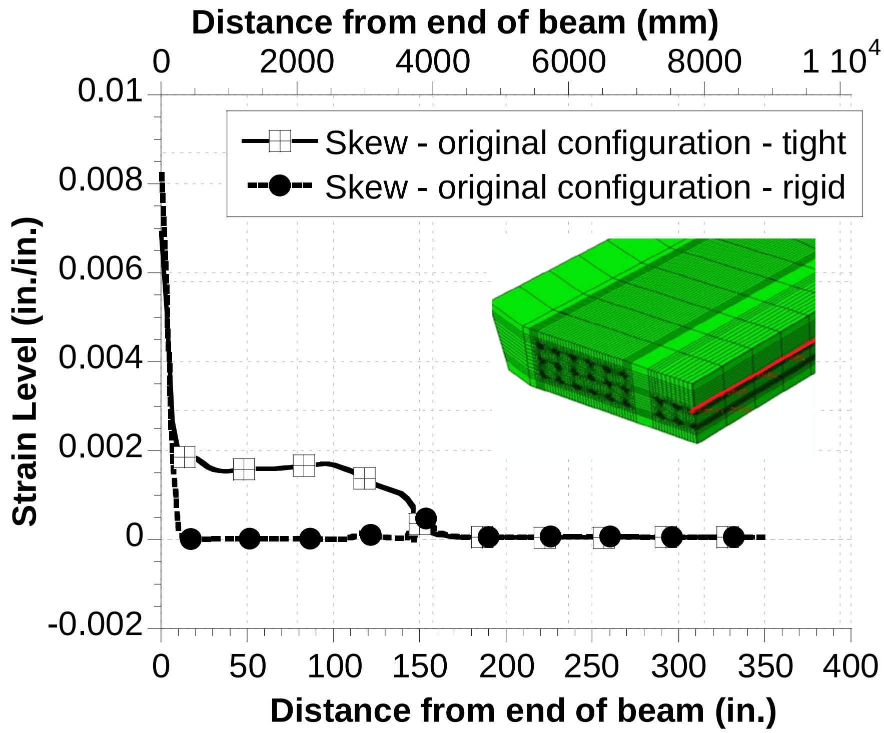

Figure A-47 Response traces along partially debonded strand No.1: Maximum principal plastic strains – Skew-symmetry U-beam models tight vs. rigid with original configuration

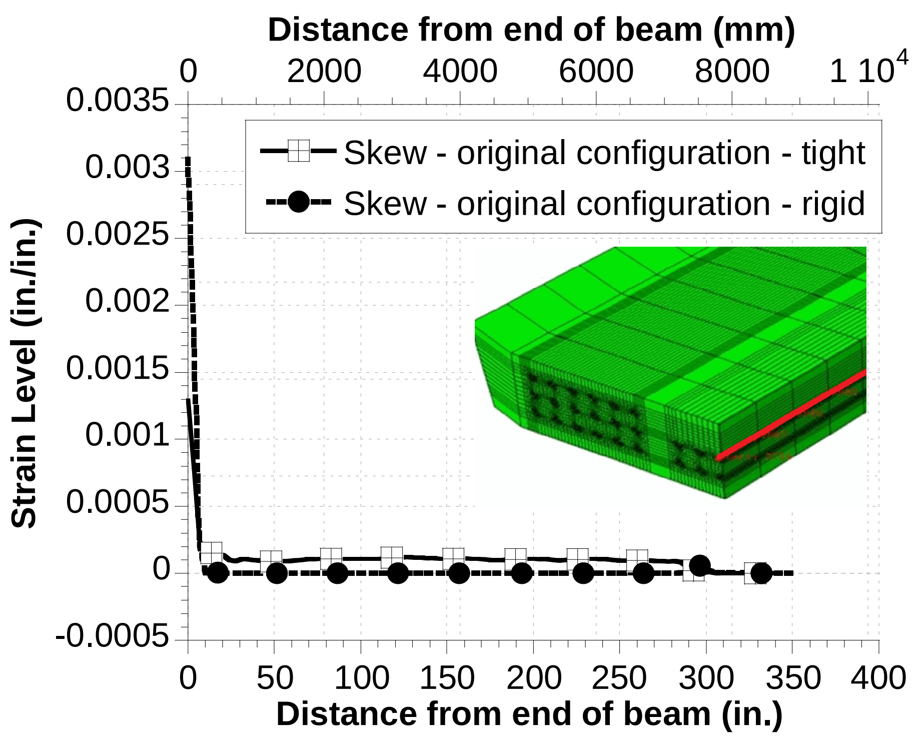

Figure A-48 Response traces along partially debonded strand No.9: PEEQT – Skew-symmetry U-beam models tight vs. rigid with original configuration

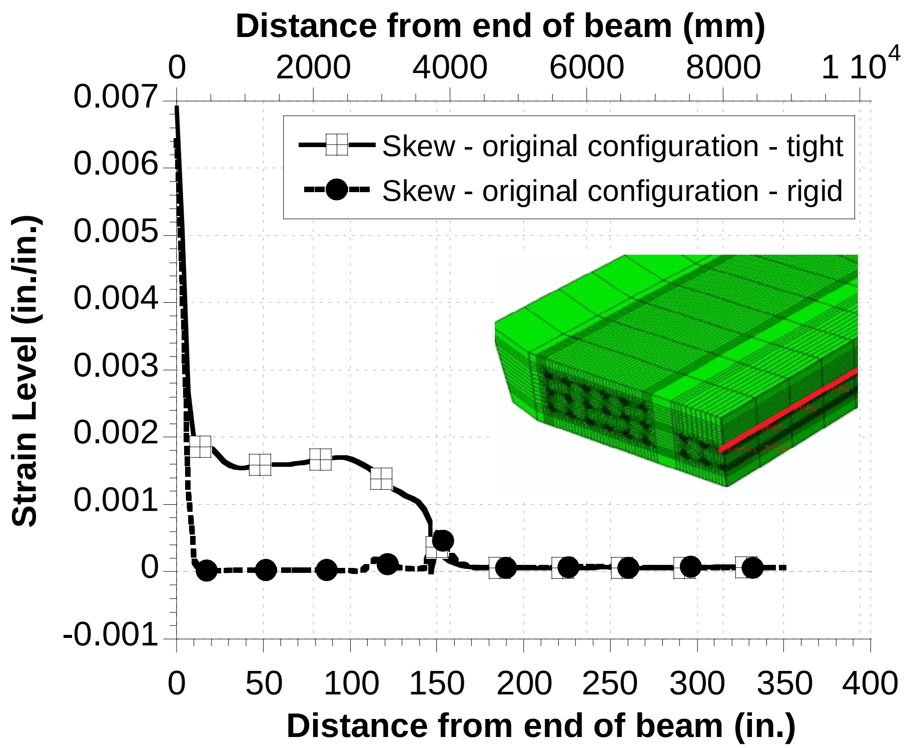

Figure A-49 Response traces along partially debonded strand No.11: Maximum principal plastic strains – Skew-symmetry U-beam models tight vs. rigid with original configuration

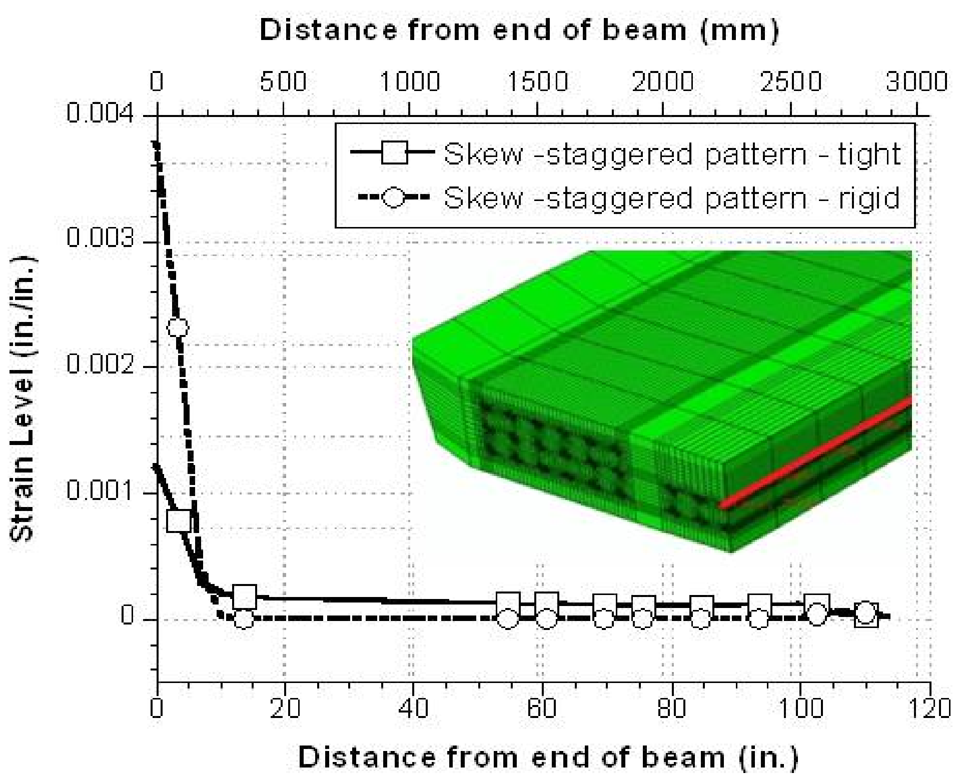

Figure A-50 Response traces along partially debonded strand No.9: PEEQT– Skew-symmetry U-beam models tight vs. rigid with staggered configuration

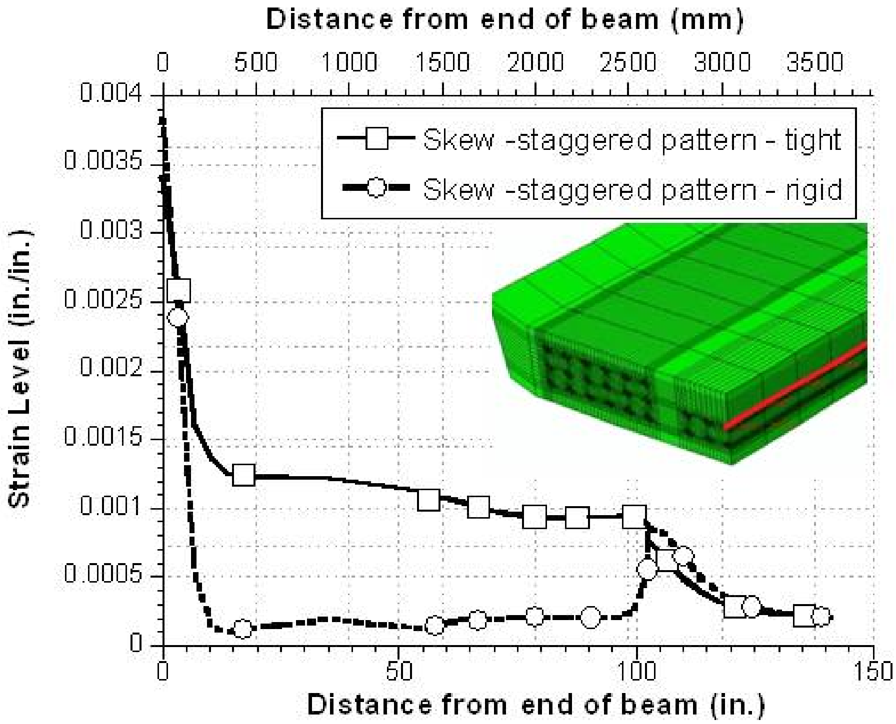

Figure A-51 Response traces along partially debonded strand No.9: Maximum principal strains – Skew-symmetry U-beam models tight vs. rigid with staggered configuration

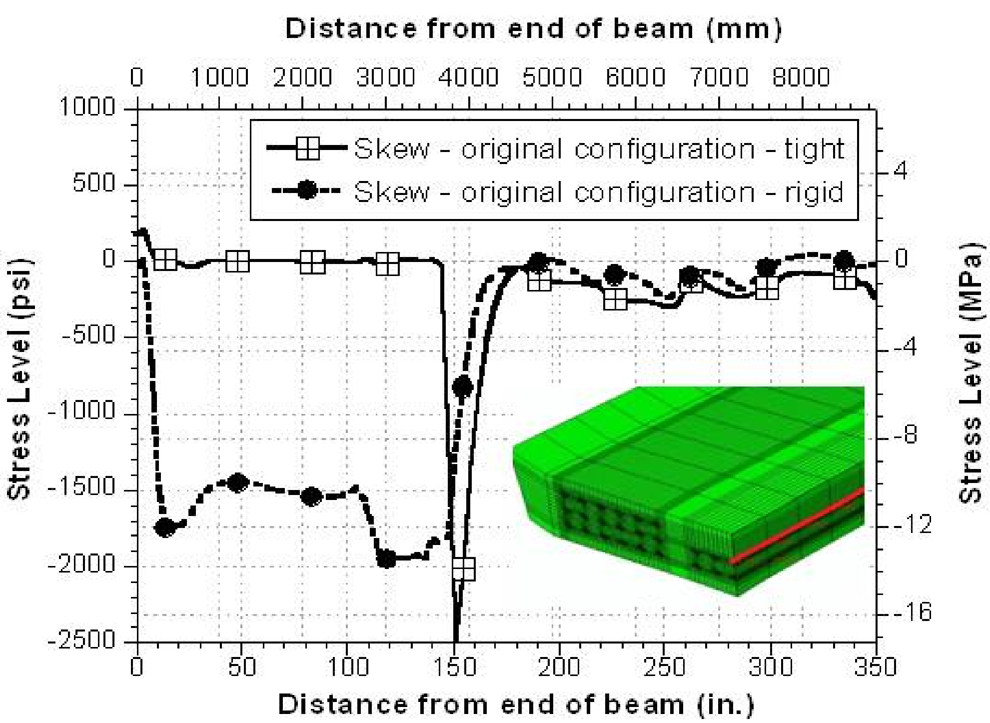

Figure A-52 Response traces along partially debonded strand No.11: Equivalent Axial stresses – Skew-symmetry U-beam models tight vs. rigid with original configuration

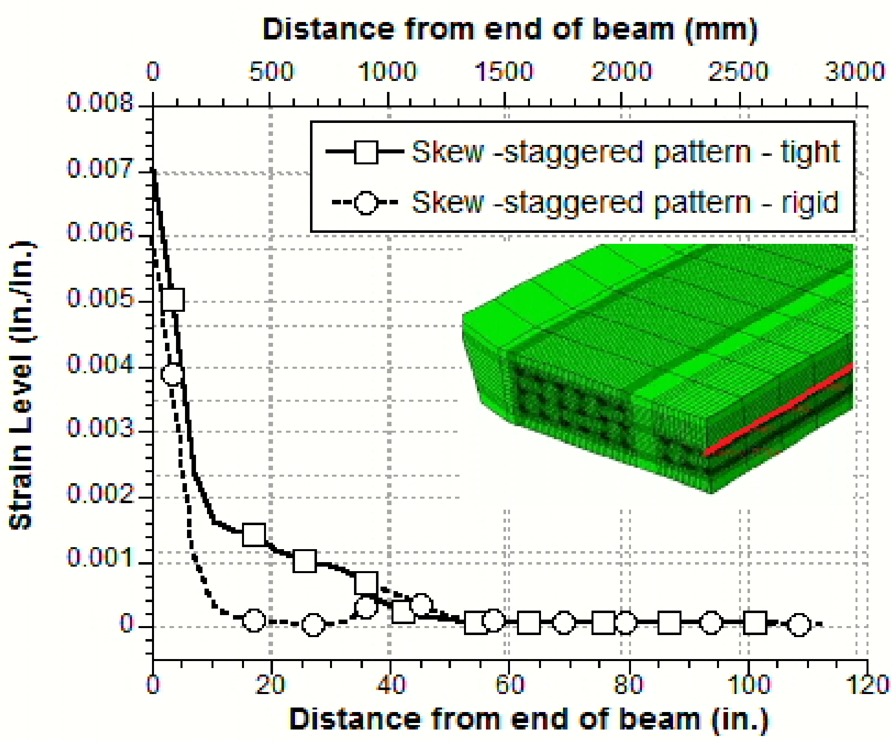

Figure A-53 Response traces along partially debonded strand No.11: Maximum principal plastic strain – Skew-symmetry U-beam models tight vs. rigid with staggered configuration

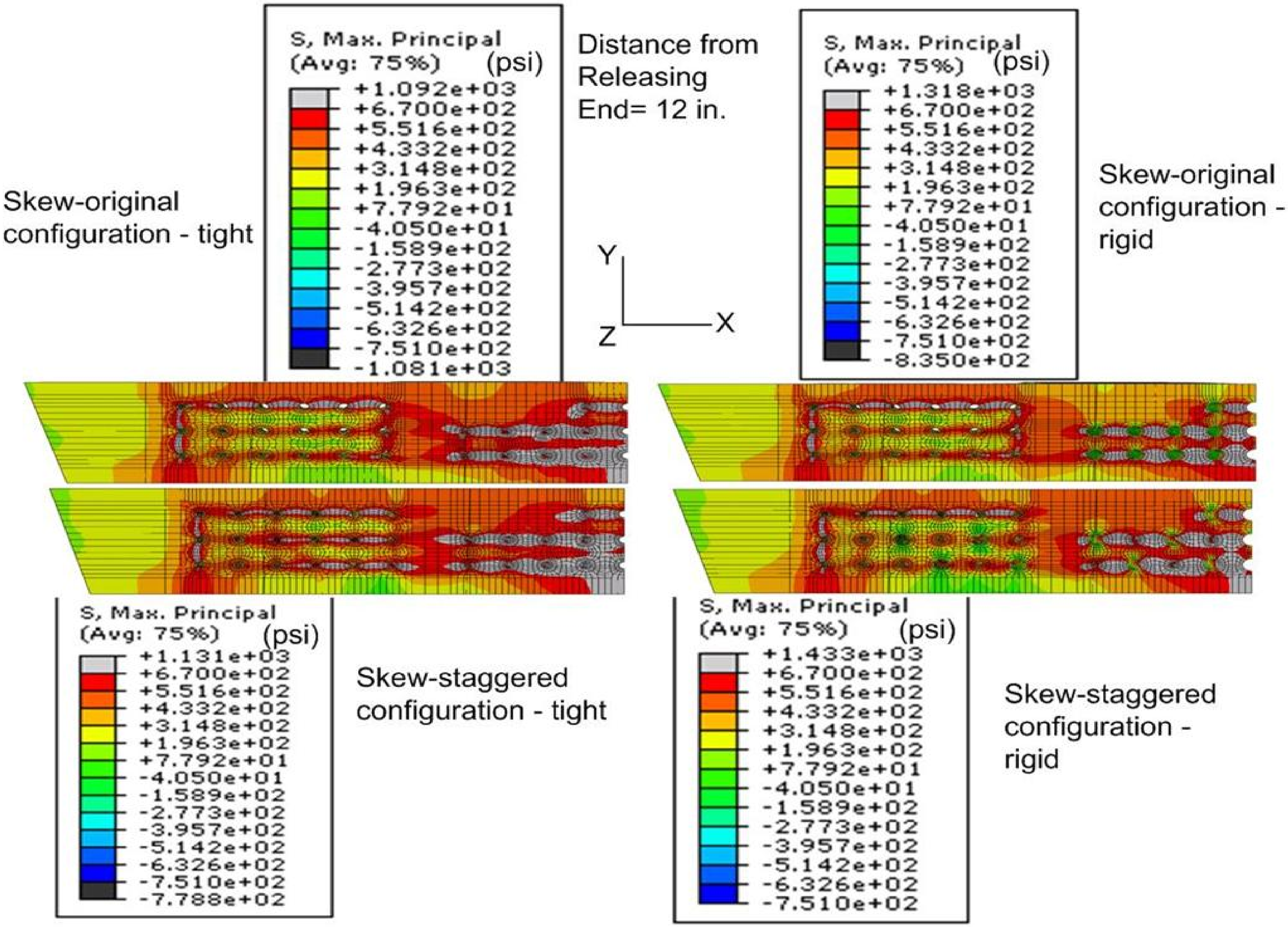

Figure A-54 Maximum principal stresses: Four skew U-beam models

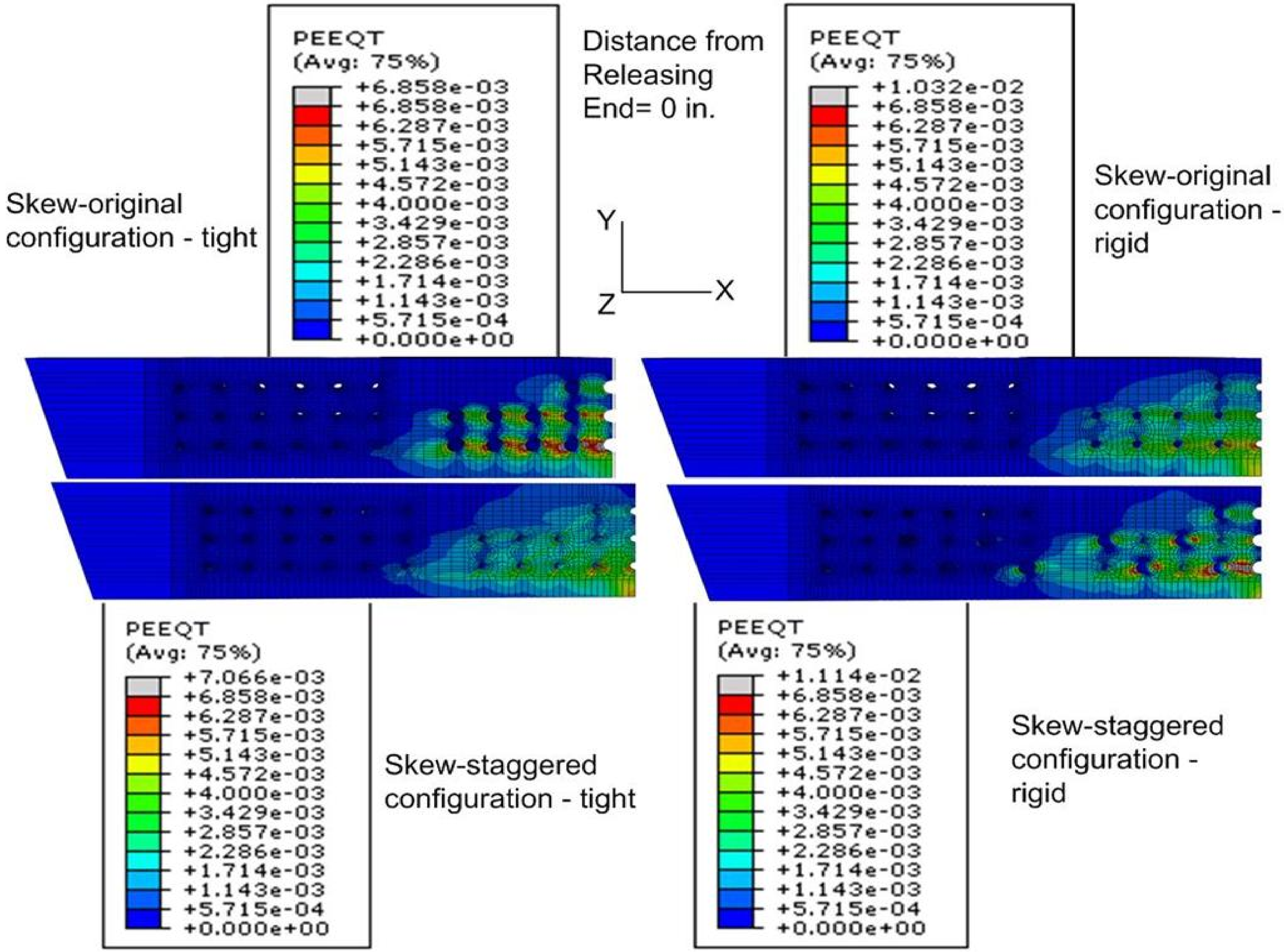

Figure A-55 Equivalent plastic strain in uniaxial tension at release end: Four skew U-beam models

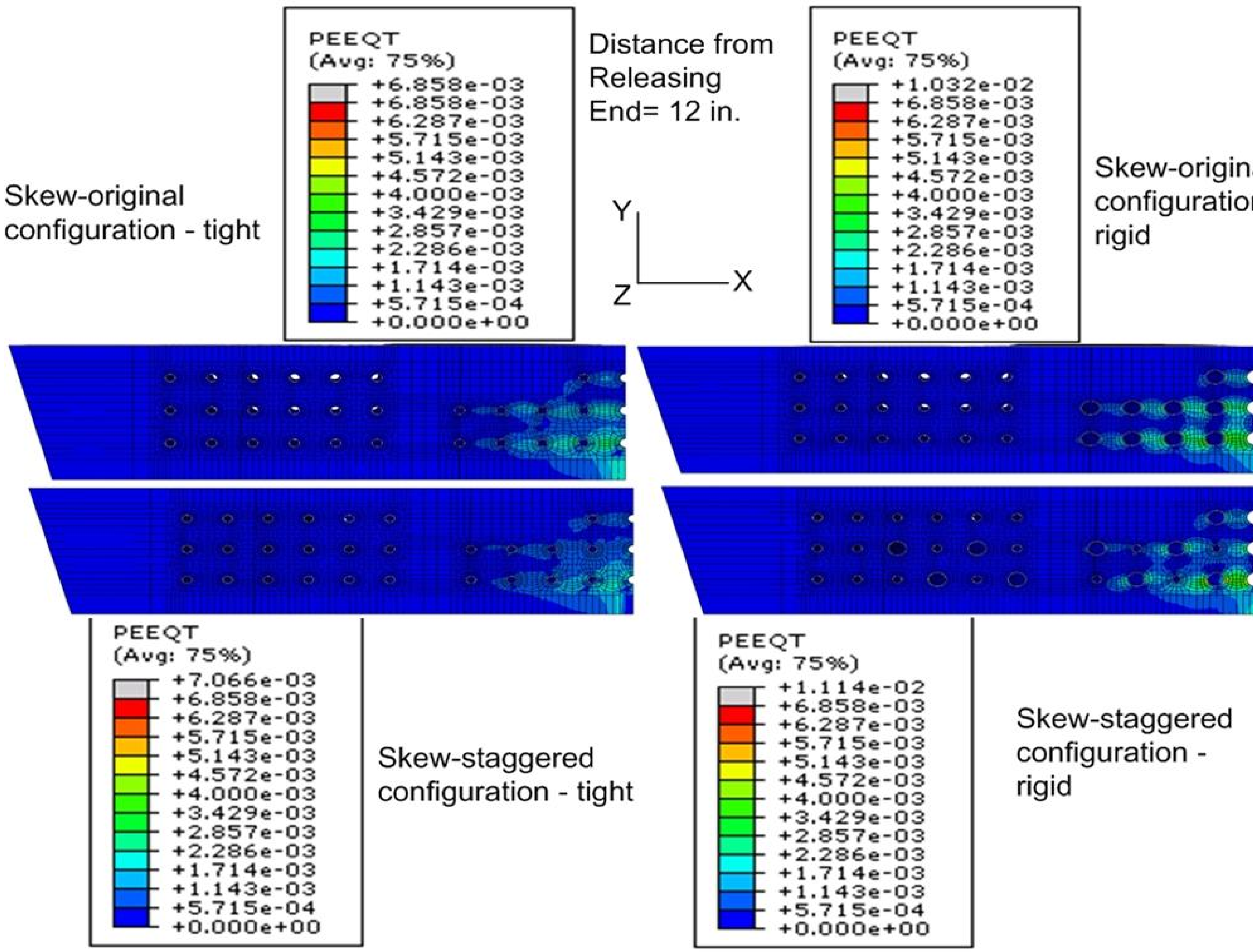

Figure A-56 PEEQT: Four skew-symmetry U-beam models at 12 in. from release end

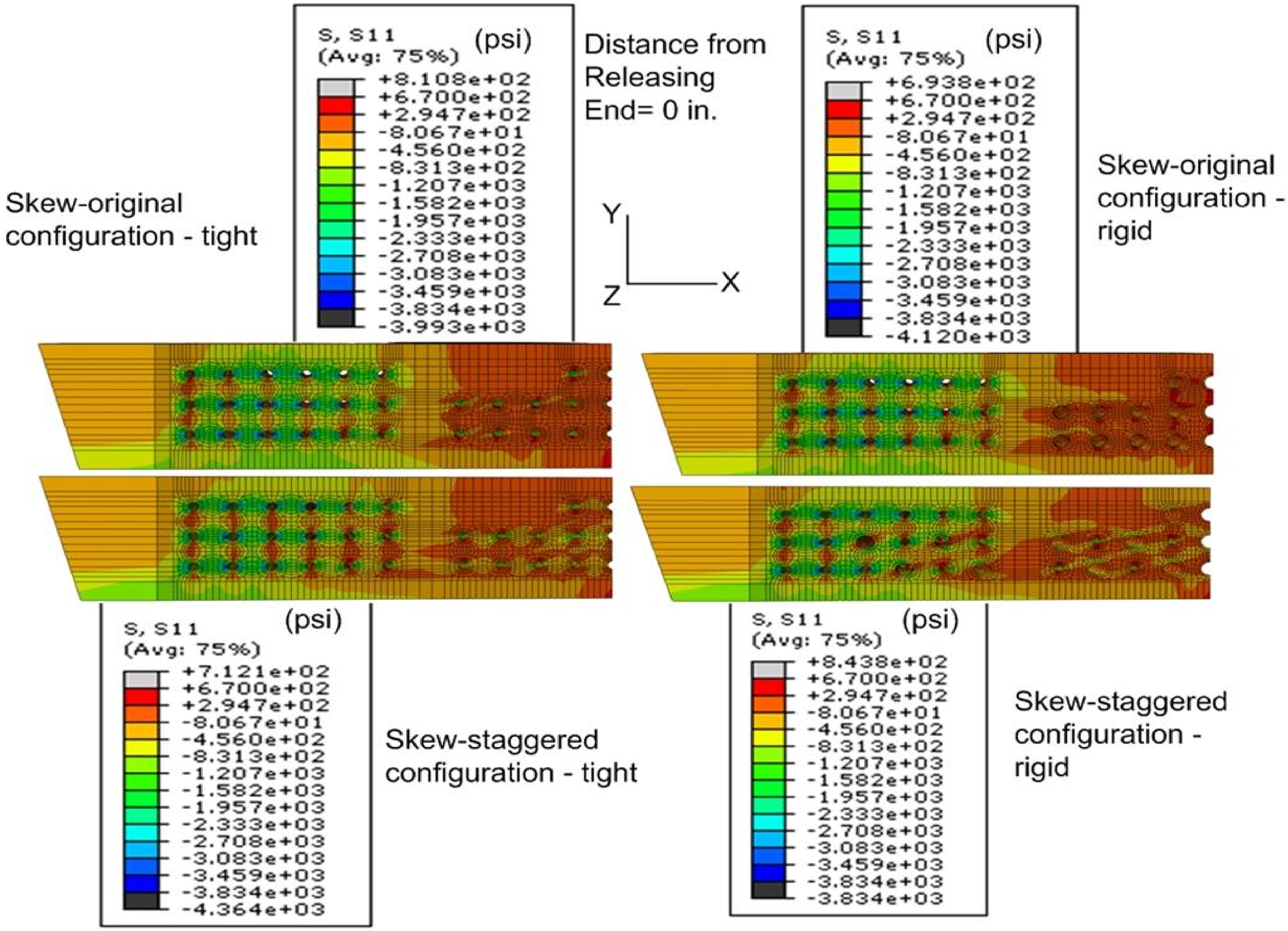

Figure A-57 Axial stresses: Four skew-beam models

REFERENCES

REFERENCES

[1] ABAQUS Documentation, *Simulia*, Version 6.9.

[2] American Association of State Highway and Transportation Officials. “AASHTO-LRFD Bridge Design Specifications,” AASHTO-LRFD Specifications, *4th Edition.* Washington, DC, 2007.

[3] American Concrete Institute (ACI). “Building Code Requirements for Structural Concrete and Commentary,” *ACI 318-08.* Farmington Hills, MI, 2008.

[4] Barnes, R.W., J.W. Grove, and N.H. Burns. "Experimental Assessment of Factors Affecting Transfer Length." *ACI Structural Journal,* November-December 2003, V.100, No.6, 740-748.

[5] Girgis, A.M., and C.Y Tuan. "Bond Strength and Transfer Length of Pretensioned Bridge Girders cast with Self-consolidating Concrete." *PCI Journal*, November-December 2005, V. 50, No. 6, 72-87.

[6] Grumbine, Tom. *Kerkstra Precast*, Personnal Communication.

[7] Florida Department of Transfportation. “Structures Design Guidelines,” *FDOT Structures Manual*, Januarry 2011, V. 1.

[8] Frosch, R.J., Donoso Personal Communication, 2011.

[9] Gamble, W.L. Reader Comments on “Release Methodology of Strands to Reduce End Cracking in Pretensioned Concrete Girders,” *PCI Journal*, July-August 2007, V.42, No. 4, 102-103.

[10] Hanson, N.W., and P.H. Kaar. "Flexural Bond Tests of Pretensioned Prestressed Beams." *ACI Journal*, January 1959, Vol.30, No.7, 783-802.

[11] Jankowiak, T., and Lodygowsky, T. “Identification of Parameters of Concrete Damage Plasticity Constitutive Model,” Foundations of Civil and Environmental Engineering, 2005, No.6, 53-69.

[12] Janney, J. "Nature of Bond in Pre-tensioned Prestressed Concrete." *ACI Journal*, May 1954, V.25, No.9, 717-736.

[13] Kannel, J., C. French, and H. Stolarski. "Release Methodology of Strands to Reduce End Cracking in Pretensioned Concrete Girders." *PCI Journal*, January-February 1997, V.42, No.1, 42-54.

[14] Koyuncu, Yilmaz, Recep Birgul, Theresa M. Alhborn, and Haluk M. Aktan. “Identifying Causes for Distress Patterns in Prestressed Concrete (PC) Girders”. *TRB 2003 Annual Meeting*.

[15] Lee, J., and Fenves, G. “Plastic-Damage Model for Cyclic Loading of Concrete Structures,” *Journal of Engineering Mechanics*, August 1998, V. 124, No.8, 892-900.

[16] Leonhardt, F. “Prestressed Concrete - Design and Construction”. *Berlin: Ernst & Sohn*, 1964.

[17] Logan, D.R. "Acceptance Criteria for Bond Quality for Pretensioned Prestressed Concret Applications." *PCI Journal*, March-April 1997, V.42, No.2, 52-90.

[18] Lubliner, J., Oliver, J., Oller, S., and Oñate, E. “A Plastic-damage model for Concrete,” *Int. J. Solids Structures*, 1989, V. 25, No.3, 299-326.

[19] Mirza, J.R., and M.E. Tawfik. "End Cracking in Prestressed Members During Detensioning,” *Modern Concrete*, V.42, No.3 , July 1978, 44-49.

[20] Moon, D.Y., J-H Kim, S-J Lee, and and G. Kim. "On Strain Change of Prestressing Strand During Detensioning Procedures," *Engineering Structures,* September 2010 V.32, No.9, 2570-2578.

[21] Naaman, A.E. “Prestressed Concrete Analysis and Design,” *Techno Press 3000*, *Ann Arbor*, *MI*, 2004, Second Edition

[22] Oh, B.H, and E.S. Kim. "Realistic Evaluation of Transfer Length in Pretensioned, Prestressed Concrete Members," *ACI Structural Journal*, November-December 2000, V.97, No.6, 821-830.

[23] Pavelchak, Matthew A. “Factors for Improving the Design and Construction of U-beams bridges: Live Load Distribution and Prestressing Strand Debonding Effectiveness”. MS Thesis, *Purdue University*, West Lafayette, IN., December 2009.

[24] Precast and Prestressed Concrete, “PCI Design Handbook”, Chicago, IL, 1999, Fifth Edition.

[25] Peterman, Robert. “The effects of as-cast Depth and Concrete Fluidity on Strand Bond,” *PCI Journal*, May-June 2007, V.52, No.3, 72-101.

[26] Russell, B.W., and N.H. Burns. “Design Guidelines for Transfer, Development, and Debonding of large Diameter Seven wire Strands in Pretensioned Concrete Girders”. Research Report 1210-5F, Center for Transportation Research, Bureau of Engineering Reserach, University of Texas at Austin, January 1993.

[27] Russell, B.W., N.H. Burns, and L.G. ZumBrunnen. "Predicting the Bond Behavior of Prestressed Concrete Beams Containing Debonded Strands." *PCI Journal*, V.39, No.5, Sep-Oct.1994, 60-76.

[28] Shahawy, M., and T. Hassan. "Effect of Strand Debonding on Prestressed Concrete Girder Performance." *American Concrete Institute, ACI Special Publication, Thomas T. C. Hsu Symposium: Shear and Torsion in Concrete Structures - At the ACI Fall 2009 Convention* 2009, No. 265 SP, 533-552.

[29] Shahawy, M., B. Robinson, and B.D. Batchelor. “An Investigation of Shear Strength Performance of Prestressed Concrete AASHTO Type II Girders”. *Structures Research Center, Florida Department of Transportation*, 1993.

[30] Shahawy, M.A., and B. De B Batchelor. "Strand Transfer Lengths in Full Scale AASHTO Prestressed Concrete Girders." *PCI Journal*, May-June 1992: V. 37, No.3, 84-96.

[31] Sun, Yi. “Effect of Strand Debonding on End Cracking in Pre-tensioned Concrete Beams,” MS Thesis, *Michigan State University*, East Lansing, MI., 2010.

[32] Thatcher, D.B., J.A. Heffington, R.T. Kolozs, G.S. Sylva III, J.E. Breen , and N.H. Burns. *Structural Lightweight Concrete Prestressed Girders and Panels.* Research Report 1852-1, Center for Transportation Research, Bureau of Engineering Research, University of Texas at Austin, January 2002.

[33] Tuan, C.Y., S.A. Yehia, N. Jongpitaksseel, and and M.K. Tadros. "End Zone Reinforcement for Pretensioned Concrete Girders." *PCI Journal*, May-June 2004, V.49, No.3, 2-16.